Universitat Autònoma de Barcelona

Transcriptional Regulation of Cell Division and Metal Uptake in Mycoplasma genitalium

Carlos Martínez Torró

TRANSCRIPTIONAL REGULATION OF CELL DIVISION AND METAL UPTAKE IN *MYCOPLASMA GENITALIUM*

Carlos Martínez Torró

2020

Doctoral thesis submitted to obtain the Doctor of Philosophy Degree in Biochemistry, Molecular Biology and Biomedicine

This work was performed at the Institut de Biotecnologia i de Biomedicina (IBB) and at the Biochemistry and Molecular Biology Department of the Universitat Autònoma de Barcelona (UAB) under the supervision of Dr. Oscar Quijada Pich, Dr. Sergi Torres Puig and Dr. Jaume Piñol Ribas

Dr. Oscar Quijada Pich Dr. Sergi Torres Puig Dr. Jaume Piñol Ribas

08193 – Cerdanyola del Vallès Phone: +34 93 586 8952 carlos.martinez.torro@uab.cat

"*Cuestiona todo, aprende algo, pero no esperes ninguna respuesta*"

EURÍPIDES

A mi abuelo

TABLE OF CONTENTS

ACKNOWLEDGMENTS

Las páginas que componen este trabajo son el diario de un viaje que empezó hace cinco años y del que me siento particularmente orgulloso, por distintos motivos. Afortunadamente, he tenido la enorme suerte de compartir camino con muchísima gente durante todo este tiempo. Gente sin la cual, sin ninguna duda, este viaje habría sido significativamente peor. Estas pocas líneas que siguen no hacen justicia a toda la ayuda, la compañía y el apoyo que me habéis proporcionado durante esta etapa, pero constituyen un agradecimiento eterno a todos los que aquí figuráis.

Tengo que empezar por las tres personas sin las que esto, literalmente, no hubiese sido posible. Por orden cronológico, tal como sucedió: Ana, muchísimas gracias por aparecer ese día en Cunit y cambiarme la vida, de proporcionarme ese punto de inflexión que necesitaba en ese momento. Haber convivido (en el laboratorio y fuera) contigo estos años ha sido de lo mejor que me ha podido pasar. Gràcies de tot cor, Òscar, per fer-ho possible, per retornar-me la passió per la ciència amb aquelles tardes de discussions infinites on tots acabàvem amb el cervell fos de plantejar tants experiments i escenaris. Era en aquells moments quan creia que, tot i que el camí fins aquí no havia sigut recte, estava fent allò que més m'agradava. I, per últim, moltíssimes gràcies, Sergi. Des del gel "monopozo" fins a les correccions d'aquesta tesi, has sigut la gran constant de la meva tesi, la persona a la qual recórrer independentment de la situació. Aquest treball és tant meu com teu. Estic enormement orgullós d'haver-te conegut i, pel camí, haver guanyat un amic increïble, algú en qui confiar plenament. Has estat una referència i la pregunta "què faria el Sergi aquí?" segurament ha estat la que més m'he plantejat durant tot aquest temps. Moltíssimes gràcies a tots tres per permetre que avui estigui escrivint això.

También imprescindible ha sido mi familia, sin la cual no habría llegado a ningún lado. Sus sacrificios constantes permitieron que yo pudiese dedicarme a estudiar. Es algo que nunca podré devolver y por lo que estoy muy agradecido, especialmente a mis padres y a mis abuelos maternos. Me sostuvieron siempre que lo necesité y su apoyo incondicional es la clave de todos mis logros. Me apena profundamente que mis abuelos no hayan podido llegar hasta aquí conmigo, pero me consuela pensar que su referencia, en especial la de mi abuelo Fabián, ha servido de guía de muchos de mis pasos. En este capítulo también entras tú, Jara. Has sido fundamental durante todo este tiempo y te

estoy enormemente agradecido. Estas líneas simbolizan el final de un viaje, pero, a la vez, también las escribo cuando nos estamos embarcando en el siguiente, uno que promete ser aún mejor, uno en el que espero seguir descubriendo cosas a tu lado. Aprovecho para extender mi agradecimiento al resto de los Lascorz Lozano: Luzía, Lorién, Azucena y Lorenzo. Muchísimas gracias, aunque sólo sea por los miles de euros en puré que habéis invertido en mí.

Muchísimas gracias a Jaume por su ayuda durante todo este tiempo y por lo mucho que me ha enseñado, no sólo durante el doctorado, sino desde la carrera. También gracias a Enrique, por darme la oportunidad de hacer la tesis en su laboratorio. Aprovecho para agradecer a Pepo y Ángel por su ayuda durante mi estancia. Y quiero acordarme especialmente a mis compañeros de laboratorio, que han sido increíbles. En especial a Lucía y Marina: poder estar con vosotras durante estos últimos años ha sido un auténtico placer y una enorme suerte. Espero que seáis conscientes de la relación tan especial que tenéis y que os cuidéis la una a la otra. Sois dos personas maravillosas y me emociona pensar en qué os vais a convertir, cómo vais a seguir creciendo. Una mención especial también a Arturo: haberte conocido ya sería una recompensa suficiente que llevarme del doctorado. Eres un tipo especial y no sabes lo feliz que me hace tener a alguien así en mi vida. El tiempo que compartimos en el laboratorio fue, posiblemente, la época en la que más he aprendido y disfrutado de mi vida, aunque hiciésemos la escritura imposible a Sergi. Una última mención especial a Miguel, un alumno maravilloso y una persona aún mejor. Vas a llegar tan lejos como tú quieras a poco que tengas algo de suerte en tu camino. ¡Mucha suerte en tu nueva etapa! Y, aunque me faltan líneas para agradeceros personalmente lo que significasteis para mí, gracias a Luis García y Luis González, a los que, para mi desgracia, disfruté demasiado poco. Gracias a Marta Hernández y Xavi Serra, que fueron una gran ayuda durante mis primeros meses. Un abrazo a Carmen y Marta Huguet (que tuvieron la desgracia de ser mis primeras estudiantes) y también a Ari. Gracias también a Rubén, compañero de lab e, inesperadamente, de piso: suerte y aprieta, que llegarás lejos. También me quiero acordar de Ignasi, otra persona que, desde prácticamente el primer día que la conocí, supe que podría llegar también tan lejos como quisiese. Gracias también a Jossy: tu dedicación y tus ganas merecen premio y seguro que lo tendrás si sigues trabajando. Por último, una mención a Núria, Laura y las dos Irenes, a las que no llegué a conocer tanto por la finalización de mi tesis, pero que siempre alegraban el laboratorio.

Tengo muchas personas a las que agradecer también del IBB, comenzando por Miguel, que siempre sospechó que los que pagaban mi contrato eran los del SAF. Gracias a la gente de Enzimo (David, Sergis, Eddi y también a los minions coloca-chantes de David), por ser el grupo más especial (para mal, sobre todo) del centro. Gracias a toda la gente de Serveis (Fran, Olga, Arais, Manu, Roger, Carles y Anna) y a los técnicos (Almu y Francesca) por hacernos la vida muchísimo más fácil. Un abrazo también a Xavi Coves, aunque sólo sea por su enorme vídeo de la Fondue 2019. Un saludo especial a Llevats, un grupo de gente enorme, y en especial a Santo y Diego. Diego, gracias por compartir conmigo (o por inocularme, mejor dicho) la pasión por el pádel y tantos grandes momentos durante estos años. Ojalá tengas la suerte que mereces y puedas estar de vuelta en dos días. Un recuerdo muy especial para el laboratorio de Immuno, donde todo empezó, en especial para Mercè, por hacerlo posible. También un saludo para Iñaki, Erika, Cristina (la primera persona que tuvo que soportarme en un laboratorio), Carme García, Sole, Javi, Carme Roura, Dolores y Diego. Y otro para la nueva generación, Andrea, Adrían y Mireia, que dejan claro que en Immuno siguen captando a gente estupenda. También muchísimas gracias al laboratorio de Nano, en especial a Naroa, Paolo, Laura (que, junto a Diego y Sergi Rodríguez, son la mejor comisión de Fondue de la historia), Marianna, Mireia, Olivia y José Vicente. Y, por último, un abrazo para EP-PDP, en concreto para Manu (mi futuro jefe y señor feudal), Marcos (la mejor persona para alguien a quien le gusta discutir) y Nathalia (siempre dispuesta a ayudar con todo). También un abrazo para Helena, Maria Torras y Marta. Aprovecho para acordarme de la Torre de Bioquímica, en especial de Jaime y Alejandro, que me levantaban la moral en los peores momentos con un partido de pádel. Gracias por dejar que me retirase como Jordan. Un agradecimiento especial también para Valen, Jordi y Guillem (¡y ánimo con lo que se os viene!).

No me quiero olvidar de mis amigos de fuera de la Autònoma. Anna Mestre, tenir-te a prop durant els darrers anys de la carrera, al laboratori, i durant i després del màster ha sigut una de les sorts més grans que he tingut mai a la vida. Gràcies per seguir al meu costat. Laia, ets una inspiració increïble i una de les persones que més admiro. Has estat un suport imprescindible durant aquests mesos i espero tornar-te a veure per aquí aviat. Sé que tiraràs endavant, perquè si hi ha algú que pot superar reptes que semblen inassolibles. María, gracias por todo, a pesar de tus audios de WhatsApp: aunque estemos a cientos de km de distancia, siempre que hablamos es como si estuviésemos a diez metros y estuvieses a punto de subir a mi piso a buscar galletas. Muchas gracias también a Jorge y Jesús, mis dos compañeros de piso durante estos últimos años. A ti,

Jorge, poco tengo que decirte ya: eres casi como familia para mí. Y a ti, Jesús, gracias por ser el mejor compañero de piso posible y la persona a la que llamaré si me tengo que mudar. También gracias a Laura que, junto con Jorge, ha sido una de las razones para volver a Cunit casi cada fin de semana: esas noches sanas de hamburguesa y cine las recordaré siempre (tú no, porque estabas dormida). Moltíssimes gràcies també a l'Alba i a l'Anna Tutusaus: mai hauria pensat que arribaríem fins aquí quan tot va començar olorant a gent en un bar prop d'Apolo. Gràcies per tantes experiències junts (i les que queden, espero!) i per ensenyar-me, especialment, el que és un festival de platja. Y dos menciones especiales, para acabar, para dos grupos de gente especial, empezando por el grupo de la Paella, a los cuales conozco desde hace ya quince años y seguimos tan cansados los unos de los otros como el primer día. En estas páginas está mi mayor plan quinquenal. Les debo muchísimo, así que muchísimas gracias. Y, por último, al grupo de Runners de la UAB, que fueron mentalmente imprescindibles durante los últimos meses de doctorado. Gracias en especial a Quique, Erik, Pablo, Ferran, Miguel, Irene, Aroha y Sergio. Habéis sido casi más fundamentales para mi salud mental que para la física.

Muchísimas gracias a todos, de todo corazón. Es un orgullo enorme haber podido pasar todos estos años rodeado de tanta gente a la que quiero y admiro. Espero haber sido capaz de devolver, ni que sea mínimamente, algo de lo mucho que me habéis aportado.

Hasta siempre,

Carlos

ABBREVIATIONS

6-Fam	6-carboxyfluorescein
ATP	Adenosine triphosphate
ATPase	Adenosine triphosphate nuclease
bp	Base pairs
CARDS	Community Acquired Respiratory Distress Syndrome
cat	Chloramphenicol acetyl transferase
CIRCE	Controlling Inverted Repeat of Chaperone Expression
Cm	Chloramphenicol
dcw	Division and Cell Wall operon
DNA	Deoxyribonucleic acid
DNase	Deoxyribonucleic acid nuclease
dNTP	Deoxynucleotide Triphosphate
DPP	2,2'-bipyridyl
DR	Downstream Region
DTT	Dithiothreitol
EDTA	Ethylenediaminetetraacetic acid
eYFP	Enhanced Yellow Fluorescent Protein
FBS	Fetal Bovine Serum
Fur	Ferric uptake regulator
gDNA	Genomic DNA
GTP	Guanosine triphosphate
GTPase	Guanosine triphosphate nuclease
HEPES	4-(2-hydroxyethyl)-1-piperazineethanesulfonic acid
HIV	Human Immunodeficiency Virus
HR	Homologous Recombination
Hrl	Histidine-rich lipoprotein
ICP-MS	Inductively Coupled Plasma Mass Spectrometry
IPTG	Isopropyl β-D-1-thiogalactopyranoside
kb	Kilobase
kDa	Kilodalton
LB	Luria-Bertani broth
LC-MS	Liquid Chromatography – Mass Spectrometry
MiniTn	Minitransposon
mRNA	Messenger RNA

MS	Mass Spectrometry
Mur	Manganese uptake regulator
ncRNA	Non-coding RNA
NRT	Non-retrotranscribed control
nt	Nucleotide
NTC	Non-template Control
Nur	Nickel uptake regulator
O/N	Overnight
ORF	Open Reading Frame
pac	Puromycin acetyl transferase
PBS	Phosphate buffered saline
PCR	Polymerase Chain Reaction
pDNA	Plasmid DNA
PVDF	Polyvinylidene Fluoride
qRT-PCR	Quantitative Real-Time PCR
RNA	Ribonucleic acid
RNase	Ribonucleic acid nuclease
RNAP	RNA Polymerase
ROS	Reactive Oxygen Species
rpm	Revolutions per minute
rRNA	Ribosomal RNA
RT	Retrotranscriptase
RT (ºC)	Room Temperature
SDS	Sodium Dodecyl Sulfate
SDS-PAGE	Sodium Dodecyl Sulfate Polyacrylamide Gel Electrophoresis
SILAC	Stable Isotope Labeling by Amino acids in Cell culture
SOB	Super Optimal Broth
SOE-PCR	Splicing by Overlap Extension – PCR
SP4	Spiroplasma-4 broth
Supp.	Supplementary
Tet	Tetracycline
TetM/TetM438	Tetracycline Resistance Marker
TO	Terminal Organelle
TSS	Transcription Start Site
UR	Upstream Region
UV	Ultraviolet light
WT	Wild-type Strain
X-Gal	5-bromo-4-chloro-3-indolyl-β-D-galactopyranoside
Zur	Zinc uptake regulator

GENERAL INTRODUCTION

GI.1 Basic biology of Mycoplasmas

Mollicutes is a class of free-living bacterial characterized by the absence of a cell wall, a low G+C content and the minute genome size of some of species (S. Razin, 1985). These unique microorganisms have a very distinct phenotype and they are a recurrent topic of evolutionary studies. It is considered that they aroused from Gram-positive bacteria through a process of degenerative evolution (Woese et al., 1980).

Table GI. 1. Characteristics and taxonomy of Mollicutes. Adapted from Razin, 2006.

Genus	Number of species	Genome size (kb)	G+C percentage (mol%)	Habitat
Mycoplasma	107	580-1350	23-40	Humans and animals
Ureaplasma	7	760-1170	27-30	Humans and animals
Entomoplasma	6	790-1140	27-29	Insects and plants
Mesoplasma	12	870-1100	27-30	Insects and plants
Spiroplasma	34	780-2220	24-31	Insects and plants
Acholeplasma	14	1500-1650	26-36	Animal and plant surfaces
Anaeroplasma	4	1500-1600	29-34	Bovine-ovine rumen
Asteroleplasma	1	1500	40	Bovine-ovine rumen

Mycoplasma is the most well-known genus among the class Mollicutes (Table GI. 1) (Shmuel Razin, 2006). They have gone through a massive genome reduction (Figure GI. 1) and, in consequence, they have a severe dependence on the host for nutrients because of its extremely limited metabolic pathways (Joel B. Baseman & Tully, 1997). Indeed, there are only three recognized mechanisms of energy generation in these bacteria: the fermentation of sugars to lactate, the oxidation of lactate or pyruvate, and the metabolism of L-arginine (Keçeli & Miles, 2002). Therefore, mycoplasmas must rely on the host in order to import several essential nutrients as purines, amino acids and

sterols (Pollack, 1997). Because of their wide demand of nutrients, they are obligated parasites and their growth *in vitro* is complex, as they need very rich media.

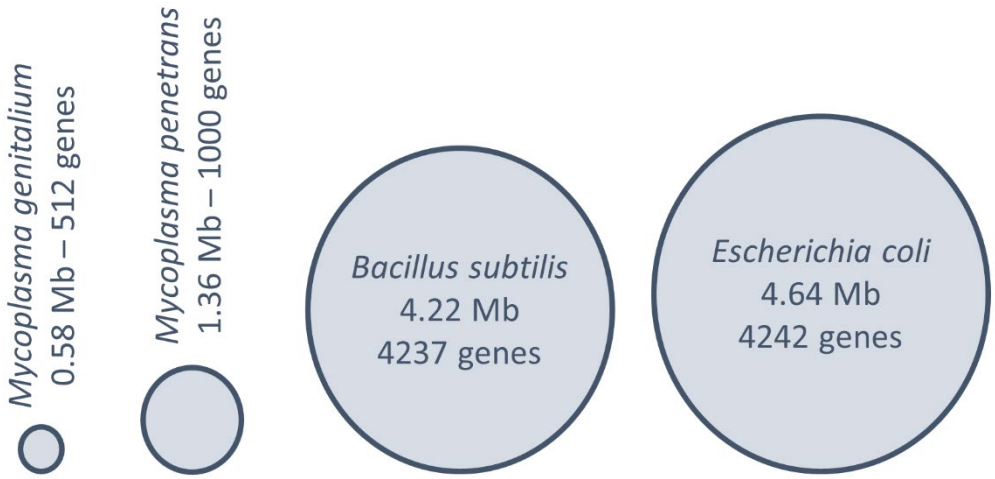

Figure GI. 1. Extensive genome reduction in mycoplasmas. Schematic comparison of one of the smallest (*M. genitalium*) and the largest (*M. penetrans*) genomes in the Mycoplasma genus with the gram-positive and gram-negative representative species *B. subtilis* and *E. coli*, respectively. The diameter of each sphere corresponds to the number of Mb of each species in cm. The number of genes is exclusively referred to the protein-coding genes.

Mycoplasma cells are small, ranging from 0.2 to 0.8 µm. Their small size and the plasticity of their membrane allow them to pass through 0.22 µm filters (Nikfarjam & Farzaneh, 2012). This fact, together with their innate resistance to antibiotics targeting the bacterial cell wall, makes them a primary cause of cell culture contamination. In addition, their detection is complicated, as the consequences of their growth on medium turbidity or cell damage are not as evident as with other contaminants. Although detection of contamination by mycoplasmas has vastly improved in recent years, the predicted incidence of mycoplasma contamination in cell cultures was astonishingly high some years ago (Rottem & Barile, 1993).

As stated in Table GI. 1, there are more than a hundred *Mycoplasma* species known, sixteen of them have a human origin and most of them are thought to be commensal species (Taylor-Robinson & Jensen, 2011). However, at least five exhibit some sort of pathogenic properties (Table GI. 2).

Table GI. 2. Basic characteristics of Mycoplasma species of human origin. Adapted from Taylor-Robinson, 2011. **Ureaplasma urealyticum* only uses urea.

Species	Primary site colonized		Metabolism		Considered pathogenic
	Genital tract	Respiratory tract	Glucose	Arginine	
M. hominis	+			+	Yes
M. fermentans	+		+	+	Yes
*U. urealyticum**	+				Yes
M. salivarum		+		+	
M. primatum		+		+	
M. pneumoniae		+	+		Yes
M. orale		+		+	
M. buccale		+		+	
M. faucium		+		+	
M. lipophilum		+		+	
M. genitalium	+		+		Yes
M. pirum	+		+		
M. spermatophilum	+		+		
M. penetrans	+		+	+	
M. amphoriforme		+	+		

There are other mycoplasma species that cause severe pathogenesis in animals, as it is the case of *M. mycoides*, *M. agalactiae* and *M. bovis*, which infect ruminants and are related to the development of respiratory diseases, mastitis and arthritis (Kumar et al., 2014; Nicholas & Ayling, 2003; Provost et al., 1987). *M. hyorhinis* and *M. hyopneumoniae* are swine pathogens that cause arthritis and enzootic pneumonia, respectively (Barden & Decker, 1971; Maes et al., 2018). And there are also avian parasites as *M. gallisepticum*, responsible for chronic respiratory disease in poultry, and *M. synoviae*, which infection leads to synovitis and upper respiratory diseases in chickens and turkeys (Stipkovits & Kempf, 1996). These microorganisms have a great impact on animal welfare and represent a massive economic burden (Minion, 2002).

GI.2 *Mycoplasma genitalium*: more than a minimal genome

GI.2.1 Clinical relevance

M. genitalium is a sexually transmitted pathogen that was first isolated nearly forty years ago from the human urogenital tract of two men with non-gonococcal urethritis (Tully et al., 1981). This microorganism has been the subject of numerous studies mostly because of its vastly reduced genome: with only 580 kb and 512 protein-coding genes, it is considered the smallest organism capable of autonomous replication.

On the other hand, since its discovery as a causal agent of non-gonococcal urethritis in men, *M. genitalium* has also been associated with cervicitis, pelvic inflammatory disease, risk of infertility spontaneous abortion and premature births (Lis et al., 2015). Moreover, there are several studies linking *M. genitalium* infections to an increased susceptibility to HIV infection (Vandepitte et al., 2014) and also to a higher shedding of the virus DNA from the cervix (Manhart et al., 2008), thus possibly facilitating its transmission. Coinfection with other pathogens like *Chlamydia trachomatis* and *Neisseria gonorrhoeae* has also been a subject of study in recent years (Lillis et al., 2019). Moreover, over the last few years, there has been a constant rise in publications describing the rapid emergence of antibiotic resistance in *M. genitalium* (Fernández-Huerta et al., 2020).

Despite its rapidly ascending clinical relevance, it is difficult to pinpoint the exact prevalence of this bacterium in the general population. It is believed to be around 1.5% in high-developed regions and about 4% in poorer countries, with no significant differences between men and women (Baumann et al., 2018). However, it could be potentially higher due to the mostly asymptomatic nature of *M. genitalium* infections (Sonnenberg et al., 2015). The prevalence in high-risk individuals could be as high as 8%, which is usually associated with particular sexual behaviors (McGowin & Anderson-Smits, 2011).

Besides the disturbing evidence that points to an emergent infectious agent, researchers also found that *M. genitalium* was becoming resistant to antibiotics. Because of the lack of a cell wall, effective treatment options for mycoplasmal infections are scarce (Table GI. 3) and there is an increasing number of clinical isolates that are resistant to macrolides and quinolones, the first and second line recommended therapies, respectively (Manhart et al., 2015). Resistance to those antibiotics in *M. genitalium* is

associated with point mutations in particular genes, as no extrachromosomal DNA has been discovered in this bacterium (McGowin & Totten, 2017). Mutations in the 23S rRNA gene confer resistance to macrolides (Jørgen S. Jensen et al., 2008), while mutations in the DNA gyrase *gyrA* and the DNA topoisomerase *parC* genes have been associated with resistance to fluoroquinolones (Shimada et al., 2010).

Table GI. 3. Susceptibility* of *M. genitalium* to various antibiotics. Adapted from Manhart *et al.*, 2015.

Class	Antibiotic	MIC Range (All Tested Isolates), µg/mL	MIC Range (Recent Clinical Isolates), µg/mL
Aminoglycosides	All	10 - >50	ND**
Amphenicols	Chloramphenicol	0.5 - 25	ND
Aminocyclitols	Spectinomycin	1 - 5	ND
Ketolides	Telithromycin	<0.00003 - 0.015	ND
	Solithromycin	<0.0032 - 16	<0.001 - 16
Lincosamides	All	0.2 - 25	ND
Macrolides	Erythromycin	<0.001 to >16	0.03 to >16
	Clarithromycin	0.0005 - 128	0.016 to >16
	Azithromycin	<0.000032 - 250	<0.0002 to >64
Monoxycarbolic acids	Mupirocin	0.25 - 1	ND
Oxazolidinone	Linezolid	4 - 128	ND
Pleuromutilins	Tiamutilin	0.0025 - 0.01	ND
Quinolones	First generation	0.06 - 32	ND
	Second generation, class I	1 - 64	ND
	Second generation, class II	0.063 to >16	0.5 to >16
	Third generation	0.03 - 4	ND
	Fourth generation, all	0.008 to >16	0.016 to >16
	Moxifloxacin	0.016 to >16	0.031 to >16
Rifamycins	Rifampin	32 - 64	ND
Streptogramins	Pristinamycin	<0.01–0.02	ND
Tetracyclines	Tetracycline	≤0.01 - 4	0.125 - 4
	Doxycycline	≤0.008 - 2.5	0.06 - 2
	Minocycline	≤0.01 - 2.5	ND

* Susceptibility is inferred from Minimum Inhibitory Concentrations (MIC). MICs below 0.01 µg/mL indicate a high susceptibility and MICs above 2 µg/mL are suggestive of resistance.
** ND = Not Determined

Although multidrug resistance (MDR) strains are still rare in Europe, they are a real threat in other regions as Australia (9.8% of the identified *M. genitalium* strains were MDR) and Japan (30.8%) mainly due to an inappropriate use of the current antibiotics (Braam et al., 2017). In consequence, treatment failures are becoming more common (Manhart et al., 2013). Despite that alternative antibiotics as pristinamycin and solithromycin are being employed to treat MDR infections, further studies are needed to determine optimal dosages for those antibiotics in order to achieve clinical cure and prevent the appearance of new resistances (Couldwell & Lewis, 2015).

GI.2.2 Infection

M. genitalium is a flask-shape organism that adheres to host target cells in order to stablish an effective infection (Figure GI. 2). *M. genitalium* cells have a differentiated tip structure, called terminal organelle, that plays a key role in host cell adherence (D C Krause et al., 1982) and it is a common feature among mycoplasmas, although its morphology differs from species to species (Hatchel & Balish, 2008). This complex structure encompasses several proteins and it is responsible for gliding motility (Krause & Balish, 2001; Hasselbring & Krause, 2007).

Several years ago, it was proposed that mycoplasmas achieved cell attachment by binding to sialylated oligosaccharides (Glasgow & Hill, 1980); this notion was supported by several studies (J. B. Baseman et al., 1982; Kasai et al., 2013; Loomes et al., 1984; Nagai & Miyata, 2006; Roberts et al., 1989). A recent report offered conclusive evidence on that aspect, as it was demonstrated that one of the main adhesins of this bacterium binds to neuraminic sugar moieties (Aparicio et al., 2018). This adhesion mechanism has been further investigated recently (Aparicio et al., 2020) and it has also been described in *M. pneumoniae* (Vizarraga et al., in press).

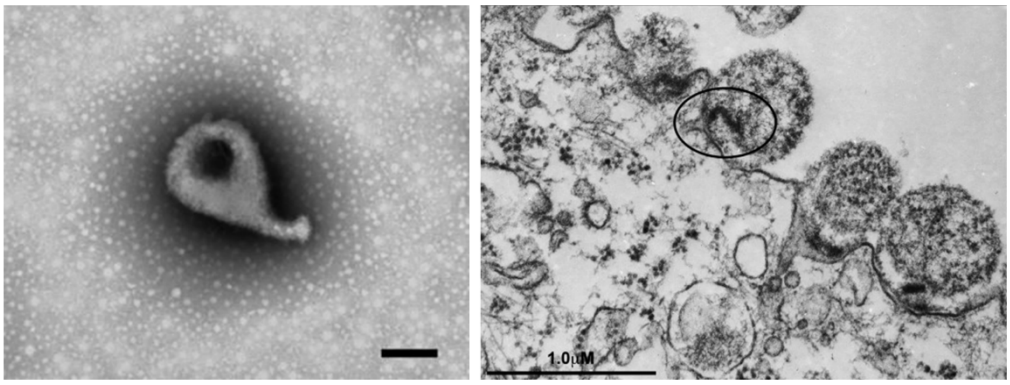

Figure GI. 2. Distinctive morphology and cell attachment of *M. genitalium*. On the left, an electron microscopy capture of *M. genitalium* with its characteristic flask-shape morphology (image extracted from Gnanadurai & Fifer, 2020, scale bar indicates 0.2 µm). On the right panel, TEM micrograph of *M. genitalium* attachment to vaginal epithelial cells. The authors highlighted the electron dense structure involved in attachment with a circle (image extracted from McGowin et al., 2009).

Host cell adherence is mediated by the two main cytadhesins of *M. genitalium*: two large surface-exposed proteins designated P140 and P110 due to its molecular weight. These two proteins and their homologues in the related species *M. pneumoniae* are essential for cytoadherence and their function is critical for infection (Duncan C. Krause, 1996). They also have a major role in the cytoskeleton of this bacterium (Proft & Herrmann, 1994), as it has been demonstrated that they are needed for both maintenance and integrity of the terminal organelle (Duncan C. Krause & Balish, 2004) as well as the regulation of its duplication (Pich et al., 2009). The participation of P110 and P140 in the motile machinery has also been demonstrated in different studies (García-Morales et al., 2016; Nakane et al., 2011). Notably, P140 and P110 stabilize each other, which means that the loss of one of them yields the same cytadherence-negative phenotype as losing both (Burgos et al., 2006).

GI.2.3 Persistence and immune system evasion

The limited treatment options and the emergence of MDR strains are two of the main reasons of *M. genitalium* high persistence. This trait could lead to health problems on asymptomatic persons, as it has been demonstrated that this small pathogen elicits pro-inflammatory cytokine secretion, even with low organism burdens (McGowin et al., 2012). Several studies have addressed the persistence of *M. genitalium* infections and, although the results differ depending on the population, it seems to range from 15 to 20% (Bradshaw et al., 2008; Manhart et al., 2013; Seña et al., 2018).

However, beyond *M. genitalium* resistance, either innate or acquired, to an ample variety of antibiotics, this bacterium has developed smart mechanisms to ensure its persistence inside the host. Almost thirty years ago, it was observed that *M. genitalium* generates spontaneous non-adherent variants that were classified as class I and class II with regards to the expression (impaired or obliterated, respectively) of P140, one of the two main cytadhesins of this pathogen (Mernaugh et al., 1993). As it was demonstrated a few years later, the generation of these variants was mediated by homologous recombination, granting *M. genitalium* a phase variation mechanism (Burgos et al., 2006). The recombination involved sequences of the adhesin genes and several repetitive DNA regions, designated as MgPa repeats, spread over the chromosome of this small pathogen (Fraser et al., 1995). Indeed, the nine scattered DNA repeats represent partial copies of the *mgpB* and *mgpC* genes that code for P140 and P110, respectively. Based on this, it has been proposed that the MgPa repeats constitute a reservoir to generate antigenic variation (Peterson et al., 1995). As it was later evidenced, these sequences allow *M. genitalium* to present an extensive heterogeneity of the *mgpB* and *mgpC* genes (Iverson-Cabral et al., 2006, 2007; Ma et al., 2007). An extensive genetic variation in the adhesin genes that correlated with the MgPa repeats was observed in clinical isolates (Figure GI. 3) (Ma et al., 2010).

This is of particular interest due to the immunodominant nature of P140 and P110 (P. C. Hu et al., 1987; Morrison-Plummer et al., 1987). *M. genitalium* not only can *switch off* the expression of its adhesins (phase variation), but also considerably modify their sequence (antigenic variation) in order to evade the immune system response. In a primate animal model, IgG from infected animals recognized preferentially the original P140 protein rather than the predominant variant after 8 weeks of infection (Wood et al., 2013). However, the conserved C-terminal domain of P140, involved in attachment, is among the most immunogenic regions (Iverson-Cabral et al., 2015).

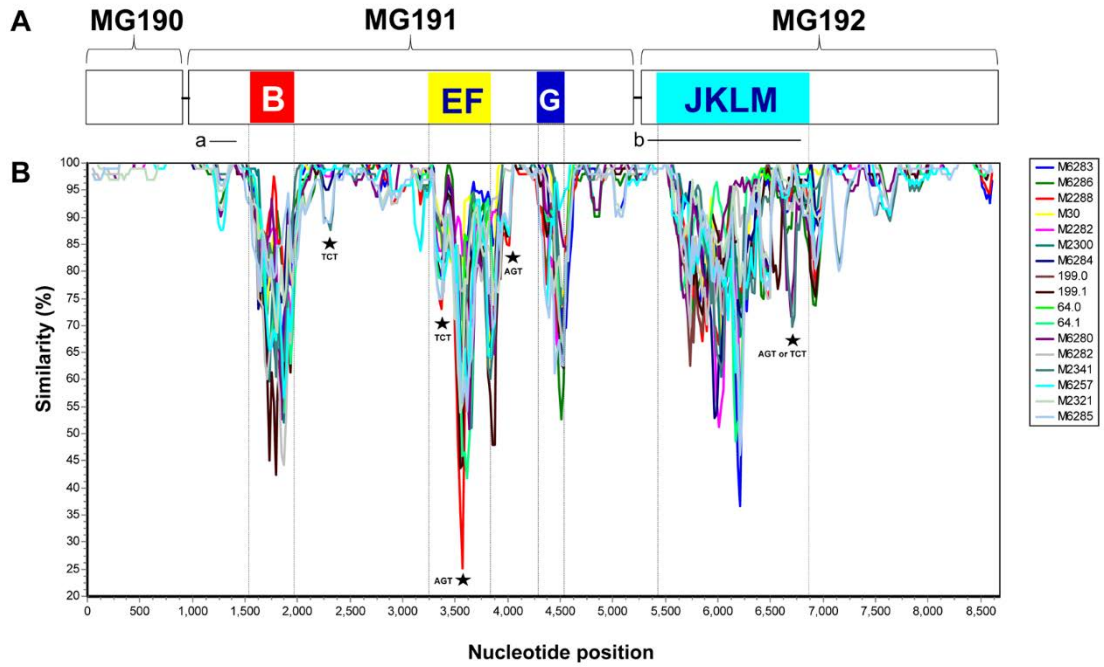

Figure GI. 3. Genetic variation of *mgpB* (MG_191) and *mgpC* (MG_192) in clinical strains when compared to the wild-type strain. The scattered MgPa regions are listed as letters (BEFGJKLM) and located above its homology region in the MgPa operon. Every color represents one of the fifteen different clinical isolates and its similarity with the G37 strain. Image extracted from Ma et al., 2010.

Phase variation, in which the expression of both adhesins is depleted, provides *M. genitalium* with another strategy to evade the immune response from the host. This phenomenon was comprehensibly assessed in a recent study (Burgos et al., 2018). The researchers found that phase variation was reversible in a great number of cases, as opposed to the non-adherent phenotype of class I and class II mutants, which is often irreversible. Therefore, *M. genitalium* could switch phases depending on the host response. Remarkably, the recombination of MgPa repeats that generates phase and antigenic variation is promoted by an alternative sigma factor encoded in the MG_428 gene (Torres-Puig et al., 2015; Torres-Puig doctoral thesis, 2017).

GI.2.4 Virulence

To date, there are no known toxins secreted by *M. genitalium*. Thus, virulence of this small pathogen is mainly associated with its capacity to stimulate the host immune response (McGowin & Totten, 2017). Actually, it has been proposed that the primary source of damage upon mycoplasma infections is self-inflicted by an inefficient immune response (Shmuel Razin et al., 1998). This topic has been thoroughly assessed in *M. pneumoniae* (Waites & Talkington, 2004), as it has been observed that potent immune

system reactions are strongly associated with more severe pulmonary injuries (Ito et al., 1995; Radisic et al., 2000).

The immunomodulation caused by mycoplasmas has been linked to its ability to persist inside the host and establish chronic infections (Shmuel Razin et al., 1998). Their exposed lipoproteins play a critical role in modulating the host immune response to a mycoplasma infection. It was evidenced in the mid-nineties that lipoproteins present on mycoplasma membranes could induce the production of proinflammatory cytokines, although by a different mechanism than lipopolysaccharides (Rawadi & Roman-Roman, 1996). A few years later, it was demonstrated that the uncharacterized lipoprotein MG309 of *M. genitalium* elicited a potent proinflammatory response via toll-like receptors (TLR) (McGowin, Liang, et al., 2009). Similarly, other researchers linked the inflammatory response induced by the lipoproteins of this pathogen to the activation of NF-κB (Y. Wu et al., 2008). Notably, it was reported that contact with lung epithelial cells triggered a differential expression of genes coding for lipoproteins in *M. pneumoniae* (Hallamaa et al., 2008), and a similar phenomenon was observed in the human-pathogen *M. hominis*, as it changed expression of lipoprotein-encoding genes upon contact with human dendritic cells (Goret et al., 2016). There has also been proposed that autophagy might also play a role in the inflammatory response induced by mycoplasma cytadherence (Shimizu, 2016).

Production of hydrogen peroxide and mycoplasma pathogenicity are intimately entwined. This reactive species is generated as a by-product of glycerol metabolism (Halbedel, Hames, et al., 2007), an essential carbon source for mycoplasma growth that is part of one of the few catabolic pathways conserved in Mollicutes (Yus et al., 2009). Glycerol also constitutes a bridge between glycolysis and fatty acid metabolism (Figure GI. 4), as glycerol-3-phosphate can be removed from the former and used for lipid synthesis (Blötz & Stülke, 2017). Although glycerol can pass the membrane by passive diffusion, mycoplasmas encode a glycerol facilitator, a membrane transporter similar to aquaporins that, in addition to glycerol uptake, also allows the facilitate diffusion of urea (Stroud et al., 2003).

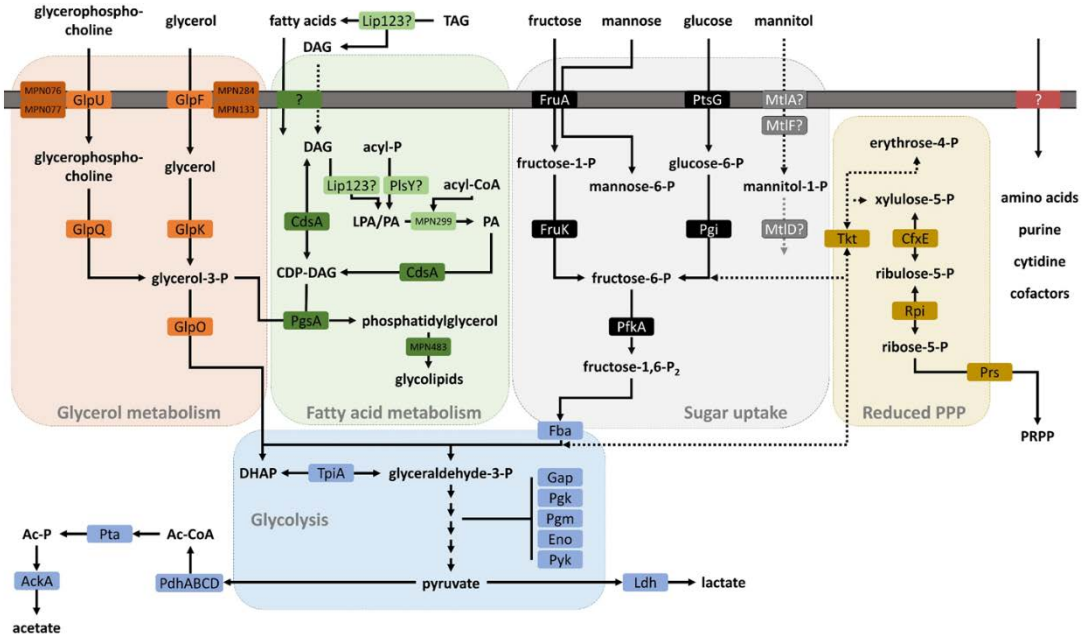

Figure GI. 4. General overview of the metabolism of *M. pneumoniae* and the relation between glycerol and the metabolism of fatty acids. Scheme extracted from Blötz & Stülke, 2017.

As it was demonstrated in a highly virulent strain of the ruminant pathogen *M. mycoides*, the uptake of glycerol is directly related to production of H_2O_2 and virulence, as this particular strain contained an operon coding for an additional glycerol transporter (Vilei & Frey, 2001). The correlation between glycerol metabolism and virulence was also proved in *M. pneumoniae*, as a mutant strain with an impaired glycerol metabolism was unable to produce H_2O_2 and did not cause any detectable damage to host cells (Schmidl et al., 2011).

The virulence of H_2O_2 is connected to its vast reactivity and the oxidative damage that it causes. Reactive Oxidative Species or ROS can harm DNA, proteins and lipids (Cross et al., 1987). Of note, human phagocytes (as neutrophils or macrophages) also use H_2O_2 as a microbiocidal, a mechanism that is called respiratory burst (Thomas, 2017). Thus, the production of ROS is a double-edged sword, as it can damage both the pathogen and the host. This is especially true for most mycoplasmas, as they do not have a gene coding for a catalase to remove H_2O_2.

Lipoproteins and peroxide production are, thus, widespread virulence factors for all mycoplasmas. Remarkably, *M. pneumoniae* also produces a toxin termed as Community Acquired Respiratory Distress Syndrome (CARDS) toxin. This protein has ADP-ribosyltransferase activity and elicits vacuolization and cell death of the host cells

(Kannan & Baseman, 2006). The toxin holds some similarity to the pertussis toxin and its immunodominance has been evidenced. In an animal model, it was observed that the CARDS toxin alone could replicate the inflammation associated with an *M. pneumoniae* infection (Hardy et al., 2009). In addition, a high expression of the toxin along with an also elevated expression of the pro-inflammatory cytokine TNF-α has been associated with more severe prognosis (G. Li et al., 2019).

GI.3 The unique biology of M. genitalium

GI.3.1 A minimal genome

M. genitalium was the second bacteria with its genome completely sequenced (Fraser et al., 1995), only behind *Haemophilus influenzae*. At the time, with 580 kb and only 470 predicted coding regions, the unraveling of its sequence marked the start of the minimal genome race. A few years after, it was speculated that the essential genes of *M. genitalium* would range between 265 and 350 (Clyde A. Hutchison et al., 1999).

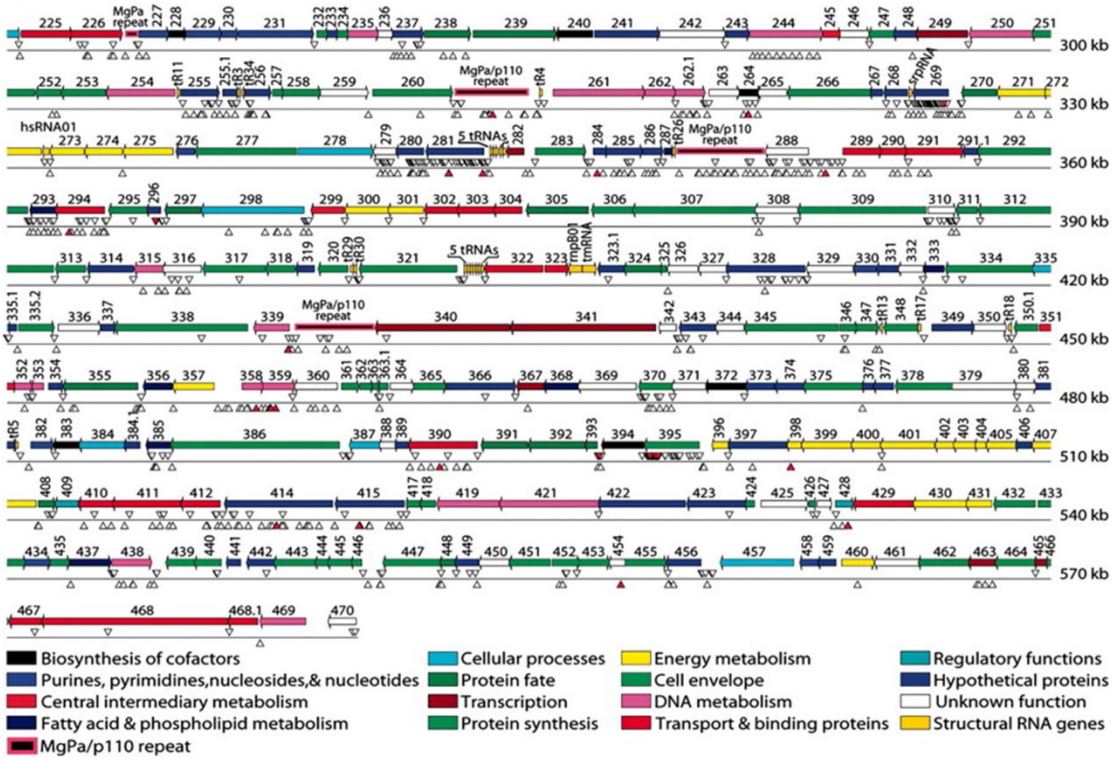

Figure GI. 5. Gene essentiality of *M. genitalium* determined by global transposition mutagenesis. Glass and his coworkers sequenced the transposon insertion site of hundreds of colonies to find out which genes were dispensable. A red triangle represents 10+ insertions. Large genomes zones without insertions can be observed, while it is also evident the existence of hot spots: genome localizations with an elevated number of transposon insertions. Image extracted from Glass et al., 2006 (the original figure was cut and this adaptation does not depict the entire genome, as its main purpose is to illustrate the method).

Since then, essentiality studies have been performed on its chromosome (Glass et al., 2006) and in the closely related species *M. pneumoniae* (Lluch-Senar et al., 2015) to determine the smallest set of genes that can sustain autonomous life. Global transposon mutagenesis found that 382 genes of *M. genitalium* were essential (Figure GI. 5), 28% of them coding for proteins of unknown function. A similar study in *M. pneumoniae* revealed the importance of non-coding regions, as they unveiled that non-coding RNAs

(ncRNAs) were involved in the regulation of the expression of essential ORFs, thus adding another layer of complexity to the minimal genome studies. The relevance of non-coding elements, including intergenic segments of unknown function, in essentiality was also addressed by a report on *Caulobacter crescentus* several years before (Christen et al., 2011).

The *M. genitalium* genome was also the first one to be produced synthetically (Gibson et al., 2008). It was followed by the genome synthesis of the ruminant pathogen *M. mycoides*, a genome comprising 1.19 Mb and 867 predicted protein-coding genes (Gibson et al., 2010). The latter was transplanted into a *M. capricolum* recipient cell and was capable of self-replication. An attempt to unravel the minimal number of genes necessary for autonomous life was performed with *M. mycoides*, and its genome was thoroughly reduced to 531 kb and 438 protein-coding genes (with a striking 31.5% of genes coding for proteins of unknown function) (C. A. Hutchison et al., 2016). Although the expected minimal genome proposed in its 1999 paper was expected to be roughly half of the experimentally determined final size, Hutchinson and his coworkers described in the 2016 report the existence of *quasi-essential* genes, not strictly needed for cell viability but required for robust growth.

In the present days, the race towards the discovery of the minimal set of genes necessary for self-replicating life has apparently come to a halt, as the interest for a minimal genome has shifted to more industry-suitable microorganisms than the slow-growing and highly demanding mycoplasmas (Vickers, 2016).

GI.3.2 Transcriptional regulation in a reduced genome

Characterization of gene regulation in mycoplasmas is still very much a work in progress due to the apparent scarceness of transcriptional regulators, likely as a result of the massive genome reduction undergone by these microorganisms. Moreover, its promoter architecture is different from what was observed in other well-characterized microorganisms as *E. coli*: despite that a robust consensus Pribnow box was seen after analyzing the transcriptional start sites of several genes, there was a weak conservation of the -35 box (Weiner III et al., 2000). This issue was investigated a few years later in *M. pneumoniae*, assessing the impact on transcription of point mutations in both the -10 and -35 boxes. Then, it was evidenced that binding of the RNA polymerase was greatly impaired upon mutation of the Pribnow box, while variations in the -35 element had a minor effect on gene expression (Halbedel, Eilers, et al., 2007). An *in silico* study in *M.*

pneumoniae characterized a consensus Pribnow sequence (TANAAT, where N is any base) from experimentally determined transcription start sites (TSS) and concluded that this element had a great relevance in *M. pneumoniae* gene expression, while they also observed the degeneration of the consensus -35 element in this bacterium and its minor role in transcription (Lloréns-Rico et al., 2015).

In addition to their unusual promoter features, mycoplasmas are thought to be heavily stripped of transcription factors. Although the list of regulators has increased through the years, it still pales in comparison to other reference microorganisms, even when compared to other Mollicutes (Table GI. 4). Some well-known transcription factors as HrcA, MraZ or Fur (involved in core cellular process as heat stress response, cellular division and metal uptake, respectively) have an homolog in mycoplasmas (Fisunov et al., 2016).

Table GI. 4. Lack of transcription factors in mycoplasmas determined by homology. Adapted from Fisunov et al., 2016.

Species	Number of putative transcription factors (% of total proteins)	Total proteins
Escherichia coli	290 (6.0%)	4820
Bacillus subtilis	238 (5.6%)	4243
Acholeplasma laidlawii	52 (3.8%)	1381
Spiroplasma melliferum	23 (2%)	1154
Mycoplasma gallisepticum	10 (1.2%)	835

Recently, there has been an increasing number of studies addressing the existence of gene regulation mechanisms alternative to conventional transcription factors. It has been proposed that some proteins could moonlight and act as regulators of gene expression. Indeed, there are enzymes that have been reported to influence gene regulation in other species, either by directly binding to DNA/RNA or modulating the activity of transcription factors (Commichau & Stülke, 2008). Notably, a few years ago it was reported that the phosphodiesterase GlpQ of *M. pneumoniae* controlled gene expression in response to the availability of glycerol-3-phosphate (Schmidl et al., 2011).

Another factor controlling transcription in mycoplasmas is DNA supercoiling, which strongly influences transcription in other bacteria (Dorman & Dorman, 2016) and might play a fundamental role in regulation upon environmental stress (Martis B. et al., 2019). Its relevance in mycoplasmas has also been assessed (W. Zhang & Baseman, 2011a). Interestingly, the existence of chromosome interacting domains (CID) was evidenced in *M. pneumoniae* and it was observed that the genes in these regions tended to be co-regulated, suggesting that the organization of the chromosome might influence gene expression (Trussart et al., 2017). These regions, as firstly described in *C. crescentus*, consist of stable spatial domains determined through Hi-C data and their organization and self-interaction are impacted by supercoiling (Le et al., 2013).

Moreover, the crucial role of RNA in regulating gene transcription is starting to gain ground in the last years. Riboswitches might represent a widespread strategy in gene regulation in mycoplasma, as there is no need for an intermediary protein: the metabolite controls transcription of the uptake or synthesis genes by direct binding to the RNA, thus acting as a sensor (Serganov & Nudler, 2013). However, only one riboswitch has been found in mycoplasmas to date (S. Mukherjee et al., 2017), although *in silico* studies might not be the best approach for riboswitch determination in these microorganisms due to their unique characteristics. In addition to riboswitches, the impact of non-coding RNAs on transcription is becoming more relevant as they are further studied, although the function of bacterial ncRNAs is still vastly unknown (Harris & Breaker, 2018). As stated above, some ncRNAs were deemed as essential for *M. pneumoniae* growth *in vitro* (Lluch-Senar et al., 2015).

Therefore, there is a plethora of factors that could regulate gene expression in mycoplasmas. Actually, a very recent report tried to obtain a comprehensive map of the gene regulatory network in *M. pneumoniae* and they concluded that transcription factors had a less important role on gene regulation in these microorganism than other alternative mechanisms such as the ones described above (Yus et al., 2019). They found that this was especially relevant when the microorganism was responding to environmental perturbations. These findings are in agreement with the robust transcriptional response to osmotic, oxidative and heat stresses observed in *M. gallisepticum* (Mazin et al., 2014). However, the conservation of transcription factors in the extremely genome-reduced mycoplasmas suggests a crucial and non-redundant role for these regulators. Therefore, the prevailing transcription factors might be essential for *in vivo* viability.

GI.3.2.1 Transcription factors in *M. genitalium*

In the closely related species *M. pneumoniae*, the presence of 9 transcription factors was reported (Figure GI. 6). Except for YlxM, which is involved in the regulation of a small ribosomal operon (Yus et al., 2019), all of them have a homolog in *M. genitalium*.

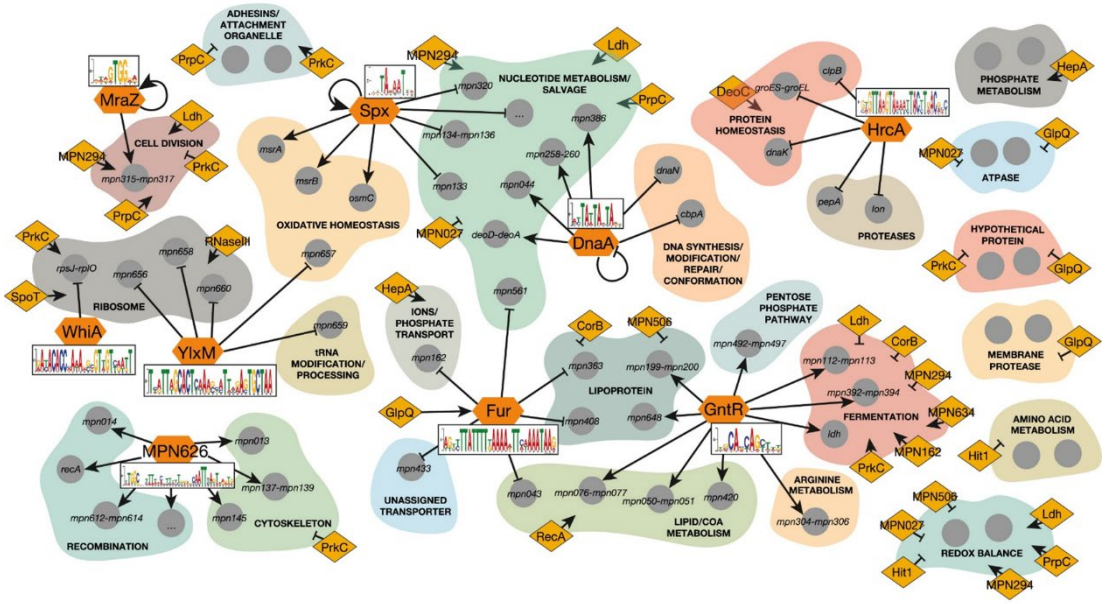

Figure GI. 6. Scheme of the regulatory network associated with transcription factors in *M. pneumoniae*. Transcription factors (orange hexagons) and their influence on cell processes depending on their targets. The proteins inside orange diamonds were also identified as regulators in this study. Image extracted from Yus et al., 2019.

Transcription factor GntR

The *M. genitalium* putative homolog for GntR is coded in the MG_101 locus. All of the transcription factors of this family have a characteristic helix-turn-helix domain in their N-terminal that is directly involved in DNA recognition and binding (Suvorova et al., 2015). The GntR homolog of *M. pneumoniae* regulates the expression of genes associated with metabolic processes as fermentation, arginine metabolism or the pentose phosphate pathway. It is an essential gene as determined both by Glass and Lluch-Senar in *M. genitalium* and *M. pneumoniae*, respectively (Glass et al., 2006; Lluch-Senar et al., 2015).

Transcription factor WhiA

WhiA was first reported to be an essential sporulation factor in *Streptomyces coelicolor*, as it regulated sporulation-specific promoters (Kaiser & Stoddard, 2011). This widely-distributed gene among Gram-positive species was later associated with other functions, such as chromosome segregation and cell division in *B. subtilis* (Bohorquez et

al., 2018; Surdova et al., 2013), envelope formation, and cell division in *Corynebacterium glutamicum* (J. H. Lee et al., 2020).

Remarkably, the WhiA homolog in mycoplasmas seems to be involved in other cell processes, as it was reported that this protein negatively regulates the main ribosomal operon of *M. pneumoniae* (Yus et al., 2019).

Transcription factor Spx

The Spx family of transcription factors has been mainly linked to oxidative and heat shock stress response (Runde et al., 2014). Recently, it has been demonstrated that Spx can inhibit translation at elevated cellular concentrations, and it is able to do it through the inhibition of genes associated with translation, as ribosomal proteins (Schäfer et al., 2018). Spx is coded by an essential gene in both *M. pneumoniae* and *M. genitalium* (Glass et al., 2006; Lluch-Senar et al., 2015), and it has been mainly related to maintenance of oxidative homeostasis in *M. pneumoniae* (Yus et al., 2019).

Transcription factor HrcA

This regulator orchestrates the response to heat stress through the recognition of the CIRCE sequences. In *M. genitalium*, these sequences were found in the promoter regions of three genes: *dnaK*, *clpB* and *lon*, that code for the chaperones DnaK and ClpB and the Lon protease, respectively. These three genes were indeed found upregulated upon heat stress (Musatovova et al., 2006). However, the profound transcriptional changes observed upon heat stress in other mycoplasmas as *M. pneumoniae* (Yus et al., 2019) or *M. gallisepticum* (Mazin et al., 2014) indicates the involvement of other mechanisms in response to heat.

Transcription factor MraZ

MraZ is a widely conserved bacterial protein, as it can be found in almost all characterized species and it is always the first gene of the division and cell wall (dcw) operon (Margolin, 2000). Its function is controversial as it has been described as a transcriptional repressor of the dcw cluster in *E. coli* (Eraso et al., 2014) and as a transcriptional activator in *M. gallisepticum* (Fisunov et al., 2016). It is not essential for growth in *M. genitalium* (Glass et al., 2006), although its overexpression is toxic in *E. coli*.

Transcription factor of the Fur family

The Fur (ferric uptake regulator) family of transcriptional regulators is involved in the acquisition of extracellular metals, such as iron (Fur), nickel (Nur), zinc (Zur) or manganese (Mur). They are transcriptional repressors that use a metal cofactor to bind DNA. Thus, when metal availability is low, Fur regulators lose the capacity to bind DNA and the expression of genes mainly involved in metal uptake and storage is derepressed (Escolar et al., 1999). As Fur-regulated genes are necessary to compete with the host for the available metals, Fur is associated with virulence (Troxell & Hassan, 2013).

In Chapter II of this thesis, we analyze in detail the regulation of metal acquisition in *M. genitalium* and the Fur homologue of this pathogen is thoroughly characterized. The results of our work were published in early 2020 (Martínez-Torró *et al*., 2020).

Alternative sigma factor σ20

The protein product of MG_428 codes for the alternative sigma factor σ20. We found that this regulator controls recombination and antigenic variation (Torres-Puig et al., 2015) and promotes horizontal gene transfer (Torres-Puig et al., 2018). This protein has homology to members of the σ70 family of sigma factors and it is able to interact with the RNA polymerase core enzyme. The deletion of MG_428 or some of the genes in its regulon severely impairs recombination in *M. genitalium*. Two genes in its regulon (*rrlA* and *rrlB*) code for two proteins that participate in a feed-forward loop essential for the function of the regulator. Due to the crucial role of recombination in immune evasion and survivance inside the host, σ20 might have a remarkable role in *M. genitalium* virulence.

Transcription factor DnaA

Besides its commonly known role as a replication-initiator protein, DnaA has also been reported to act as a transcription factor that binds to a consensus sequence deemed as the DnaA box (Messer & Weigel, 1997). It has been evidenced that it can act as a transcriptional repressor or activator. In *B. subtilis*, DnaA controls the expression of a vast number of genes and it is proposed that its regulatory function might change with regards to the growth phase and replication stress (Washington et al., 2017). Its role in mycoplasmas beyond transcription initiation has not been assessed, although it has been observed in *M. genitalium* that putative DnaA boxes are significantly different from the already described in *E. coli* (Hernández-Solans et al., poster presentation at ASM Microbe Congress, 2016). This assessment was later corroborated in *M. pneumoniae*, as

a study concluded that the consensus sequence of DnaA boxes was more relaxed than in *E. coli* (Blötz et al., 2018).

GI.3.3 A limited (but increasing) genetic toolset

The basic tools for functional genomic analyses in M*. genitalium* are mostly limited to random mutagenesis with transposons and targeted mutagenesis by allele exchange. Regarding the latter, targeted gene disruption through homologous recombination with a suicide plasmid was first described in *M. genitalium* twenty years ago (Dhandayuthapani et al., 1999). This is not a common feature among mycoplasmas, as the generation of mutants in this species was strictly associated with the laborious process of random mutagenesis and screening. Notably, in the closely related *M. pneumoniae*, double crossover events are rare and strain-specific (Krishnakumar et al., 2010).

On the other hand, random mutagenesis by transposon delivery has been the main genetic tool available for mycoplasmas. The most widely used transposon in mycoplasma was the Tn4001 isolated from *Staphylococcus aureus* (Lyon et al., 1984), which was later successfully proved in *M. pneumoniae* (Hedreyda et al., 1993) and also in *M. genitalium* (Reddy et al., 1996). This transposon was used for the first global transposon mutagenesis in *M. genitalium* (Clyde A. Hutchison et al., 1999). Its instability once transposed probably due to an inadequate expression of the transposase was later improved with the creation of the MiniTn4001, in which the transposase was placed outside the inverted repeats to diminish unwanted transposition events (Pour-El et al., 2002). The MiniTn4001 transposon was then further optimized for *M. genitalium* (Pich, Burgos, Planell et al., 2006). A new transposon which transformation efficiency is reportedly higher than the MiniTn4001 was recently engineered (Montero-Blay et al., 2019). In this transposon, the regulatory region of the transposase and the selectable marker are changed to improve their transcription in a broad range of Mycoplasma species.

Due to the lack of cell wall, there are few viable options to use as selectable markers. In *M. genitalium*, the three most widely-used antibiotic resistance markers were the tetracycline resistance protein, the aminoglycoside resistance protein and the chloramphenicol acetyltransferase. A few years ago, a new functional marker in *M. genitalium* was described: the puromycin *N*-acetyltransferase (Pac) of *Streptomyces alboniger* (Algire et al., 2009).

In the last ten years, there has been an increasing development and adaptation of genetic tools for use in mycoplasmas. The discovery of functional extrachromosomal DNA elements could represent a breakthrough in mycoplasma studies. Although replicative plasmids were observed in *M. mycoides* (Bergemann et al., 1989), the evidence of these elements in mycoplasmas was scarce. However, studies with constructed oriC plasmids in different mycoplasma species (Lartigue et al., 2003) laid the groundwork for more recent publications reporting the creation of several oriC plasmids for many mycoplasma species: there are now functional replicative plasmids for *M. gallisepticum* (S.-W. Lee et al., 2008), *M. synoviae* (Shahid et al., 2014), *M. bovis* (J. Li et al., 2015), *M. hyopneumoniae* (H. Z.A. Ishag et al., 2016) and *M. hyorhinis* (Hassan Z.A. Ishag et al., 2017), among others. Until recently, though, there were no stable extrachromosomal DNA elements described in *M. genitalium*. Two years ago, it was reported that a replicative plasmid containing the oriC of *M. pneumoniae* could be used in *M. genitalium* (Blötz et al., 2018). Previous experiments in this laboratory with replicable plasmids containing the own oriC sequence of *M. genitalium* revealed high rates of chromosome integration (Torres-Puig *et al.*, unpublished data).

Moreover, the Cre-lox technology was adapted to *M. genitalium* in our laboratory (Mariscal et al., 2016). This could be of great relevance for future studies in *M. genitalium*, as it provides the possibility of unmarked genetic modifications in a bacterium with a limited pool of functional selectable markers, thus allowing consecutive rounds of genome edition. To ensure a tight control of the Cre recombinase, its transcription was under the control of a modified version of the inducible promoter P*xyl*/*tet*O_2, previously described as functional in *M. agalactiae* (Breton et al., 2010).

Finally, the adaptation to mycoplasmas of the promising CRISPRi (CRISPR interference) technology has also been studied in our laboratory. This is a modification of the CRISPR system that uses a Cas9 without endonuclease activity. Therefore, when this modified Cas9 is coexpressed with a guide RNA, it is able to effectively repress the expression of several target genes (Qi et al., 2013). This method has been proved in *M. pneumoniae* and targeted gene regulation was achieved (Mariscal et al., 2018). The generation of knockdowns could be of major interest when studying essential genes encoded in the *M. genitalium* genome.

GI.4 Bacterial Cell Division

Cell division is an essential process in bacteria that has been extensively studied through the years. There are currently models that encompass the whole chronology of cell division in reference bacteria as *B. subtilis* and *E. coli*. These models center around the bacterial divisome, a macromolecular structure responsible for carrying out cytokinesis, in which the FtsZ protein has a predominant role.

FtsZ is a tubulin-like protein which relevance is highlighted by its remarkably widespread conservation (a copy of *ftsZ* can be found in almost all bacterial species, except for chlamydiae and the mycoplasmas *Ureaplasma urealyticum* and *Mycoplasma mobile*) (Margolin, 2000) and the essentiality of the gene in which its encoded (Dai & Lutkenhaus, 1991). This protein polymerizes and depolymerizes through GTP hydrolysis and eventually form a ring-like structure at midcell named as the Z-ring (A. Mukherjee & Lutkenhaus, 1998). The Z-ring serves as the scaffold of the bacterial divisome and it recruits several proteins involved in cell division (Errington et al., 2003).

However, in order to exert the necessary constriction for cytokinesis, FtsZ needs to be tethered to the membrane, as this GTPase cannot attach itself to the membrane. This function is performed by two proteins in *E. coli*: FtsA and ZipA, which are also involved in the recruitment of proteins into the divisome (Pichoff & Lutkenhaus, 2002). While the latter is mainly present in Gammaproteobacteria, FtsA is an actin-like protein widely conserved in prokaryotes, and the gene in which is encoded is usually immediately upstream of *ftsZ* (Margolin, 2000).

FtsA interacts with the conserved C-terminal domain of FtsZ to recruit the GTPase to the membrane (Haney et al., 2001). Then, this actin-like protein can regulate the assembly and curving of FtsZ polymers upon binding of ATP (Figure GI. 7), although no ATPase activity for FtsA has been observed (Loose & Mitchison, 2014). The binding of ATP also plays a role in the ability of FtsA to attach to the membrane (Krupka et al., 2014). Thus, FtsA is crucial to stabilize the formation of FtsZ polymers and to promote the organization of those filaments into the dynamic filament network that will eventually become the Z ring.

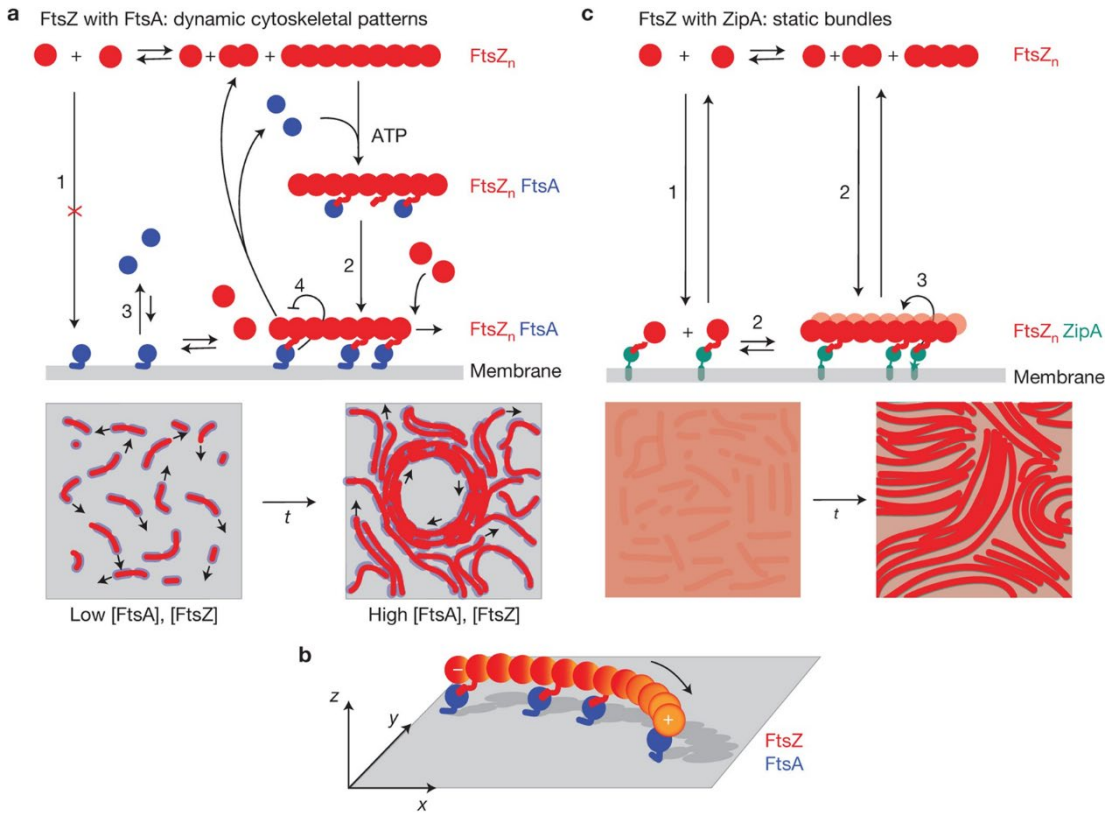

Figure GI. 7. Model for FtsZ-FtsA interaction and tethering to the membrane. FtsA promotes the formation of a dynamic and reorganizing filament network, while ZipA is only able to organize FtsZ into static bundles. **(a)** According to this model, FtsA would interact with cytoplasmatic FtsZ polymers and then the FtsA-FtsZ filament would be recruited to the membrane. Once FtsZ is recruited into the membrane, lateral interactions between filaments can organize into a dynamic filament network. **(b)** Scheme of a curved FtsZ polymer anchored to the membrane by FtsA. **(c)** Recruitment of FtsZ to the membrane through ZipA. This protein is able to tether to the membrane monomeric FtsZ as well as polymers, possibly by its higher affinity for FtsZ with regards to FtsA. Then, FtsZ can initiate polymerization and organize into thick bundles. Image extracted from Loose & Mitchison, 2014.

The assembly of the divisome begins once FtsZ is anchored to the membrane and the Z ring is formed. In well-characterized microorganisms like *E. coli* and *B. subtilis*, this process involves the recruitment of several transmembrane proteins that, together with the Z ring, provide the necessary constriction force to carry out cytokinesis. Lately, the treadmilling dynamics of FtsZ caused by its GTPase activity have also been associated with the location and activity of enzymes responsible for cell wall synthesis, suggesting that bacteria have coupled the cytoskeletal motion to wall synthesis to ensure a correct cell division (Bisson-Filho et al., 2017; Yang et al., 2017).

Due to its predominant role in cell division, FtsZ and the Z ring structure constitute the main targets in the regulation of cytokinesis. There are several proteins involved in

promoting the assembly and stability of the Z ring as well as there are others directly associated with its disassembly and localization. Among the former, besides the aforementioned FtsA and ZipA, there are a few positive regulators described, although its low conservation across bacteria suggest that these organisms have developed different mechanisms to modulate the Z ring assembly and stability (Huang et al., 2013). One of the most studied positive regulators is ZapA, which stabilizing function has been connected to the stimulation of lateral association of FtsZ filaments (Monahan et al., 2009). It has also been reported that ZapB, which is mainly restricted to Gammaproteobacteria, has a role in stimulating Z ring formation (Ebersbach et al., 2008) and its participation in chromosome segregation has also been discussed (Espéli et al., 2012).

As for the negative regulation of FtsZ polymerization and Z ring assembly, there are two major mechanisms described: the Min system and nucleoid occlusion (Figure GI. 8). The main goal of these regulatory systems is the prevention of the Z ring mislocalization, as they ensure that its formation is only viable at midcell, between the two nascent chromosomes. The Min system blocks the Z ring formation at the cell poles by directly inhibiting the polymerization of FtsZ (Edwards & Errington, 1997; Z. Hu & Lutkenhaus, 2003); while nucleoid occlusion prevents division before chromosome segregation (Bernhardt & De Boer, 2005; L. J. Wu & Errington, 2004).

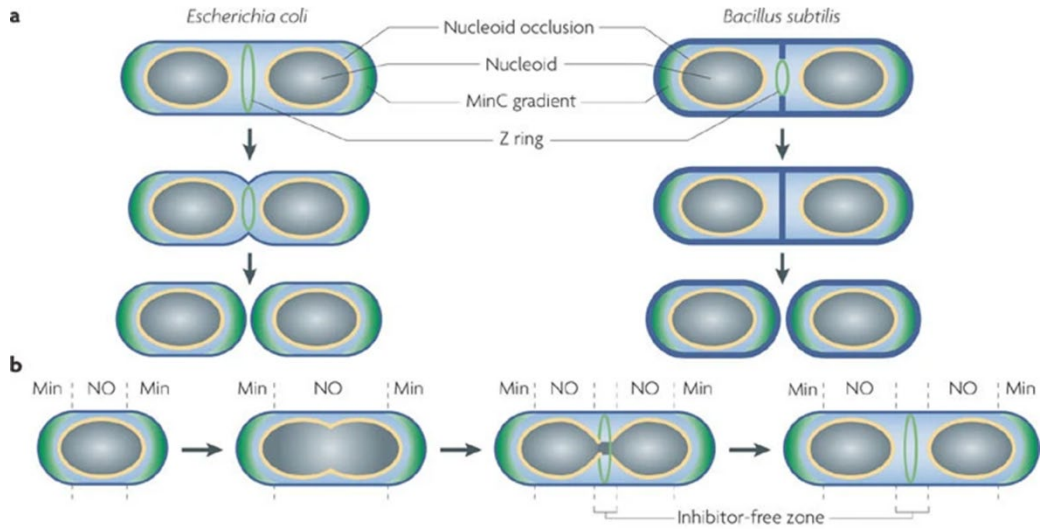

Figure GI. 8. Negative regulation of the Z ring formation in the reference microorganisms *E. coli* and *B. subtilis*. (a) The two different mechanisms by which these microorganisms divide with regards to the peptidoglycan wall. (b) The nucleoid occlusion system (represented as a yellow envelope of the chromosome) and the Min system (its higher concentration at the poles is

highlighted with a green gradient) ensure the correct localization of the Z ring. Image extracted from Adams & Errington, 2009.

Remarkably, despite its extreme conservation and its crucial role in cytokinesis, it was discovered a few years ago that FtsZ was not essential for growth in bacterial variants that lack a cell wall. These variants are called L-forms and were firstly described almost ninety years ago (Klieneberger, 1935), although their characterization is much more recent. It was demonstrated that a few mutations in *B. subtilis* led to a cell-wall-less organism that was able to proliferate without the divisome machinery (Leaver et al., 2009). The membrane composition and fluidity of these mutants was deemed as critical for their proliferation (Mercier et al., 2012). The switch to L-forms has been associated with several stresses, as persistence inside the host, osmotic shock and antibiotic resistance (Kawai et al., 2018; Monahan et al., 2014; Ramijan et al., 2018).

The lack of cell wall could be the reason why the cell-wall-less mycoplasmas *U. urealyticum* and *M. mobile* do not encode FtsZ in their chromosome (Margolin, 2000). In addition, research conducted in our laboratory determined that the *ftsZ* gene of *M. genitalium* was not essential for *in vitro* growth (Lluch-Senar et al., 2010). Therefore, there is an alternative mechanism to carry out cytokinesis in these organisms. However, the conservation of *ftsZ* in almost all mycoplasma species hints to an important function of its gene product in these genome-reduced microorganisms. Thus, *M. genitalium* could provide insightful knowledge about the function and dynamics of FtsZ in the cell-wall deficient mycoplasmas.

GI.5 Metal Acquisition in Bacteria

Transition metals are critical for cell growth and survival, as they have a key role in bacterial metabolism. These elements are used by proteins for structural reasons, as part of catalytic reactions or for electron transfer, among others (Holm et al., 1996). Crucial cell processes as DNA replication and transcription or cellular respiration require metal ion cofactors and it has been reported that almost half of the enzymes with characterized structures require metals (Andreini et al., 2008).

However, in spite of its biological relevance, they also constitute a double-edged sword, as an excess of metal ions is toxic (Hood & Skaar, 2012). Although toxicity can be caused by several mechanisms depending on the metal and some of them are still unknown, there are three widely accepted detrimental consequences of metal excess: the generation of oxidative stress, the mismetallation of proteins originated by a highly concentrated metal binding to low-affinity sites, and the alteration of protein structures by binding to free thiol groups (Schalk & Cunrath, 2016). Therefore, cell viability heavily relays on metal homeostasis.

Microorganisms have developed highly optimized mechanisms to ensure both metal availability and a low concentration of free intracellular metal ions to minimize toxicity. As metal elements cannot be synthetized, bacteria must scavenge them from their surroundings. The response to metal deprivation differs between microorganisms and elements, but it often involves high affinity transport systems and the secretion of chelators to acquire the extracellular metal (Merchant & Helmann, 2012).

Therefore, metal uptake is strongly related to virulence, as both host cells and pathogenic bacteria are competing for a pool of limited and essential resources. In consequence, one of the most basic defenses against pathogens consists of restricting their access to metals, a mechanism called nutritional immunity (Weinberg, 1975). Moreover, due to the damaging effect that a metal excess can cause on microorganisms, macrophages can actively increase their copper uptake to eliminate bacteria from their phagosomal compartments (White et al., 2009).

The struggle between host and microorganisms to acquire metal is well documented, especially for iron uptake. Although the former has several mechanisms to reduce the availability of iron, bacteria have developed systems to combat metal scarcity. The

secretion of iron chelators, known as siderophores, is the most well-known bacterial feature to sequester iron from the host. Siderophores can bind iron with higher affinity than host proteins as lactoferrin and transferrin (Schalk, 2008), and then deliver the metal ion through highly specific transport systems or via shuttle mechanism (Stintzi et al., 2000). Beyond iron, a similar battle for the acquisition of zinc and manganese has also been described (Kehl-Fie & Skaar, 2010).

The use of siderophores as well as other metal acquisition systems is tightly controlled due to the double-edged nature of metal. To ensure that there is no metal uptake when it is not necessary, there are proteins that act as sensors (Giedroc & Arunkumar, 2007). These sensors usually bind to DNA to regulate the expression of genes involved in metal transport and storage.

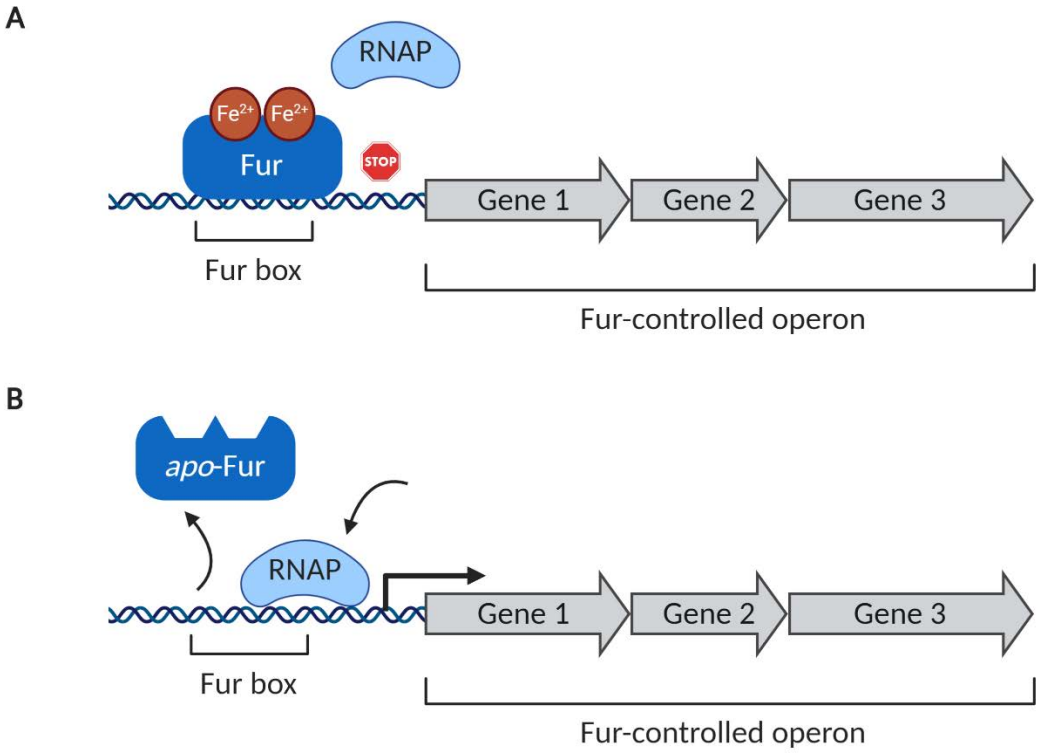

Figure GI. 9. Schematic representation of Fur transcriptional regulation. (A) Fur is bound to its iron cofactors and is able to bind to the Fur box in the promoter region of a Fur-controlled operon. The access of the RNA polymerase (RNAP) is blocked by Fur and the transcription of the downstream genes is repressed. **(B)** Without its cofactors, the non-metallated Fur (*apo*-Fur) cannot bind to the Fur box and the downstream genes are transcribed. This figure was created with BioRender.

The Fur family represents an important group of metal sensors in bacteria. They were first linked to iron acquisition (Ferric uptake regulator), but homologues involved in the regulation of other metals is well-documented (Zur for zinc, Nur for nickel and Mur for

manganese). Fur is a transcriptional repressor that binds to a certain DNA sequence known as Fur box, a sequence that was initially described as a 19-bp inverted repeat in *E. coli* (De Lorenzo et al., 1987). More recent studies showed slight variations of this configuration, as the Fur box could be described as three repeats of the hexameric motif GATAAT (F-F-F arrangement) or two hexamers in the forward orientation and a third one in the reverse orientation (F-F-x-R configuration, where x is a base pair that serves as a spacer) (Lavrrar & McIntosh, 2003). Remarkably, it was evidenced in *B. subtilis* that the three Fur homologues in this bacterium (Fur, Zur and PerR, which is involved in oxidative stress response) were able to distinguish their own operators despite that the regulatory boxes of all three regulators shared significant sequence similarities (Fuangthong & Helmann, 2003).

Fur binds to the Fur boxes as two overlapping dimers (Lavrrar & McIntosh, 2003), blocking the access of RNA polymerase, and thus effectively inhibiting transcription of genes involved in iron uptake and storage. In order to do so, each monomer of Fur needs Fe^{2+} (Escolar et al., 1999). Consequently, transcription of the repressed genes will be resumed when iron is not available. Interestingly, the crystallization of Fur from *E. coli* and *Vibrio anguillarum* revealed the existence of a zinc binding site (Althaus et al., 1999; Zheleznova et al., 2000). Further studies demonstrated that zinc binding was not required for DNA binding, although its presence was deemed as essential for the stabilization of the Fur dimer (D'Autréaux et al., 2007) (Figure GI. 10). The analysis of several Fur and homologues structures uncovered the widespread presence of zinc-binding sites, acting as a structural metal or as a regulator (Fillat, 2014).

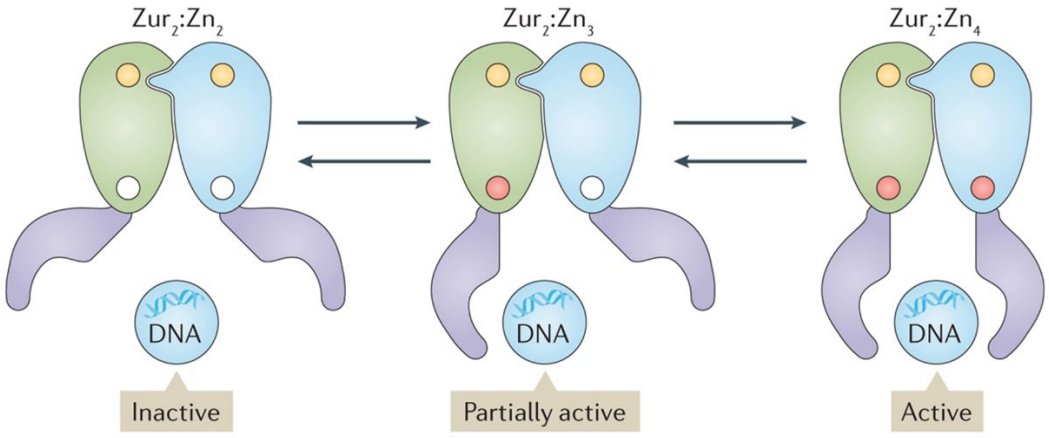

Figure GI. 10. Role of zinc in structure and binding of the Zinc uptake regulator (Zur) in *B. subtilis*. The ability of Zur to repress genes is depending on the metal sufficiency. When the repressor is fully metallated ($Zur_2:Zn_4$, on the right), it dimerizes and it can bind tightly to the DNA, thus

blocking the transcription of the downstream genes. However, if there is not enough free Zn^{2+} available (Zur_2:Zn_2), only the structural sites (represented as yellow circles) responsible for the dimerization will be occupied and the protein would not be able to recognize its regulatory boxes, and the genes in its regulon will be transcribed. This figure was extracted from Chandrangsu et al., 2017.

Some studies have demonstrated a higher complexity of Fur regulation that transcend its role as a classical on/off repressor. It has been reported that Fur can act as a transcriptional activator of virulence-related genes in *Neisseria meningitidis* (Delany et al., 2004). Similarly, Fur regulates the expression of the virulence protein CagA in *Helicobacter pylori* (Pich et al., 2012; Vannini et al., 2014). The link between Fur and virulence has also been established in *Salmonella enterica*, as it was reported that the regulator stimulates the expression of a protein crucial for epithelial invasion (Teixidó et al., 2011). Furthermore, the non-metallated Fur protein (*apo*-Fur) can also regulate gene expression: it can activate transcription of an efflux pump involved in secreting siderophores in *S. aureus* (Deng et al., 2012); and investigations in the closely related *H. pylori* (Carpenter et al., 2013) and *Campylobacter jejuni* (Butcher et al., 2012) evidenced the existence of a whole *apo*-Fur regulon in these human pathogens.

However, there is a shortage of available information regarding metal regulation in mycoplasmas, despite its parasitic nature that confronts them with the host to obtain essential trace elements as metals. Although in some mycoplasma species a Fur putative protein has been annotated based on sequence similarity, there are little to none data addressing the response to metal starvation in these bacteria. There is one published report characterizing the transcriptional response to iron depletion in *M. hyopneumoniae* (Madsen et al., 2006), a swine parasite, although the researchers did not unravel the underlying regulatory network.

The studies on mycoplasmas could have further relevance due to the deficiency of working antibiotics against these pathogens and the abrupt rise of multi-resistant strains. As metal elements are critical for cell metabolism, ascertaining the mechanism by which these microorganisms are able to ensure their acquisition could shed a light in the development of new drugs.

OBJECTIVES

CHAPTER I: REGULATION OF CELL DIVISION AND FTSZ LOCALIZATION DYNAMICS IN A CELL WALL-LESS BACTERIUM

- To determine the transcriptional changes associated with the loss of *mraZ* and *mraW* in *M. genitalium*.
- To characterize null mutants for *mraZ*, *mraW*, *ftsZ* and the whole division and cell wall operon.
- To establish the possible role of MraZ and MraW in cell division.
- To investigate the FtsZ dynamics in *M. genitalium*.

CHAPTER II: RESPONSE TO METAL STARVATION INVOLVES FUR-DEPENDENT AND INDEPENDENT REGULATORY PATHWAYS

- To investigate the transcriptional changes observed in *M. genitalium* under iron-limiting conditions.
- To define the Fur regulon and to determine the DNA binding site for Fur in this pathogen.
- To establish the role of Fur in the physiology of *M. genitalium*.
- To determine the possible function of the Fur-regulated genes.
- To define the metallome of *M. genitalium*.

CHAPTER I

REGULATION OF CELL DIVISION AND FTSZ LOCALIZATION DYNAMICS IN A CELL WALL-LESS BACTERIUM

CI.1 Introduction

Cell division is an essential process in both prokaryotic and eukaryotic cells. Due to its critical nature, it is also a mechanism subject to a tight and extremely complex regulation to ensure the cell viability (Vicente et al., 1998). In the model organism *Escherichia coli*, the **d**ivision and **c**ell **w**all (*dcw*) cluster contains up to sixteen genes that encapsulate the whole division process: from the biosynthesis of the peptidoglycan wall to the cytokinesis (Ayala et al., 1994), in which the tubulin-like FtsZ protein plays a major role.

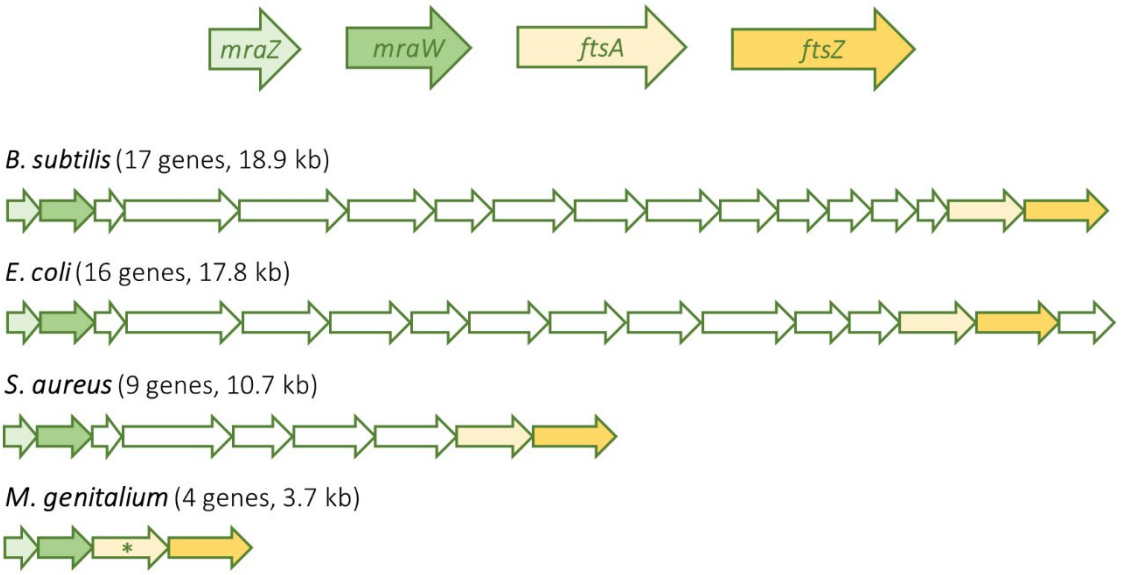

Figure I. 1. Schematic representation of the division and cell wall operon in three representative microorganisms (*Bacillus subtilis*, *Escherichia coli* and *Staphylococcus aureus*) and *Mycoplasma genitalium*. The three genes conserved in M. genitalium (mraZ, *mraW* and *ftsZ*) as well as *ftsA* are highlighted with different colors to show their position in the respective clusters. The third gene of the operon in *M. genitalium* is marked with an asterisk as its gene product is a putative *ftsA* homologue.

Despite their extremely reduced genome and their lack of a cell wall, Mollicutes also encode a shortened version of the *dcw* operon (Figure I. 1) (Y. Zhao et al., 2004). Interestingly, cell division is closely entwined with motility in some of these microorganisms. It was demonstrated that the duplication of the Terminal Organelle (TO) and its migration to the opposite pole precede cytokinesis in *Mycoplasma pneumoniae* (Duncan C. Krause & Balish, 2001). It was also evidenced in this microorganism that there was no variation in DNA content between cells with one TO and cells with a nascent TO near the original, suggesting that the duplication of the TO

might be the first step of cell division in this species (Seto et al., 2001). In addition, another study suggested that gliding motility ceased upon the creation of a new organelle and it was only resumed once the new TO moved to the opposite pole (Hasselbring et al., 2006), thus suggesting a remarkable coordination between motility and division.

The strict relation between gliding motility and cytokinesis is quite probably preserved in the closely related *M. genitalium* (Figure I. 2). However, the viability of nonmotile cells suggests that motility is not essential for cell division (Pich et al., 2006). This is in agreement with the existence of nonadherent (and, thus, gliding-deficient) phase variants. Therefore, there is a mechanism in place in *M. genitalium* that ensures viability if the cell loses its ability to adhere and glide through the host cells.

Figure I. 2. Terminal Organelle (TO) duplication and cell division in *M. genitalium*. From left to right: a single cell (1) with a chromosome (highlighted in blue) duplicates its TO before DNA replication (2). The chromosome replication begins once the TO has ended its migration to the opposite pole (3) and then gliding motility is partially resumed to carry out cytokinesis (4) and eventually produce two daughter cells (5).

This mechanism might be encoded in its reduced version of the *dcw* cluster, which it only contains four genes in *M. genitalium*: *mraZ*, *mraW*, a gene that codes for a hypothetical protein and *ftsZ*. Little is known about the exact function of MraZ and MraW, in spite of the vast conservation of the two genes in which they are encoded, even in their position inside the operon, as the two genes are always placed at the beginning of the cluster (Vicente et al., 1998). However, their presence even in the cell-wall-less Mollicutes indicates a global role beyond cell wall synthesis.

The first gene of the operon is *mraZ*, which codes for a transcriptional regulator (see GI.3.2.1 Transcription factors in *M. genitalium*). A few years ago, it was unveiled that MraZ acts as a transcriptional repressor of the *dcw* operon in *E. coli* (Eraso et al., 2014). Eraso and his collaborators evidenced that MraZ could negatively regulate its own expression as well as the transcription of the first 11 genes of the cluster. In addition, they determined through Electronic Mobility Shift Assays (EMSA) that MraZ binds to

direct repeats contained in its immediate upstream region. Interestingly, the deletion of this highly conserved gene did not result in any discernible phenotype, although its overexpression was proven as lethal, as cells became filamentous.

The effect of increased levels of MraZ in cell filamentation were corroborated in two posterior studies performed in *Corynebacterium glutamicum* (Maeda et al., 2016) and *Mycoplasma gallisepticum* (Fisunov et al., 2016). In the former, it was also confirmed that MraZ negatively regulates the transcription of the *dcw* operon. However, Fisunov and his collaborators reported an opposite phenotype, as they described a transcriptional activation of the cluster upon *mraZ* overexpression. Thus, MraZ has been described as both a transcriptional repressor and activator of the division and cell wall operon.

Regarding the gene product of *mraW*, the second gene of the *dcw* operon in *M. genitalium*, it has been published that MraW is an RNA methyltransferase that targets the 16S rRNA (Kimura & Suzuki, 2010). Although its function has not been determined yet, there are several studies that address the effects of its deletion. Kimura and Suzuki reported that the *mraW* mutant had an altered non-AUG initiation and translation fidelity, thus suggesting that MraW could be potentially playing a role in start codon selection. The defective mutant of *mraW* in *S. aureus* also exhibited an anomalous translation fidelity, a slight increase in doubling time and a higher sensitivity to oxidative stress (Kyuma et al., 2015). It was found that the tolerance to aminoglycosides in *E. coli* decreased in the *mraW* mutant (Zou et al., 2018). And a very recent study in enterohaemorrhagic *E. coli* linked the deletion of *mraW* to a reduced motility and a decreased DNA methylation in an wide range of promoters and genes (Xu et al., 2019).

MraZ and MraW are strictly related. Eraso described that the toxic effects caused by the overexpression of *mraZ* could be overcome by co-overexpressing *mraW* (Eraso et al., 2014). In addition, the *mraZ* gene is always accompanied by *mraW* at the beginning of the *dcw* operon. Remarkably, no chromosomes with orphan *mraZ* genes have been documented. However, a small representation of bacteria conserve *mraW* despite the lack of *mraZ*, suggesting the existence of an MraZ-independent activity for MraW.

The third gene of the operon (MG_223) codes for a hypothetical protein of unknown function. However, in the mollicute *Spiroplasma kunkelii*, which has also a dcw operon with four genes, the third gene was characterized as *ftsA* (Y. Zhao et al., 2004). Curiously,

Zhao and collaborators compared the sequence identity of these four genes between several Mollicutes and found that, although the sequences of MraZ, MraW and FtsZ were fairly similar, the product of the third gene of the operon had little sequence homology among species. This would suggest that the product encoded by the third gene of the operon has diverged in Mollicutes, perhaps as an adaptation to the particularities of each membrane.

The *ftsZ* gene is almost universally conserved in bacteria and so is its position as one of the last genes of the *dcw* operon (Margolin, 2000). It is essential in *E. coli* (Dai & Lutkenhaus, 1991) and *B. subtilis* (Beall & Lutkenhaus, 1991), among others. It codes for FtsZ, a GTPase that is the ancestral homologue of tubulin (Margolin et al., 1996). This protein is able to assemble in a polymer-dynamic ring-like structure named the Z ring (Sun & Margolin, 1998). The assembly serves as a scaffold for other division-related proteins that are recruited into the structure to effect cell division (Errington et al., 2003).

Notably, in spite of its high conservation among bacteria and its critical function in cell division, it was evidenced that *ftsZ* is not essential in *M. genitalium* for *in vitro* growth (Lluch-Senar et al., 2010). Other Mollicutes as *Ureaplasma urealyticum* and *Mycoplasma mobile* do not even encode a copy of *ftsZ* in their chromosome (Margolin, 2000). Interestingly, it has been reported lately that FtsZ is non-essential in some Gram-positive and Gram-negative bacteria that have the ability to switch to a wall-free state, also known as L-forms (Mercier et al., 2014). Although this could justify the dispensability of *ftsZ* in the wall-less *M. genitalium*, its conservation in such a reduced genome remains intriguing.

All in all, the reduced genome and dcw cluster of *M. genitalium*, as well as the existence of an FtsZ-independent cytokinesis mechanism, offer a privileged context to study the function of MraZ and MraW in cell division. In addition, the conservation of FtsZ albeit the motility-driven cytokinesis described in this bacterium constitutes an intriguing challenge. In this chapter, we provide fundamental inputs regarding the role of MraZ, MraW and FtsZ in *M. genitalium*.

CI.2 Results

CI.2.1 Identification of putative regulation boxes in the *mraZ* promoter region

Two independent studies (Eraso et al., 2014; G. Y. Fisunov et al., 2016) revealed that MraZ was able to bind to unique sequences within its own promoter. Although the two studies were undertaken in two phylogenetically distant microorganisms (*E. coli* and *M. gallisepticum*), the described regulatory region was highly conserved in both cases. This prompted us to conduct an *in silico* study to identify putative MraZ binding sites within the *mraZ* promoter region of several phylogenetically diverse microorganisms.

To this end, up to 250 bp of the immediate upstream sequence of *mraZ* were aligned. The alignment revealed an exquisitely well-conserved sequence that consisted of three GTG(G/T) boxes separated by six nucleotides (Figure I. 3A). Thus, the putative *mraZ* binding site sequence consensus could be defined as GTG(G/T)-N_6-GTG(G/T)-N_6-GTG(G/T). In addition, adenine was the predominant nucleotide in the spacer regions between the boxes (Figure I. 3B), and it was especially abundant in the three nucleotides closest to each box. The nucleotide pattern before each box was remarkably similar, so the composition of the spacer regions might be important for regulation. Remarkably, a fourth box was observed in *M. genitalium*, *Neisseria gonorrhoeae, Mycobacterium tuberculosis* and *Burkholderia pseudomallei*.

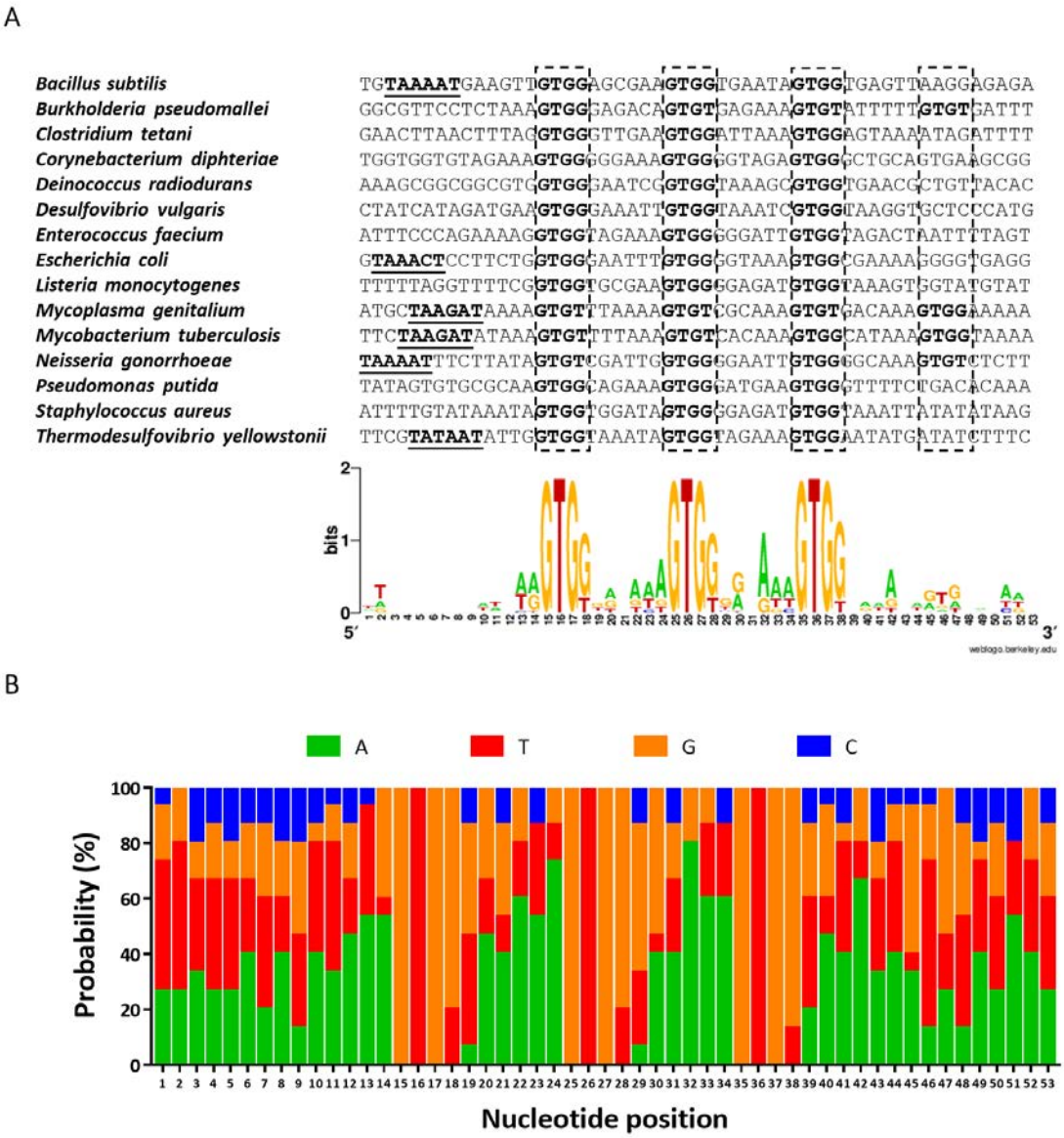

Figure I. 3. Characterization of the upstream region of *mraZ* in representative and phylogenetically diverse microorganisms. (A) Consensus putative regulatory boxes achieved through the bioinformatic analysis of the upstream region of *mraZ* of several reference bacteria. In bold, the three GTG(G/T) boxes, with 6 nucleotides between them. A fourth GTG(G/T) box was highlighted when present if the distance with the previous one was 6 nucleotides. In bold and underlined, reported or predicted Pribnow boxes. At the bottom, the sequence pattern generated with Weblogo (Crooks et al., 2004) from the corresponding alignment. (B) Probability of finding each nucleotide in the promoter region of *mraZ*. The upstream region of the bacteria listed before was examined to detect a nucleotide pattern before a putative mraZ box. Each tick on the x axis represents a nucleotide. The three consensus GTG(G/T) boxes are located in positions 15-18, 25-28 and 35-38, whereas the occasional fourth is in the 45-48 range.

CI.2.1.1 Study of the *mraZ* upstream region and dcw operon structure

We also performed a more throughout analysis of the *mraZ* untranslated region (UTR) in order to identified other conserved features such as the length and distance between the boxes and the start codon in phylogenetically diverse microorganisms (Table I. 1). Although the UTR length was over a hundred nucleotides long in all cases except for *Thermodesulfovibrio yellowstonii*, there were marked differences in the length of this region among all the studied species. As for the distance between the boxes and the start codon, it ranged from 213 in *Corynebacterium diphtheriae* to 3 nucleotides in *T. yellowstonii*, being between 20-60 the most common distance observed.

Table I. 1. Analysis of the *mraZ* upstream region of selected bacteria. The length of the untranslated region (UTR), the nucleotides between the third box and the reported start codon, the number of genes of the operon and the presence of *ftsZ* were examined in each of the previously studied species. GP stands for Gram-positive and GN for Gram-negative.

Microorganism (Gram stain)	UTR length (bp)	Nucleotides from last box to start codon (bp)	Operon length (*mraZ* to *ftsZ*)	*ftsZ* in the operon
Bacillus subtilis (GP)	125	32	17	Yes
Burkholderia pseudomallei (GN)	388	85	15	Yes
Clostridium tetani (GP)	239	27	13	No
Corynebacterium diphtheriae (GP)	809	213	13	Yes
Deinococcus radiodurans (GP)	278	145	4	No
Desulfovibrio vulgaris (GN)	153	12	15	Yes
Enterococcus faecium (GP)	169	39	10	Yes
Escherichia coli (GN)	601	20	15	Yes
Listeria monocytogenes (GP)	202	33	11	Yes
Mycoplasma genitalium	309	15	4	Yes
Mycobacterium tuberculosis	1706	42	17	Yes
Neisseria gonorrhoeae (GN)	278	52	17	Yes
Pseudomonas putida (GN)	294	35	15	Yes
Staphylococcus aureus (GP)	143	30	9	Yes
Thermodesulfovibrio yellowstonii (GN)	70	3	17	Yes

Next, the number of genes in the operon and the presence of the *ftsZ* gene were also investigated. We found that the average number of genes in the dcw operon was 13 ± 4. That number went up to 14 ± 3 when *M. genitalium* (4) and *D. radiodurans* (4) were

excluded of the analysis. The *ftsZ* gene was found in the same operon or chromosomal region as *mraZ* in almost all cases. Only in *Deinococcus radiodurans* and in *Clostridium tetani* (in which the two genes are separated by more than 500 kb) *ftsZ* was placed outside of the *mraZ* operon. The gene coding for FtsZ was usually the last of the operon and it was always preceded by *ftsA*.

CI.2.1.2 Analysis of the *mraW* promoter in *mraZ*-less genomes

As previously stated, despite the *mraZ* gene is always accompanied by a copy of *mraW*, some bacteria possess an orphan *mraW* gene. It is the case of *Vibrio cholerae*, *Streptococcus pyogenes*, *Helicobacter pylori* or *Chlamydia pneumoniae*, among others. In these bacteria, *mraW* is the first locus of the *mraW* gene cluster. Notably, large untranslated regions (UTR) were also found upstream of *mraW*. In this case, though, the alignment of the UTR sequences did not yield any consensus sequence or DNA motif.

Table I. 2. Promoter region of *mraW* and its operon organization in species with *mraW* and without *mraZ*. A large UTR upstream of *mraW* is present in all analyzed genomes. The number of genes in the operon and the presence of *ftsZ* were also examined. Genomes that lack the gene coding for tubulin-like cell-division protein *FtsZ* are marked with one asterisk; bacteria with two chromosomes are marked with two asterisks.

Microorganism (Gram stain)	Class	UTR length (bp)	Operon length (genes)	*ftsZ* in the operon
Acholeplasma laidlawii	Mollicutes	70	1	No
Arcobacter butzleri (GN)	Epsilonproteobacteria	59	2	No
Brucella melitensis (GN)**	Alphaproteobacteria	473	15	Yes
Campylobacter jejuni (GN)	Epsilonproteobacteria	158	2	No
Chlamydia pneumoniae (GN)*	Chlamydiales	243	3	No
Chlamydia trachomatis (GN)*	Chlamydiales	277	3	No
Helicobacter pylori (GN)	Epsilonproteobacteria	178	2	No
Mycoplasma penetrans	Mollicutes	227	2	No
Nautilia profundicola (GN)	Epsilonproteobacteria	56	2	No
Streptococcus mutans (GP)	Bacilli	86	4	No
Streptococcus pneumoniae (GP)	Bacilli	165	4	No
Streptococcus pyogenes (GP)	Bacilli	473	4	No
Vibrio cholerae (GN)**	Gammaproteobacteria	757	13	Yes

The absence of *mraZ* is particularly frequent in Epsilonproteobacteria (Table I. 2). It was also absent in all the studied streptococci. The chlamydiales class was also an interesting study case due to the reported absence of *ftsZ* in these microorganisms. Overall, the *mraZ*-less operons were significantly shorter and did not contain an FtsZ coding gene, except for two noteworthy exceptions: *Vibrio cholerae* and *Brucella melitensis*. In these two microorganisms, the number of genes and the operon structure was very similar to that observed when *mraZ* is present. Intriguingly, these microorganisms also share an uncommon feature among bacteria, as both have two chromosomes. Excluding these two, the average number of genes of a *mraW* operon was 3 ± 1 genes, which is markedly different from the average number of genes observed in the *mraZ* operon (13 ± 4 genes).

CI.2.1.3 Dcw cluster in Mollicutes

The most observed structure of the division operon in Mollicutes was the one that consisted of four genes: *mraZ* as the first gene, followed by *mraW*, a 1000-1200 nucleotides-long gene coding for a hypothetical protein and *ftsZ* as the last gene, as previously reported (Y. Zhao et al., 2004). This was the case of *M. genitalium*, *M. pneumoniae*, *M. agalactiae*, *M. hominis* and *M. gallisepticum*, among others.

However, there were slight variations of this genetic arrangement in other Mollicutes. *Ureaplasma urealyticum* and *Mycoplasma mobile* contained a three-gene operon with *mraZ*, *mraW* and a gene coding for a hypothetical protein. This was a unique case due to the lack of *ftsZ* in their genome despite having a copy of *mraZ*. There were also found two Mollicutes (listed in Table I. 2) in which *mraZ* was not present: *Acholeplasma laidlawii* and *Mycoplasma penetrans*. These are two curious arrangements: *mraW* in *Acholeplasma laidlawii* was apparently not a part of any operon, as it had not any gene directly downstream; as for *M. penetrans*, *mraW* was the first gene of a two-gene cluster and it was followed by a 1200 bp gene coding for a hypothetical protein. In both cases *ftsZ* was found at a very distant position on the chromosome. *Mycoplasma hyorhinis* also had a three-gene operon, although on this occasion it lacked a gene coding for a hypothetical protein and its cluster was formed by *mraZ*, *mraW* and *ftsZ*. Lastly, the cattle pathogen *Mycoplasma mycoides* also exhibited a unique division operon setup, as it held a five-gene operon consisting of *mraZ*, *mraW*, a small ORF, a 1200 nucleotides-long gene coding for a hypothetical protein and *ftsZ*.

CI.2.2 Construction of the *mraZ* and *mraW* mutants

To create the *mraZ* and *mraW* mutants, we first obtained an intermediate strain named *mraZWCm*. In this strain, the *mraZ* and *mraW* genes were deleted from the chromosome and replaced by a chloramphenicol resistance marker under the control of the MG_438 promoter (Figure I. 4).

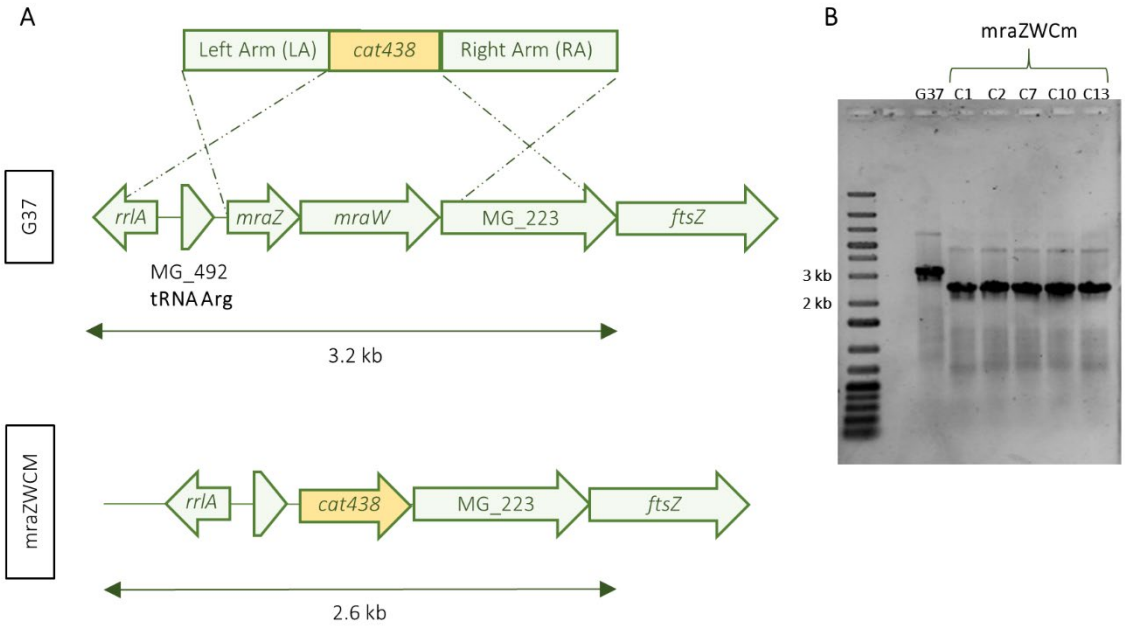

Figure I. 4. Construction of the intermediate strain *mraZWCm*. **(A)** Both *mraZ* and *mraW* genes were deleted by homologous recombination and replaced by a chloramphenicol resistance marker. **(B)** Screening of the *mraZ* and *mraW* deletion by PCR. C10 was selected as the master strain.

Then, three different constructions were introduced into the *mraZWCm* strain to create the *mraZ* and *mraW* mutants, and a reference strain (*mraREF*) carrying both *mraZ* and *mraW* along with the new selectable marker used; this reference strain was created for control purposes (Figure I. 5). In all cases, the first one hundred bases immediately upstream of the start codon of *mraZ* were preserved, as it contained the putative regulatory region. Therefore, the antibiotic marker used for selection was placed before the conserved upstream region of the *mraZ* promoter. Moreover, the selectable marker was introduced in the antisense orientation with respect to *mraZ*, thus minimizing the potential polar effects on the dcw operon. Additionally, a transcriptional terminator was introduced at the 3' end of the tetracycline resistance marker to control polar effects on the *mraZ* upstream genes. The three different constructions were transformed into the *mraZWCm* mutant to obtain the reference strain *mraREF* and the *mraZ* and *mraW* mutants.

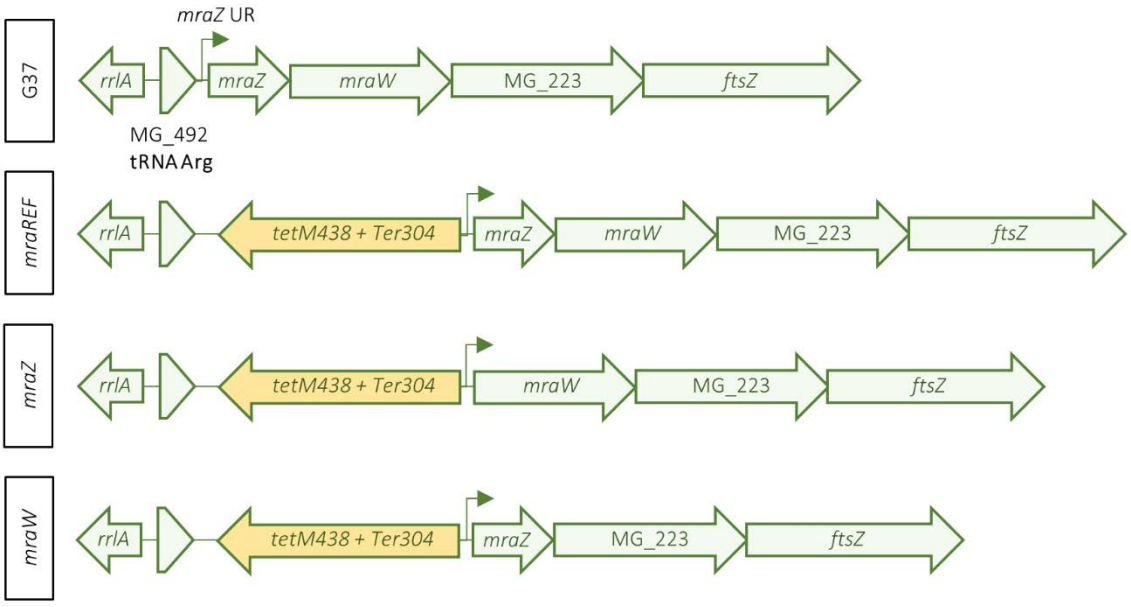

Figure I. 5. Schematic representation of the dcw operon and its immediate surroundings in the different mutant strains. The putative regulatory region (stated as *mraZ* UR) is located upstream of the *mraZ* ORF (~100 bp) is conserved in all cases.

CI.2.3 Effect of *mraZ* on the operon transcription

MraZ has been described as a transcriptional regulator of the division and cell wall operon. Therefore, we investigated the existence of transcriptional changes in the dcw operon in the *mraZ* mutant by qRT-PCR. First, we demonstrated that the cell division genes were transcribed at WT levels in the *mraREF* strain and then used this strain for further comparison (Figure I. 6A). Indeed, as it was reported in *E. coli*, deletion of *mraZ* induced a strong activation (log2 fold change of 4) of the three remaining genes of the dcw cluster (Figure I. 6B). In contrast, deletion of *mraW* had no significant effect on transcription of *mraZ* and *ftsZ*, although there was a slight upregulation of MG_223 (Figure I. 6B). These results were in agreement with the previously reported study in *E. coli*.

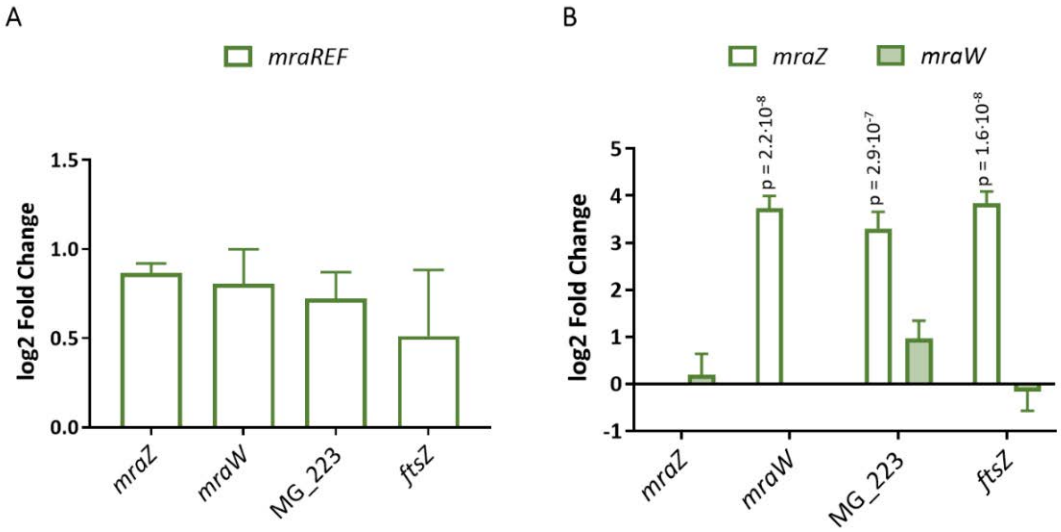

Figure I. 6. Transcriptional activation of the division operon upon deletion of *mraZ* analyzed by qRT-PCR. (A) Transcription levels of the operon in the mraREF strain when compared to the wild-type strain. Bars represent the mean of three independent biological replicates. **(B)** Alteration of the division and cell wall cluster of *M. genitalium* after depletion of *mraZ* or *mraW*. The depicted data is the average log2 fold change when compared to the reference strain of at least four independent biological repeats. Statistically significance was assessed using the Student's T Test and the p-value of biologically significant values (log2 ± 1) is stated above the corresponding bar if significant (p-value < 0.05).

Next, we conducted a genome-wide transcriptional study by RNA-Seq to assess if MraZ controlled transcription of additional genes. The RNA-Seq analysis confirmed that loss of MraZ induced a robust activation of the dcw cluster (Table I. 3). However, no other genes were activated in the *mraZ* mutant. On the other hand, the deletion of *mraW* had no effect neither on the operon transcription nor on the transcription of other genes.

Table I. 3. Global transcriptional changes of *mraZ* and *mraW* mutants determined by RNA-Seq. Only genes which transcription was statistically (p-value < 0.05) and biologically (above or below the log2 ± 1 arbitrary cutoff) significant for any of the two strains are included. Data was obtained from the analysis of three independent biological repeats of each mutant. Relevant fold changes and p-values with respect to the reference strain are highlighted in bold.

Gene	*mraZ*		*mraW*	
	Log2 Fold change	p-value	Log2 Fold change	p-value
mraZ	**-4.64**	**0**	0.10	0.24
mraW	**3.02**	**0**	**-3.84**	**0**
MG_223	**2.08**	**$2 \cdot 10^{-139}$**	-0.21	**0.02**
ftsZ	**2.34**	**$9.3 \cdot 10^{-218}$**	-0.21	**0.03**

CI.2.4 Proteomics of the *mraZ* strain

Next, we wanted to check if the transcriptional changes observed in the *mraZ* mutant were also associated with changes in protein abundance. To this end, we conducted a SILAC test for the *mraZ*, *mraW* and wild-type strains (Kani, 2017). This technique allows the determination of protein abundance among samples by growing each strain in two different conditions: one culture is grown in standard conditions (light medium) and the other strain is grown with an amino acid labeled with a heavy isotope as heavy lysine (marked with ^{13}C) (heavy medium). Then, the labeled amino acid is incorporated to the proteome of the strain growing in heavy medium. Thus, the two samples can be analyzed together by mass spectrometry, as the proteins that belong to the labeled strain are heavier than the non-labeled ones.

As expected, there was a considerable increase in MraW and FtsZ levels in the *mraZ* mutant: peptides that belong to these proteins were 14-fold and 25-fold more abundant than in the G37 strain, respectively (Figure I. 7, Supplementary Table I. 5 , Supplementary Table I. 6). In addition, MG223 could only be detected in the absence of the transcriptional regulator, suggesting that this protein was overexpressed in this background when compared to the G37 and *mraW* mutant strains. Therefore, the overexpression at the mRNA level of the operon correlated with a notable increase in the concentration of the corresponding proteins. Conversely, deletion of *mraW* did not have a significant effect on the concentration of MraZ or FtsZ, although the latter was almost 2-fold more abundant in the *mraW* mutant than in the wild-type strain (Figure I. 7, Supplementary Table I. 7, Supplementary Table I. 8). Thus, *mraW* inactivation did not impact transcription nor translation of the division operon.

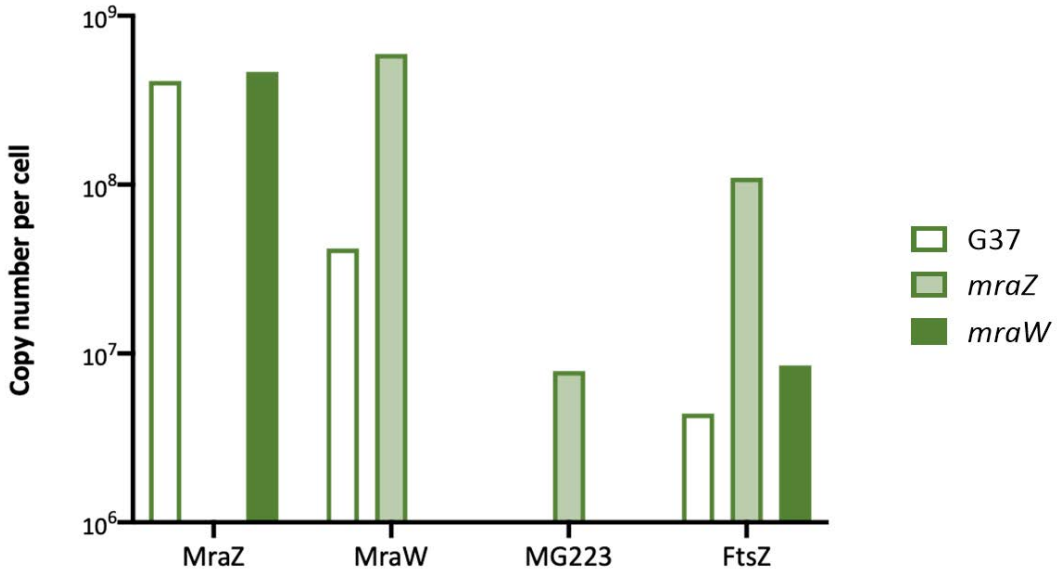

Figure I. 7. Copy number per cell of the dcw operon proteins in the mutant strains. The data is the average of two independent measures for each strain. The absence of a bar does not strictly indicate the absence of the protein, as it could be present but under the detection threshold.

CI.2.5 Impact on cell growth of depleting *mraZ*

We observed that cultures of the *mraZ* mutant always required more time to grow than cultures from the WT strain or the *mraREF* mutant. Therefore, to determine the existence of a growth delay of the *mraZ* mutant cells, the duplication times of the *mraZ* mutant and other relevant strains were measured. For this purpose, we adapted a colorimetric assay previously reported by Karr and colleagues (Karr et al., 2012). This method is exhaustively described in Materials and Methods (M.7 Growth Analysis). The calculated duplication time for the strain without *mraZ* was 11.54 ± 0.38 h, while the wild-type and the *mraREF* were clocked at 8.38 ± 0.28 h and 8.81 ± 0.29 h, respectively (Figure I. 8). These results were consistent with the four days of culture that were necessary for the *mraZ* mutant to grow compared to the standard three days of culture of the wild-type strain. Interestingly, the *mraW* mutant also exhibited a slight delay in growth when compared to those strains, as its calculated duplication time was 9.96 ± 0.53 h.

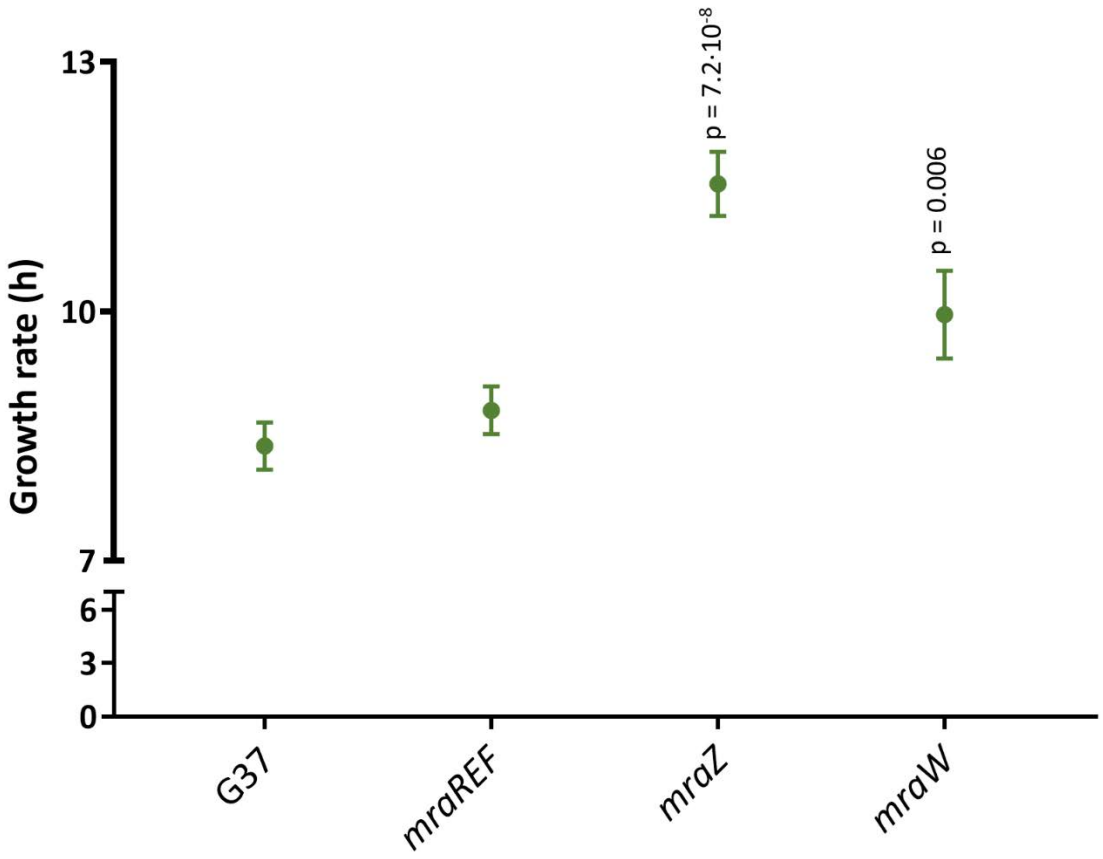

Figure I. 8. Absence of *mraZ* or *mraW* impairs the growth of *M. genitalium*. The duplication time data was collected after several independent biological repeats. Statistical significance was assessed using a paired T-test and statistically significant values (p-value < 0.05) are stated above the upper standard error bar of each strain.

Then, we wondered whether the slow growth associated with the loss of *mraZ* could be due to defects in cell division. Thus, we analyzed this mutant by Scanning Electron Microscopy (SEM). At first glance, the *mraZ*-depleted cells showed a marked phenotype. Cells in this mutant appeared more elongated than the observed in the wild-type strain and there was a substantial number of cells in division (Figure I. 9A and B). Interestingly, in certain cases, we observed an early duplication of the terminal organelle before the cell had completed cytokinesis (Figure I. 9C). The aberrant enlarged morphology and the higher number of cells in division seemed to be associated with an impaired cytokinesis mechanism, as cells apparently struggled to separate from each other (Figure I. 9D). Therefore, activation of the cell division operon as a result of MraZ depletion leads to cell division defects associated with an impaired cytokinesis.

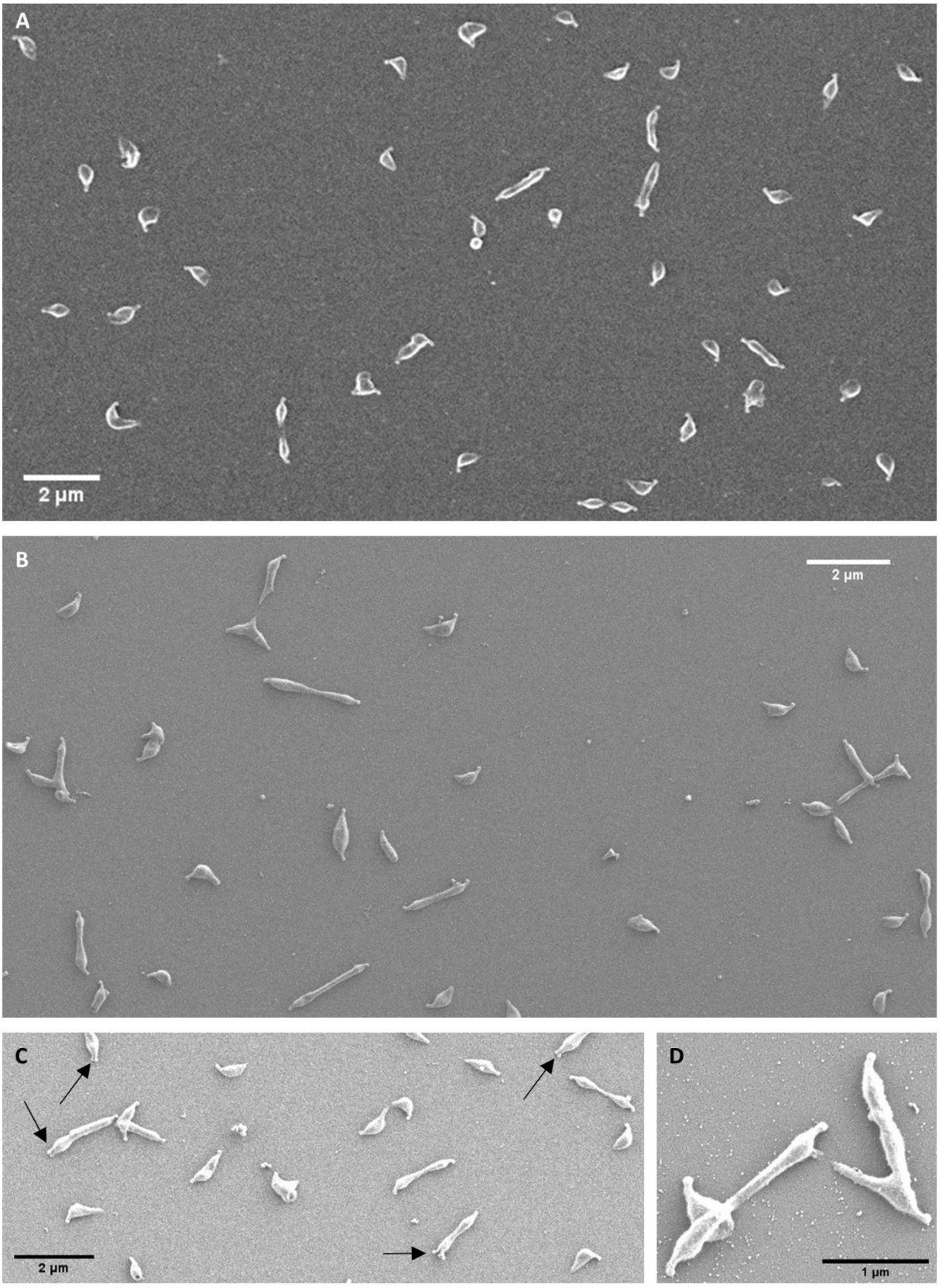

Figure I. 9. The *mraZ* strain exhibits division deficiencies. (A) A SEM micrograph of the wild-type strain, exhibiting the characteristic flask-shape form of *M. genitalium*. **(B)** An overall view of the *mraZ* strain by SEM. The low number of single cells and the considerable length of the dividing

cells hints to a possible defect in cell division. **(C)** Premature terminal organelle duplication is pointed with arrows. Cells still attached to another cell begin too early another process of cell replication. **(D)** Enlarged view of the *mraZ* mutant cells illustrates the aberrant cellular morphology of this strain.

On the other hand, the impact of the loss of *mraW* on cell morphology was less apparent. The cells from the *mraW* mutant were undistinguishable from those of the WT strain (Figure I. 10A). Occasionally, some elongated cells characteristic of the *mraZ* mutant could be spotted in this strain (Figure I. 10B and C).

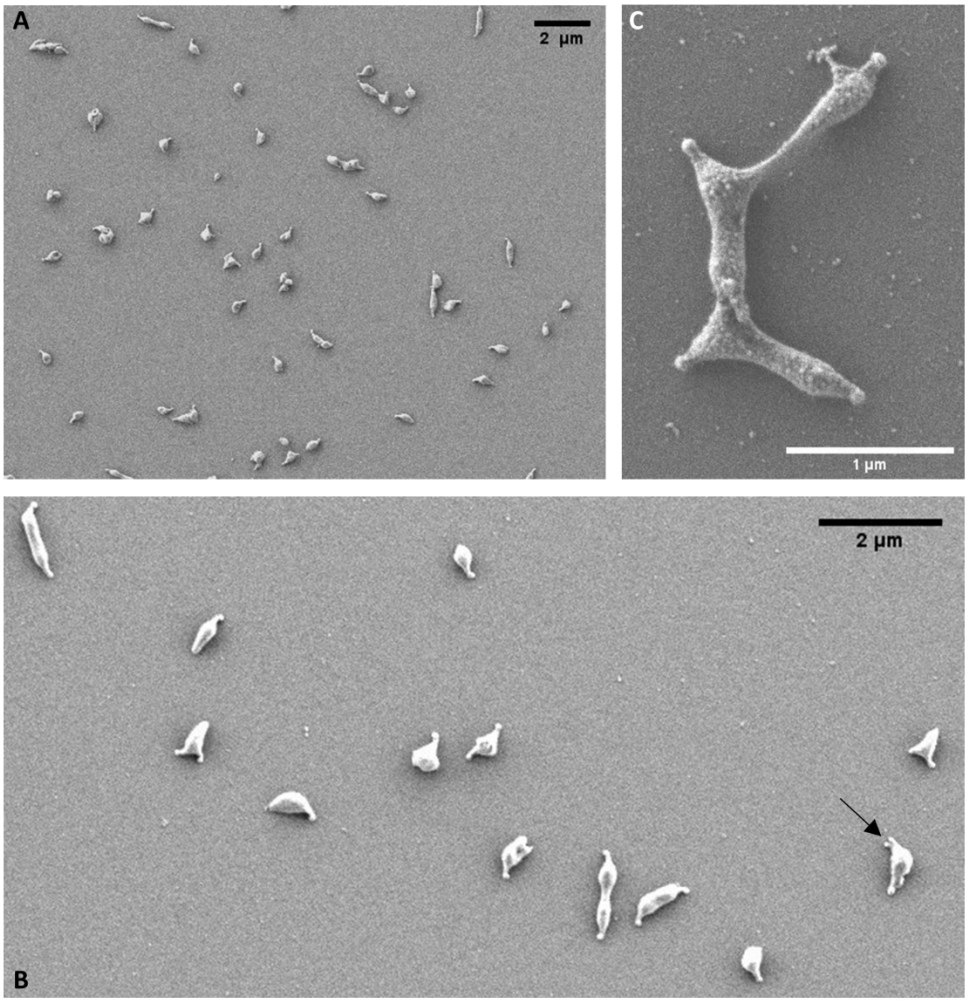

Figure I. 10. The loss of *mraW* has not the same impact on cell morphology and division as the absence of *mraZ*. (A) An overview of the *mraW* mutant observed with SEM. The cell morphology is similar to that of the wild-type strain. **(B)** Duplication of the terminal organelle before the cytoplasmatic separation of the two dividing cells, as observed in the *mraZ* mutant. **(C)** Aberrant cell division observed in the *mraW* mutant.

To further confirm the cell division defects of the *mraZ* mutant, we used the ImageJ software (Hartig, 2013) to measure cell length from both single and dividing cells, as well as the number of cells in division. Our results showed that cells lacking *mraZ* were indeed larger than the cells from other strains, particularly those in division (Figure I. 11A). Single cells from the *mraZ* mutant were 14% larger than cells from the *mraREF* strain, and the percentage increased to 34% when comparing dividing cells. In addition, we found that the percentage of cells in division in the *mraZ* mutant was remarkably higher (38.44%) than the observed in the wild-type and reference strains (13.35% and 12.99%, respectively) (Figure I. 11B). As expected, cell length from both single cells and dividing cells of the *mraW* mutant was identical to *mraREF* cells (Figure I. 11A). However, we observed a slight increase in the percentage of dividing cells (19.0%) when compared to both the wild-type and *mraREF* strains (Figure I. 11B).

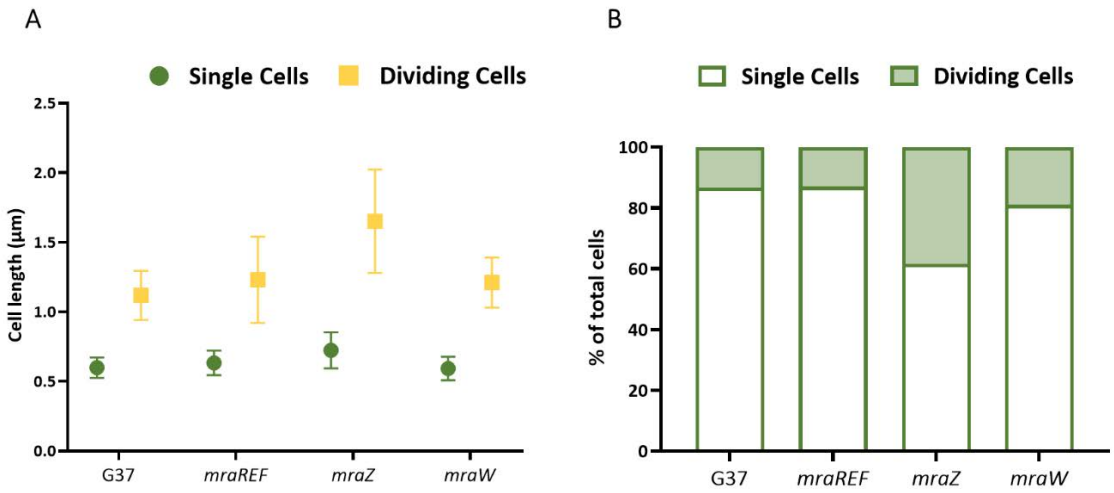

Figure I. 11. Cytokinesis is impaired upon loss of *mraZ*. **(A)** Mean length (µm) of the single (represented by a green circle) and dividing (yellow square) cells for the four analyzed strains. **(B)** Percentage of single and dividing cells in the reference and mutant strains. The left bar in each strain represents the percentage of single cells and the right bar states the percentage of cells in division.

CI.2.6 Complementation of the *mraZ* mutant strain

To confirm that the phenotypical alterations observed in the *mraZ* mutant were due to the loss of the MraZ protein, we introduced a copy of the *mraZ* gene by transposon delivery. Because MraZ controls its own expression, the *mraZ* gene was cloned into the MiniTn4001 minitransposon (Pich, Burgos, Planell, et al., 2006) along with its upstream region to allow autoregulation. Upon transformation of the minitransposon into the *mraZ* mutant, several colonies were picked up, propagated and analyzed. First, we confirmed the presence of *mraZ* in the chromosome of the transformants by PCR. Then, we determined the transcriptional levels of the cell division genes by qRT-PCR, as they were up-regulated in the mutants. The obtained data were compared to both the parental mutant strain and the *mraREF* strain (Figure I. 12).

Transcription of the operon was not restored to *mraREF* levels in none of the analyzed clones (Figure I. 12A). In fact, transcription levels of the cell division genes remained almost unchanged, despite the mRNA levels of *mraZ* were considerably higher than the observed in the *mraREF* strain. In light of these results, a new construct was tested in which the *mraZ* gene in the minitransposon was under the control of a constitutive endogenous promoter. Again, transcription of the cell division genes was still derepressed (Figure I. 12B). Unexpectedly, *mraZ* transcript levels were lower when transcription was driven by a constitutive strong promoter than by its own promoter region. Furthermore, despite *mraZ* messenger levels were almost 2-fold more abundant in C1 than in C2, transcription of *mraW*, MG_223 and *ftsZ* was similar in these clones. Thus, expression of the operon did not seem to correlate with the transcription levels of the ectopic *mraZ* copy.

As *mraZ* is always accompanied by the *mraW* gene in the genome, we cloned the two genes along with the upstream region of *mraZ* in the same minitransposon. We wanted to test whether the presence of an *mraW* copy immediately downstream of *mraZ* had an effect on MraZ function. Once more, transcription levels of the cell division genes were not restored (Figure I. 12C).

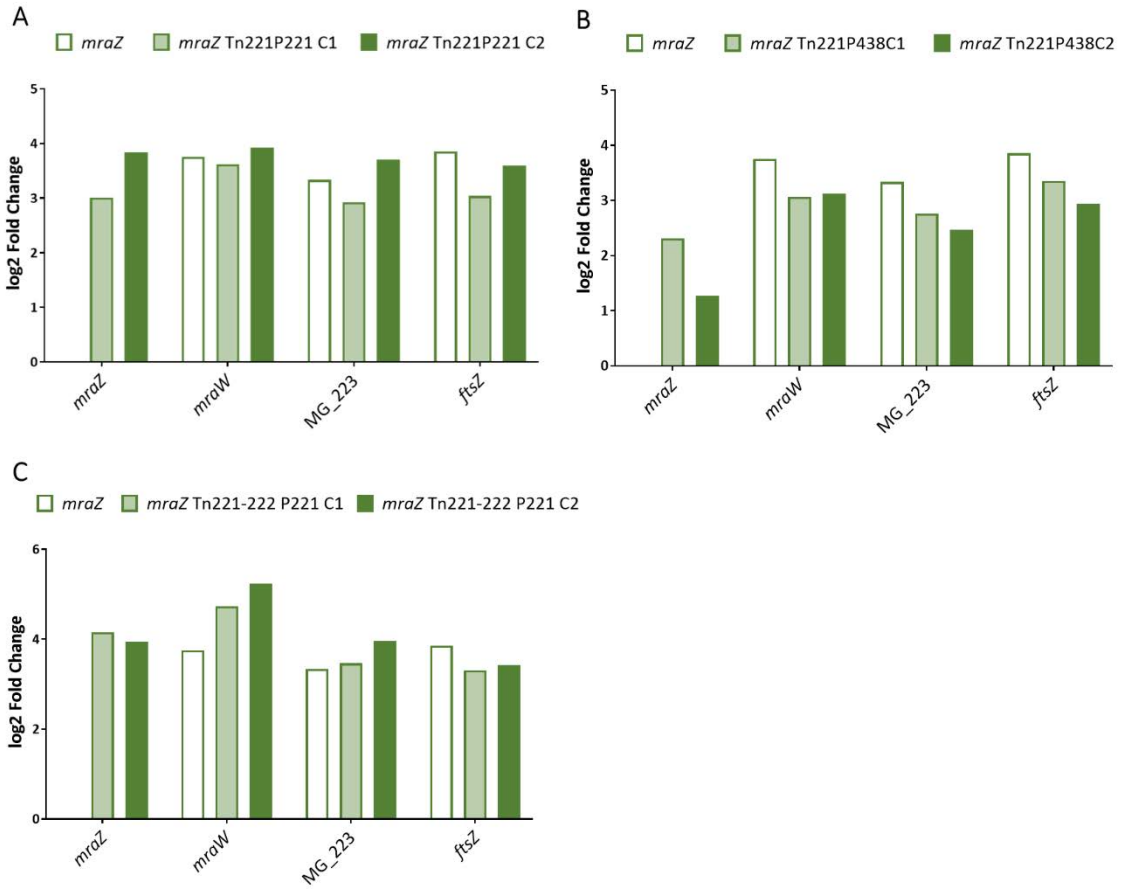

Figure I. 12. An ectopic copy of *mraZ* delivered by transposon does not restore the transcription levels of the division operon. (A) Transcriptional analysis of two individual clones in which *mraZ* and its upstream region was delivered by transposon as determined by qRT-PCR. RNA from the *mraREF* strain was extracted and analyzed in the same experiment and then compared to the data obtained from the six clones. Data from the *mraZ* mutant is the arithmetic mean of seven biological repeats. No biological repeats were performed of the individual clones. **(B)** qRT-PCR data obtained from two clones in which *mraZ* was under the control of the MG_438 promoter. RNA from the *mraREF* reference strain was also analyzed in the same experiment and then compared to the data obtained from the six clones. Data from the *mraZ* mutant is the arithmetic mean of seven biological repeats. No biological repeats were performed of the individual clones. **(C)** An additional copy of *mraW* downstream *mraZ* does not rescue the *mraREF* transcription phenotype. Results from two different clones that were analyzed by qRT-PCR along with the reference strain. Data from the *mraZ* mutant is the arithmetic mean of seven biological repeats. No biological repeats were performed of the individual clones.

As *mraZ* complementation could not be achieved by delivering an ectopic copy of this gene in *trans*, we decided to reintroduce the *mraZ* gene in the cell division operon. In particular, we placed the *mraZ* copy after the *ftsZ* gene, thus assessing if complementation could be achieved in *cis*. The new copy was introduced into the *mraZ* mutant by homologous recombination, using the chloramphenicol resistance marker (Figure I. 13A). In the resulting transformants, *mraZ* expression was under the control of its own promoter (Figure I. 13B).

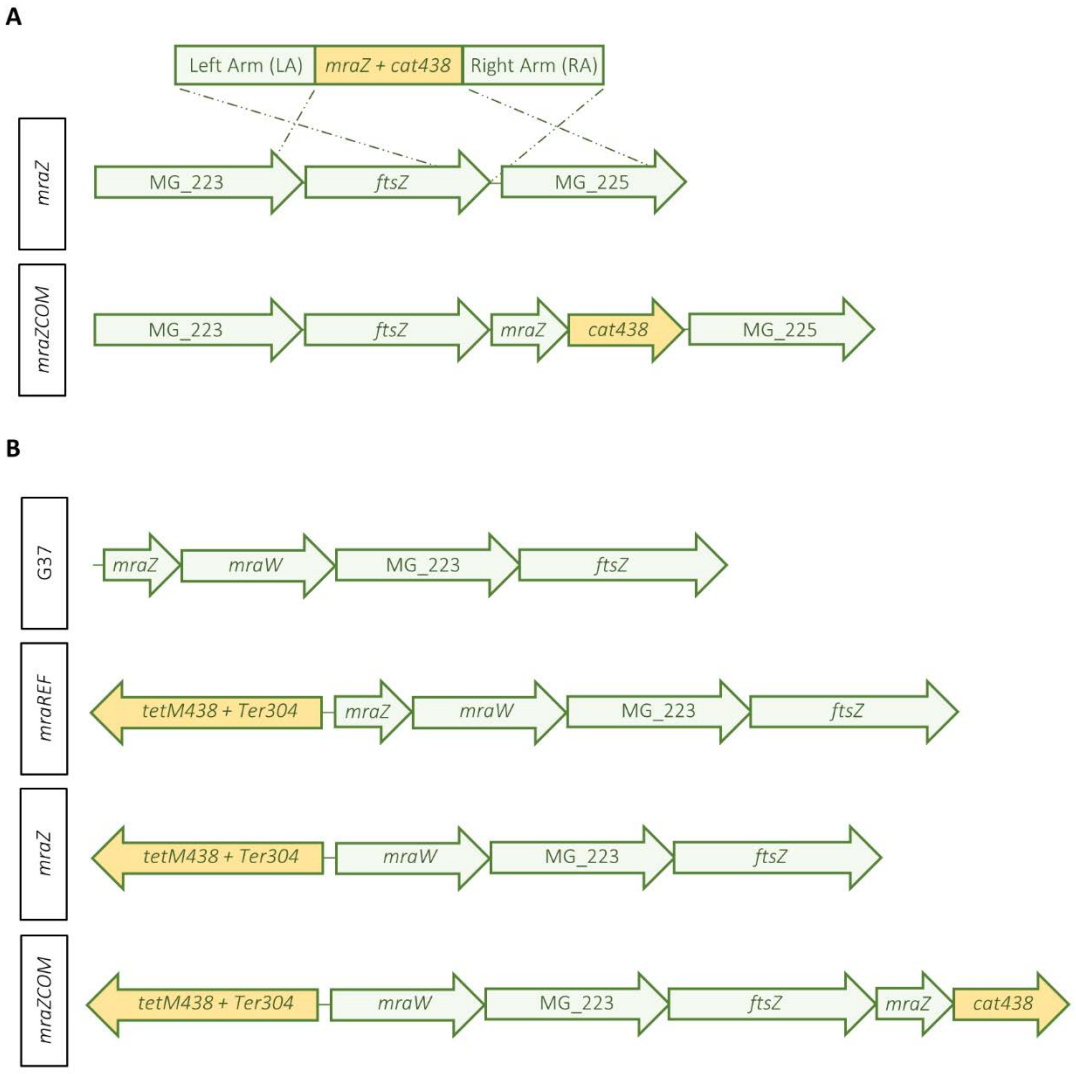

Figure I. 13. Complementation of the *mraZ* mutant by homologous recombination. (A) Construction of the complemented strain, placing the copy of *mraZ* and the chloramphenicol resistance marker between *ftsZ* and MG_225. **(B)** Schematic representation of the cell division operon in the complemented *mraZCOM* strain with respect to the parental (*mraZ*) and reference strains (G37, *mraREF*).

The newly generated strain, designated *mraZCOM*, was characterized by qRT-PCR. Transcription levels of the cell division genes in the *mraZCOM* strain were similar to those of the *mraREF* strain (Figure I. 14A). Notably, transcription of *mraW* was slightly above the biological significance threshold (1.28 log2 fold change) and the placement of *mraZ* as the last gene of the operon also had a negative impact on its own transcription levels (-1.08 log2 fold change).

Once the transcription of the operon was checked, the *mraZCOM* strain was further analyzed to assess if the other phenotypical alterations observed in the *mraZ* mutant had been restored. As expected, the growth rate of the new mutant (8.53 ± 0.38 h) resembled the one obtained for the *mraREF* (8.71 ± 0.29 h) and wild-type strains (8.38 ± 0.28 h) (Figure I. 14B). These results were in agreement with what was observed when growing the complemented strain in a flask, as it achieved full growth a full day before the parental *mraZ* strain, which was clocked at 11.54 ± 0.39 h. Next, the cells of the *mraZCOM* strain were scrutinized using SEM to study their morphology as well as to evaluate the percentage of cells in division. Then again, the overall characteristics of the complemented strain as examined by SEM were very similar to the wild-type strain at a first glance (Figure I. 14C). The follow-up analysis of cell length and percentage of dividing cells confirmed the initial observation, as the *mraZCOM* strain parameters were nearly identical to the previously calculated for the wild-type and the *mraREF* strains. Therefore, a *mraZ* copy after the operon successfully complemented the mutant strain.

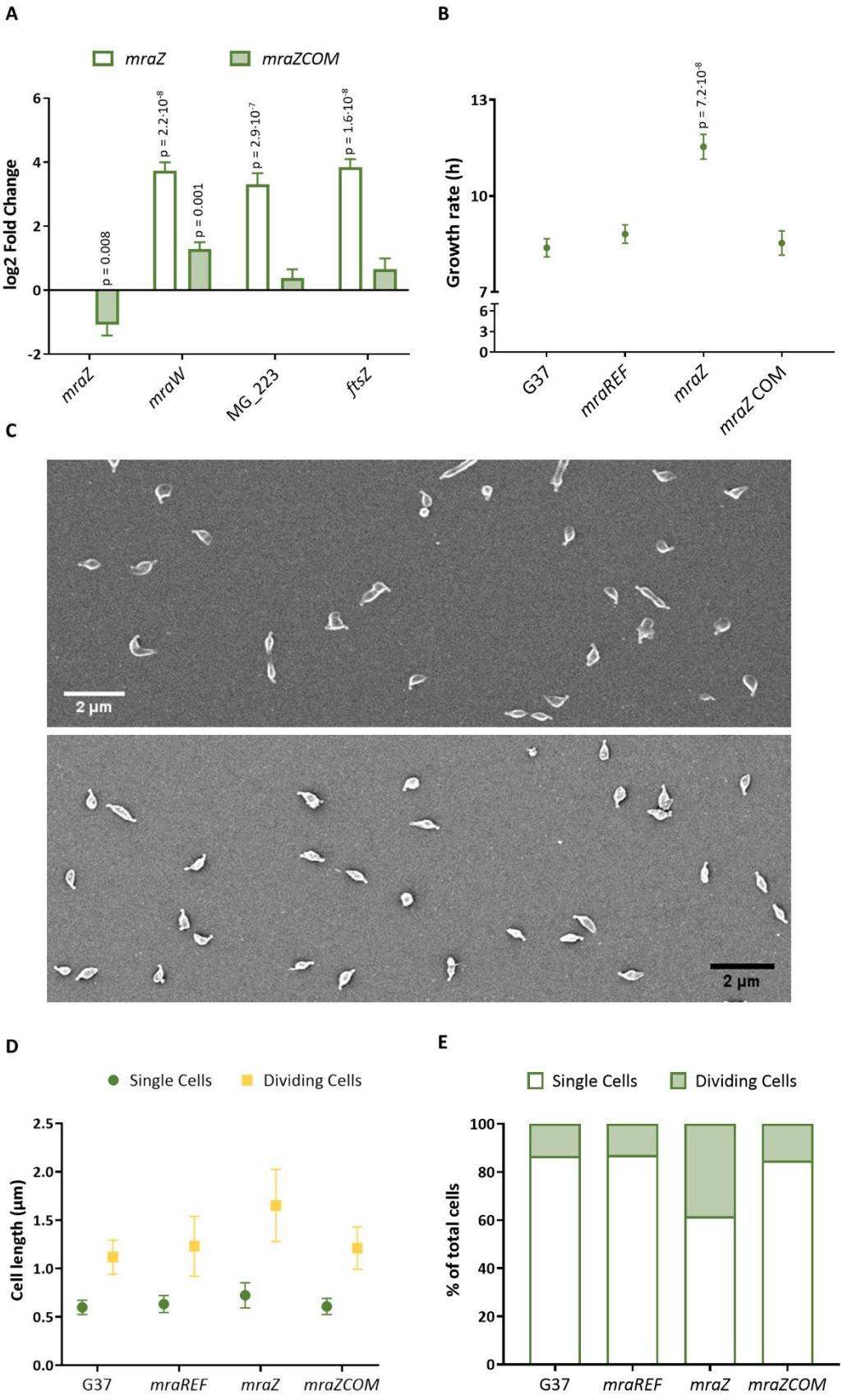

Figure I. 14. Restoration of the *mraREF* phenotype after introducing a new *mraZ* copy in cis in the mutant strain. (A) qRT-PCR data of the complemented strain confirms the complementation of

the mutant strain by homologous recombination. Bars represent the mean of at least four independent biological repeats. Statistically significant values assessed by a paired T-test are above the corresponding bar if biologically significant (log2 fold change ± 1). **(B)** Duplication time of the *mraZCOM* strain compared to its parental strain (*mraZ*) and to the wild-type and mraREF strains. Statistical significance was assessed using a paired T-test. Significant values ($p < 0.05$) are indicated above its corresponding experimentally determined value. **(C)** SEM micrographs of the wild-type strain (top panel) and the *mraZCOM* complemented strain (bottom panel). Scale bars represent 2 µm. **(D)** Single and dividing cell length of the wild-type, *mraREF*, *mraZ* and the *mraZCOM* strains. Several micrographs of each strain were analyzed using the ImageJ software. More than 150 cells from each strain were studied. **(E)** Percentage of single and dividing cells as observed in SEM micrographs for the four tested strains.

CI.2.7 Overexpression of *mraZ*

As mentioned earlier, MraZ overexpression activates transcription of the cell division operon in *M. gallisepticum* (Fisunov et al., 2016). Therefore, we decided to assess the effect of overexpressing MraZ in *M. genitalium*. To this end, we introduced an additional copy of the *mraZ* gene into a wild-type background. Two different promoters were tested to drive expression of the additional *mraZ* copy: a constitutive strong promoter (*P438*) and the *mraZ* own promoter (*P221*). In addition, we assessed the effect of co-expressing *mraZ* and *mraW*. For control purposes, we also obtained a construct (*mraZmut P438*) where the *mraZ* gen carried a frameshift mutation introducing a premature stop codon. The different constructs were cloned into a minitransposon and introduced into *M. genitalium*.

This time, instead of analyzing individual clones, we tested RNA isolated from pools of mutants to obtain a much broader view of the transcriptional changes. In keeping with the results reported in *M. gallisepticum*, we observed the activation of the cell division operon (Figure I. 15). This up-regulation was independent of the promoter driving *mraZ* transcription and was not affected by the co-overexpression with MraW.

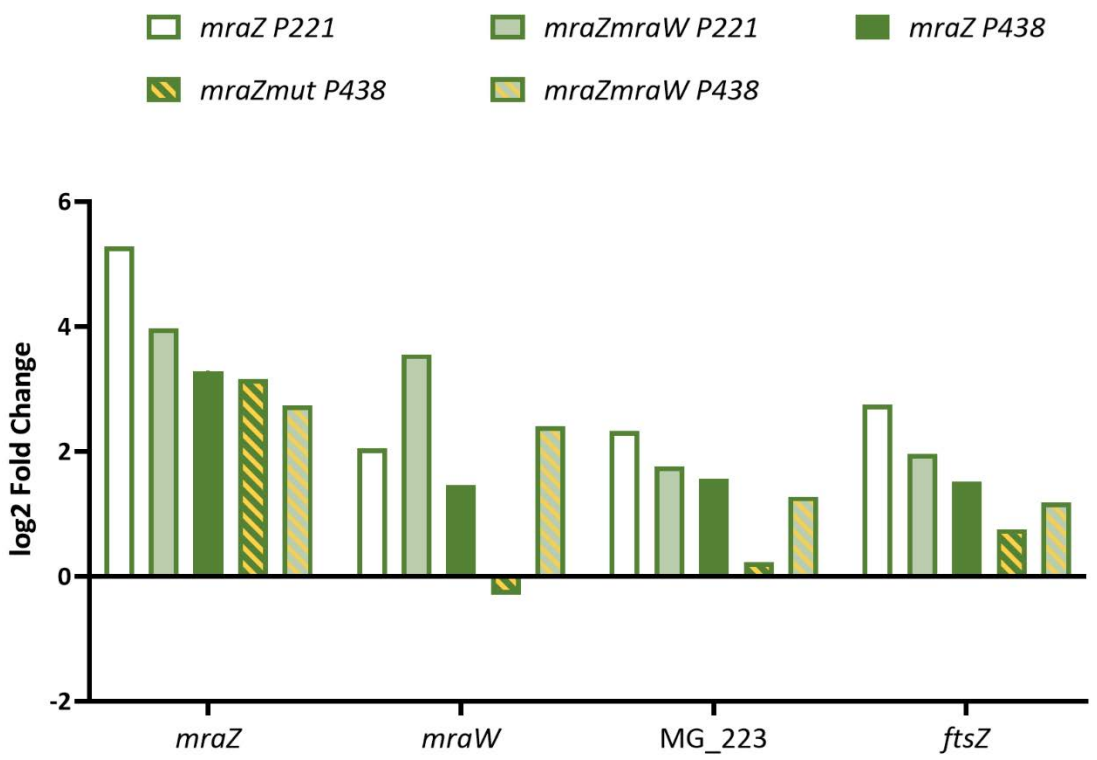

Figure I. 15. Overexpression of *mraZ* leads to higher transcription levels of the operon. qRT-PCR data from several strains overexpressing *mraZ* (with or without *mraW*). G37 was transformed with one of the constructions, the RNA from the entire culture was extracted and later analyzed and compared to the G37 strain.

CI.2.8 Cell division without the entire *dcw* cluster

As several genes of the dcw cluster seem to be dispensable for growth in *M. genitalium* (Glass et al., 2006), we decided to test whether the entire cluster could be deleted from the chromosome. The whole operon was deleted by homologous recombination and replaced by a chloramphenicol resistance marker under the control of the MG_438 promoter (Figure I. 16).

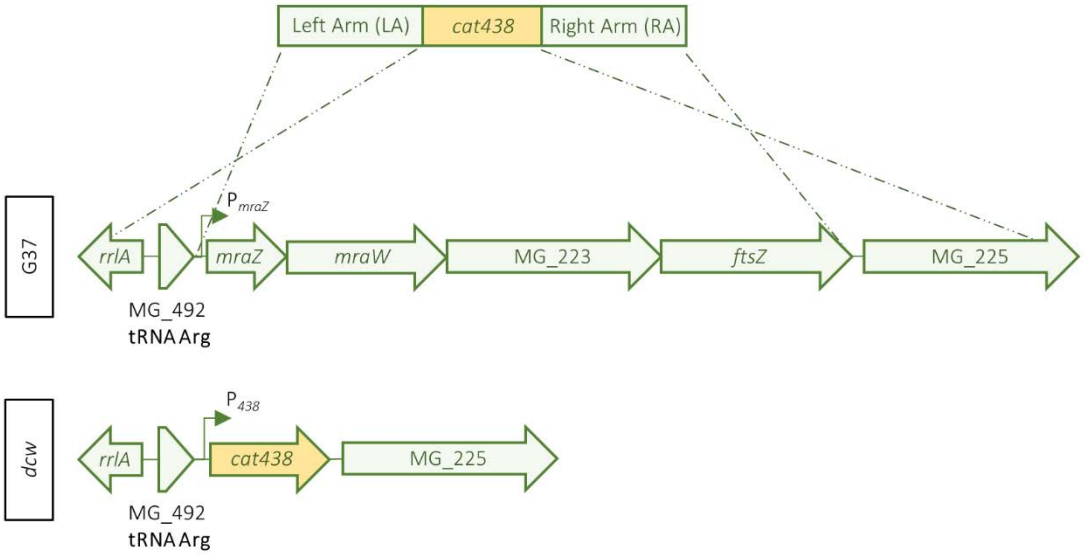

Figure I. 16. Design and creation of the *dcw* strain. The four genes of the operon are replaced by a chloramphenicol acetyltransferase under the control of the MG_438 promoter.

The dcw-depleted mutant was first examined by SEM. Notably, the number of cells in division appeared to be higher (30.53%) than in the wild-type strain (13.35%) (Figure I. 17A and D). Of note, the percentage of cells in division was similar to that observed in the *mraZ* mutant (38.44%). In addition, we observed some aberrant cell divisions, suggesting an impaired cytokinesis and a premature duplication of the terminal organelle before the separation of the two daughter cells (Figure I. 17B). The cell length was largely unaffected with regards to the wild-type strain (Figure I. 17C).

Remarkably, this mutant exhibited a significant growth delay, as the duplication time of the strain was notably higher (10.13 ± 0.33 h) than that of the wild-type (8.38 ± 0.28 h) and the reference strains (8.81 ± 0.29 h) (Figure I. 17E). Interestingly, the growth rate was very similar to the observed in the *mraW* strain (9.96 ± 0.53 h).

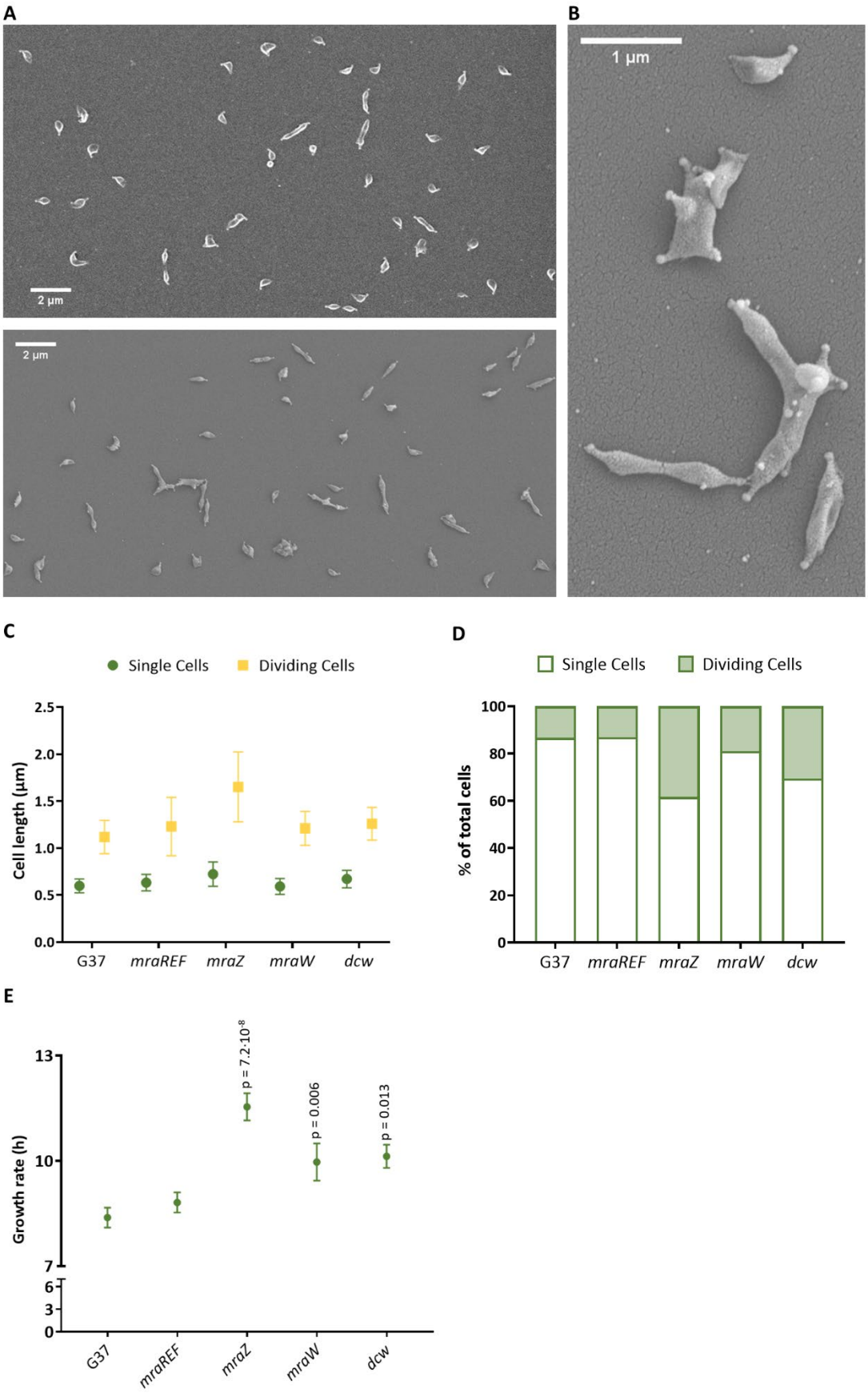

Figure I. 17. Deletion of the *dcw* operon has an impact on cell fitness and morphology. (A) Comparison between the wild-type strain (top panel) and the *dcw* mutant (bottom micrograph)

using SEM. **(B)** Aberrant cell divisions observed in a *dcw* SEM micrograph. Cells with multiple terminal organelles were frequently upon deletion of the division operon. **(C)** Cell length of the newly created strain as compared to the wild-type and the other characterized mutants. The length was calculated using ImageJ and represents the mean of at least 150 cells per strain. **(D)** Percentage of cells in division in each of the studied strains. **(E)** Duplication time of all the mutants studied as well as the reference and wild-type strains. Statistical significance was assessed by a paired T-test and statistically significant values ($p < 0.05$) compared to the wild-type strain are exhibited upon their corresponding growth rate value.

These results raised important questions regarding the contribution of FtsZ in *M. genitalium* cell division. Therefore, we decided to characterize an *ftsZ* mutant to put the phenotype in context of the other mutants described in this chapter. SEM analysis revealed an impaired cytokinesis in the *ftsZ* mutant (Figure I. 18B and C). There was a slight increase in the percentage of cells in division in this strain (22.44%), a percentage closer to the *dcw* mutant (30.53%) than to the G37 strain (13.35%) (Figure I. 18E). However, the cell length and the duplication time were very similar to the observed in the wild-type strain (Figure I. 18D and F).

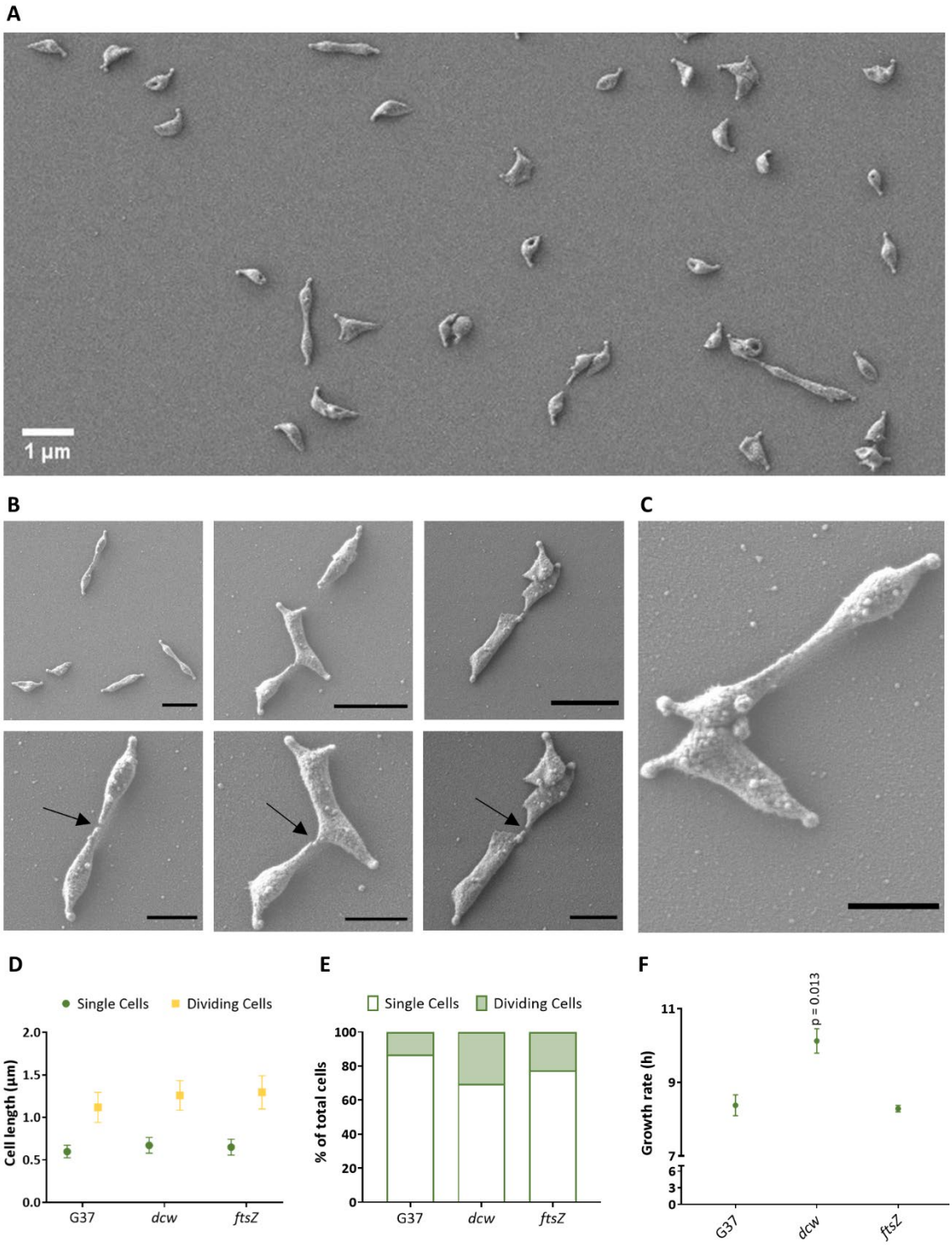

Figure I. 18. Characterization of the morphology, division and duplication time of the *ftsZ* mutant. **(A)** Overall view of the *ftsZ* mutant in SEM. Scale bar indicates 1 µm. **(B)** Micrographs of some aberrant divisions in the *ftsZ* strain. The images of the second row belong to the same field as the ones in the first row, but with a higher magnification. Arrows point to abrupt breaking points. Scale bar for the first row represents 1 µm and 0.5 µm for the second row. **(C)** Hindered cell fission in the *ftsZ* strain. Scale bar represents 0.5 µm. **(D)** Cell length of the *ftsZ* mutant with respect to the mutant of the whole operon and the wild-type strain. **(E)** Percentage of single and dividing cells in each strain. **(F)** Growth rate of *ftsZ* compared to the wild-type and the *dcw* strains.

Significance was assessed using a paired T test. Significant values are placed above the mean duplication time of each strain.

CI.2.9 Single-cell FtsZ dynamics in *M. genitalium*

The analysis of the *ftsZ* mutant does not shed light on the specific function of FtsZ in *M. genitalium* cell division. Moreover, our findings raised important concerns regarding the importance and functionality of FtsZ in this bacterium. Therefore, to explore the role of this protein, we created a fluorescent protein fusion to follow the expression and localization of FtsZ. To this end, the *mcherry* fluorescent marker was introduced by homologous recombination at the end of the *ftsZ* gene. Therefore, *ftsZ* was under the control of its own promoter.

In addition, the P65 protein (coded in the MG_217 ORF) was used to label the Terminal Organelle (TO) of *M. genitalium* (Burgos et al., 2008). Thus, the *eyfp* fluorescent marker was fused to the MG_217 gene by homologous recombination. The observed fluorescent signal was strong and exceptionally focused, and it facilitated the identification of dividing cells, which exhibited fluorescent foci at opposite poles (Figure I. 19). The sharpness of the foci allowed the recognition of early stages of division, as the duplication of the terminal organelle results in two proximal foci at one pole. In conclusion, the recognition of the TO (P65 signal) facilitates the identification of the subcellular localization of FtsZ.

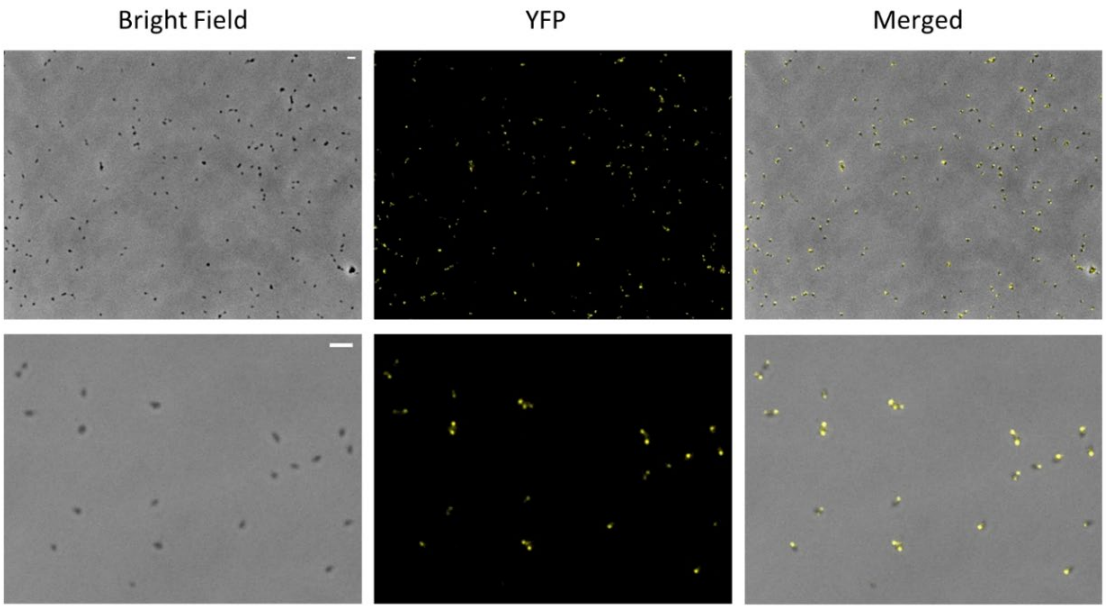

Figure I. 19. P65:YFP fluorescence in a wild-type background is ubiquitous and polar. The first set provides an overall view of the *217YFP* strain, while the second is a magnified micrograph from another photo. In the last row, cells in division can be spotted due to the opposite fluorescent signal. A recent duplication of the terminal organelle can also be detected in the last micrograph of the second row (top left corner). The scale bar is placed at the upper right corner of the bright field images and represents 2 µm.

When the expression of the FtsZ:mCherry fusion was investigated in the WT strain, we did not observe fluorescent cells (n = 2772 cells) (Figure I. 20, first row). Given that FtsZ expression was markedly higher in an *mraZ*-depleted background, we decided to explore FtsZ localization in the *mraZ* mutant. This time, we observed a large number of cells (56.63%; 6458 out of 11403 cells) exhibiting FtsZ:mCherry fluorescence (Figure I. 20, second row). In parallel, the *ftsZ*:*mcherry* construct was also analyzed in the *mraW* strain. Surprisingly, some fluorescent cells could be identified (1.58%; 110 out of 6942 cells) (Figure I. 20, third row).

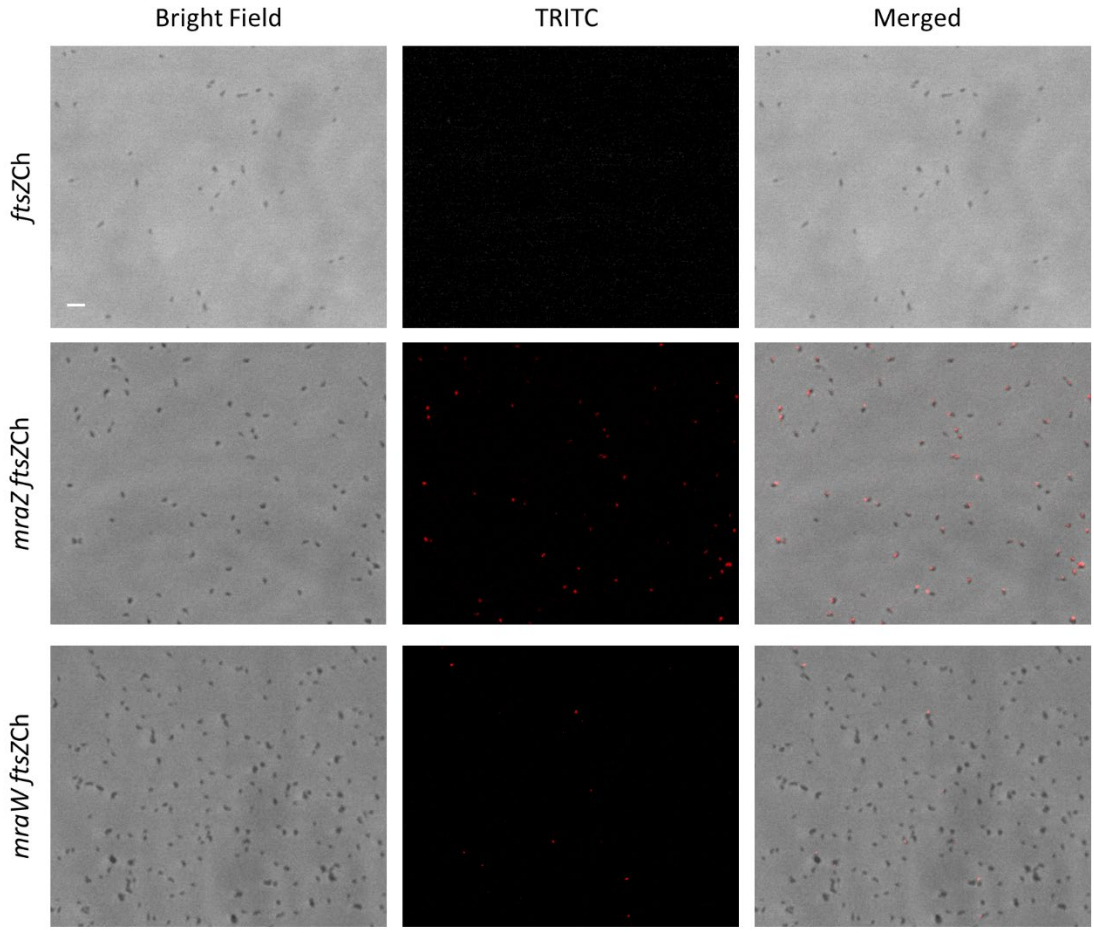

Figure I. 20. Single cell analysis suggests a low expression of FtsZ in a G37 strain. Each row represents three fluorescence microscopy images: the bright field (without fluorescence), the TRITC channel (only mCherry fluorescence) and the resulting overlay. The scale bar (located in the first image, lower left) represents 2 µm. All images are shown at the same magnification.

Remarkably, there were two significant traits of the fluorescent signal in the *mraZ ftsZ*Ch strain. One of them was associated with the intensity of the fluorescence, a parameter that markedly differed among cells. On the other hand, the FtsZ:mCherry signal seemed to be frequently located at one of the cell poles. This last remark was confirmed by the P65:eYFP fusion (Figure I. 21). The *mraZ ftsZ*Ch *217YFP* strain revealed that the location of the FtsZ:mCherry signal was opposite to the yellow focus in single cells and it started to shift to the cell center when the duplicated terminal organelle began to separate from the parental one. Notably, the yellow and red fluorescent signals never overlapped, suggesting the existence of a regulatory system that prevents the polymerization of FtsZ near the terminal organelle of *M. genitalium*. In addition, we observed that the intensity of the FtsZ foci was higher when it was localized at the mid-cell.

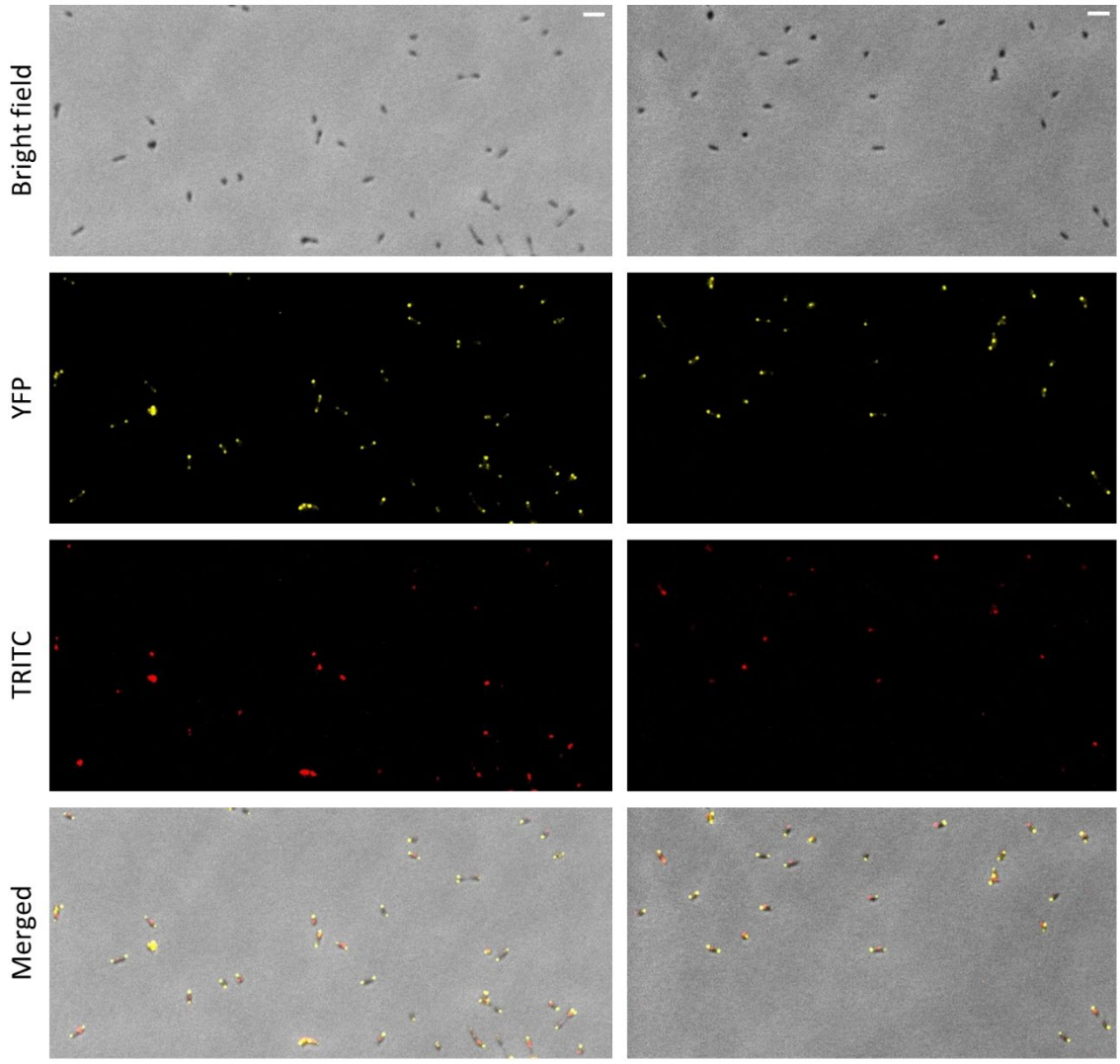

Figure I. 21. FtsZ location depends on the terminal organelle. Micrographs corresponding to two different fields of the *mraZ ftsZCh 217YFP* strain. The yellow fluorescence is always polarized at one of the two (or both) cell poles and has an impact on the FtsZ:mCherry position, as the two fluorescence signals do not overlap. Scale bar is placed in the bright field image of each set and represents 2 µm.

Given the sharpness, location and interplay of the two fluorescent signals, the *mraZ ftsZCh 217YFP* strain constituted a suitable platform to study chromosome segregation and cytokinesis dynamics in *M. genitalium*. Thus, cells from this mutant were also stained with Hoechst to determine the spatial relationship between the chromosomal location, the terminal organelle and the FtsZ foci (Figure I. 22A). In addition, it also offered a great insight into the FtsZ dynamics throughout the cell division process (Figure I. 22B).

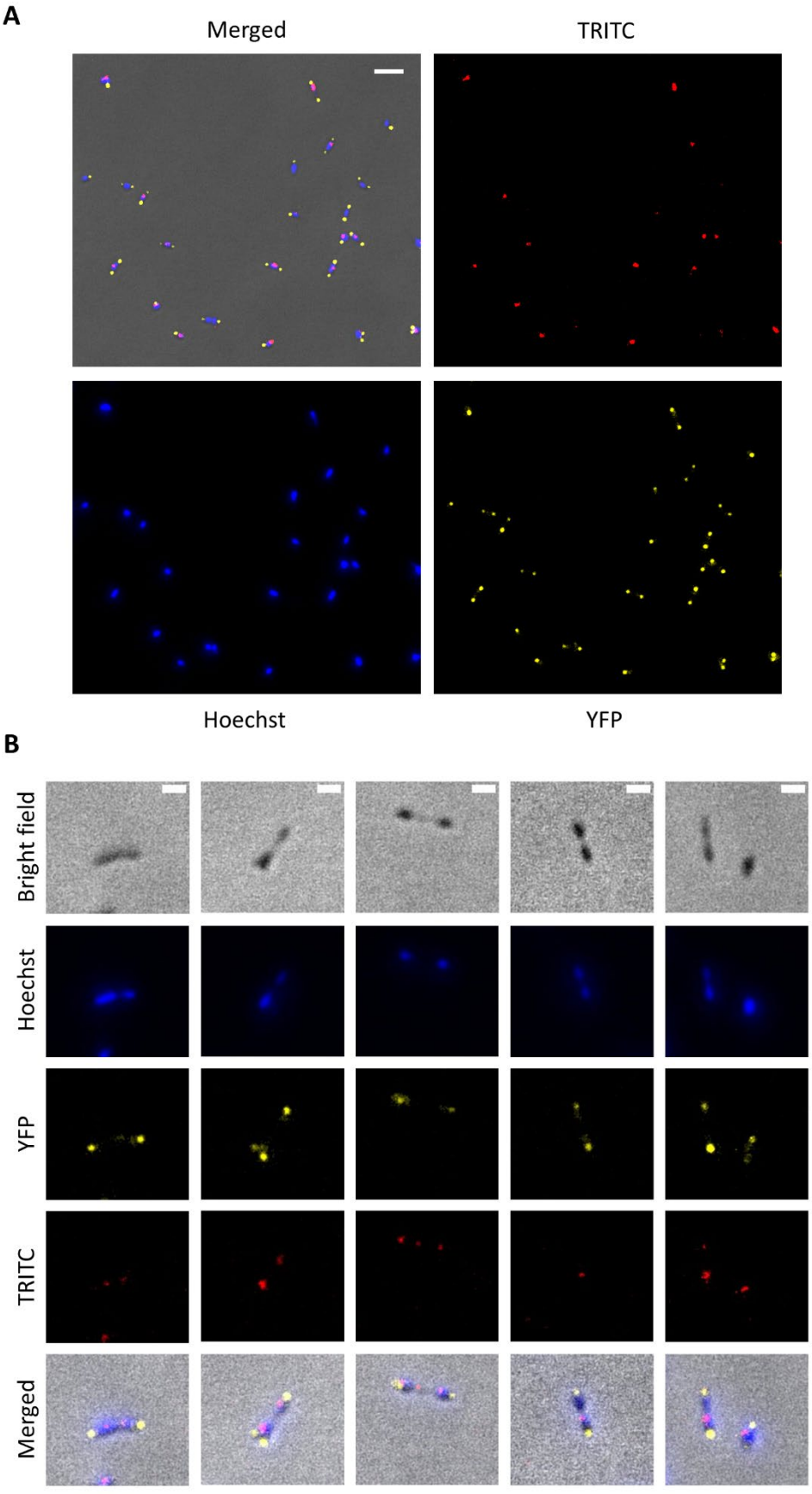

Figure I. 22. Cytokinesis tracking through the combination of the three fluorescent signals. (A) Micrographs of the same microscopic fields for each of the three fluorescent channels in the *mraZ*

*ftsZ*Ch 217YFP strain and the resulting overlay. The scale bar is located at the upper right corner of the merged image and represents 2 µm. **(B)** FtsZ:mCherry foci after chromosome segregation and before cytokinesis is completed. Micrographs of dividing cells with remaining FtsZ:mCherry fluorescence between the two chromosomes during the last steps of cytokinesis. Scale bar is placed at the top right corner of the bright field images and represents 1 µm.

The use of the three different signals shed light on the cell cycle of this bacterium, as it made possible to pinpoint the location of the terminal organelle, the chromosome and FtsZ throughout the cell replication. In addition, they provided valuable information about how the terminal organelle and the division machinery impacted the chromosome replication and segregation. The analysis of this strain allowed us to identify eight different stages of cell division in *M. genitalium* (Figure I. 23).

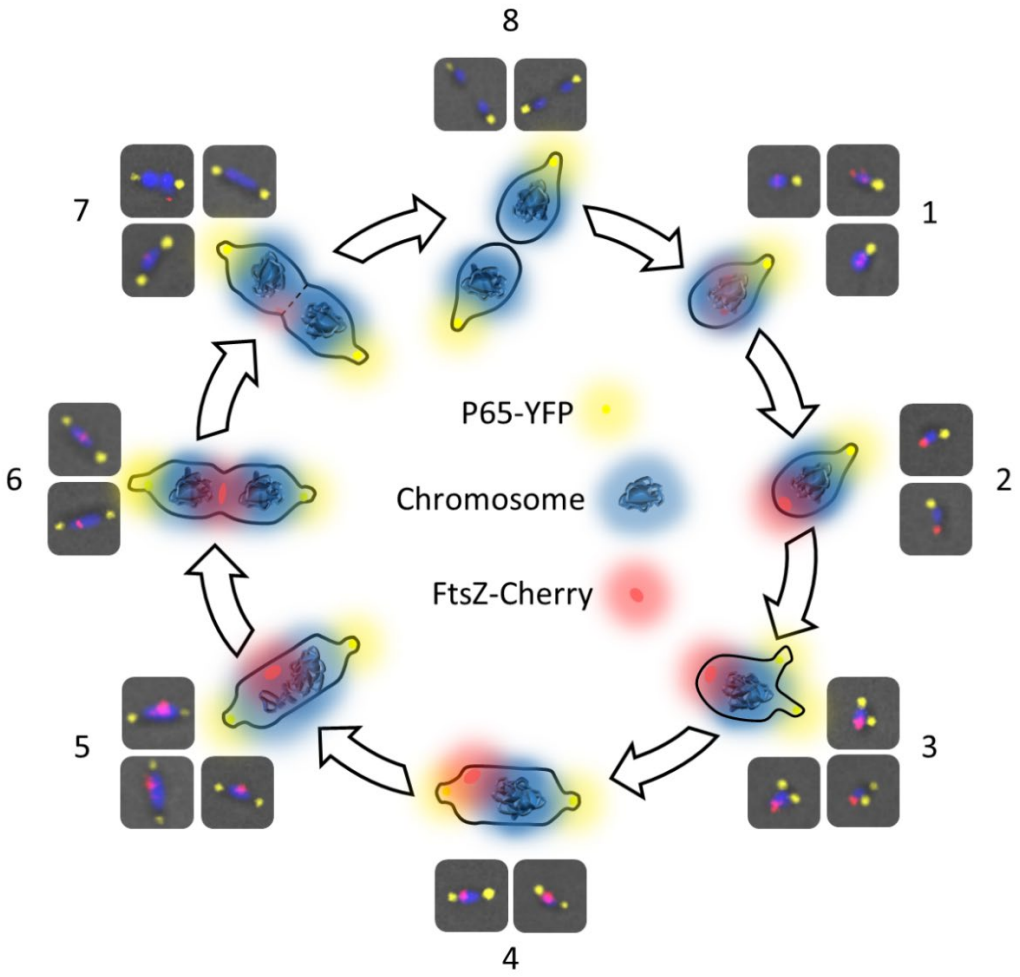

Figure I. 23. Fluorescent tracking of the cell cycle of *M. genitalium* from a single cell until complete cytokinesis. Each stage is illustrated by fluorescence microscopy micrographs of the *mraZ ftsZ*Ch 217YFP strain.

The process starts when a dim and disperse FtsZ:mCherry fluorescence begins to appear in single cells (Step 1) before it concentrates at one cell pole (step 2). Then, coinciding with terminal organelle duplication (step 3), the FtsZ fluorescent focus starts to shift to the midcell (step 4). As the cell elongates driven by the two terminal organelles pushing for opposite directions, FtsZ fluorescence intensifies at midcell (step 5) and slowly fades away during cytokinesis (step 6) as the two chromosomes are distributed in the original and daughter cells. After the chromosome relocation and the final stages of cytokinesis, FtsZ is degraded (step 7) and two daughter cells emerge (step 8).

Therefore, the fluorescence analysis of this strain demonstrates an active participation of FtsZ in the cell division of *M. genitalium*, as well as an underlying regulatory mechanism that prevents the colocalization of the division machinery and the terminal organelle. To our knowledge, this is the first study addressing FtsZ localization during cell division in mycoplasmas.

CI.3 Discussion

The results presented in this chapter demonstrate that MraZ is as a transcriptional regulator of the *dcw* cluster in *M. genitalium*. Supporting this notion, *mraZ* depletion leads to a strong activation of the other three genes of the operon. This finding correlates with proteomics data showing that the proteins coded by these three loci are more abundant in the *mraZ* null mutant. Therefore, our results are in agreement with previous data obtained in *E. coli* (Eraso et al., 2014). However, in keeping with a recent study conducted in *M. gallisepticum* (G. Y. Fisunov et al., 2016), we also observed a notable increase in transcription of the cell division cluster upon MraZ overexpression. Thus, our work confirms previous contradicting data by Eraso and Fisunov in two phylogenetically distant species. Remarkably, the fact that MraZ overexpression is lethal in *E. coli* and a *mraZ* null mutant was not characterized in *M. gallisepticum*, makes our study in *M. genitalium* the only one addressing at the same time the effect of the loss and excess of MraZ in the same bacterium.

The overexpression of *mraZ* led to a notable increase in the transcription of *mraW*, MG_223 and *ftsZ*, and this effect was neither dependent on the promoter used to drive expression of the ectopic copy of *mraZ* nor dampened by co-overexpressing *mraW*. However, the transcriptional activation observed after the addition of an ectopic copy was not as strong as the associated with the loss of the regulator. In addition, the *mraZ* mutant had a distinctive phenotype.

The thorough characterization of the *mraZ* mutant revealed several growth and replication alterations. This strain exhibited a significant delay in growth, severe morphological alterations and a remarkably high percentage of cells in division. Therefore, although the transcriptional activation was achieved both when knocking out the regulator and after its overexpression, the notable defects associated with the loss of *mraZ* highlights the importance of gene regulation. This could be because the strains with two copies of *mraZ* are still able to have a tighter control on the operon regulation than the strain lacking *mraZ*.

Our results suggest that the levels of *mraZ* messenger are tightly controlled and an alteration on those levels has important downstream transcriptional consequences. This is further confirmed by the several complementation assays performed to restore the wild-type phenotype. We found that it was not possible to return to the transcription

levels of the wild-type strain when introducing a copy of *mraZ in trans*, regardless of the promoter used. The restoration of the transcription as well as the other growth defects associated with the loss of *mraZ* was only achieved after placing the new copy of *mraZ* after the last gene of the *dcw* operon. Although transcription of *mraZ* as the last gene of its operon was considerably lower than in the *mraREF* strain, the characterization of the complemented strain evidenced that it was phenotypically identical to the wild-type and the reference strains.

It is tempting to speculate that the oligomerization status of MraZ could determine the sense of the regulation of the *dcw* operon, that is activation or repression. Supporting this notion, it has been reported that MraZ is able to form dodecamers in *E. coli* (M. A. Adams et al., 2005) and octamers in *M. pneumoniae* (Chen et al., 2004). In addition, Fisunov and collaborators found that free MraZ protein formed dodecamers in *M. gallisepticum*, but they also observed that MraZ could form 24-mer or octamers depending on the protein concentration when it was complexed with its promoter (Fisunov et al., 2016). They speculate that an MraZ octamer binds to each box, thus forming a 24-mer structure when all the boxes are occupied. Therefore, the effect of MraZ on transcription could depend on its concentration and the number of boxes occupied. However, the mechanism underlying its binding to the boxes, its affinity for each one of the three (or four, as there is an additional box in *M. genitalium* and others) and the possible existence of cooperative binding are still unknown.

Because of the severe cellular disfunction caused by the loss of MraZ, it seems reasonable to think that this protein is a transcriptional repressor and that the activation observed upon its overexpression is due to an adaptation to the ectopic copy of *mraZ*. Because of the critical function of MraZ in the regulation of division and the already stablished fact that it regulates its own expression (Eraso et al., 2014), its role as a transcriptional activator would be biologically questionable. There are several cases of positive autoregulation reported, as more than 30 transcription factors in *E. coli* are classified as auto-activators (Hermsen et al., 2010). This approach, however, might present some issues in a cell division context, as positive feedback slows down cellular responses, due to the amount of time needed to achieve the necessary concentration of transcription factor (Y. T. Maeda & Sano, 2006). On the other hand, negative autoregulation provides a fast response (Rosenfeld et al., 2002), and it is also associated with a high stability, as the concentration of the regulator is maintained within optimal limits (Becskel & Serrano, 2000). These are two crucial traits when it comes to a critical

process as cell division. Moreover, there are other several negative regulatory networks involved in the control of cell division, as the Min system and nucleoid occlusion (Bernhardt & De Boer, 2005; Edwards & Errington, 1997; Z. Hu & Lutkenhaus, 2003; L. J. Wu & Errington, 2004). A negative autoregulation by MraZ could also explain why there was no discernible phenotype associated with its deletion in the *E. coli* mutant, as this microorganism duplicates every 20 minutes in rich medium and the *dcw* operon is probably derepressed most of the time.

Regarding MraW, previous work in *E. coli* suggests that it works as an antagonist of MraZ function (Eraso et al., 2014). Accordingly, the lethal phenotype of overexpressing *mraZ* was reversed when it was co-transcribed with *mraW*. As the overexpression of *mraZ* is not toxic in *M. genitalium*, we could not properly test this antagonism, but we observed that adding an extra copy of *mraW* immediately downstream of an ectopic copy of *mraZ* did not have an effect on the transcriptional activation caused by the regulator.

Notably, we were able to describe a distinct phenotype for the *mraW* mutant. The growth rate of the mutant strain (9.96 ± 0.53 h) was slightly slower than that of the *mraREF* (8.81 ± 0.29 h) and the wild-type (8.38 ± 0.28 h) strains. In addition, a small percentage of cells (1.58%) exhibited FtsZ:mCherry fluorescence in a *mraW*-less background, a notably lower percentage than the observed in the *mraZ* mutant (56.63%), but nonetheless a significant number because no fluorescent cells could be detected in a wild-type background. The fluorescence data is also consistent with the proteomics results: there was a notable spike in FtsZ expression upon depletion of mraZ (peptides belonging to FtsZ were 20-fold more abundant than in the G37 strain) and only a meager increase was detected in the mraW null mutant (2-fold). Remarkably, the loss of mraW had no effect on the transcription of the operon.

Thus, it could be possible that MraW has a regulatory role, although at a translational level. MraW is an RNA methyltransferase and the influence of these proteins in translation is well-documented. It has been reported that MraW specifically methylates the C1402 residue of the 16S rRNA (Kimura & Suzuki, 2010). This residue is involved in translation initiation and its mutation leads to an increased doubling time in *E. coli* (Jemiolo et al., 1985). The mutant of *mraW* has been directly related to an altered translation fidelity (Kyuma et al., 2015). Furthermore, the existence of species with orphan *mraW* genes establishes a role for MraW independent from MraZ function.

Our results together with the already existent reports on this protein suggest that MraW could indeed have a role in translational regulation. Thus, MraW might act as a secondary regulator, modulating the translation of the polycistronic mRNA that contains the MraZ coding region. This would be consistent with its reported role as a partial antagonist of MraZ (Eraso et al., 2014), as the overexpression of MraW could reduce the levels of MraZ. The proposed model would also be consistent with the milder effects on growth rate and cell division of the *mraW* mutant with regards to the loss of *mraZ*, as in the *mraW* strain there is a higher layer of regulation provided by MraZ. The vast conservation of both genes across the bacteria kingdom denotes a remarkably optimized system.

Due to the slow growth rate of *M. genitalium*, the cell division operon is likely repressed by MraZ for the most part of the cell cycle. This is in agreement with the already discussed effects associated with the deregulation of the cluster. Accordingly, no FtsZ fluorescence could be observed in a wild-type context, which could imply a minor role of the tubulin-like protein in this bacterium. This notion is supported by the apparent lack of phenotype *in vitro* displayed by the *ftsZ* mutant, which characteristics and duplication time are very similar to that of the G37 strain. It was already described that the *ftsZ* mutant was viable in *M. genitalium* (Lluch-Senar et al., 2010), and we demonstrate here that none of the genes of the cell division operon are essential for *in vitro* growth. Therefore, the lack of fluorescence in a wild-type background and the unaltered duplication time of the defective mutant might hint to a secondary role for FtsZ in *M. genitalium* in the tested conditions.

Conversely, the conservation of *ftsZ* in the reduced genome of *M. genitalium* suggests that its gene product has a relevant function in this bacterium. Due to the increased expression of FtsZ in the *mraZ* mutant, we were able to determine the FtsZ dynamics in *M. genitalium*. Remarkably, we found that FtsZ clusters at the cell pole opposite to the Terminal Organelle (TO). Then, when the TO duplicates and it migrates to the opposite cell pole, FtsZ foci shift to the midcell. Intensity of the FtsZ foci increases when it arrives to the midcell and the two chromosomes start to segregate. This pattern strongly suggests a clear role for FtsZ in *M. genitalium* division. In addition, the position of FtsZ seems to be regulated. Although *M. genitalium* does not apparently possess a Min system as the one described in *E. coli* (Fu, 2001; Z. Hu & Lutkenhaus, 2003; Raskin & De Boer, 1999) or *B. subtilis* (Edwards & Errington, 1997), it is very plausible that there is a regulatory system in place that prevents the formation of a Z ring close to the TO.

Interestingly, *M. genitalium* codes for a divIVA homolog (MG211), a key protein in the Min system of *B. subtilis* (Edwards & Errington, 1997). In addition, we observed that the FtsZ foci were often located between the two segregating chromosomes, suggesting that there could be a nucleoid occlusion mechanism in *M. genitalium* yet to be determined.

Finally, we were able to delete the whole dcw operon of *M. genitalium*. Although an essentiality study in the closely related bacterium *M. pneumoniae* disclosed that the four genes of the operon were not essential for *in vitro* growth (Lluch-Senar et al., 2015), we are the first to describe a complete knockout of the cluster. Interestingly, this mutant exhibited a slower growth (10.13 ± 0.33 h) than the *ftsZ* mutant (8.29 ± 0.09 h), as well as a higher percentage of dividing cells (30.53% in the *dcw* mutant and 22.44% in the *ftsZ* strain). Thus, our results hint to a potentially relevant role of the *dcw* operon in cell division beyond FtsZ, as the loss of the whole operon is notably more deleterious for growth than the loss of *ftsZ* alone.

Overall, the results presented here shed some light on the function of MraZ as a transcriptional regulator and reveal the existence of an intricate mechanism controlling MraZ activity. In addition, this is the first study to associate a distinctive phenotype to the loss of MraZ, which is probably due to the high levels of expression of several cell division proteins and the interference with the alternative division system. Moreover, we also propose a possible role for MraW in regulation. Finally, the analysis of the FtsZ cell dynamics indicates the existence of a regulation of the Z ring location and formation in *M. genitalium*.

CHAPTER II

RESPONSE TO METAL STARVATION INVOLVES FUR-DEPENDENT AND -INDEPENDENT REGULATORY PATHWAYS

CII.1 Introduction

Urethritis or inflammation of the urethra is a medical condition intimately related to sexually transmitted infections (STI). Non-gonococcal urethritis is the most common treatable sexually transmitted syndrome in men (Horner et al., 2016; Moi et al., 2015) and it is frequently associated with infections by *Chlamydia trachomatis* and *Mycoplasma genitalium*. M. genitalium is an emergent human pathogen that has been also associated with several syndromes in women including cervicitis, endometritis and pelvic inflammatory disease (Jørgen Skov Jensen, 2017; McGowin & Totten, 2017). Appreciation of the significance of *M. genitalium* in human disease has been hampered by in vitro culture limitations and lack of commercial molecular-based tests for rapid detection of this bacterium (Bradshaw et al., 2018). Prevalence of *M. genitalium* infections range from 0.7% to 3.3% in the general population, but this percentage increases dramatically in specific populations at high risk of STI (Anagrius et al., 2005; Horner et al., 2016). In this sense, *M. genitalium* is more prevalent than any other bacterial STI in HIV-positive men who have sex with men (Soni et al., 2010).

Remarkably, numerous studies indicate that *M. genitalium* is rapidly developing resistance to all current standard antibiotic treatments, and is bound to become a major untreatable STI (Bradshaw et al., 2018; Martin et al., 2017). Supporting this idea, prevalence of mutations associated with azithromycin resistance, the first-line therapy to treat *M. genitalium* infections, rises up to 50% in particular contexts. Moreover, recent studies document a rapid emergence of mutations associated with resistance to the fourth-generation fluoroquinolone moxifloxacin, which is used as the second-line therapy to treat *M. genitalium* infections in Europe. Compounding this problem is the observation made years ago that 60% to 80% of *M. genitalium* infections fail to respond to tetracyclines, which are still used in many parts of the world as primary treatment for non-gonococcal urethritis. Overall, treatment of *M. genitalium* is increasingly challenging with resistant cases requiring costly drugs, which often have limited availability (Deguchi, 2017; J.S. Jensen et al., 2016). In consequence, there is an urgent need to identify novel therapeutic targets and to develop alternative antimicrobial strategies to combat *M. genitalium* infections.

Metal acquisition systems are fundamental components of bacterial pathogens as they are essential to compete with the host for available limited resources. Accordingly, bacteria have developed diverse strategies to acquire metals within the host. For

example, many bacteria have the ability to scavenge iron from storage proteins found in the circulatory system, such as hemoglobin and transferrin, or on mucosal surfaces such as lactoferrin. To this end, they synthesize and secrete molecules with high affinity for metals, known as metallophores, to confiscate these otherwise inaccessible essential elements (Neumann et al., 2017). On the other hand, some bacteria produce potent cytotoxins meant to destroy target host cells and release the intracellular content to increase nutrient availability. Interestingly, the expression of many of these cytolysins, including the shiga toxin from *Shigella dysenteriae*, the diphtheria toxin from *Corynebacterium diphtheriae*, the exotoxin A from *Pseudomonas aeruginosa* or the *cagA* cytotoxin of *Helicobacter pylori*, responds to changes in iron availability (Litwin & Calderwood, 1993; Merrell et al., 2003). Additionally, it has been shown that *H. pylori* exploits the *cagA* cytotoxin to perturb host trafficking systems and increase metal supply at the sites of infection (Tan et al., 2009, 2011). Therefore, there is a tight connection between metal acquisition systems and bacterial virulence.

While essential for survival, freely available metals are toxic both for the host and the pathogen. Therefore, expression of metal acquisition systems is usually controlled by regulatory proteins that sense and coordinate the response to changes in metal availability. Transcriptional regulators of the Fur (Ferric Uptake Regulator) family are widespread in bacteria and they control the acquisition and storage of transition metals (Troxell & Hassan, 2013). So far, Fur regulators have been shown to coordinate gene expression in response to changes in iron (Fur), zinc (Zur), nickel (Nur) and manganese (Mur) availability (J. W. Lee & Helmann, 2007). In the presence of metal, Fur proteins bind to specific DNA sequences, known as Fur boxes, located within the promoter region of target genes and block RNA polymerase binding. Conversely, when metals are scarce, Fur proteins are unable to bind their DNA targets and transcription of the regulated genes is de-repressed. Remarkably, inactivation of the fur locus often leads to important colonization defects and attenuated virulence in many pathogenic bacteria, including *H. pylori*, *Staphylococcus aureus*, *Campylobacter jejuni*, *Listeria monocytogenes*, *Actinobacillus pleuropneumoniae*, *Bacillus cereus* and *Vibrio cholerae* (Pich & Merrell, 2013). However, so far, only few studies have addressed the response to iron starvation in mycoplasmas (Madsen et al., 2006; Yus et al., 2019) and the mechanisms controlling metal homeostasis in these bacteria remain essentially unknown.

In this study, we demonstrate that a metalloregulator of the Fur family is involved in the regulation of nickel acquisition in *M. genitalium*. A Histidine-rich lipoprotein and an

energy coupling factor-type ABC transporter system arise as the main nickel acquisition systems of this bacterium. In addition, we reveal the existence of Fur-independent regulatory pathways controlling metal homeostasis in this pathogen. The results of this study may facilitate the development of novel therapeutic strategies to control *M. genitalium* infections based on molecules targeting the metal acquisition systems identified.

CII.2 Results

CII.2.1 Global response of *M. genitalium* to iron starvation

We conducted a genome-wide RNA-Seq analysis to investigate transcriptional changes following metal depletion in *M. genitalium*. To this end, we shocked the cells with the metal chelator 2,2'-bipyridyl (DPP) and compared transcription to that of *M. genitalium* cells grown under routine culture conditions. DPP has been shown to bind iron with high affinity, although it can also coordinate other transition metals, especially when used at high concentrations. Our analysis revealed a robust response to metal starvation, with more than eighty differentially expressed genes belonging to diverse functional categories (Figure II. 1 and Supplementary Table II. 3). Remarkably, we observed a pronounced up-regulation of the molecular chaperone *dnaK* (4-fold) and the protease genes *clpB* (14-fold) and *lon* (7-fold), which are important to preserve protein integrity in bacteria. Likewise, transcription of several genes involved in DNA repair including the excinuclease *uvrC* (MG_206), the ATP-dependent helicase *uvrD* (MG_244) or the recombinase *recA* (MG_339), was induced under metal-depleted conditions. Transcript levels of the HPr kinase gene *hprK* (MG_085) and the glycerol uptake facilitator *glpF* (MG_033), involved in the regulation of carbon metabolism and sugar transport, also increased upon metal depletion. In addition, we observed a marked activation of three genes, MG_149, MG_321 and MG_439, coding for predicted lipoproteins.

Of note, we found that clusters of genes with related functions were consistently co-regulated. For instance, transcription of an operon coding for the different subunits of a putative ABC-type metal transporter system (MG_304, MG_303 and MG_302) increased by 5-fold upon iron starvation. Similarly, genes coding for a putative oligopeptide ABC-type transporter system (*oppBCDF*) were up-regulated by 4-fold. Moreover, transcription of the MG_241 and MG_242 genes, which are co-transcribed with the *uvrD* locus, was also activated 9- and 6-fold, respectively. These genes code for two proteins with two transmembrane segments, indicating a membrane-associated function.

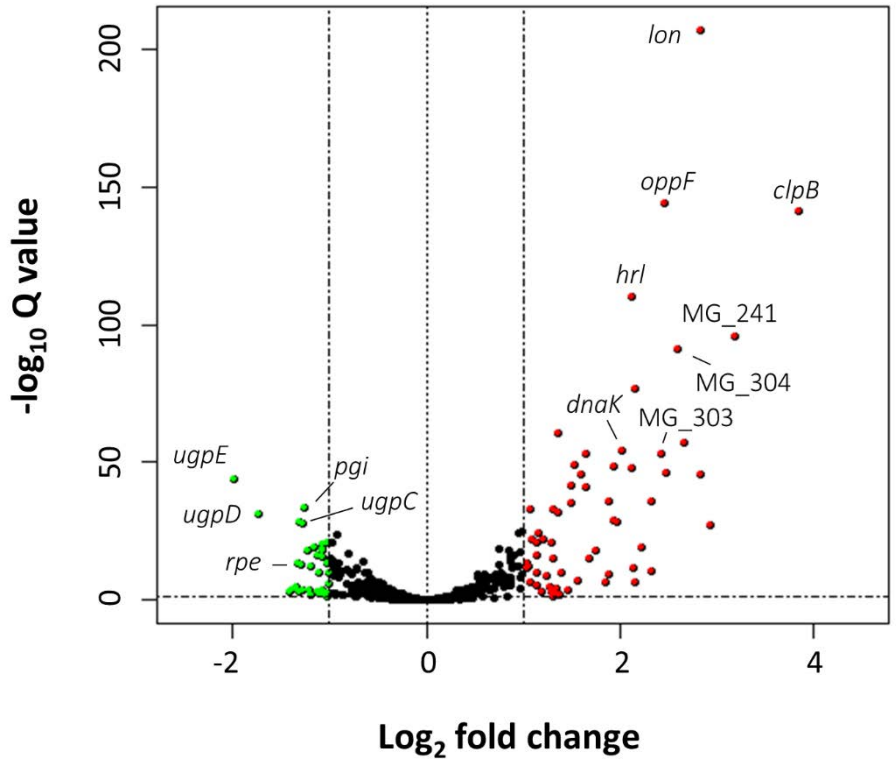

Figure II. 1. Global transcriptional changes after treatment with DPP determined by RNA-Seq. The volcano plot exhibits the differences in transcription of the treated strain with respect to the untreated G37. Each spot represents a single gene and its position depends on the log2 fold change compared to the wild-type (horizontal axis) and the statistical significance of the transcriptional changes (vertical axis). Thus, a spot located at the top right corner (as *lon*) indicates a strong overexpression and an elevated significance of the value (an extremely low p-value). Some genes are highlighted due to its biological relevance or its log2 fold change. Red spots represent transcriptional activation, while green spots are for underexpressed genes. The fold change cutoff was set at log2 ±1.

On the other hand, transcription of an operon coding for an ABC transporter system involved in glycerol-3-phosphate uptake (*ugpCAE* genes) was down-regulated by 3-fold upon the shock with 2,2'-bipyridyl. In addition, metal starvation inhibited transcription of several genes related to carbohydrate metabolism, including the glycolytic enzymes glucose-6-phosphate isomerase (*pgi*, MG_111) and fructose bisphosphate aldolase (*fba*, MG_023). Similarly, we detected decreased transcript levels of the ribulose-phosphate 3-epimerase (*rpe*, MG_112) and the UTP-glucose-1-phosphate uridylyltransferase (*galU*, MG_453) genes. Therefore, metal depletion prompts an important remodeling of the metabolic flux in *M. genitalium*. Furthermore, we found that transcription of the stringent response regulator gene *relA* was also inhibited, which is consistent with a coordinated response to nutrient deprivation. In summary, the response of *M.*

genitalium to metal starvation is both robust and diverse, and it likely involves several regulatory proteins and pathways.

CII.2.2 Role of Fur in the regulation of metal homeostasis in M. genitalium

The MG236 protein of *M. genitalium* shows sequence homology to metalloregulators of the Fur family, which controls metal homeostasis in many bacteria. Moreover, the predicted three-dimensional structure of the MG236 protein using the SWISS-MODEL protein structure homology-modelling server (Waterhouse et al., 2018) reveals a striking similarity to that of a Fur regulator from *C. jejuni* (Figure II. 2A). Our analyses indicate that *fur* in *M. genitalium* is co-transcribed with several genes coding for two ribosomal proteins (MG_232 and MG_233), the ribosomal-processing cysteine protease Prp (MG_234), the apurinic endonuclease IV Nfo (MG_235) and the unknown protein MG_237 (Figure II. 2B). To assess the possible implication of the *M. genitalium* Fur homolog in the regulation of metal acquisition, we obtained a null mutant by allelic exchange. In the resulting fur mutant strain, the MG_236 gene is replaced by the tetracycline resistance marker (*tetM*). The terminator sequence of the *dnaK* gene, identified by the TranstermHP software (Kingsford et al., 2007), was placed after the *tetM* marker to prevent overexpression of the MG_237 gene. For control purposes, we also generated a complemented strain carrying an ectopic copy of the *fur* gene. Primer extension analyses revealed that transcription of *fur* in the wild-type strain was driven by a promoter located in the upstream region of the MG_232 gene (Figure II. 2B). Therefore, in the complemented strain, we imposed transcription of the transposon-encoded *fur* copy by the MG_232 promoter. However, all of the analyzed clones overexpressed *fur* as compared to the wild-type strain (Figure II. 3). This is likely due to the presence of other promoters within the insertion site that increase transcription driven by the MG_232 promoter.

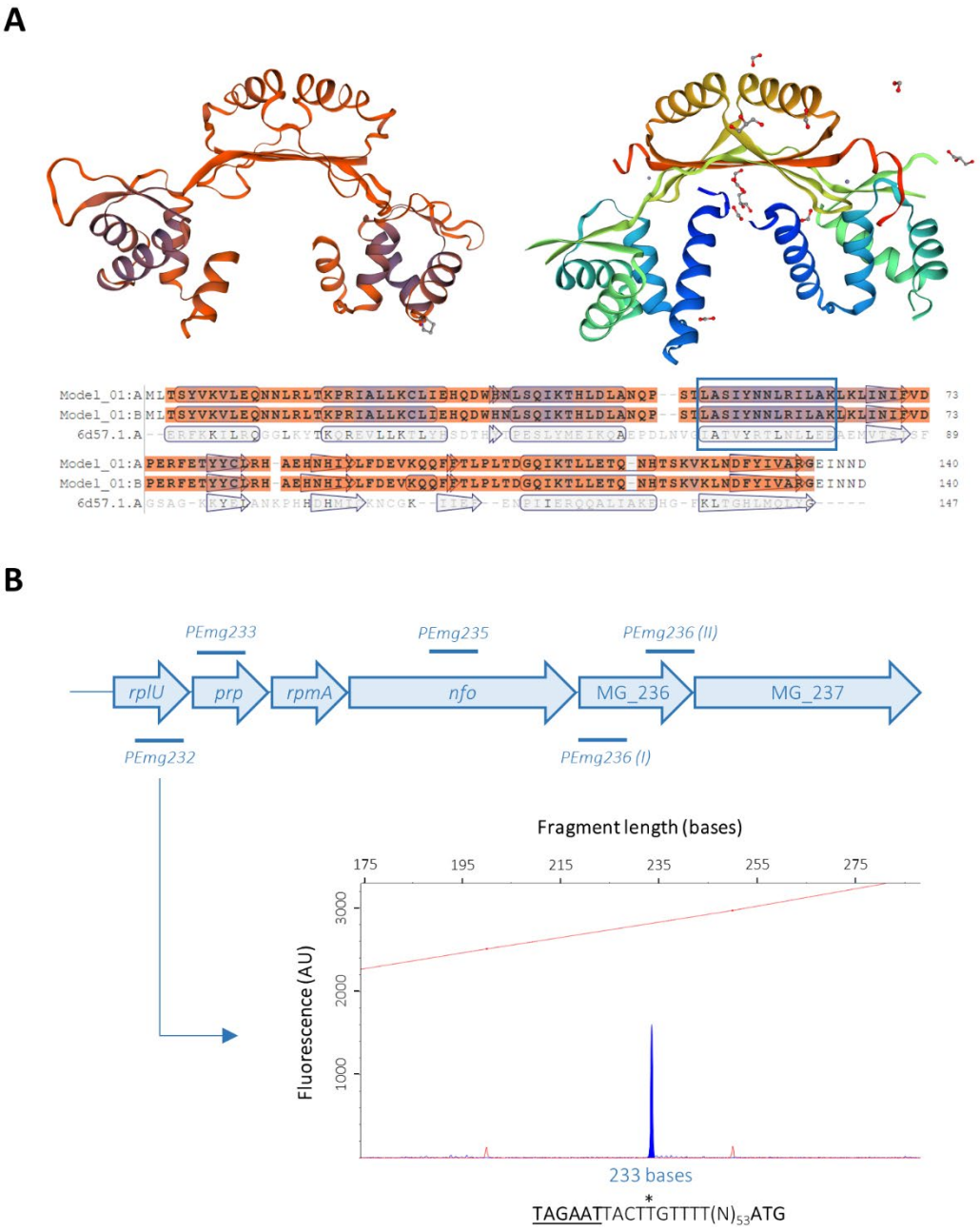

Figure II. 2. Homology of the *M. genitalium* MG236 protein to transcriptional repressors of the Fur family and determination of the MG_236 transcriptional start site (TSS). (A) The amino acid sequence below the predicted structure indicates with colors the QMEAN of each amino acid compared to the *Campylobacter jejuni fur* homolog S1 dimer (Sarvan et al., 2018). QMEAN is a composite estimator based on global (the whole structure) and local (each residue) quality estimates using four individual terms. Overall scores below -4 are considered models with low quality. The global QMEAN of MG236 modelled after the Fur homologue of *C. jejuni* is -2.83. As for the local QMEAN values attributed to each residue, reddish amino acids have a lower quality than blueish residues. The local QMEAN values are represented in the predicted homodimer, indicating the protein regions with a better alignment. The described DNA binding helix is highlighted in the amino acid sequence with a blue rectangle. **(B)** Representation of the *fur* operon in *M. genitalium* and primer extension analyses to obtain the TSS. The multiple

oligonucleotides tested are above or below the region where they hybridized. The exhibited peak was obtained with the primer PEmg232. The other oligonucleotides tested did not yield additional TSS. The Pribnow box (underlined) and the experimentally determined +1 site (marked with an asterisk) are indicated below the fluorescence peak. Red peaks represent ROX size standards and the primer extension peak is indicated in blue. Electropherogram generated with Peak Scanner.

Transcriptional changes in the *fur* mutant under standard culture conditions were also assessed by RNA-Seq. We observed the activation (~4-fold) of the histidine-rich lipoprotein gene (*hrl*, MG_149) and three genes (MG_302, MG_303 and MG_304) comprising a putative metal uptake system with homology to CbiMNQO transporter systems (Supplementary Table II. 4). As mentioned above, these genes were also up-regulated in the wild-type strain upon metal starvation. Reintroduction of an ectopic MG_236 copy to the *fur* mutant restored wild-type levels of transcription of the Fur-regulated genes (Supplementary Table II. 4). Transcript levels of the MG_237 gene were slightly lower in both the *fur* mutant and the complemented strain (~2-fold), indicating some polar effects derived from the replacement of the fur gene by the *tetM* marker. qRT-PCR analysis confirmed the Fur-regulated expression of the *hrl* gene and the putative ABC-type metal transporter (Figure II. 3).

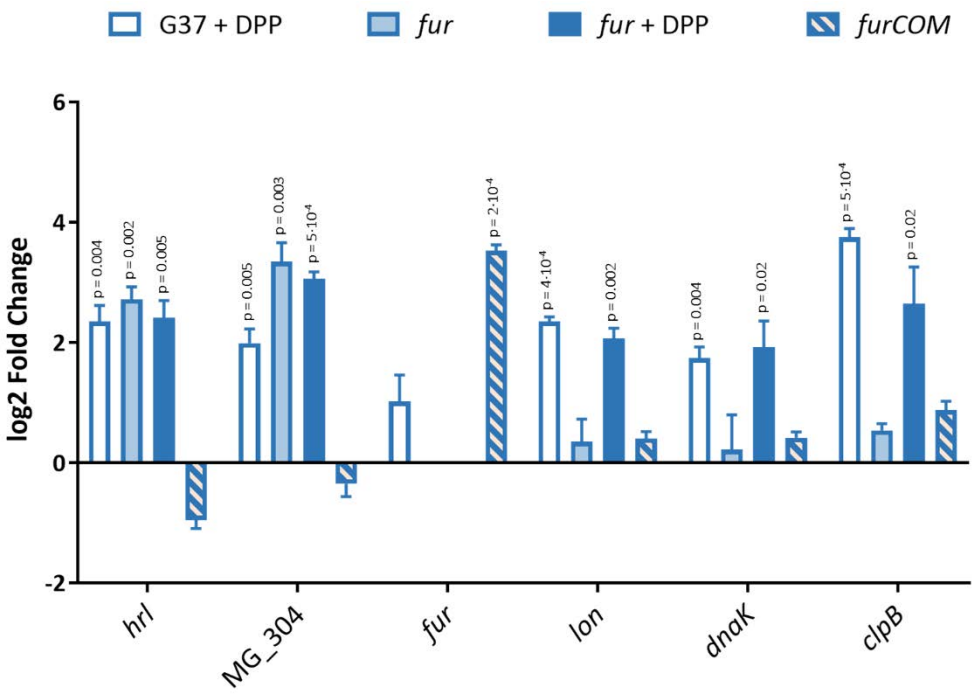

Figure II. 3. qRT-PCR analysis of *M. genitalium* G37, a *fur* mutant and its complemented strain derivative (*furCOM*) under standard growth conditions and upon the addition of 2,2'-bipyridyl. Bars represent the mean log2 fold-changes of three independent biological repeats. Statistical significance of mean fold-changes above the arbitrary cutoff >1 for biological significance was assessed using a paired *t* test. P-values are located above each column when differences to the

G37 strain are statistically significant ($p < 0.05$). The ectopic location of the *fur* gene in the complemented strain leads to a marked *fur* overexpression.

CII.2.3 Control of metal homeostasis by Fur-independent pathways

To get further knowledge on the regulatory mechanisms controlling metal homeostasis in *M. genitalium*, we investigated the existence of transcriptional changes in the *fur* mutant upon shock with the chelator DPP. Despite the absence of the transcriptional regulator, a strong transcriptional response was still observed, and we identified up to one hundred differentially expressed genes upon metal depletion (Figure II. 4 and Supplementary Table II. 5).

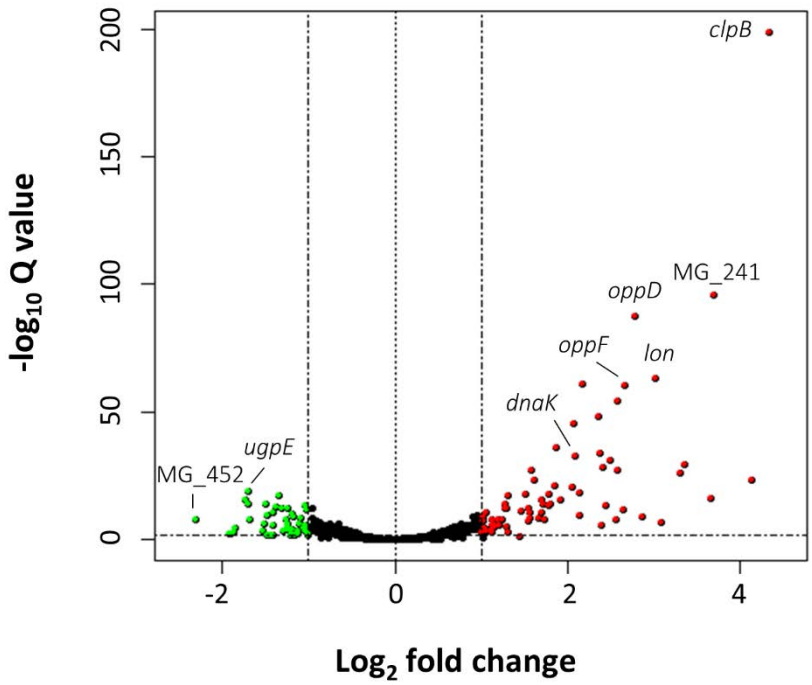

Figure II. 4. Transcriptome changes in the *fur* mutant after a shock with 2,2'-bipyridyl as determined by RNA-Seq. Volcano plot of the RNA-Seq data of the *fur* mutant: in the x axis, log2 fold changes in transcription; in the y axis, the statistical significance (a higher number represents a lower p-value). Green and red spots indicate transcriptional repression and activation, respectively. The threshold for biological significance was arbitrarily set a log2 ±1.

We observed a good overlap between the response to metal starvation in the fur mutant and that in the wild-type strain. However, transcription of *hrl* and the *cbiO* transporter operon (MG_302-MG_304) remained unchanged, indicating that activation of these genes in response to metal deprivation is entirely dependent on Fur. The existence of genes that respond to Fur and metal starvation, and many others that only respond to variations in metal availability, was confirmed by qRT-PCR analyses (Figure II. 3). Overall,

our results demonstrate the existence of a global Fur-independent response to metal starvation in *M. genitalium*.

CII.2.4 Proteomic analysis of the fur mutant

Then, we wondered whether the transcriptional changes observed in the *fur* mutant were conserved at the protein level. To this end, we used 2D-DIGE and LC-MS to examine the differences in protein abundance between the wild-type strain and the *fur* mutant under standard culture conditions. (Figure II. 5). We identified sixteen protein spots with significant changes in expression and above the 2-fold arbitrary cutoff in the *fur* mutant compared to the wild type strain (Supplementary Table II. 6). In all cases, changes were consistent with higher expression levels in the *fur* mutant. Mass spectrometric analyses determined the presence of the Hrl (MG149) polypeptide in two spots (log2 fold change 2.22 and 2.60, respectively). Remarkably, the apparent molecular mass of this lipoprotein (16 kDa or below) was lower than the expected (32 kDa); this suggests a proteolytic cleavage at the center of the protein. A similar observation was previously documented by Shimizu and coworkers (Shimizu et al., 2008).

The different subunits of the metal transporter system (MG304-MG303-MG302) were not identified in any of the analyzed spots. However, in other spots, we also identified the presence of the MG338 lipoprotein (log2 fold change 2.45 and 2.60, respectively) and the Beta subunit of the Pyruvate dehydrogenase component E1 (MG273, PdhB). In addition, we identified the Methionine sulfoxide reductase A in three different spots (log2 fold change from 2.23 to 2.49) and the 30S ribosomal proteins S7 (log2 fold change 2.54) and S9 (log2 fold change 2.19 and 2.54, respectively), in one and two spots, respectively. Analysis of five protein spots did not produce any significant identification results.

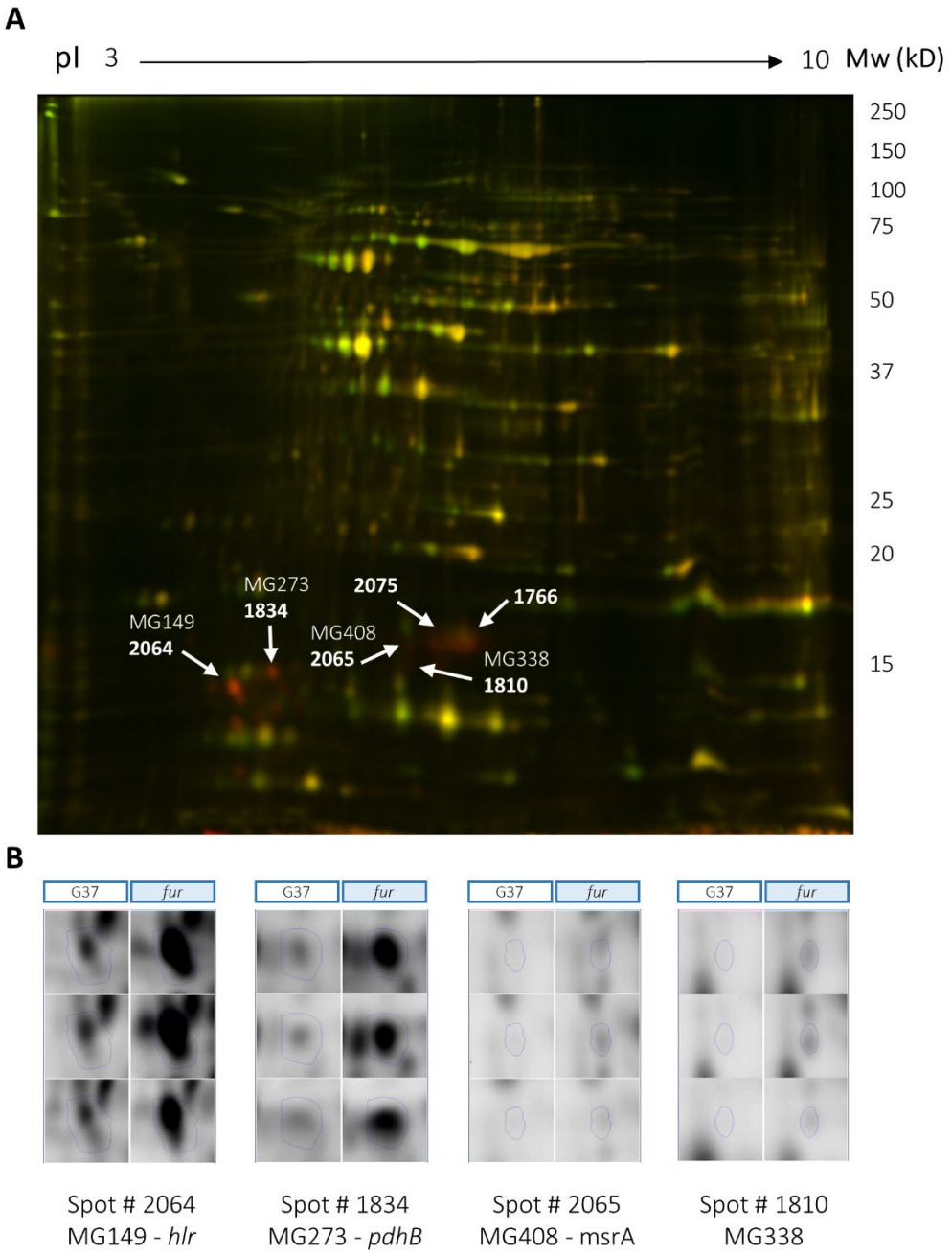

Figure II. 5. 2D-DIGE analysis of the *M. genitalium* wild-type strain and the *fur* mutant. (A) Superimposed images in pseudocolor from Cy3 (green, G37 proteins) and Cy5 (red, *fur* proteins) labelled samples run on a 2D-DIGE gel. The positions of some of the differential proteins are marked and labelled. **(B)** Fluorescence images corresponding to each of the three replicate samples of the WT and *fur* samples for some of the differential proteins identified.

CII.2.5 Identification of a regulatory element in Fur-regulated promoters

M. genitalium Fur-regulated genes seem to be controlled by σ70-dependent promoters. Of note, we recognized a conserved sequence with dyad symmetry near the putative Pribnow boxes of these promoters (Figure II. 6). To assess the possible contribution of this conserved sequence to Fur-regulation, we created a transcriptional fusion of the *hrl* promoter to the *mcherry* fluorescent marker. The resulting Hrl_{WT}:CatCh cassette was introduced to *M. genitalium* by transposon delivery. All transformants analyzed, designated G37-Hrl_{WT}CatCh, exhibited marginal mCherry fluorescence (Figure II. 7). This is consistent with low levels of expression of the mCherry marker in a wild-type background driven by the *hrl* promoter.

Figure II. 6. Identification of a putative Fur box sequence in *M. genitalium* and M. pneumoniae. MPN162, MPN433 and MPN043 are the respective homologs of MG_149 (*hrl*), MG_304 and MG_033 (*glpF*) in *M. pneumoniae*. Sequences in bold correspond to the conserved palindromic regions identified within the promoters of Fur-regulated genes of *M. genitalium* and *M. pneumoniae*. The graphic is a sequence logo generated with the conserved sequences. The overall height of each stack indicates the sequence conservation at that position. The putative -10 promoter elements are underlined. The scrambled promoter sequence used to generate the mutant strain is located below the consensus Fur box sequences and the mutated residues are marked in red.

Then, we tested the expression of the Hrl_{WT}:CatCh cassette in a fur mutant background. To this end, we first determined the insertion site of the minitransposon carrying the *mcherry* reporter in the different G37-Hrl_{WT}CatCh mutants described above (Supplementary Table II. 7). Clone 1, with the minitransposon inserted in the intergenic region within the MG_339 and MG_340 genes, was selected for further analysis. In order to allow direct comparison of mCherry expression in different strain backgrounds, the Hrl_{WT}:CatCh cassette was introduced into the *fur* mutant at the same chromosomal

location as in clone 1 by homologous recombination. In the resulting *fur*-Hrl$_{WT}$CatCh transformants, we observed mCherry fluorescence in all the clones analyzed (Figure II. 7). Using the same procedure, an *hrl* promoter with a scrambled Fur box was also introduced to the wild-type strain in the intergenic region within the MG_339 and MG_340 genes by homologous recombination. mCherry fluorescence was observed in both mutant backgrounds (Figure II. 7). Overall, these data demonstrate the participation of the identified conserved sequence in Fur-regulation.

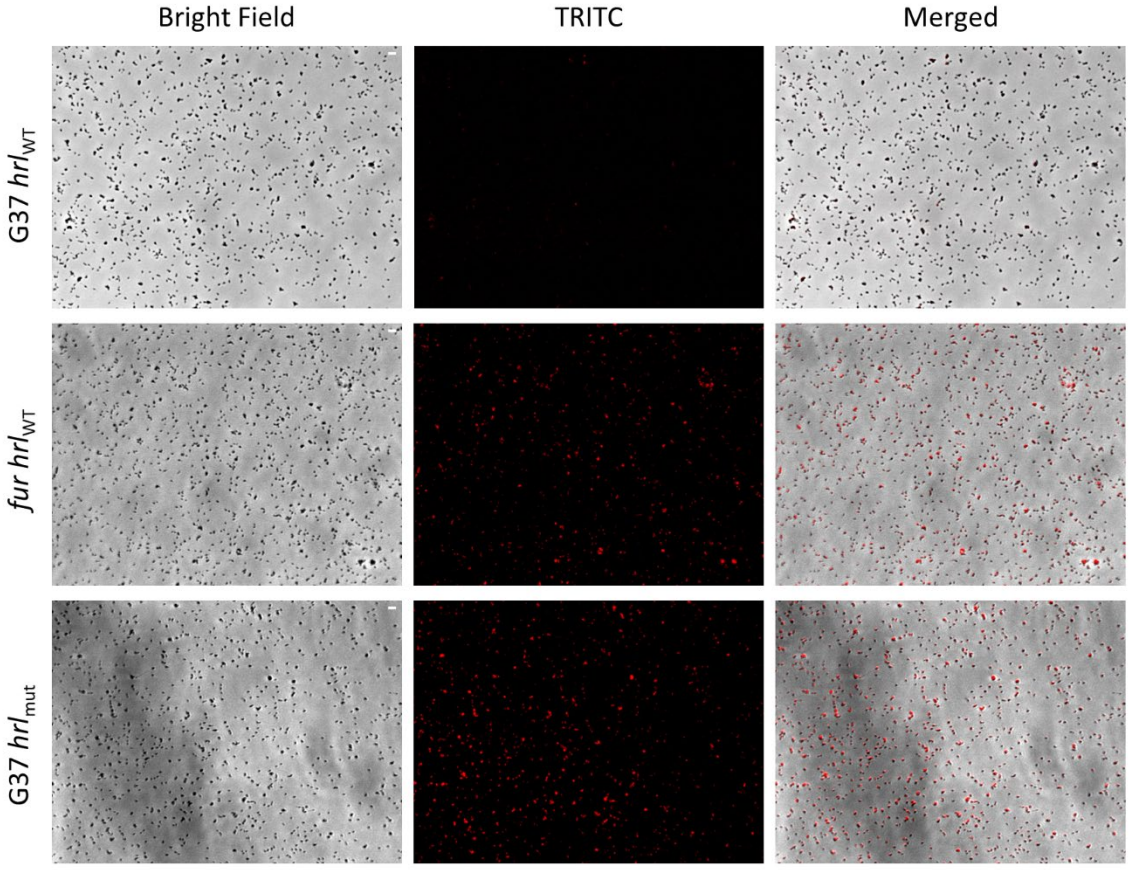

Figure II. 7. Expression of the mCherry reporter under the control of the *hrl* promoter of *M. genitalium* analyzed by fluorescence microscopy. Each row contains a series of three images corresponding to the phase contrast, the Texas Red channel and the resulting overlay, respectively. Scale bar is at the upper right corner of the bright field images and represents 2 µm.

To obtain quantitative data, we assessed *mcherry* expression in these mutants by qRT-PCR (Figure II. 8). As expected, transcript levels of the *mcherry* reporter were higher in the *fur* mutant than in the wild-type background (~6-fold). Similarly, the presence of a mutated *hrl* promoter increased transcription of the *mcherry* reporter in a wild-type background (~4-fold). In addition, we also tested the effect of the iron-chelator 2,2'-bipyridyl on *mcherry* expression. We found that *mcherry* transcription was metal

dependent in the wild-type strain (Figure II. 8). Transcriptional analysis confirms the fluorescence data described earlier.

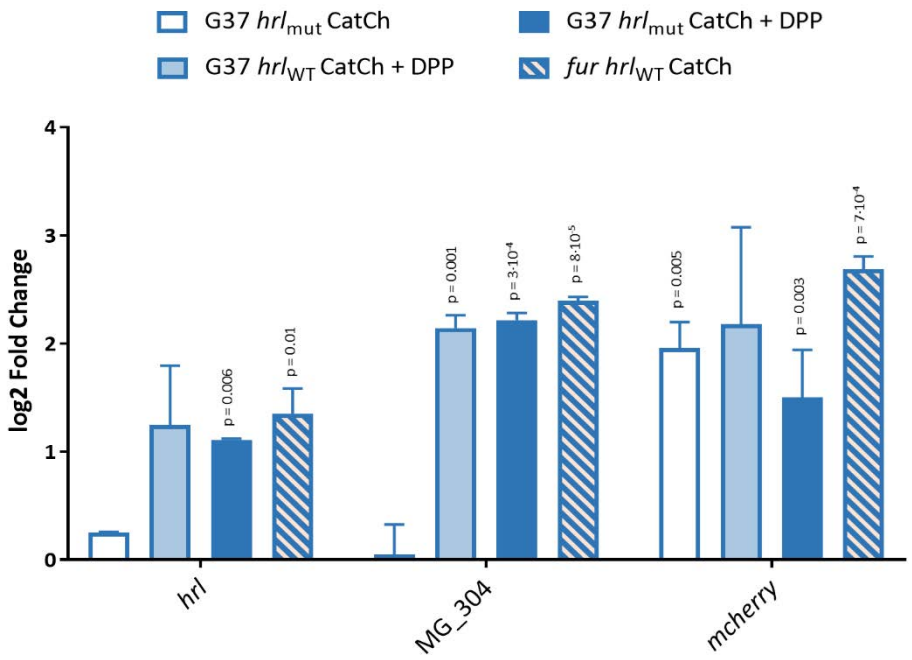

Figure II. 8. Transcription of the *mcherry* tag in the reporter strains in standard growth conditions and after addition of 2,2'-bipyridyl determined by qRT-PCR. Bars represent the mean log2 fold-changes of three independent biological repeats. Statistical significance of mean log2 fold-changes above the arbitrary cutoff >1 for biological significance was assessed with Student's T test. Statistically significant values ($p < 0.05$) are indicated above the error bars. Transcription of *hrl* and MG_304 was also analyzed for control purposes.

CII.2.6 Determination of the metallome of M. genitalium

The study of metal acquisition systems of *M. genitalium* prompted us to determine the metal content (metallome) of this pathogen under routine culture conditions. Culture medium of this bacterium is extraordinarily rich and it contains a significant amount of transition metals as supported by ICP-MS analysis (Supplementary Table II. 8). In pellets of the wild-type strain, zinc was the most abundant transition metal identified (~100µg g^{-1}), followed by iron (~20µg g^{-1}) and copper (~3 µg g^{-1}) (Figure II. 9). Other metals such as nickel, manganese or cobalt were scarce or undetectable in our analysis. Treatment of the pellets with EDTA did not reveal any difference in metal accumulation. In contrast, cells from the *fur* mutant contained about 10-fold more nickel than the wild-type strain. In contrast, the intracellular metal content was effectively restored in the complemented *fur* mutant. Cobalt was also detected at higher levels in the *fur* mutant (~5-fold), but this result varied largely among the different repeats. Therefore, our data

indicate that Fur may be implicated in the regulation of nickel acquisition in *M. genitalium*.

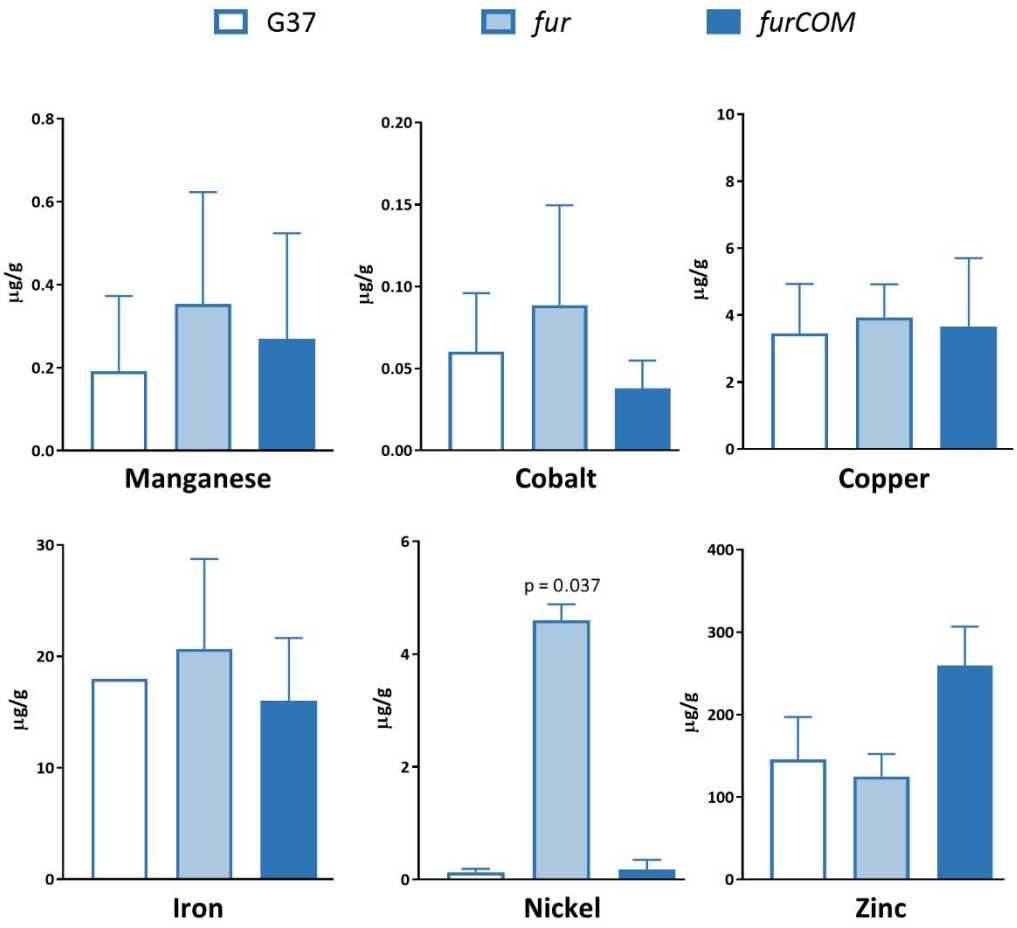

Figure II. 9. Analysis of metal accumulation in *M. genitalium* by inductively coupled plasma mass spectrometry (ICP-MS). Statistical significance of the mutant strains with respect to the G37 strain was assessed with Student's T test- Statistically significant values ($p < 0.05$) are indicated with their corresponding p-values.

CII.2.7 Effect of transition metals on Fur regulation

Finally, we tested the effect on *fur* and key Fur-regulated genes of an excess of different transition metals added to the SP-4 medium. We did not observe any transcriptional differences upon supplementation with 1 mM $CoCl_2$, $FeCl_2$ or $NiCl_2$ (Figure II. 10A). However, the addition of 1 mM ZnCl2 triggered a significant downregulation of *hrl* and a slight decrease on MG_304 transcription (Figure II. 10B). Expression of *fur* was not significantly altered in any of the conditions tested. Altogether, our data indicates that *M. genitalium* Fur might use zinc as a cofactor to regulate gene expression.

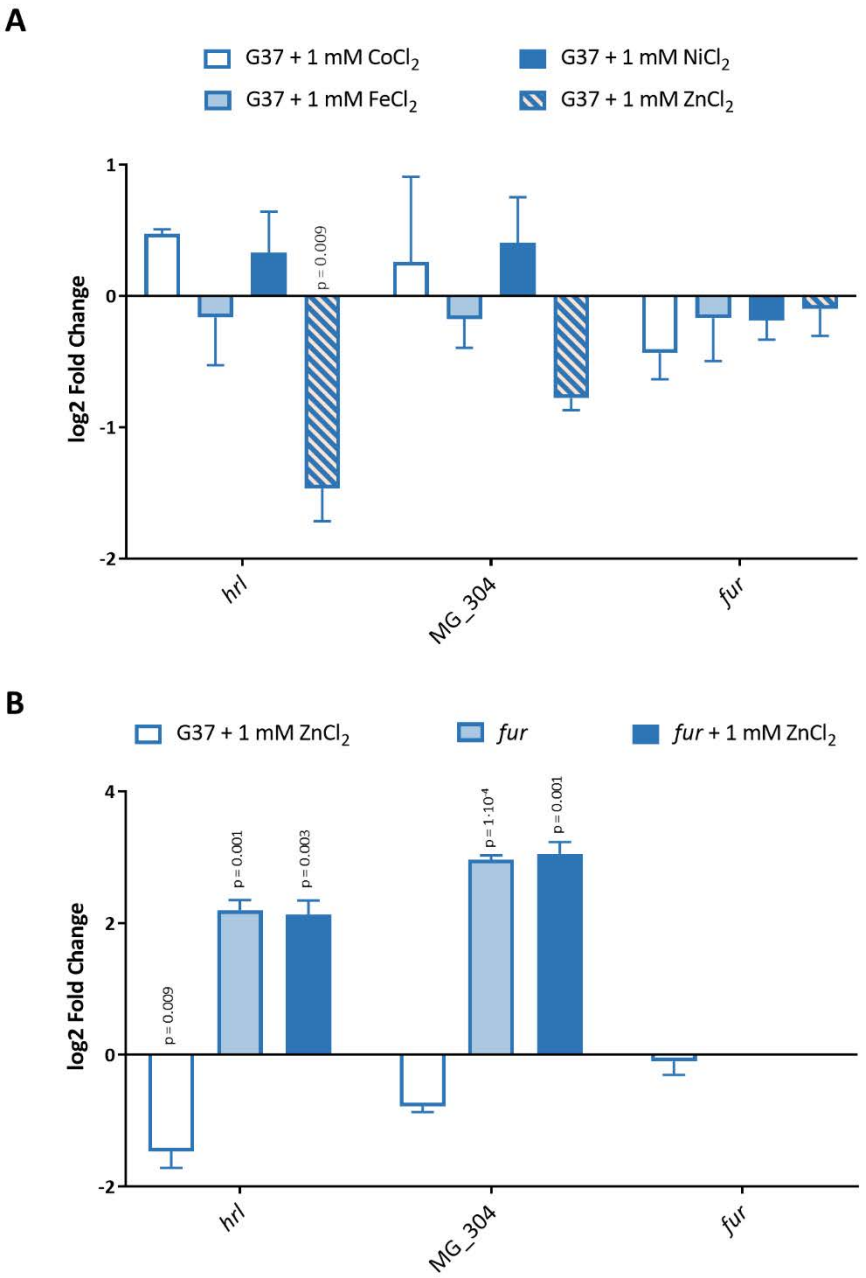

Figure II. 10. Response to an excess of metal in the G37 and *fur* strains. (A) qRT-PCR analysis of key Fur-regulated genes in the wild-type strain upon addition of 1 mM $FeCl_2$, $NiCl_2$, $ZnCl_2$ or $CoCl_2$. **(B)** qRT-PCR analysis of key Fur-regulated genes in the G37 and *fur* strains upon addition of 1 mM $ZnCl_2$. In both graphics, bars indicate the mean log2 fold-changes of three independent biological repeats. Statistical significance of mean log2 fold-changes above the arbitrary cutoff > 1 was assessed with Student's T test. Statistically significant values ($p < 0.05$) are indicated above the corresponding columns.

CII.3 Discussion

Sequestration of micronutrients represents one of the first lines of defense of the host against bacterial infection. To counteract this defensive strategy, termed nutritional immunity (Hood & Skaar, 2012), bacteria display a large repertoire of dedicated transporters to guarantee a sufficient supply of essential elements. Several years ago, Tryon and Baseman reported the ability of the respiratory pathogen *M. pneumoniae* to acquire human lactoferrin by a saturable and specific manner (Tryon & Baseman, 1987). Lactoferrin is an iron-binding protein found at high concentrations in mucosal secretions that shows antibacterial activity both in vitro and in vivo (Bullen et al., 2005). However, the same study concluded that *M. genitalium* does no bind either lactoferrin or transferrin. Therefore, despite the clinical relevance of this emerging mucosal-surface pathogen, studies addressed to identify the metal acquisition strategies of *M. genitalium* are essentially non-existent.

Herein, we show that metal starvation elicits a broad transcriptional response in *M. genitalium*, suggesting that regulation of metal homeostasis in this bacterium involves different regulatory pathways. In this sense, we found that iron regulates transcription of several chaperone and protease genes under the control of the HrcA repressor, which coordinates the heat stress response in *M. genitalium* (Musatovova et al., 2006). Similarly, transcript levels of *relA*, a major regulator of the nutrient-starvation response in bacteria (Hauryliuk et al., 2015), decrease upon metal depletion. On the other hand, we found a significant activation of an operon coding for an oligopeptide permease (Opp) transporter system (MG_077-MG_078-MG_079 and MG_080). Oligopeptide and dipeptide permeases have been found to be significantly up-regulated during iron starvation in other pathogenic bacteria (Hempel et al., 2011; Merrell et al., 2003) and they have been implicated in metal acquisition in *S. aureus* (Hiron et al., 2010) and *E. coli* (Létoffé et al., 2006). Moreover, some oligopeptide-binding proteins can accommodate heme in its binding pocket (Tanaka & Pinkett, 2019), hence providing a new strategy to acquire iron from the host. In addition, the oligopeptide transport ATP-binding protein OppD has been shown to be critical for survival of the avian pathogen *Mycoplasma gallisepticum* within the respiratory tract (Tseng et al., 2017), supporting the relevance of oligopeptide permeases in mycoplasma infection.

Additionally, our results also show that metal depletion activates transcription of the glycerol uptake facilitator gene (*glpF*). This finding is notable because glycerol

metabolism is involved in hydrogen peroxide production in mycoplasmas and it represents a widespread virulence factor of these unique pathogens (Großhennig et al., 2013; Hames et al., 2009; Pilo et al., 2005). Therefore, an increased glycerol uptake capacity could enhance the cytotoxic potential of *M. genitalium* under metal limited conditions. On the other hand, we found that metal starvation inhibits transcription of several genes involved in carbohydrate metabolism. Moreover, we also observed decreased transcript levels of the gene coding for the Ribulose-phosphate 3-epimerase, an enzyme that has been shown to use zinc as a cofactor for catalysis along with cobalt and manganese (Liang et al., 2011). Thus, our results indicate that metal deprivation prompts an important metabolic reprogramming in *M. genitalium*, with altered expression of several genes encoding for putative transporters and metabolic enzymes.

The MG_236 gene of *M. genitalium* codes for a Fur homologue, which are widespread metalloregulators controlling metal homeostasis in bacteria. Other human mycoplasmas including the respiratory pathogen *M. pneumoniae* (MPN329) and the STI pathogen *Mycoplasma penetrans* (MYPE1200), also contain putative Fur proteins. In a previous report, the MG_236 gene was classified as essential for *M. genitalium* growth under laboratory culture conditions (Glass et al., 2006). However, we successfully deleted the MG_236 gene by allelic exchange using standard procedures. Transcriptional analysis of the *fur* mutant revealed the activation of a gene coding for a Histidine-rich lipoprotein (MG149) and a putative metal transporter system with homology to CbiMNQO uptake systems (MG302-MG303-MG304), which are putatively implicated in cobalt import in association with the cobalamin (vitamin B12) biosynthetic pathways. The *hrl* gene was previously shown to be markedly induced upon hyperosmotic shock in *M. genitalium* (W. Zhang & Baseman, 2011b). The overlap between osmotic stress and metal starvation in bacteria has been previously documented (Gancz et al., 2008; Gancz & Merrell, 2011). In the upstream region of the Fur-regulated genes, we recognized a conserved sequence with dyad symmetry with the consensus gcTTATTTtgAA-N3-TTcaAAATAAgc located near the predicted -10 promoter elements (Figure II. 6). Proximity of the predicted Fur binding sites to key promoter elements is in agreement with the classic repressor role of Fur regulators, which bind to the DNA and prevent RNA polymerase binding. Of note, the putative Fur binding sites identified in *M. genitalium* differ considerably from the conventional Fur boxes originally described in E. coli (De Lorenzo et al., 1987; Escolar et al., 1998). However, divergent Fur operators have been identified in mycobacteria and streptomycetes (Milano et al., 2001). Despite the presence of a Fur metalloregulator in *M. genitalium*, our analyses

demonstrate that the transcriptional response to metal deprivation in this emerging pathogen is mainly Fur-independent.

In the respiratory pathogen *M. pneumoniae*, the presence in the genome of a pseudopalindromic sequence resembling the putative Fur boxes identified in this work was already pinpointed in two comprehensive transcriptional studies (Güell et al., 2009; Yus et al., 2019). Candidate Fur binding sites in *M. pneumoniae* are located in the upstream region of the MPN162 (*hrl* homolog), MPN433 (*cbiO*) and MPN043 genes (*glpF*) (Figure II. 6). Fur overexpression in M. pneumoniae induces transcriptional changes in genes containing the identified Fur boxes (Güell et al., 2009). Unlike in *M. pneumoniae*, our results indicate that *glpF* expression is regulated by metal deprivation but not Fur in *M. genitalium*, which likely reflects the exquisite adaptation of these human pathogens to their respective infection niches.

On the other hand, we demonstrate that *M. genitalium* cells grown in a nutrient rich environment preferentially accumulate zinc, iron and copper, likely through constitutive metal transporters. This metal accumulation profile is similar to that described in *E. coli* by Zhao and co-workers (S. Zhao et al., 2018). According to this report, *E. coli* and Enterococcus faecium acquire preferentially iron, manganese and zinc, while nickel and cobalt are predominant in *S. aureus* and *Klebsiella pneumoniae*. Remarkably, ICP-MS analysis of a *M. genitalium fur* mutant revealed increased concentrations of nickel compared to the wild-type strain, establishing an important role for Fur in the acquisition of nickel in this urogenital pathogen. In addition, we found that high levels of zinc inhibit the expression of genes under the control of Fur, suggesting that it might function as a cofactor of this transcriptional regulator in *M. genitalium*. This is in agreement with a recent report, showing that thiolutin, which binds zinc with high affinity, modifies transcription of Fur-regulated genes in *M. pneumoniae* (Yus et al., 2019).

Nickel participates in different biological processes and they are considered essential micronutrients. Nickel is a cofactor of urease, Ni-Fe hydrogenases some superoxide dismutases, enzymes that do not seem to be present in *M. genitalium*. However, *M. genitalium* is a facultative anaerobic organism, which is relevant because many Ni^{2+}-containing enzymes are active under low-oxygen conditions. Thus, we anticipate that *M. genitalium* encounters oxygen depletion during infection, which opens the possibility to the existence of unknown Ni^{2+}-containing enzymes in this bacterium.

A search for conserved domains within Hrl using the MOTIF tool reveals up to 13 hits, most of them belonging to known proteins involved in nickel, cobalt and zinc transport such as RcnA, ZnuA, CbtA, ZntC, CzcD or Zip (Supplementary Figure II. 1). For example, RcnA belongs to the Nickel/Cobalt Transporter (NicO) Family and it is believed to catalyze Co^{2+} and Ni^{2+} efflux in E. coli (Rodrigue et al., 2005). As mentioned earlier in this text, the putative metal transporter regulated by Fur in *M. genitalium* shows homology to CbiMNQO uptake systems (Rodionov et al., 2006). The CbiMNQO protein complex belongs to the ECF (Energy Coupling Factor) subtype of ABC transporters, which are composed of two ATP-binding cassette ATPases (EcfA-MG304 and EcfA'-MG303) and a transmembrane coupling subunit (EcfT-MG302). These three core ECF proteins should interact with cognate substrate-binding subunits (EcfS), which confer ligand specificity. In *M. genitalium*, no *ecfS* gene has been identified in the vicinity of the metal responsive ECF-type operon identified in this study. Therefore, it is tempting to speculate that Hrl may function as a substrate-binding subunit of the CbiMNQO-like uptake system. Alternatively, although metallophores have not been described in mycoplasmas, Hrl may exhibit metallophore-like activity and cooperate with a yet to be identified EcfS protein to facilitate nickel uptake. Histidine rich proteins are present in other mycoplasma species, where they are usually annotated as ZIP zinc transporter proteins. Experiments are under way to establish the exact role of Hrl and the CbiMNQO-like transporter in metal uptake.

Given the tight link between metal acquisition systems and virulence, Fur-regulated proteins constitute good therapeutic candidates for drug development. Transporters from the ECF family, which are not present in humans, have been proposed as potential antimicrobial targets. Assessment of the likelihood to find a selective, low-molecular weight molecule that binds with high affinity to the target, which is usually referred to as druggability assessment, identified up to twelve druggable pockets within a reference ECF transporter system (Bousis et al., 2019). An alternative approach to prevent metal acquisition could be either the inhibition of binding of the S-components to the ECF module or the inhibition of their ability to bind metals. In this sense, compounds inhibiting Hrl activity may also prevent *M. genitalium* growth in vivo. Of note, it has been shown that Hrl from *M. genitalium* (Shimizu et al., 2008) and *M. pneumoniae* (Shimizu et al., 2007) elicit a prominent pro-inflammatory response and stimulate cytokine production through activation of NF-KB. Therefore, Hrl represents important virulence protein and a key therapeutic drug target of *M. genitalium*. In addition, Fur regulators are absent in eukaryotes and they also constitute attractive antibacterial targets. Several

attempts have been made to develop therapies based on inhibition of Fur activity in other pathogens. Remarkably, several small peptides that inhibit Fur function have been shown to decrease pathogenic *E. coli* strain virulence in a fly infection model (Mathieu et al., 2016).

In summary, in this study we describe the Fur regulon of *M. genitalium* and identify the proteins mediating nickel acquisition in this emerging human pathogen. Furthermore, our results show a complex, multilayered transcriptional response to metal deprivation in this bacterium, suggesting a central role for metal regulatory systems in the survival of this urogenital pathogen within the host.

GENERAL DISCUSSION

GD.1 Cell division in *M. genitalium*

GD.1.1 MraZ as a transcription factor

Previous publications in *E. coli* (Eraso et al., 2014) and *M. gallisepticum* (Fisunov et al., 2016) laid the groundwork for the present study, as the results in this work show, univocally, that *mraZ* codes for a transcriptional regulator of the division and cell wall (dcw) operon. Interestingly, although both referenced studies agreed about MraZ as a transcription factor, the two reports came to opposite conclusions about the role of the protein as a regulator: it was a transcriptional repressor of the cluster according to Eraso and his coworkers and a transcriptional activator for Fisunov and his colleagues.

MraZ is a widely conserved protein among bacteria, not only in sequence but also in its position: it is always the first gene of the dcw operon (Vicente et al., 1998). Consequently, it does not seem probable that its role in *E. coli* would be much different than its role in *B. subtilis*, *S. aureus* or *M. gallisepticum*. Nonetheless, the two studies on *mraZ* did not offer a complete picture of its function, as overexpression of this gene on *E. coli* is toxic and the mutant of *mraZ* in *M. gallisepticum* was not characterized. Therefore, both reports were offering a different but perhaps compatible perspective of depleting or overproducing MraZ, respectively.

In this work, a mutant strain lacking the *mraZ* gene is analyzed, as well as several strains carrying and ectopic copy of this transcription factor and overexpressing it at different levels. The derepression of the operon upon depletion of *mraZ* is observed, as Eraso reported; however, an overexpression of *mraZ* indeed yielded an activation of the division cluster. Therefore, these results are in agreement with both research works and provide a more probable outcome for an almost universally conserved protein in the known bacteria world. The results here presented suggest that *mraZ* is a transcriptional repressor, due to the large upregulation observed when it is knocked out and the distinctive phenotype associated with its deletion. However, it is not a classical repressor and it cannot be ruled out that it might also function as an activator of the cluster under certain unknown conditions.

There are some examples of transcriptional repressors that can switch to auto-activators depending on the cellular context. One of the more remarkable and fascinating cases is the CI repressor of the lambda phage (Figure GD. 1). This protein has a key role in the switch from lysogenesis to lytic cycle. In the prophage stage, CI prevents the lysis by

repressing the two promoters linked to the cycle as it was in detail described by Maurer, Meyer and coworkers (Maurer et al., 1980; Meyer et al., 1980; Meyer & Ptashne, 1980). It had been previously reported that CI was able to modulate its own transcription, acting as an activator in low concentration and as a repressor once a certain threshold was reached (Ptashne et al., 1976). In the same study, it was also noted that the repressor was efficiently transcribed but inefficiently translated, due to the lack of a strong ribosome binding site in the mRNA header.

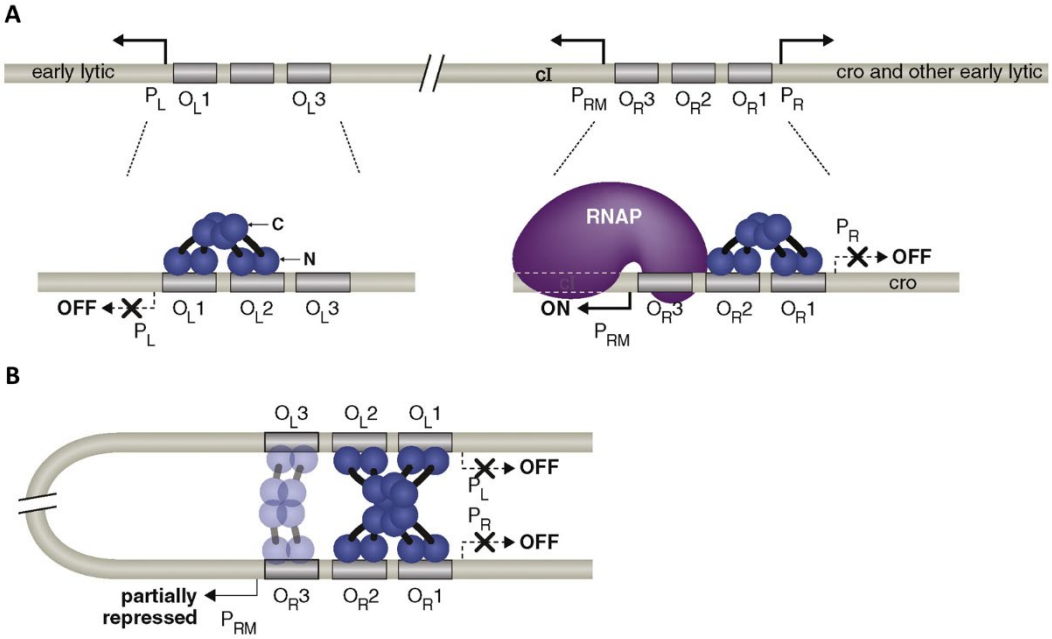

Figure GD. 1. Transcriptional repression or activation mediated by CI depending on its oligomerization and concentration. (A) The transcription factor has high affinity with the O_L1 and O_R1 regions. It can bind another dimer to the O_L2 and O_R2, respectively, due to its ability to form higher-order oligomers cooperatively. When it is bound to these four operator sites, it represses the transcription of the transcription factor Cro and the genes involved in the early lytic cycle, while it enhances its own transcription from the P_{RM} promoter. **(B)** Once there is a high concentration of CI, the two tetramers (the one bound at the O_R region and the one at the O_L region) can interact forming an octamer that cause a loop of DNA, as these regions are spatially separated by 2.4 kb. Then, two new dimers of CI are able to bind to the O_R3 and O_L3 operator sites. Once there is a CI dimer bound to O_R3, the transcription from PRM is stopped. Therefore, CI is able to regulate its own transcription depending on its concentration. Image adapted from Hochschild & Lewis, 2009.

The switch from activator to repressor of its own expression is related to the affinity to the operator sites. The phage contains six operators in two regions separated by 2 kb: O_R1, O_R2 and O_R3 at the O_R region; and O_L1, O_L2 and O_L3 at the O_L region. Both O_L1 and O_R1 are high affinity sites. Once a dimer of CI is bound to these two sites, it can cooperatively bind another dimer to O_L2 and O_R2 (Johnson et al., 1979), thus forming

two tetramers. When these four sites are occupied, the two tetramers are able to octamerize by forming a DNA loop between O_R and O_L and transcription of the lytic genes is totally repressed (Dodd et al., 2001). This loop can further increase the transcription of cI (Anderson & Yang, 2008). It is in this situation when a tetramer of CI can bind to O_R3 and O_L3 (the two sites with minor affinity) and shut down the promoter P_{RM}, which drives its own transcription. Thus, transcription of CI depends on the concentration, oligomerization and affinity with its operator sites.

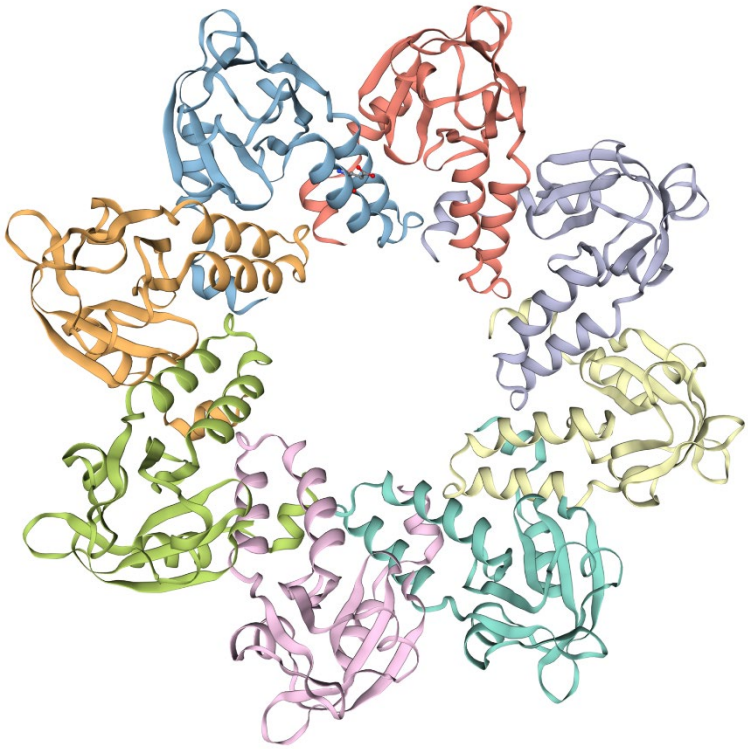

Figure GD. 2. Predicted model of the MraZ protein of *M. genitalium* using the published structure of *M. pneumoniae* as a template using the SWISS-MODEL tool. MraZ forms a homo-octamer (each monomer is highlighted with a different color) as its homologue in *M. pneumoniae*.

Like the CI transcription factor, it has also been reported that MraZ is able to multimerize (Figure GD. 2). The crystal structure of this transcription factor was firstly described in *M. pneumoniae* (Chen et al., 2004) and is almost identical to the one coded in *M. genitalium* (their sequence identity is above 80%). In that publication, it was stated that MraZ formed an octameric ring-shaped structure. However, the structure of this protein in *E. coli* (which holds a 29% sequence identity with the one from *M. pneumoniae*) suggested that it oligomerizes as a dodecamer (M. A. Adams et al., 2005). In the recent study of MraZ in *M. gallisepticum* (Fisunov et al., 2016), Fisunov and his collaborators investigated further the multimerization of MraZ and, after performing a size exclusion chromatography of the native complex, they came to the conclusion that the free MraZ

protein formed a dodecamer, but when combined with an oligonucleotide containing its promoter region, it was able to form octamers and 24-mers, depending on its low or high concentration, respectively. As the highly conserved promoter region of *mraZ* has three MraZ binding boxes, they proposed that each MraZ octamer binds to one box, thus forming a 24-mer complex when the three octameric rings are bound to its box.

Therefore, as it occurs with the CI protein of the lambda phage, it is possible that the impact of MraZ on the operon transcription is depending on its concentration and, consequently, its oligomerization. A thoroughly designed experiment analyzing the operon transcription with several degrees of mutations in its binding sites combined with also different levels of *mraZ* gene expression could shed some light into this matter. Due to the dispensability of the operon in this species as well as that the overexpression of *mraZ* has no discernible toxic effect, *M. genitalium* provides excellent conditions to further investigate this protein.

GD.1.2 The conservation of the *dcw* operon in *M. genitalium*

The division and cell wall operon in Mollicutes is already extremely reduced when compared to other microorganisms. The lack of cell wall as well as its low predicted gene redundancy might justify the fact that the cluster in these unique organisms consists of only four genes (Y. Zhao et al., 2004). In addition, in some Mollicutes as *Ureaplasma urealyticum* and *Mycoplasma mobile*, the operon is further reduced as there is not even a copy of *ftsZ* in their chromosome (Margolin, 2000).

FtsZ was also reported to be dispensable for in vitro growth in *M. genitalium* (Lluch-Senar et al., 2010). Moreover, an essentiality study in the closely related *M. pneumoniae* also revealed that the four genes of the operon were not essential, although *mraZ* and *mraW* were characterized as fitness genes, suggesting that their truncation had more impact on cell duplication that the interruption of the MG_223 homolog and *ftsZ* (Lluch-Senar et al., 2015). This is in agreement with our results, as the deletion of *ftsZ* has no discernible phenotype, while the *mraZ* and *mraW* mutants exhibited a notable growth delay. This, as already discussed in Chapter I, highlights the importance of regulation.

Moreover, we were able to delete the whole *dcw* operon. Although the characterization of this mutant exposed a slight impairment of cell division, this strain confirmed that neither of the four genes of the cluster is necessary for *in vitro* growth. These results indicate that the motile machinery is probably the primary force driving cytokinesis in

M. genitalium. The close coordination between motility and cell division has been thoroughly studied in *M. pneumoniae* (Hasselbring et al., 2006; Krause & Balish, 2001; Seto et al., 2001), although the viability of *M. genitalium* gliding-deficient strains established that motility is not essential for cytokinesis (Burgos et al., 2007; Pich et al., 2006).

Thus, why is the *dcw* operon conserved in such a reduced genome? It could be explained by the existence of phase variants: *M. genitalium* cells can become nonadherent depending on the spontaneous recombination of its two main adhesins, coded by the genes *mgpB* and *mgpC* (Burgos et al., 2006). Deprived of their characteristic cytoskeleton, nonadherent cells would need the *dcw* operon to divide. This would be critical *in vivo*, as it has been described that *M. genitalium* changes its two main adhesins to avoid recognition by the host immune system (Iverson-Cabral et al., 2006, 2007; Ma et al., 2007, 2010). Some of these changes might result in reversible nonadherent variants (Burgos et al., 2018) that would require FtsZ in order to remain viable until they become adherent again. Remarkably, we tried several times to delete the adhesins by homologous recombination in the *ftsZ* mutant and we were unsuccessful. Therefore, it might be not possible to create a nonadherent strain in a *ftsZ*-null background.

The long-lasting cytokinesis reported in the *M. genitalium ftsZ* mutant (Lluch-Senar et al., 2010) could also help to explain both the conservation and the role of the tubulin-like protein in this bacterium. Although its deletion seemed to have no effect on the growth rate, it was stated that cytokinesis in the mutant was almost 4-fold slower than in the wild-type strain (3.7 h vs 1.07 h, respectively). The defects on cytokinesis are corroborated in this work, as it appears that the *ftsZ* mutant struggles to separate the two daughter cells in the late stages of cytokinesis, resulting in a slight increase in the percentage of dividing cells as well as in the length of the cells in this stage. This is not relevant *in vitro*, but could be of paramount importance *in vivo*, as it was stated that dividing cells in the closely related microorganism *M. pneumoniae* did not move (Hasselbring et al., 2006). Accordingly, an impaired cytokinesis could have a considerable impact on *M. genitalium* viability and persistence *in vivo*.

Overall, although neither *ftsZ* nor the whole *dcw* cluster are essential for in vitro growth, their conservation in such a reduced genome strongly suggests a relevant role of their gene products *in vivo*. As we demonstrate by fluorescence microscopy, there is an interplay between the motile machinery and the proteins of the division system coded

in the *dcw* operon. The deregulation or the complete absence of these proteins are probably the causes of the observed growth alterations in the *mraZ* and *dcw* mutants, as in both cases the balance of the two division systems is compromised.

GD.2 A complex metal regulation

The transcriptional changes detected in *M. genitalium* after inducing metal-starvation with 2,2'-bipyridyl indicate that the response of this microorganism goes well beyond the metalloregulator Fur. There is an alteration in the expression of genes that code for proteins associated with other regulatory pathways, as DnaK, Lon or ClpB that are linked to the heat-shock repressor HrcA (Musatovova et al., 2006) or the stringent response regulator RelA. On the contrary, the transcriptional response to the loss of *fur* is limited to four genes.

This disparity between the range of the transcriptional responses in the samples treated with 2,2'-bipyridyl and the *fur* strain is considerable. However, so it is the stress difference: in the latter the absence of the metalloregulator is putatively creating a false deficiency of one metal, whereas the use of the unspecific chelator is effectively depleting several metals. In *E. coli*, a thoroughly well-characterized bacterium, there are thirteen described metalloregulators, four of them being global regulators (which affect the transcription of a large number of genes involved in several functions) and the other nine described as local regulators (regulating only one gene or a small transcription unit) (Yamamoto, 2014). It is highly probable that *M. genitalium* counts with more than one metal sensor that will be triggered upon DPP treatment. In addition, it has been reported that bacteria can activate alternative pathways in response to metal limitation, as a functional substitution attempt (Merchant & Helmann, 2012).

GD.2.1 Potential implications for virulence

The addition of DPP had a deep impact on the transcription of many genes (Figure GD. 3). The changes on the energy metabolism that indicated a swift to glycerol metabolism (associated with the potential increase in H_2O_2 production) has been already addressed on the Chapter II discussion. However, the production of peroxide is not the only virulence factor that has been described in mycoplasmas.

The importance of lipoproteins in the wall-less mycoplasmas is critical and it has a tight association to its virulence (McGowin, Liang, et al., 2009; McGowin & Totten, 2017; Rawadi & Roman-Roman, 1996; Shimizu et al., 2008). Remarkably, it has been evidenced that they can change its lipoprotein profile due to stress, as an interaction with host cells (Goret et al., 2016; Hallamaa et al., 2008) or during an osmotic shock (W. Zhang & Baseman, 2011a).

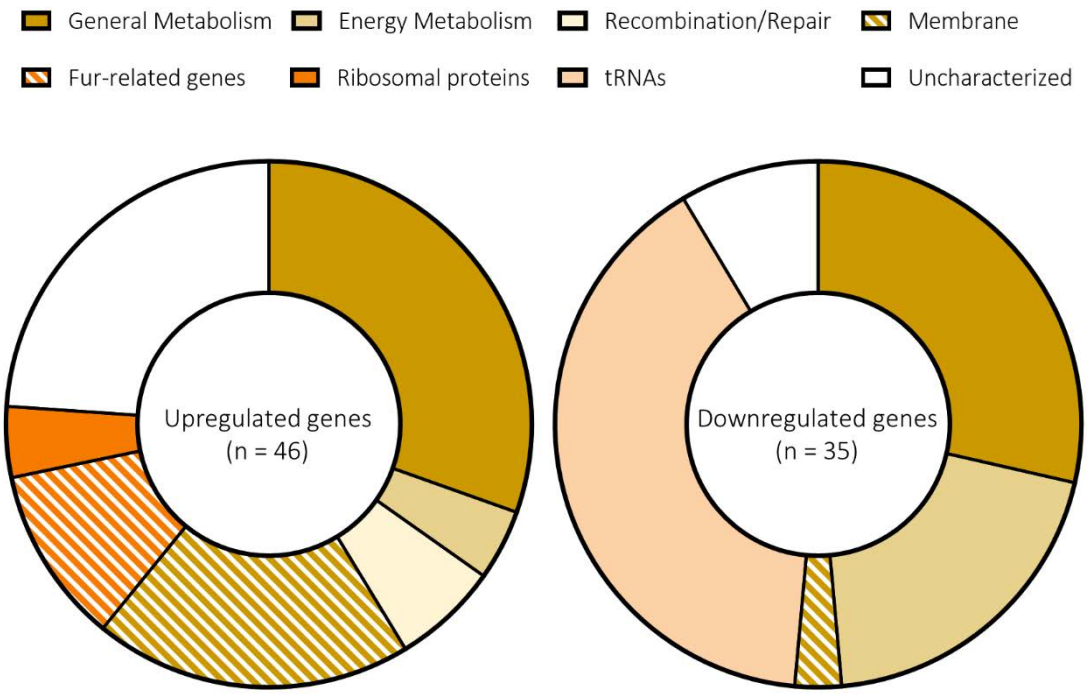

Figure GD. 3. Functional classification of the genes which expression was affected by 2,2'-bipyridyl in the G37 strain. The genes above or under the arbitrary threshold for biological relevance were classified with regards to the assigned functions of the proteins they code to. Genes are divided with respect to their upregulation or downregulation upon addition or the chelator.

In this work, we demonstrate that potentially there is a profound change in the surface lipoproteome of *M. genitalium* upon metal deprivation. As evidenced in Figure GD. 3, metal starvation induces the transcriptional activation of a large subset of genes coding for membrane-associated proteins. This could be of great relevance in *M. genitalium* pathogenesis due to the aforementioned relation between lipoproteins and virulence. In fact, *hrl*, one of the targets of Fur in *M. genitalium*, codes for a potential virulence factor, as it was evidenced that Hrl activates the transcription factor NF-κβ (Shimizu et al., 2008). In addition, the observed upregulation of *glpF* (which codes for the glycerol uptake facilitator GlpF) might led to an increased peroxide production. Therefore, *M. genitalium* could be potentially increasing its virulence when it is subjected to a metal depletion stress.

Interestingly, the mRNA associated with many MgPa repeats was remarkably upregulated. This phenomenon was not observed in the other RNA-Seq analysis performed in this study. Thus, this suggests that the strong activation of these regions is part of the response to the metal depletion. As these regions are scattered among the genome and the observed MgPa activation is widespread, its increased transcription could be because of the triggering of a specific activator. The consequences of their

upregulation and the possible role in the generation of phase and antigenic variants are unknown.

GD.2.2 Transcription factor-independent regulation

There are at least eight putative transcription factors in *M. genitalium* (see GI.3.2.1 Transcription factors in *M. genitalium*). Notably, despite the vast range of the response to the chelator, only the transcription of *fur* was differentially expressed when compared to the untreated sample (Table GD. 1).

Table GD. 1. Transcriptional alteration of eight putative transcription factors of *M. genitalium* upon treatment with DPP determined by RNA-seq. Only *fur* has a biologically significant log2 fold change, indicated in bold.

Transcription factor (Locus tag)	log2 fold change	p-value
gntR (MG_101)	-0.090	0.412
whiA (MG_103)	-0.103	0.576
spx (MG_127)	0.297	0.007
hrcA (MG_205)	-0.378	0.003
mraZ (MG_221)	-0.061	0.647
fur (MG_236)	**1.033**	$5.4 \cdot 10^{-15}$
sig20 (MG_428)	-0.385	0.007
dnaA (MG_469)	-0.515	0.001

Interestingly, *fur* was upregulated in this context while the rest of its operon remained unaltered, except for the MG_237 gene, which is located immediately downstream of *fur*. Although this could be attributed to the existence of an undiscovered promoter, the primer extension results and the transcriptional profile of the operon in a metal-depleted background rule out this option (Figure GD. 4). After a close examination of the transcription of the *fur* operon after a 2,2'-bipyridyl shock, it seems that the increased expression of *fur* and MG_237 could be attributed to a reduced degradation (or a higher stability) of the mRNA after the transcription of MG_234.

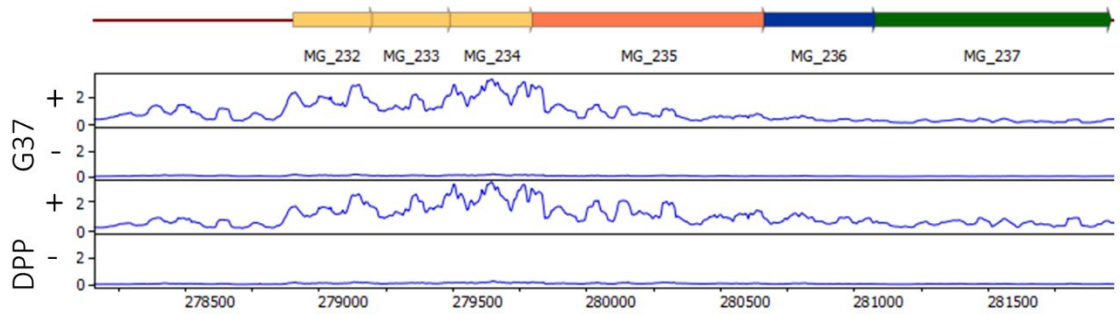

Figure GD. 4. Transcriptional profile of the *fur* operon after treatment with DPP determined by RNA-Seq. The expression of the + strands of the untreated (top) and treated (bottom) samples are fairly similar.

The activation of the Fur-regulon genes upon treatment with DPP could be entirely attributed to Fur, as these genes were not found upregulated when the *fur* strain was treated with DPP with regards to the untreated sample. Still, the Fur-related genes (MG_149, the MG_304 operon and *fur* itself) only accounted for a small percentage of the total differentially expressed genes (10.9% of the upregulated genes, 6.2% if all genes are considered).

A recent publication in *M. pneumoniae* detailed the increasing percentage of transcription regulation that is considered transcription factor-independent (Yus et al., 2019). The authors stated that only 20% of the regulation is associated with transcription factors when the bacterium is responding to different stresses. This would be in agreement with our results, as the stress induced by metal depletion led to the differential expression of a high number of genes. They enumerated other alternative regulatory systems as the genome organization, the DNA supercoiling, the availability of nucleoside triphosphate or riboswitches as mechanisms behind the response to cell perturbations. DNA supercoiling has been related to global transcriptional changes (Dorman & Dorman, 2016; Martis B. et al., 2019; W. Zhang & Baseman, 2011a).

The publication of Zhang and Baseman is particularly interesting because it was performed on *M. genitalium* and it evidenced a broad response to osmotic shock. They observed a high number of co-transcribed operons and this also is observed to a certain degree in this work. This phenomenon was studied several years ago in *M. genitalium*, as it was observed that the apparent scarcity of terminators caused by the small intergenic spaces led to the co-transcription of functionally unrelated genes (Benders et al., 2005). More recent studies had related the co-transcription of regions to the chromosome organization (Le et al., 2013; Trussart et al., 2017). Thus, the different regulation of chromosomal domains upon metal starvation could explain some of the

transcription factor-independent regulation detailed in this study, especially when it comes to the co-transcription of functionally unrelated clusters.

GD.2.3 Riboswitches and ECF transporters

Riboswitches are found in mRNA sequences usually at the 5' UTR, that can bind metabolites which ultimately would be affected by its posterior translation (Serganov & Nudler, 2013). Thus, they are mRNA regions that act as sensors for specific metabolites, without intermediate molecules, and are able to tune down the expression of the downstream genes when the metabolite is in excess. To date, only one riboswitch has been detected in mycoplasmas (S. Mukherjee et al., 2017). Riboswitch prediction tools as Denison Riboswitch Detector (Havill et al., 2014), Riboswitch Scanner (S. Mukherjee & Sengupta, 2016) or RiboSW (Chang et al., 2009) were not capable of finding any riboswitch conserved sequence in *M. genitalium* genome, although *in silico* predictors might not be the best tool to determine their presence in these unique microorganisms.

These sensors have been associated with Energy-Coupling Factor (ECF) transporters and metal uptake. One of the most studied riboswitches is directly related with cobalamin, in which adenosylcobalamin (AdoCbl) binds to the leader region of the mRNA that codes the proteins involved in cobalamin biosynthesis and inhibits its translation by alteration of the ribosome binding site (Nahvi et al., 2002). The existence of riboswitches controlling the expression of metal transporters by binding to nickel and cobalt has also been reported (Furukawa et al., 2015).

Notably, the Fur-controlled operon of *M. genitalium* (MG_304, MG_303, MG_302) codes for an ECF transporter with homology to the CbiMNQO and NikMNQO systems that are involved in cobalt and nickel uptake, respectively. The CbiMNQO system was first described in *Salmonella typhimurium* as part of a cluster which other genes linked to the biosynthesis of vitamin B_{12} (Roth et al., 1993). As the cobalt acquisition is essential for the biosynthesis of cobalamin, several ECF transporters have been characterized as cobalt transporters of the CbiMNQO family depending on their colocalization with other genes related to the cobalamin biosynthetic pathway (Rodionov et al., 2006). The presence of cobalamin-riboswitches regulating these systems have been reported (Cheng et al., 2011). However, the presence of a riboswitch in the promoter region of MG_304 has not been determined. The identification of this regulatory element as well as its ligand could be of great importance due to its possible use as targets for antimicrobial drugs (Deigan & Ferré-D'Amaré, 2011; Machtel et al., 2016; Mulhbacher

et al., 2010). A more extensive study of this operon is currently underway in our laboratory.

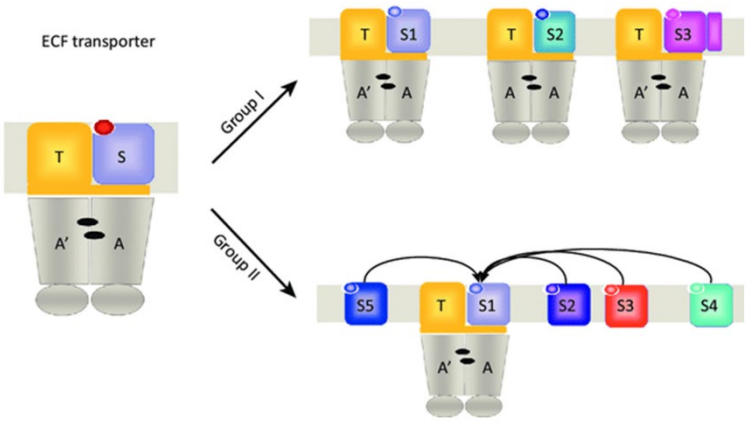

Figure GD. 5. Modularity of ECF transporters. This family of transporters can be divided in two groups, depending on the EcfS subunit. In group I, there is a dedicated module for each substrate-binding subunit, that is also coded in the same operon as the energy-coupling module. In group II, the same energy module can bind to several EcfS subunits that are coded in other genome regions. Image extracted from P. Zhang, 2013.

M. genitalium also codes for another essential ABC transporter with high homology to the CbiMNQO family: the gene product of MG_179, MG_180 and MG_181. This operon, though, is not under the control of Fur, as determined in this work. Its transcription was not affected in the mutant strain and its upstream region does not contain a Fur box. Surprisingly, it was found upregulated in the *fur* mutant after a shock with DPP, but that upregulation was not observed in the metal-deprived G37 strain. Neither operon contains a gene coding for a solute-binding subunit (EcfS), as both ABC transporters are formed by two putative CbiO subunits (EcfA) that act as ATP-binding proteins and one CbiQ subunit (a transmembrane coupling protein, EcfT, that acts as a permease). This is not infrequent, as the EcfS components can be coded in different chromosomal locations than the other complex components, thus offering a modular mechanism where different substrate-binding subunits share the same energy-coupling subunits (Rodionov et al., 2009) (Figure GD. 5). A study on *Lactobacillus lactis* revealed that one energy-coupling module interacted with the eight different EcfS subunits coded in its chromosome (Ter Beek et al., 2011). This is a cost-effective solution that would be reasonable to find at a minimal bacterium as *M. genitalium*.

Given that the two energy-coupling subunits in *M. genitalium* are essential (Glass et al., 2006; Lluch-Senar et al., 2015) and that it has been reported that the same module can

interact with several EcfS subunits in other bacteria, it is probable than their role exceeds metal uptake. The upregulation of the MG_304 operon together with the elevated increase in transcription and translation of *hrl* and its gene product, respectively, could suggest that Hrl acts as the substrate-binding subunit of that transporter. A transporter that, at the same time, is also upregulated to fulfill its other essential functions besides the metal transport. Nevertheless, the already characterized cobalt and nickel S subunits have distinctive particularities: they need a small integral membrane protein (CbiN or NikN) and they have seven transmembrane domains instead of the six helices of other EcfS (P. Zhang et al., 2010). A bioinformatic analysis evidences that Hrl is mainly an extracytoplasmic protein with a small transmembrane domain as an anchor; thus, its structure is very different from the reported S subunits with seven transmembrane domains. Therefore, Hrl does not seem to be an EcfS subunit, although its extremely high content in histidines and the fact that is strongly overexpressed in a fur mutant clearly suggests that it has a role in metal acquisition.

All in all, the presence of two ECF transporters that lack a S subunit is probably related to the reported modularity of this family. As of now, experiments to determine the presence of substrate-binding subunits in *M. genitalium* are in the works.

CONCLUSIONS

CHAPTER I: REGULATION OF CELL DIVISION AND FTSZ LOCALIZATION DYNAMICS IN A CELL WALL-LESS BACTERIUM

— There is a conserved sequence within the promoter region of *mraZ* across bacterial species. The conserved motif consists of three GTG(G/T) boxes separated by six nucleotides. There is an additional fourth box in *M. genitalium*.

— Depletion of MraZ activates transcription of the division and cell wall operon, which is associated with a severe growth delay and an impaired cytokinesis.

— Loss of MraW does not change gene expression, although it slightly increases the duplication time and it is associated with a higher expression of FtsZ.

— Wild-type transcriptional levels of the *dcw* operon in a *mraZ* mutant can only be restored when an ectopic copy of *mraZ* is inserted in *cis*.

— Overexpression of *mraZ* causes a transcriptional activation of the operon, although it is milder than the associated with the loss of the regulator.

— The entire division and cell wall operon is dispensable for *in vitro* growth in *M. genitalium*. Loss of this operon results in a notable growth delay and cytokinesis defects. However, these defects are less severe than the observed upon deletion of *mraZ*.

— The P65:YFP fusion allows an excellent tracking of the terminal organelle position in virtually all cells in the population without major phenotypic drawbacks.

— In single cells, FtsZ localizes opposite to the Terminal Organelle (TO) and it shifts towards midcell after the replication and migration of a new TO. There is no overlap between the major cytoskeleton structure of *M. genitalium* and FtsZ.

CHAPTER II: RESPONSE TO METAL STARVATION INVOLVES FUR-DEPENDENT AND INDEPENDENT REGULATORY PATHWAYS

- The MG_236 gene of *M. genitalium* codes for a transcriptional regulator of the Fur family.

- Fur-regulated genes code for an uncharacterized histidine-rich lipoprotein (Hrl) and three subunits of an uncharacterized ABC transporter (MG304, MG303, MG302).

- There is a conserved palindromic sequence within the promoter region of Fur-regulated genes, which is likely the Fur operator.

- Deletion of Fur is responsible for the differential expression of several proteins, including Hrl, the gene product of the Fur-regulated gene MG_149.

- There is an extensive Fur-independent transcriptional response to metal starvation in *M. genitalium*.

- Determination of the metallome of *M. genitalium* reveals an increased nickel uptake in the *fur* mutant.

- Excess of zinc causes a stronger repression of the Fur-regulated genes.

MATERIALS AND METHODS

M.1 Biologic Material

M.1.1 Bacterial growth

M.1.1.1 Culture and transformation of *Escherichia coli* strains

E. coli XL1-Blue strain was used for cloning procedures due to its recombination deficiency and its high transformation efficiency. It is also endonuclease I (*endA*) deficient, thus providing an improved yield of miniprep DNA. This strain is resistant to tetracycline (coded in the F' episome) and nalidixic acid (because of a mutation in the A subunit of DNA gyrase). Its complete genotype is listed as follows: *endA*1 *gyrA*96 *thi* $^{-}$1 *recA*1 *relA*1 *lac glnV*44 *hsdR*17(r_K^- m_K^+) F' [::Tn10 proAB$^+$ lacI^q Δ(lacZ)M15].

E. coli XL1-Blue was grown in Luria-Bertani (LB) medium. This is one of the most widely used broths for the growth of bacteria and it is composed of 10 g/L tryptone (Scharlau Microbiology), yeast extract 5 g/L (Scharlau Microbiology) and NaCl 10 g/L (Scharlau Microbiology). 1.5% agar (w/v) was added for LB plates. The medium was autoclaved at 121ºC for 15 minutes and stored at RT (liquid) or 4ºC (plates).

Super Optimal Broth (SOB) medium was used for XL1-Blue competent cell preparation. The composition of this medium is 20 g/L tryptone (Scharlau Microbiology), 5 g/L yeast extract (Scharlau Microbiology), NaCl 0.5 g/L (Scharlau Microbiology) and 2.5 mM KCl. The broth was adjusted to pH 7 with 2M KOH and autoclaved at 121ºC for 15 minutes. $MgCl_2$ 2mM prepared fresh and was added fresh before use.

Liquid cultures were inoculated in a laminar flow cabinet and grown at 37ºC and 250 rpm in an orbital shaking incubator with a maximum 1:5 volume proportion for proper aeration. An isolated colony or 10 µL from a working stock were used to inoculate 3 mL of LB. 20 µl from a working stock were used to inoculate 50-100 mL of LB to obtain greater quantities of plasmid DNA for electroporation purposes. For larger volumes, 1% inoculum from a starter culture grown until $OD_{600} \approx 1$ was used. Antibiotic selection was added to the culture in all cases to prevent plasmid loss.

Solid cultures were also inoculated in a laminar flow cabinet to isolate single colonies upon transformation. A Digralsky spreader was used to spread the transformant cells on the plate. Plates were incubated at 37ºC overnight in an incubator. Colonies were picked up with a sterile wood stick or a pipette tip and expanded in 3 mL LB overnight at 37ºC. Once characterized, *E. coli* strains were preserved in LB with 15% glycerol (v/v) at -80ºC.

The following LB supplements were used:

- **Ampicillin** (Sigma-Aldrich): stock solution was prepared at 200 mg/mL in MilliQ H_2O and sterilized filtering through a 0.22 µm filter (Merck-Millipore). The stock was conserved at -20ºC and used at a final concentration of 100 µg/mL (1:2000).
- **Tetracycline** (Sigma-Aldrich): stocks were prepared at 5 mg/mL in 70% ethanol and sterilized by filtering the solution through a 0.22 um filter (Merck-Millipore). The 1 mL aliquots were conserved at -20ºC and covered in aluminum foil to protect the antibiotic from the light, as it is a photosensitive compound. The working concentration for XL1-Blue strain is 10 µg/mL (1:500).
- **Isopropyl β-D-1-thiogalactopyranoside (IPTG)** (Sigma-Aldrich): stocks were prepared at 1M in sterile MilliQ H_2O and stored at -20ºC. IPTG is used at a working concentration of 1mM (1:1000) and it induced transcription of genes under the control of the lac operator.
- **5-bromo-4-chloro-3-indolyl-β-D-galactopyranoside (X-Gal)** (VWR Chemicals): stocks were prepared dissolving 40 mg of X-Gal in 1 mL N,N-dimethylformamide. X-Gal is used in LB plates as it is an analogue of lactose that yields an insoluble blue compound used to distinguish a successful cloning with blue/white screening. It is used at a final concentration of 40 µg/mL (1/1000). These plates need to be stored in the dark covered with aluminum foil as X-gal is photosensitive.

E. coli XL1-Blue competent cells were obtained following the inoue method described in Sambrook et al., 1989. Transformation of *E. coli* XL1-Blue cells was performed as described in Sambrook et al., 1989, where cells were shocked at 42ºC for 90 seconds.

M.1.1.2 Culture of *Mycoplasma genitalium*

M. genitalium was grown in Spiroplasma Medium 4 (SP4). The medium is prepared in two steps: base and supplementation. The base is composed of PPLO Broth 3.5 g/L (Becton Dickinson), Bactotryptone 10 g/L (Becton Dickinson), Bactopeptone 5.3 g/L (Becton-Dickinson) and Glucose 5 g/L (Sigma-Aldrich). The mix is dissolved in MilliQ H_2O and adjusted to pH 7.8 with NaOH 2M. To prepare SP4 agar plates, Bactoagar 0.8% (w/v) was added before autoclaving at 121ºC for 15 minutes.

After autoclavation and once the SP4 base was cooled down (not under 56ºC if solid SP4 is desired), it was supplemented. For 500 mL SP4 broth preparation 50 mL 2% Yeastolate

(w/v) (Becton Dickinson), 6 mL 0.1% Phenol Red pH 7 (w/v) (Sigma-Aldrich), 25 mL 10x CMRL (Life Technologies), 17.5 mL fresh yeast extract, 85 mL Fetal Bovine Serum (Life Technologies), 1.71 mL glutamine 29.2 mg/mL (Sigma-Aldrich) and 250 µL ampicillin 200 mg/mL (Sigma-Aldrich) were added to the base. The pH was adjusted again to 7.8 with NaOH 2M and the mixture was filtered through a 0.22 µm Stericup (Merck-Millipore) to ensure the medium was clear of any residual live yeast cell.

The following components were used with SP4 when needed:

- **Yeastolate 2%**: 8 g Yeastolate (Becton-Dickinson) dissolved in 400 mL MilliQ H_2O and autoclaved at 121ºC for 15 minutes. Stored at 4ºC.
- **Yeast extract 25%** (w/v): 250 g of fresh yeast was dissolved in 1 L MilliQ H_2O and autoclaved at 115ºC for 10 minutes. Then, it was centrifuged at 400g for 10 minutes to pellet the yeast cells. Supernatants were autoclaved again at 115ºC for 10 minutes and aliquoted in 20 mL. For extra security, the aliquots were centrifuged again at 400g for 10 minutes before storing them at -20ºC.
- **Phenol Red 0.1 pH 7**: 0.4 g Phenol Red (Sigma-Aldrich) dissolved in 400 mL MilliQ H_2O. The pH was adjusted carefully to 7 using NaOH 2M. Stored at 4ºC after autoclaving at 121ºC for 15 minutes.
- **Fetal Bovine Serum (FBS)** (Life Technologies): it was heated up to 56ºC for 30 minutes in order to inactivate the complement system. Then, it was aliquoted in sterility in a laminar flow cabinet and 43 mL aliquots were stored at -20ºC.
- **Ampicillin** (Sigma-Aldrich): stock solution was prepared as described before and used at a final concentration of 100 µg/mL (1:2000) to prevent bacterial contamination.
- **Tetracycline** (Sigma-Aldrich): stock solution was prepared as described before. It was used at a working concentration of 2.5 µg/mL (1:2000) to select strains carrying the marker gene tetM438 (Pich et al., 2006). It was used avoiding light exposure as it is photosensitive.
- **Chloramphenicol** (Sigma-Aldrich): stocks were prepared at 34 mg/mL in 70% ethanol and sterilized by filtering through a 0.22 µm filter (Merck-Millipore). Aliquots of 1 mL were stored at -20ºC. It was used at a working concentration of 17 µg/L (1:2000) to select strains carrying the marker gene catM438 (Calisto et al., 2012) that provides chloramphenicol resistance.
- **Puromycin** (Life Technologies): the stock solution (10 mg/mL) was stored at -20ºC. It was used at a final concentration of 3.3 µg/mL (1:3000) to select strains

carrying the *pac* marker (described in Algire et al., 2009) under the control of the MG_438 promoter (Torres-Puig et al., 2015), as with tetracycline and chloramphenicol gene markers. Puromycin stock solution was kept in the dark as it is a photosensitive compound.

M. genitalium cultures were inoculated in a class 2 laminar flow cabinet and incubated at 37ºC in a 5% CO_2 atmosphere. Liquid cultures were grown in 5, 20 or 35 mL of SP4 in 25, 75 or 175 cm^2 tissue culture flasks (SPL Life Sciences), respectively. The inoculum used varied highly depending on the strain or the experiment, ranging from 15 µL to 200 µL. Cultures were kept at 37ºC until mid-log phase (usually about 3-4 days) and then they were processed. For adherent strains, the medium was aspirated and cells were recovered with fresh medium using a cell scrapper (SPL Life Sciences). For non-adherent strains, the cells were centrifuged at 18000g for 15 minutes. Then, the supernatant was discarded and pelleted cells were recovered in the desired medium.

For solid cultures, the plated quantity depended on the experiment that was being performed. For viability assays, the cellular suspensions were serially diluted until 10^{-6} and 10 µL drops of different dilutions were plated. For transposon delivery, 100 µL of a 0, 10^{-1} and 10^{-2} dilutions were plated onto SP4 agar plates. And to achieve homologous recombination with a suicide plasmid, 200 µL of non-diluted cellular suspension were plated. Individual colonies could be observed after 10-14 days using a binocular stereomicroscope. The isolated colonies were selected with a permanent marker using the stereomicroscope and recovered in the laminar flux cabin using sterile cut microtips. These colonies were cultured in 25 cm^2 flasks with 5 mL of SP4 and the proper concentration of the selection marker. Some growth can be observed after 7-10 days depending on the strain and the mutant can be recovered by aspiring the medium and residual agar and scrapping the cells in 1 mL of fresh SP4. Stocks were stored at -80ºC without the addition of glycerol, due to the high concentration of FBS in SP4 medium that permits cryopreservation.

M.1.1.3. Transformation of Mycoplasma genitalium

M. genitalium was transformed by electroporation as described by Reddy et al., 1996, adapting a protocol used to *M. pneumoniae* transformation by Hedreyda et al., 1993. The protocol used in this laboratory is a slightly modified version detailed as follows:

— Inoculum of a *M. genitalium* strain in a 75 cm^2 flask with 20 mL SP4.

- After 3 days at 37ºC and 5% CO_2, the culture usually reached the mid-log phase. Then, 10 mL of SP4 were discarded and cells were scrapped in the remaining volume.
- The scrapped cells in 10 mL SP4 were filtered through a 0.45 µm filter (Millipore) to disaggregate cell clusters and increase transformation efficiency. Then, 3-5 mL were inoculated in a new 75cm2 flask with 15-17 mL of fresh SP4 or 8-10 mL were seeded in a 175cm2 flask with 25-27 mL of fresh SP4 if several transformations (4+) were desired. The flask was left overnight at the incubator.
- The next day, medium was aspirated and cells were washed three times with Electroporation Buffer (8mM HEPES, 272 mM sucrose, pH 7.2-7.4). Then, cells were scrapped in the remaining residual medium, recovered in a microtube and the volume was adjusted depending on the number of transformations to be performed.
- 100 µL of the cellular suspension were mixed with 10 µg (for transposition) or 30 µg (for gene replacement using a suicide plasmid) of plasmid DNA.
- Immediately after mixing the cells with the plasmid DNA, the mixture was placed into a 0.2mm gapped electroporation cuvette (VWR) and electroporated at 2500 V, 250 Ω and 25 mF with an electroporation system (ECM 620-630 BTX). Electroporation time constants ranged from 4.0 to 6.0 milliseconds. After electroporation, cuvettes were immediately put on ice.
- After 15 minutes on ice, cells were resuspended with 1 mL of fresh SP4 and transferred to a sterile microtube. Tubes were incubated at 37ºC and 5% CO_2 for 3 hours in order to allow the expression of the resistance marker.
- Finally, cells were plated on SP4 agar cells with the corresponding antibiotic. As a control, viable cells on SP4 agar without antibiotic could also be seeded.

There were two modifications to this protocol if the parental strain was non-adherent:

a) The culture was not filtered through a 0.45 µm filter but forced through a 25G needle syringe 5-7 times. This is because of the natural aggregation of non-adherent cells that would highly decrease the number of cells that passed through the filter.
b) As they do not adhere to the plastic, the three washes with electroporation buffer were performed by centrifuging the cells three times at 18000g for 15 minutes.

M.1.1.4 *M. genitalium* strains

Chapter I strains

Table MM. 1. Strains used or created for Chapter I: Regulation of Cell Division and FtsZ Localization Dynamics in a Cell Wall-Less Bacterium.

Strain	Description	Source
WT or G37	*Mycoplasma genitalium* G37 is the reference strain. It was isolated for the first time from the urogenital tract of a male patient with non-gonococcal urethritis.	ATCC:33530
mraZWCm	This strain lacks both the MG_221 and MG_222 genes and it is resistant to chloramphenicol. This strain was used as an intermediate strain. The promoter of the selectable marker was placed in sense with the downstream genes. The *mraZ* putative operator was also deleted. Genotype: ΔMG_221::*tetM*, ΔMG_222::*tetM*.	This work
mraREF	This strain was used as the reference strain for *mraZ* and *mraW* mutants. The selectable marker did not disrupt any gene and was placed upstream of the putative *mraZ* regulative region and in antisense with respect to *mraZ* to prevent polar effects. It is resistant to tetracycline. Genotype: *tetM*.	This work
mraZ	This strain lacks the MG_221 gene and it is resistant to tetracycline. The *mraREF* mutant was used as the parental strain. The selectable marker is orientated in the antisense direction to prevent polar effects to the downstream genes of the operon. The marker is located upstream of the mraZ putative operator. Genotype: ΔMG_221::*tetM*.	This work
mraW	This strain lacks the MG_222 gene and it is resistant to tetracycline. The *mraREF* mutant was used as the parental strain. The selectable marker is orientated in the antisense direction to prevent polar effects to the downstream genes of the operon. The marker is located upstream of the mraZ putative operator. Genotype: ΔMG_222::*tetM*.	This work
mraZCOM	This is the *mraZ* mutant complemented with an ectopic copy of *mraZ*. The new copy was located downstream of *ftsZ* by HR. This strain is resistant to tetracycline and chloramphenicol. Genotype: ΔMG_221::*tetM*, *cat*.	This work

mraZ Tn221 P221	This is the *mraZ* complemented with an ectopic copy of *mraZ* in trans. The gene was under the control of its own promoter. It is resistant to chloramphenicol and tetracycline. Genotype: ΔMG_221::*tetM*, Tn*CmR*-P_{221}MG_221.	This work
mraZ Tn221 P438	This is the *mraZ* complemented with an ectopic copy of *mraZ* in trans. The gene was under the control of the MG_438 promoter. It is resistant to chloramphenicol and tetracycline. Genotype: ΔMG_221::*tetM*, Tn*CmR*-P_{438}MG_221.	This work
mraZ Tn221-222 P221	This is the *mraZ* complemented with a copy of *mraZ* followed by an extra copy of *mraW*. The two genes were under the control of their own promoter. It is resistant to chloramphenicol and tetracycline. Genotype: ΔMG_221::*tetM*, Tn*CmR*-P_{221}MG_221:MG_222.	This work
mraZ P221	This strain was created to overexpress *mraZ* under its own promoter. A minitransposon containing an ectopic copy of *mraZ* was transformed into the G37 strain. It is resistant to chloramphenicol. Genotype: Tn*CmR*-P_{221}MG_221 (pool).	This work
mraZ P438	This strain was created to overexpress *mraZ* under the control of the MG_438 promoter. A minitransposon containing an ectopic copy of *mraZ* was transformed into the G37 strain. It is resistant to chloramphenicol. Genotype: Tn*CmR*-P_{438}MG_221 (pool).	This work
mraZmut P438	This strain overexpresses a copy of *mraZ* with a frameshift mutation which prevents its translation. It is resistant to chloramphenicol. Genotype: Tn*CmR*-P_{438}MG_221_{FS} (pool).	This work
mraZmraW P221	This mutant carries an extra copy of *mraZ* and *mraW* introduced by minitransposon. The two genes are under the control of their own promoter. It is resistant to chloramphenicol. Genotype: Tn*CmR*-P_{221}MG_221:MG_222 (pool).	This work
mraZmraWP438	This mutant carries an extra copy of *mraZ* and *mraW* introduced by minitransposon. The two genes are under the control of the MG_438 promoter. It is resistant to chloramphenicol. Genotype: Tn*CmR*-P_{438}MG_221:MG_222 (pool).	This work
ftsZ	This strain lacks for the MG_224 gene and it is resistant to chloramphenicol. Genotype: ΔMG_224::*cat*.	This work

dcw	This is a strain that lacks the whole division and cell wall operon and it is resistant to chloramphenicol. Genotype: ΔMG_221::*cat*, ΔMG_222::*cat*, ΔMG_223::*cat*, ΔMG_224::*cat*.	This work
ftsZCh	The fluorescent *mcherry* tag was added by homologous recombination (HR) to the MG_224 gene. This strain is resistant to chloramphenicol. Genotype: *cat*, *ftsZ*:*mcherry*.	This work
217YFP	The fluorescent eYFP reporter was fused to the MG_217 gene through HR. This strain is resistant to puromycin. Genotype: *pac*, MG_217:*eyfp*.	This work
mraZ ftsZCh	This is a strain that lacks *mraZ* and has the mCherry tag fused to *ftsZ*. This strain is resistant to tetracycline and chloramphenicol. Genotype: *cat*, ΔMG_221::*tetM*, *ftsZ*:*mcherry*.	This work
mraZ ftsZCh 217YFP	This strain is the mutant of *mraZ* with the two fluorescent fusions *ftsZ*:Ch and MG_217:*eyfp*. It is resistant to tetracycline, chloramphenicol and puromycin. Genotype: *cat*, *pac*, ΔMG_221::*tetM*, *ftsZ*:*mcherry*, MG_217:*eyfp*.	This work
mraW ftsZCh	This is the *mraW* mutant strain and it has the mCherry tag fused to *ftsZ*. This strain is resistant to tetracycline and chloramphenicol. Genotype: *cat*, ΔMG_222::*tetM*, *ftsZ*:*mcherry*.	This work

Chapter II strains

Table MM. 2. Strains used or created for Chapter II: Response to Metal Starvation Involves Fur-Dependent and -Independent Regulatory Pathways.

Strain	Description	Source
WT or G37	*Mycoplasma genitalium* G37 is the reference strain. It was isolated for the first time from the urogenital tract of a male patient with non-gonococcal urethritis	ATCC: 33530
fur	This strain lacks the MG_236 gene and it is resistant to tetracycline. The resistance marker has a transcription terminator at its 3' end to reduce polar effects derived from its promoter. Genotype: ΔMG_236::tetM.	This work
fur COM	This strain is the defective mutant of MG_236 complemented with a minitransposon bearing an ectopic copy of MG_236 under the control of its own promoter. Genotype: ΔMG_236::tetM, MG_438::TnCmMG_236.	This work
G37-Hrl_{wt}:CatCh	This strain carries a selectable marker fused to a *mcherry* tag (Cat:Ch) under the control of the promoter region of the gene hrl. This region contains a putative Fur box. The strain was used to assess the transcriptional repression associated with the fur box. Genotype: TnPacHrlwt:cat:mcherry.	This work
G37-Hrl_{mut}:CatCh	This strain carries a selectable marker fused to a *mcherry* tag (Cat:Ch) under the control of the scrambled promoter region of the gene hrl. This construction was placed in the same genomic location as in the G37-Hrlwt:CatCh strain to replicate the genetic context. Genotype: TnPacHrlmut:cat:mcherry.	This work
fur-Hrl_{wt}:CatCh	This strain lacks the MG_236 gene and has the Cat:Ch fusion under the control of the promoter region of the gene hrl. This construction was placed in the same genomic location as in the G37-Hrlwt:CatCh strain to replicate the genetic context. This strain was used to assess the fluorescence of the marker under the control of a fur box in a fur defective context.	This work

fur-Hrl_{mut}:CatCh	This strain lacks the MG_236 gene and has the Cat:Ch fusion under the control of the scrambled promoter region of the gene hrl. This construction was placed in the same genomic location as in the G37-Hrlwt:CatCh strain to replicate the genetic context. This strain was used to assess the fluorescence of the marker under the control of a scrambled fur box in a fur defective context.	This work

M.2 DNA Manipulation

M.2.1 Plasmid DNA extraction

Extraction of plasmid DNA (pDNA) was carried out using a 3 mL of an O/N *E. coli* culture and the *FastPlasmid Mini Kit* (5 Prime) or the *GeneJET Miniprep Kit* (Thermo Scientific), following the instructions of the manufacturer. The quantity of plasmid DNA obtained depended on the copy number of the plasmid. For a high copy number plasmid, up to 10 µg of pDNA were usually obtained. Minipreparations were used for cloning purposes.

If larger amounts of pDNA were needed, a 50 or 100 mL O/N *E. coli* culture was processed using the *GenElute HP Midiprep Kit* (Sigma-Aldrich), following manufacturer's instructions. In order to increase the concentration, pDNA was precipitated after elution with 0.8 volumes of isopropanol and 0.1 volumes of 0.3 M ammonium acetate. The mix was centrifuged at 18000g and 4ºC for 30 minutes. The supernatant was discarded and the pellet was washed once with 70% ethanol. Then, the supernatant was discarded again and the pellet was vacuum dried. The dried pellet was resuspended with 100 mL Electroporation Buffer, as midipreparations were used to transform *M. genitalium*. Suspension was left O/N at 4ºC and stored at -20ºC after quantification. Typically, up to 300 µg of pDNA could be obtained.

M.2.2 Genomic DNA extraction from *M. genitalium*

To isolate genomic DNA (gDNA) from *M. genitalium*, the following protocol (adapted to our lab by Torres-Puig) was followed:

- Inoculum of the desired *M. genitalium* strain to screen in a 25 cm^2 flask with 5 mL of SP4 and supplemented with the required antibiotics. The culture was grown until late exponential phase.
- The medium was aspirated and cells were washed twice in 1 mL PBS. Then, cells were scrapped off in 1 mL PBS, transferred to a microcentrifuge tube and centrifuged at 16000 g for 10 minutes. For non-adherent strains, cells were centrifuged in SP4 and washed twice in PBS.
- PBS was aspirated and the pellet (usually a small one) was lysed using 20-50 µL of lysis buffer (0.1 M Tris-HCl pH 8.5, 0.05% Tween-20, 250 µg/mL proteinase K). An optimal disaggregation of the pellet by pipetting up and down was important to achieve a good lysis. The mix was incubated at 37ºC for 1 hour.
- Then, proteinase K was inactivated at 95ºC for 10 minutes.

— Lysates were stored at 20ºC.

2 µL of the lysate were used for PCR screening and 5 µL were usually enough for Sanger sequencing.

M.2.3. DNA quantification

DNA quantification was determined using a NanoDrop 1000 Spectrophotometer (Thermo Scientific), following the manufacturer's instructions.

M.2.4 DNA Amplification

DNA amplification for molecular cloning purposes was carried out with *Phusion High Fidelity DNA polymerase* (Thermo Scientific), following manufacturer's instructions. Taq DNA polymerase (Sigma-Aldrich) was employed in mutant screenings. 20 ng of DNA template were usually used, 200 µM of dNTP mix (Sigma-Aldrich), 0.2 µM of each oligonucleotide and 0.6 U of the Phusion polymerase or 1.25 U of the Taq polymerase.

Usually, PCR fragments were joined by Splicing by Overlap Extension (SOE) PCR. This method is based in the use of oligonucleotides with a 5' overhang that is complementary to the 3' end of the fragment to be fused with. Both fragments are amplified separately, purified and they are mixed in the next PCR reaction. In this new reaction, they will be annealed together and using the forward primer of the first fragment and the reverse oligonucleotide of the second fragment they will generate a new product. This technique is used to merge several DNA fragments without using ligation reactions.

M.2.5 Agarose gel electrophoresis

Agarose gels were used to separate DNA fragments. Depending on the size of these fragments, the concentration of agarose (SeaKem LE Agarose) ranged from 0.7-2% (w/v) and it was diluted in 1xTAE buffer (40 mM Tris, 20 mM acetic acid and 1 mM EDTA). Usually, DNA samples were already mixed with a commercial loading buffer (*Phusion Green HF buffer* or *FastDigest Green buffer*, both from Thermo Scientific). If not, samples were diluted with loading buffer (40 mM Tris-Acetate pH 8, 1 mM EDTA, Bromophenol Blue 250 µg/mL, xylene cyanol 250 µg/mL and 30% glycerol) before loading them into the agarose gel.

Electrophoresis gels were run at 70-90V for 60-90 minutes in 1x TAE Buffer. Molecular weight was estimated using *GeneRuler™ 1 kb Plus DNA Ladder* (Thermo Scientific). Then, the agarose gel was stained with *RedSafe* (iNtRON Biotechnology) or *Midori Green Advance* (NIPPON Genetics). Both DNA staining solutions were used at 0.02% (v/v). The gel was incubated with the staining buffer for 30 minutes in an orbital shaker. Then, it was visualized under UV or black light in a *GelDoc™ XR+ Imaging System* (Bio-Rad) for screening purposes or under a *Spectroline TC-365A* transilluminator (Spectronics Corporation) to recover DNA bands from the agarose gel. DNA from agarose gels was later extracted using *NucleoSpin Gel and PCR Clean-up* kit (Macherey-Nagel), following manufacturer's instructions.

M.2.6 DNA restriction

DNA fragments were digested using *FastDigest™* restriction enzymes (Thermo Scientific), following the manufacturer's instructions.

M.2.7 DNA ligation

DNA fragments were ligated into previously digested plasmids with T4 DNA ligase (Sigma-Aldrich or Thermo Scientific). Reactions were performed at room temperature for 1-2 hours or 15-30 minutes, depending on the specifications of the ligase and the DNA ends (longer time for blunt ends, shorter for sticky ends).

M.2.8 DNA sequencing

Sanger sequencing reactions were performed with the *BigDye® 3.0 Terminator* kit (Applied Biosystems) and analyzed in an ABI PRISM 3130xl Genetic Analyser (Applied Biosystems). Reactions were performed at Servei de Genòmica i Bioinformàtica (UAB).

M.2.9 Plasmid construction

Plasmids were constructed depending on the desired approach.

— To generate knock-out mutants, the gene of interest was replaced with a resistance marker. This was achieved via transformation with a suicide plasmid that contained 1 kb of both upstream and downstream regions of the gene to be replaced flanking the antibiotic cassette. The resistance marker was under the control of a constitutive promoter.

— To re-introduce or overexpress genes, a miniTn4001-derived transposon bearing a copy of the gene of interest was employed. The extra copy was amplified from genomic DNA of *M. genitalium* usually adding a 5' tail with the sequence of the MG_438 promoter (the same that drives the transcription of the resistance marker) or, in some cases, its own promoter. It was cloned into the pMTnTetM438 (Pich et al., 2006b), pMTnCat (Calisto et al., 2012) or pMTnPac (Torres-Puig, 2017) plasmids previously digested with *Apa*I-*Xho*I and used to transform M. genitalium.

— To introduce fluorescent fusion proteins in the chromosomal loci, the fluorescent marker gene was fused to the gene of interest with SOE-PCR. In order to allow the expression of the marker, the stop codon of the gene to which it was fused was deleted. An antibiotic resistance gene was placed downstream of the fluorescent marker, under the control of the MG_438 promoter. The whole cassette containing the gene of interest and the fluorescent and resistance markers was flanked with the upstream and downstream sequences of the gene of interest introduced by SOE-PCR. Then, it was cloned in an *Eco*RV-digested pBE and it was transformed into *M. genitalium*.

Plasmids used in this work and their construction are explained in greater detail in the Appendices (A.1.1 and A.2.1). Maps were created with the Snapgene Software (GSL Biotech).

M.2.10 Oligonucleotides

All oligonucleotides used in this work can be found in the Appendices (A.1.2 and A.2.2) organized by Chapter.

M.3 RNA Manipulation

M.3.1 RNA extraction

Total RNA extraction was achieved using the *RNAqueous Total RNA Isolation Kit* (Thermo Scientific). *M. genitalium* strains were grown in 75 cm^2 flasks until mid-log phase and then washed thrice with 1x PBS (Sigma-Aldrich). After drying thoroughly, 500 µL of the lysis buffer provided in the kit were added to the flask and the cells were scrapped and recollected in an Eppendorf tube. Then, the extraction was performed following manufacturer's instructions. Eluted RNA was treated with *Turbo DNA-free Kit* (Thermo Scientific) to remove the remaining gDNA and then quantified using a NanoDrop 1000 Spectrophotometer. RNAs were later stored at -80ºC.

For RNAseq analysis, *miRNeasy Mini Kit* (QIAgen) was used to extract total RNA of *M. genitalium*. This kit was used instead of the *RNAqueous Total RNA Isolation Kit* due to its capacity to also extract miRNAs and 5S rRNA that could not be purified with the previous kit. Late exponential phase cultures grown in 25 cm^2 flasks were scrapped off in 5 mL of fresh SP4 and subcultured in two new 25 cm^2 flasks (2.5 mL of the scrapped off *M. genitalium* strain and 2.5 mL of fresh SP4 in each flask) and incubated at 37ºC for 6 hours. Then, flasks were washed thrice with 1x PBS and cells were scrapped off after adding 500 µL of *QIAzol Lysis Reagent*. Extraction was performed following manufacturer's instructions. Traces of genomic DNA were removed using the *RNAse-free DNase Set* (QIAgen), following manufacturer's instructions. Then, RNAs were quantified using a NanoDrop 1000 Spectrophotometer and stored at -80ºC until used. RNA quality was assessed using the *Agilent RNA 6000 Nano Kit* (Agilent Technologies) in an Agilent 2100 Bioanalyzer (Agilent Technologies).

M.3.2 qRT-PCR analyses

Synthesis of cDNA for quantitative Real-Time PCR analysis was performed using *iScript cDNA Synthesis Kit* (Bio-Rad). 1 µg of total RNA for each strain to be analyzed was retrotranscribed following manufacturer's instructions. Negative controls without reverse transcriptase were also carried out. qRT-PCR reactions were performed in 96 or 384-well plates using the *iTaq™ Universal SYBR® Green Supermix* (Bio-Rad) and the protocol was carried out in CFX96 or CFX384 Real-Time PCR Detection Systems (Bio-Rad) at Laboratori de Luminiscència i Espectroscòpia de Biomolècules (UAB). Each well contained 3 µL of diluted cDNA (1/15), 1 µL of each oligonucleotide and 5 µL of the iTaq mix. The protocol was set as follows:

1. Initial denaturation (95ºC – 3 minutes)
2. Denaturation (95ºC – 10 s)
3. Annealing (56ºC – 20 s)
4. Elongation (72ºC – 20 s)

   } 40x (plate read after every cycle)

5. Denaturation (95ºC – 10 s)
6. Melting curve (temperature increments of 0.5ºC every 5 s from 65ºC to 95ºC. Plate read after every increment)

Data from qRT-PCR in this work comes from at least three biological repeats. A technical repeat for each sample was also performed in each plate and the mean value was used to determine the cycle quantification (C_q) value. Non-template (NTC) and non-reverse transcribed (NRT) controls were analyzed as well as a measure of the purity of the samples. For NTC controls, RNase-free water was used as template for amplification, thus allowing the detection of contaminants in the RT kit or in the oligonucleotides used. For NRT controls, RNase-free water was mixed with 1 µg of RNA without buffer or the retrotranscriptase. This control is useful to discover gDNA presence in the samples. No fluorescence signal should be detected in any of these controls.

As for the last step of the protocol, melting curves are a good detector of non-specific amplicons, as each set of primers should only yield one product. If there is more than one peak in the melting curve of an analyzed gene, it is recommended to employ a new set of oligonucleotides.

Raw data was analyzed using CFX Manager software (Bio-Rad). Relative gene expression was calculated using the Pfaffl method (Pfaffl, 2001), which considers the amplification efficiencies of the target genes. Normalization was achieved by geometric averaging of multiple reference genes (Vandesompele *et al*., 2002). The cutoff for differential gene expression was set on the arbitrary 2-fold cutoff (or 0.5 for downregulated genes) or the equivalent log2 = 1 fold change (or -1 for downregulated genes).

The genes coding for the alpha subunit of the DNA-directed RNA polymerase (MG_177), the ribosomal protein L13 (MG_418) and the 2,3-biphosphoglycerate-independent phosphoglycerate mutase (MG_430) were used as housekeeping genes to normalize expression between samples.

M.3.2.1 Primer design and amplification efficiency

Oligonucleotides for qRT-PCR were designed using Primer3Plus software (Rozen & Skaletsky, 2000). The guidelines for qRT-PCR primer selection employed are the following: 18-22 nucleotides long, GC content of 40-50%, a yielded amplicon of about 200 bp and an annealing at the 5' end of the target genes.

The amplification efficiency was tested for each new set of oligonucleotides. A calibration curve using serially diluted genomic DNA as a template was determined. Considering an ideal efficiency (100%), each dilution should be amplified in C_q increments of 2 units. A linear regression of the logarithm of the template quantity versus the cycle quantification value allowed the calculation of the amplification efficiency with the following equation:

$$Efficiency(\%) = \left(10^{-\frac{1}{slope}} - 1\right) \cdot 100$$

Amplification efficiencies ranging from 85 to 110% were considered suitable for qRT-PCR analysis.

M.3.3 RNAseq analyses

RNA libraries were prepared with *TruSeq Stranded Total RNA Library Prep Kit* (Illumina) and analyzed using a HiSeq 3000 System (Illumina) at the Genomics Unit (CRG). cDNA clusters were immobilized in sequencing lanes of 2x50 reads. Reverse and complementary sequences were computed with the Read2 primer. Data analysis and sequence alignment was performed using the in-house *Map* software (Piñol, unpublished work) with Bowtie2 tool (Langmead and Salzberg, 2012) in the End-to-End mode and Forward-Forward paired-ends.

Sequences were piled up using SAMtools (Li *et al.*, 2009), setting no limit to the number of sequences in the alignment. *FeatureCounts* (Liao *et al*., 2014) was used to convert reads to counts in the different ORFs, without counting the multi-mapping reads and disabling multi-overlapping reads. The counts were submitted to the R/Bioconductor package *DESeq2* (Anders and Huber, 2010; Love *et al*., 2014) for statistical analysis. *DESeq2* analysis used a parametric fitType and a zero-mean normal prior on the non-intercept coefficients. Data was then sorted by log2 fold change and the changes were considered statistically significant if their p-values were below 0.05.

Three biological repeats of each strain or condition tested were used to conduct the analysis.

M.3.4 Primer extension analyses

20 µg of previously quantified RNA was used to perform a primer extension analysis. Due to the high amount of RNA needed and the usual yield of ~500 ng/µL in ~50 µL after the RNA extraction and DNase treatment (see 1.3.1), a previous precipitation with ethanol is recommended. Prior to the retrotranscription, the 20 µg of RNA, 0.5 µL of a 50 µM 6-Fam-labelled primer and 1.5 µL of 10 mM dNTPs were mixed together and heated at 65ºC for 5 minutes in a thermal cycler. Then, the mix was cooled down in ice and the remaining components were added: 3 µL of 10x buffer, 3 µL of 25 mM $MgCl_2$, 2 µL of 0.1M DTT, 1.5 µL of RNaseOUT (40 U/µL) and 1.5 µL SuperScript® III Retrotranscriptase (200 U/µL). All the components (except for the labelled oligonucleotide) are supplied with the *SuperScript® IIII First-Strand Synthesis System* (Thermo Scientific).

The retrotranscription was carried out following the manufacturer's instructions: 50ºC for 50 minutes followed by 5 minutes at 85ºC for enzyme inactivation. Then, the labelled cDNA was treated with 2U RNase H at 37ºC for 20 minutes. After the treatment, it was precipitated with 0.1 volumes of 3 M sodium acetate and 2.5 volumes of absolute ethanol. The pellet was finally dissolved in 10 µL of highly deionized formamide (Thermo Scientific). Before the analysis, the pellet was mixed with 0.5 µL of ROX400HD or ROX500 markers (Thermo Scientific). The fragments were separated in an ABI 3130xl Genetic Analyzer at the Servei de Genòmica i Bioinformàtica (UAB) and the obtained files were analyzed with *PeakScanner* software (Thermo Scientific).

M.4 Protein Analysis

M.4.1 Protein extraction and quantification

M. genitalium cultures were grown in 75 cm^2 flasks until late exponential phase. Then, they were washed four times with 1x PBS and thoroughly dried. Cells were scrapped off in 100 µL of 1x PBS and lysed with 6x Laemmli sample buffer (0.375 M Tris-HCl pH 6.8, 12% SDS, 60% glycerol, 0.6% β-mercaptoethanol and 0.003% bromophenol blue). Then, samples were boiled for 10 minutes to denature proteins and immediately cooled down before storing them at -20ºC. Protein concentration was determined with *Pierce BCA Protein Assay Kit* (Thermo Scientific), following manufacturer's instructions.

M.4.2 Protein electrophoresis

Proteins were loaded into denaturing polyacrylamide gels to separate them according to their molecular weight. SDS-PAGE gels were prepared according to standard procedures (Shapiro *et al*., 1967) using 40% acrylamide:bisacrylamide (37:5:1) solution (Bio-Rad or Panreac) and polymerized in the *Mini-PROTEAN® handcast system* (Bio-Rad). The final concentration of acrylamide in the resolving (or running) gel ranged between 10 and 15%, depending on the molecular weight range of the target proteins. Acrylamide concentration on the stacking gel was fixed at 4%. *PageRuler™ Unstained Protein Ladder* (Thermo Scientific) was used as a molecular weight marker. For Western Blotting, *PageRuler™ Plus Prestained Protein Ladder* (Thermo Scientific) was the selected ladder.

Gels were run with the amperage fixed at 20-30 mA for 90-120 minutes in 1x Running Buffer (25 mM Tris, 192 mM glycine, 0.1% SDS). The endpoint was determined with the bromophenol blue front and depended on the target molecular weight range to be resolved.

M.4.3 Staining

Once the electrophoresis was over, gels were washed with distilled water to remove traces of SDS and then stained with Coomassie solution (0.1% Coomassie R250 (w/v), 10% acetic acid (v/v), 40% methanol (v/v)) for 30 minutes in agitation. Gels were unstained in 10% acetic acid and sponges were used to accelerate the process.

Colloidal Coomassie G-250 was used if a higher sensitivity was needed (Dyballa and Metzger, 2009). After electrophoresis, gels were washed with distilled water and stained

for 1 hour. Afterwards, they were unstained with 10% ethanol (v/v) and 2% orthophosphoric acid (v/v).

M.4.4 2D-DIGE

Total protein for 2D-DIGE analysis was extracted as described in Párraga-Niño et al., 2012. Cells were washed thrice in PBS and lysed in lysis solution (8 M urea, 2 M thiourea, 2.5% CHAPS, 2% ASB-14, 60 mM DTT, 40 mM Tris-HCl pH 8.8 and protease inhibitor cocktail) and then sonicated. Protein solutions were further purified by a modified TCA-acetone precipitation (2D-CleanUp Kit, GE Healthcare) and, finally, dissolved in the DIGE labelling buffer (8 M urea, 4% w/v CHAPS, 30 mM Tris pH 8.0). Protein concentration was calculated using Bio-Rad RCDC Protein Assay (Bio-Rad, UK), following manufacturer's instructions. Triplicate protein samples of each of the strains were labelled using Cy3 or Cy5 cyanine dyes and separated in three two-dimensional electrophoresis gels as described in Párraga-Niño et al., 2012. Fluorescence images of the gels were obtained on a Typhoon 9400 scanner (GE Healthcare). Cy3 and Cy5 images were scanned at excitation/emission wavelengths of 532/580 nm and 633/670 nm, respectively. Image analysis and quantification of relative protein abundances were performed using SameSpots (Nonlinear Dynamics, UK). The analysis and identification of the differentially expressed proteins was performed at Vall d'Hebron Institut d'Oncologia (VHIO) by Francesc Canals and Marta Monge.

M.4.5 SILAC test for quantitative proteomics

To discover the differentially expressed proteins in the mutant strains, we used a SILAC (Stable Isotope Labeling by Amino acids in Cell culture) protocol created at Serrano's Lab (CRG) for *M. pneumoniae*. This protocol was facilitated to us and adapted to *M. genitalium*. As this test requires the growth of *M. genitalium* in Hayflick's medium (as described in Yus et al., 2012 for *M. pneumoniae*), first we tried to grow the wild-type strain of *M. genitalium* in this medium. Once we confirmed that *M. genitalium* was able to grow in Hayflick's medium, we followed the protocol:

- Grow *M. genitalium* cells from stock in a 25 cm^2 flask with 5 mL of Hayflick plus 15 mM light (^{12}C) or heavy (^{13}C) lysine or 8 mM of unmarked or marked (S-adenosyl methionine, also known as SAM) methionine.
- Once the cultures are grown, split cells 1:10 in same conditions. Remaining cells can be washed with PBS and stored at -80ºC.

- Once the cultures are fully grown again, wash the cells with PBS and store them at -80ºC.
- Prior to sending them to the proteomics facility, thaw pellets on ice and resuspend in 20 µL 1% SDS diluted in TE. Boil for 5 minutes, vortex and measure protein concentration in Nanodrop.

Once these steps were completed, we sent the samples on ice to the Proteomics Facility at the CRG. The results were analyzed in Serrano's Lab.

M.5 Epifluorescence Microscopy

M. genitalium strains were grown on µ-Slide 8 well plates (Ibidi) overnight at 37ºC with 5% CO_2. Strains were inoculated into 200 µL of fresh SP4. The initial inoculum depended on the stock concentration and usually ranged between 2 µL and 8 µL. The next day, cells were washed thrice with 1x PBS with $CaCl_2$ and $MgCl_2$ (Sigma-Aldrich) and visualized on a *Nikon Eclipse TE 2000-E* microscope (Nikon) using a 100x objective lens with immersion oil.

Images were captured with a *Nikon Digital Sight DS-SMC* camera (Nikon) controlled by *NIS-Elements BR* software (Nikon). The camera was user-programmed to take different captures of the same field, the number of which depended on the experiment. Usually, a phase contrast capture was followed by the different photos under fluorescence exposure and then the macro finished with another phase contrast photo to ensure that the cells had not moved during the process. To detect eYFP fluorescence, cells were excited at 500 nm for 1 second and the fluorescence was collected at 542 nm; for mCherry fluorescence, the samples were exposed at 560 nm for 2 seconds and captured at 630 nm; for Hoechst 33342, the exposure was at 387 nm for 800 ms and the light was captured at 447 nm.

Acquired images were analyzed with *ImageJ* software (NIH). Cells were automatically counted with the GDSC plug-in.

M.6 Scanning Electron Microscopy

Scanning Electron Microscopy (SEM) was performed as described previously (Pich *et al*., 2008). *M. genitalium* cultures were grown to mid-log phase over glass coverslips in a 24-well plate with fresh SP4. The glass coverslip was marked with a diamond tip scriber in one side and placed in one of the wells with 1 mL of fresh SP4. They were marked for two main reasons: to identify the mutant (1) and the side in which the mycoplasmas were attached (the non-marked side). Thus, the mark had to be univocal and recognizable to correctly allow the discrimination of the sample and the growth side. Usually, due to the small surface of the coverslips, they were marked with numbers that allowed unambiguous recognition of both sides (for instance, the number 8 wouldn't be an appropriate choice because it would not allow to determine in which side the bacterium was attached).

The inoculum depended on the stock concentration and usually ranged between 5-10 µL of *M. genitalium* strains. The mutants were grown overnight and washed thrice with 1 mL 1x PBS. Then, the cells were fixed with 1% glutaraldehyde (v/v) dissolved in PBS for one hour in the dark. Samples were washed again with PBS and dehydrated sequentially with increasing ethanol solutions (25, 50, 75 and 100% ethanol), 10 minutes for each solution. Once in 100% ethanol, samples were sent to Servei de Microscòpia (UAB) and immediately critical-point dried in a K850 Critical Point Drier (Emitech) and then they were sputter coated with gold. Samples were observed using a *MERLIN FE-SEM* microscope (ZEISS).

Images were analyzed with *ImageJ* software (NIH).

M.7 Growth Analysis

To measure the replication rates of several *M. genitalium* strains, a mid-log phase culture grown in a 25 cm^2 flask with 5 mL SP4 was used. The medium was aspirated and the cells were resuspended in 3 mL of fresh SP4. Then, 300 µL of the cellular suspension were inoculated in the first (or seventh) row of a 96-well plate. 100 µL of the first well was inoculated into the next well (second/eighth) row) that contained 200 µL of fresh SP4, thus diluting 1/3 the initial concentration (Figure MM. 1). This process was repeated four more times (until the sixth/twelfth row), therefore achieving a final 1/243 dilution. In the sixth/twelfth well, 100 µL were discarded after mixing by pipetting up and down three times to leave the final volume at 200 µL. The 96-well plated was sealed with transparent tape to diminish condensation and incubated at 37ºC and 5% CO_2 for 7 days.

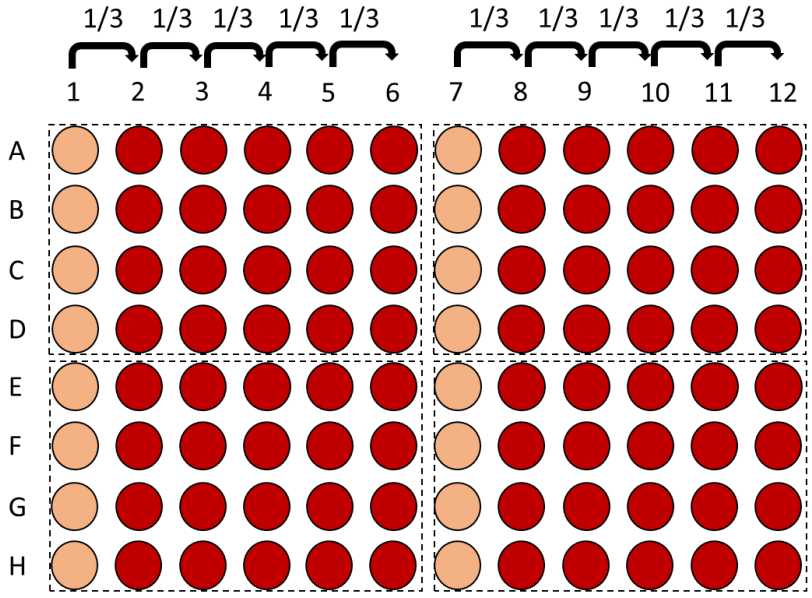

Figure MM. 1. Schematic representation of a 96-well plate used for growth kinetics of *M. genitalium* strains. 300 µL of each strain was inoculated in the first (or seventh) row and it was diluted sequentially with SP4 until the sixth (or twelfth) row. For instance, 300 µL of a G37 strain was seeded at the A1 well; 100 µL of the A1 well was inoculated into the A2 well that contained 200 µL of SP4. Next, 100 µL of the A2 well was seeded into the A3 well, 100 µL of the A3 well was transferred to the A4 well. This process was repeated until the A6 well was reached. Then, after pipetting up and down several times, 100 µL of the A6 well were discarded in order to leave the final volume at 200 µL. Four technical repeats were performed for each strain (A1-A6, B1-B6, C1-C6 and D1-D6, for instance), as it is represented by a dotted line square.

The plate was placed into a *Tecan Sunrise Absorbance Microplate Reader* (Tecan) inside the incubator. This microplate reader was used to extrapolate the replication rates by measuring the colorimetric change of the medium at 550 nm. The alteration of the

spectrum is related to the microorganism growth, as the metabolism of the bacteria acidifies the initial pH from 7.8 (red) to 6 (yellow). Then, a growth curve was generated for each dilution and the inflection point was inferred. Next, the inflection points were plotted in a graphic, using the Napierian logarithm of the dilution as the x coordinate for each dilution. Once all the inflection points were plotted and aligned, the equation of the line was obtained and the doubling time (g) was inferred using the slope (μ, growth rate constant) of the line, as described in the formula for exponential growth of bacteria ($g = \ln 2/(1/\mu)$). This method is an adaptation of the one reported in Karr et al., 2012.

For each analysis, there was a total of 400 lectures, one every half hour for up to eight days. The readings were stored in an Excel datasheet and analyzed as described after the measurements were over. In order to obtain the readings, a proprietary software of the Tecan spectrophotometer (Magellan) was used. A new software was developed recently by Jaume Piñol to ease the downstream analysis of the data. In addition, a Python script was designed to organize each dataset (the absorbance values of the dilutions of the four technical replicates) in an individual Excel sheet. Then, the same script analyzed the data and provided the curve parameters needed to extrapolate the duplication time. Once all the parameters were calculated, the script was designed to summarize all the growth data in a global Excel sheet, thus providing the average replication time for each strain using the four technical repeats per plate. The Python script can be consulted and downloaded at the following link: shorturl.at/hozGZ.

After running this script, the user must run the Solver complement for each dilution in order to obtain the real adjusted value. Thus, this program reduces the analysis of the reads from several hours to less than five minutes, as it only takes seconds to calculate the adjusted values for each dilution using Solver. The results of each technical repeat are gathered as they are calculated in the Global sheet, as the script has set the necessary formulas to gather the values to calculate the average replication time for each strain.

M.8 ICP-MS

Aiming to assess the metal uptake of *M. genitalium*, dried pellets of *M. genitalium* were analyzed using Inductively Coupled Plasma Mass Spectrometry (ICP-MS). Although this is an analysis technology that can detect elements at very low concentrations, the scarce levels of biomass achieved with *M. genitalium* grown in a culture flask were insufficient to be analyzed (two 175 cm^2 flasks yielded less than a microgram in dried weight).

To obtain greater levels of biomass, *M. genitalium* strains were grown in a 2 L sterilized Erlenmeyer at 37ºC for five days in an orbital shaking incubator. One liter of SP4 broth was prepared as described for each strain, although the pH of the SP4 base was not adjusted to 7.8 due to the lack of a 5% CO_2 atmosphere in the incubator. Thus, the final pH of the broth was 7.2.

The cultures were processed after five days. The content of the Erlenmeyer was poured into a 1 L centrifuge bottle and centrifuged at 7000 rpm (12500g) in a JLA-8.1000 rotor for 40 minutes. Then, the supernatants were discarded and the pellets were resuspended in 10 mL PBS Ca^{2+} Mg^{2+} (Sigma-Aldrich) and transferred into sterile 13 mL tubes. They were centrifuged again at 12500 rpm (18000g) in a JA-25.50 rotor for 15 minutes. Next, the supernatants were discarded again and the pellets were washed in the same tube with 10 mL of fresh PBS Ca^{2+} Mg^{2+} and centrifuged once again in the same conditions previously described. After that, the supernatant was aspired thoroughly and stored at -80ºC until they were sent for analysis at the *Servei de Química Analítica* (UAB). As a control, 10 mL of each liter of SP4 were stored at 4ºC before the inoculation and they were analyzed in order to assess the total metal uptake of *M. genitalium*.

APPENDICES

A.1 Appendix of Chapter I

A.1.1 Plasmid constructions

Supplementary Table I. 1. List of plasmids used to create the strains used in Chapter I.

Plasmid name	Description	Source
pΔmraZW	Suicide vector pBE (Pich, Burgos, Planell, et al., 2006) derivative used to knock out *mraZ* and mraW by homologous recombination. This strain was used as a scaffold to create the *mraZ*, *mraW* and *mraREF* strains Selectable marker: chloramphenicol.	This work
pmraZWTcTer	A pBE derivative used to reintroduce both *mraZ* and mraW into the double-knockout strain. The tetracycline resistance is placed upstream of both genes and in the antisense orientation, to prevent polar effects. The selectable marker also has the MG_305 transcription terminator at its 3' end. Selectable marker: tetracycline	This work
pΔmraZ	Suicide vector pBE derivative used to create the *mraZ* defective mutant. Selectable marker: tetracycline.	This work
pΔmraW	Suicide vector pBE derivative used to create the *mraW* defective mutant. Selectable marker: tetracycline.	This work
pdcw	A pBE derivative used to delete the whole division and cell wall operon (*dcw*) of *M. genitalium*. The four genes of the operon and the upstream region were replaced by a *cat* marker. Selectable marker: chloramphenicol.	This work
pftsZ	Suicide vector pBE derivative used to create the *ftsZ* defective mutant. Selectable marker: chloramphenicol.	This work
pmraZCOM	pBE derivative used in the *cis* complementation of the *mraZ* mutant. Selectable marker: chloramphenicol.	This work
pMTn221P221	Minitransposon miniTn4001 (Calisto et al., 2012) derivative carrying a *mraZ* copy under the control of its own promoter. Used to create the *mraZ* overexpressing strains and in *trans* complementation assays of the *mraZ* mutant. Selectable marker: chloramphenicol.	This work

pMTn221P438	Minitransposon miniTn4001 derivative carrying a *mraZ* copy under the control of the MG_438 promoter. Used to create the *mraZ* overexpressing strains and in *trans* complementation assays of the *mraZ* mutant. Selectable marker: chloramphenicol.	This work
pMTn221222P221	Minitransposon miniTn4001 derivative bearing a copy of *mraZ* followed by a copy of *mraW* under the control of its own promoter. Used to create the *mraZ* overexpressing strains and in *trans* complementation assays of the *mraZ* mutant. Selectable marker: chloramphenicol.	This work
pMTn221mutP438	Minitransposon miniTn4001 derivative carrying a *mraZ* copy with a frameshift under the control of the MG_438 promoter. Used in the creation of the *mraZ* overexpressing strains. Selectable marker: chloramphenicol.	This work
pftsZCh	Suicide vector pBE derivative used to fuse the *ftsZ* gene to the *mCherry* fluorescent marker. Selectable marker: chloramphenicol.	This work
p217YFP	Suicide vector pBE derivative used to fuse MG_217 to the *eYFP* fluorescent marker. Selectable marker: puromycin.	This work

A.1.1.1 Construction of pΔmraZW and generation of *mraZWCm*

In order to generate a reference strain that could be compared to the *mraZ* and *mraW* null mutant strains, these two genes were both knocked out with the pΔmraZW plasmid (Supplementary Figure I. 1). This construction allowed the substitution of both genes for a chloramphenicol acetyltransferase marker by bearing the upstream and downstream regions of *mraZ* and *mraW* flanking the antibiotic resistance gene. The originated strain (*mraZWCm*) was used as a platform to generate the *mraZREF*, *mraZ* and *mraW* strains.

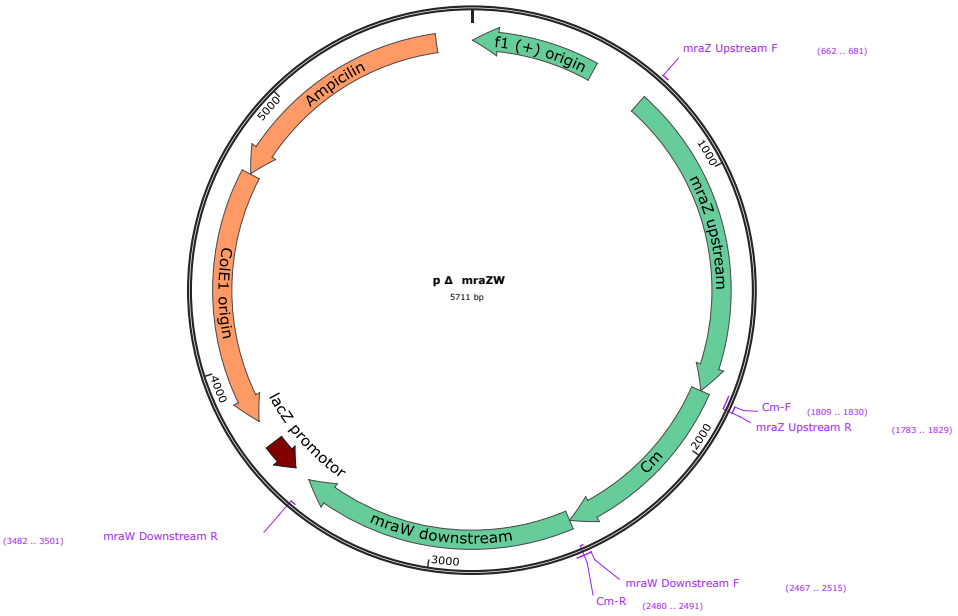

Supplementary Figure I. 1. Map of pΔmraZW plasmid. Oligonucleotides used in its construction are highlighted.

The upstream region of *mraZ* was amplified by PCR with the oligonucleotides *mraZ Upstream F* and *mraZ Upstream R*. The downstream region was amplified using *mraW Downstream F* and *mraW Downstream R* as primers. The chloramphenicol

acetyltransferase was amplified from a pMTnCat (Calisto *et al*., 2012) using the Cm-F[1] and the Cm-R primers. Both *mraZ Upstream R* and *mraW Downstream F* oligonucleotides had overlapping sequences to the 5' and 3' end of the chloramphenicol acetyltransferase marker, respectively. Thus, by SOE-PCR it was possible to join the mraZ upstream fragment and the *cat* marker (*mraZ Upstream F* and *Cm-R* used as primers) as well as the marker to the mraW downstream sequence (*Cm-F* and *mraW Downstream R*). Finally, both regions were amplified together using the *mraZ Upstream F* and *mraW Downstream R* oligonucleotides. This fragment was cloned into an *Eco*RV-digested pBE and transformed into a *M. genitalium* G37 strain.

A.1.1.2 Construction of *mraREF*, *mraZ* and *mraW* strains

Due to the possible polar effects generated by an antibiotic resistance marker, the *mraZ* and the *mraW* strains were compared to the *mraREF* strain. This strain was used as a reference as it had a tetracycline resistance marker (*tetM*) upstream of *mraZ*, as it was the case with both mutant strains. The three strains were generated after transforming their respective plasmids into the *mraZWCm* strain. These plasmids have homology with the upstream and downstream region of *mraZ* and *mraW* and contain a tetracycline resistance marker in antisense in order to reduce the polar effects derived from the constitutive promoter. Moreover, the antibiotic marker, under the control of the constitutive promoter of the MG_438 gene, has a transcription terminator from the downstream region of the MG_305 gene at its 3' end. This transcription terminator was identified using the TransTermHP software (Kingsford et al., 2007). The immediate

[1] The Cm-F oligonucleotide is the same as the Tc-F and Pac-F, as it accounts for the MG_438 promoter sequence and this sequence is used to drive the transcription of the three antibiotic resistance markers. It is listed as Cm-F instead of Tc-F (its original name, as stated in the oligonucleotides list) to avoid any confusion.

upstream zone of *mraZ* (105 bp upstream of the start codon) was preserved in all cases, as it was thought to contain the promoter and regulatory motifs.

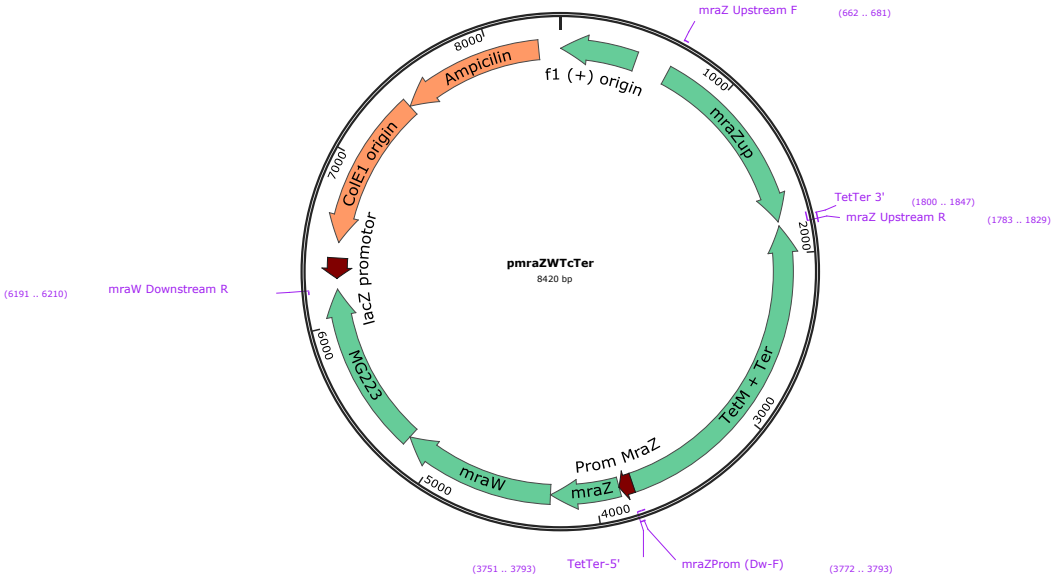

Supplementary Figure I. 2. Map of pmraZWTcTer plasmid. Oligonucleotides used in its construction are highlighted.

The pmraZWTcTer plasmid (Supplementary Figure I. 2) was constructed also by SOE-PCR. The upstream and downstream regions were the same used in the construction of the pΔmraZW plasmid. The resistance marker with the transcription terminator at its 3' end was amplified from the pMG_236 plasmid (A.2.1 Plasmid Constructions of Chapter II) using the *TetTer-5'* and *TetTer-3'* oligonucleotides. These oligonucleotides had overlapping regions with the *mraZ* promoter and the *mraZ* upstream region, respectively, to allow the total amplification of the different fragments by SOE-PCR. The second fragment was amplified with the *mraZProm (Dw-F)* and *mraW Downstream R* oligonucleotides. The upstream region was put together with the marker using the *mraZ Upstream F* and *TetTer-5'* primers and the downstream region was merged with the antibiotic resistance gene using the *TetTer-3'* and *mraW Downstream R* oligonucleotides. Both regions were later amplified together with *mraZ Upstream F* and *mraW Downstream R* as primers. The whole amplicon was cloned into an *EcoRV*-digested pBE and cloned into the *mraZWCm* strain.

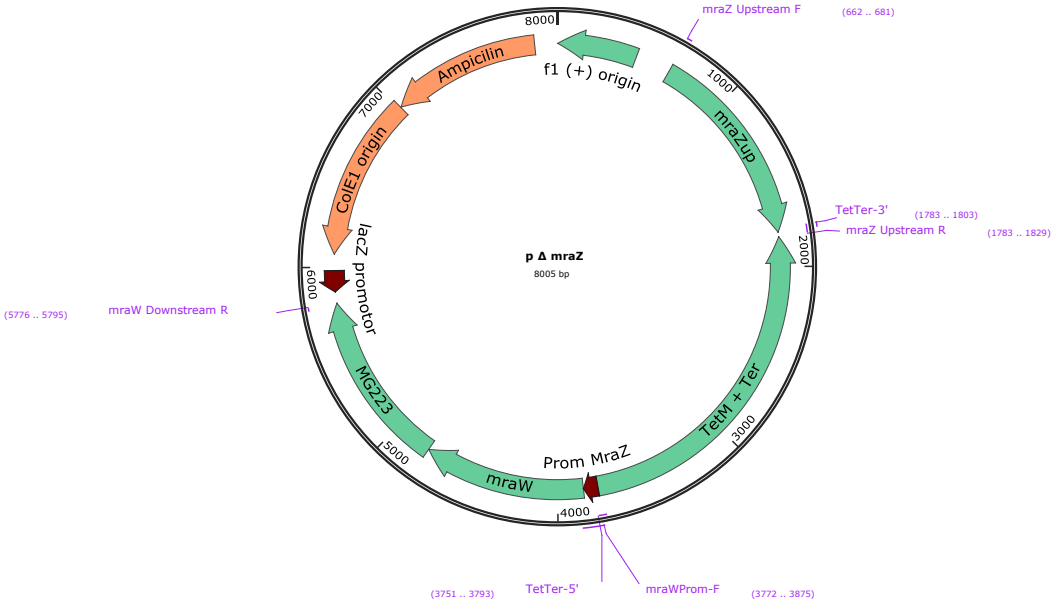

Supplementary Figure I. 3. Map of pΔmraZ plasmid. Oligonucleotides used in its construction are highlighted.

As for the pΔmraZ plasmid (Supplementary Figure I. 3), it was constructed in a similar way to the pmraZWTcTer plasmid. It contained the same upstream and downstream regions, but it lacked the *mraZ* ORF. The promoter region was just upstream from *mraW* thanks to a large oligonucleotide (*mraW Prom-F*) that annealed with the 5' of mraW in its 3' end and contained an 80+ nucleotide long 5' tail that annealed with the immediate upstream region of the *mraZ* gene. Thus, the putative regulatory region was preserved to ensure that the possible phenotypical effects associated with the strain were directly related to the loss of *mraZ*.

As already mentioned, the upstream region and the tetracycline resistance marker were amplified as stated in the pmraZWTcTer plasmid (amplified using the *mraZ Upstream F* and *TetTer-5'* oligonucleotides). The *mraW* gene and the downstream region were amplified using the *mraWProm-F* and *mraW Downstream R* primers. Then, the two fragments could be merged because of the sequence overlap created by the *TetTer-5'* oligonucleotide, which contained a tail complementary to the regulatory region of *mraZ* that was present in the second fragment because of the *mraWProm-F* oligonucleotide. Thus, the final product was amplified using again the *mraZ Upstream F* and *mraW Downstream R* oligonucleotides. This was cloned into an *EcoRV*-digested pBE and cloned into the *mraZWCm* strain.

Supplementary Figure I. 4. Map of pΔmraW plasmid. Oligonucleotides used in its construction are highlighted.

The procedure to construct the pΔmraW plasmid (Supplementary Figure I. 4) was very similar to the one used with the pmraZWTcTer plasmid. The upstream region and the *tetMP438* marker were amplified as already described. As for the *mraZ* and downstream fragment, an oligonucleotide (*mraZ-R*) containing the 3' end of *mraZ* and a tail complementary to the 5' end of the MG_223 gene was used. So, in order to put the MG_223 gene just downstream of the *mraZ* stop codon, the *mraZ* ORF and its promoter region were amplified with the mraZProm (Dw-F) and mraZ-R oligonucleotides; and 1 kb of the MG_223 gene was amplified as usually with the mraW Downstream F and mraW Downstream R primers. Then, as the 3' end of the mraZ product was complementary to the 5' of the MG_223 fragment, both fragments were merged using the mraZProm (Dw-F) and mraW Downstream R oligonucleotides. As for the upstream part, it was amplified using the mraZ Upstream F and mraZ-R oligonucleotides, as the TetTer-5' oligonucleotide had a tail complementary to the regulatory region of mraZ, as stated previously. Finally, the whole fragment was put together with the mraZ Upstream F and mraW Downstream R primers. Then, it was cloned into an *Eco*RV-digested pBE and cloned into the *mraZWCm* strain.

A.1.1.3 Construction of the *mraZ* complementation and overexpressing strains

The complementation of the *mraZ* mutant was firstly performed in *trans*, placing the ectopic *mraZ* copy in a minitransposon. There were several versions of this minitransposon, as the complementation was tried using two different promoters (the own *mraZ* promoter and the constitutive promoter of the MG_438 gene) and a copy of *mraW* was also placed after *mraZ* in one of the versions. Depending on the promoter, the forward primer used to amplify *mraZ* changed: *MG221P221-F(ApaI)* for its own promoter and *COMmg221-F(ApaI)* for the MG_438 promoter. Equally, the reverse primer used depended on if the transposon included only a copy of *mraZ* or if it was accompanied by mraW: for the former, *COMmg221-R(XhoI)* was used, while *COMmg222-R(XhoI)* was the one used if *mraW* was placed after *mraZ*. These different constructions were also used to overexpress *mraZ* in a wild-type background. In addition, another construction that contained a frameshift in *mraZ* was also constructed with the forward primer *COM221mut-F(ApaI)*. All of these constructions were amplified from gDNA of *M. genitalium*, digested with *Xho*I and *Apa*I and cloned into an equally digested MiniTn4001CmR. Then, they were transformed into the G37 and *mraZ* strains.

To analyze the complementation in *cis*, a new plasmid was constructed to place a *mraZ* copy after the *ftsZ* gene by homologous recombination (Supplementary Figure I. 5). The upstream region (*ftsZ*) was amplified using the *mg224-F(cherry)* and the 224*mraZ*-R primers. This last oligonucleotide overlapped with the 3' of *ftsZ* and it left a hanging 3' end which was complementary to the 5' of *mraZ*. Then, we amplified the *mraZ* + CmR construction from a MiniTn4001CmR in which we have previously cloned the *mraZ* ORF to try *trans* complementation. This amplification was done using the *mraZ-F* and *Cm-R* primers. The last part of the construct contained the downstream region of *ftsZ* (a short intergenic region of 45 bp and a large part of MG_225) and it was amplified by PCR using the *mg224-Dw-F(Cm)* and *mg224-Dw-R(Cm)* oligonucleotides. The *mg224-Dw-F(Cm)* oligonucleotide had a 5' hanging end which overlapped with the 3' end of CmR. All three parts were fused together using SOE-PCR and cloned into an *Eco*RV-digested pBE and later transformed into the *mraZ* mutant.

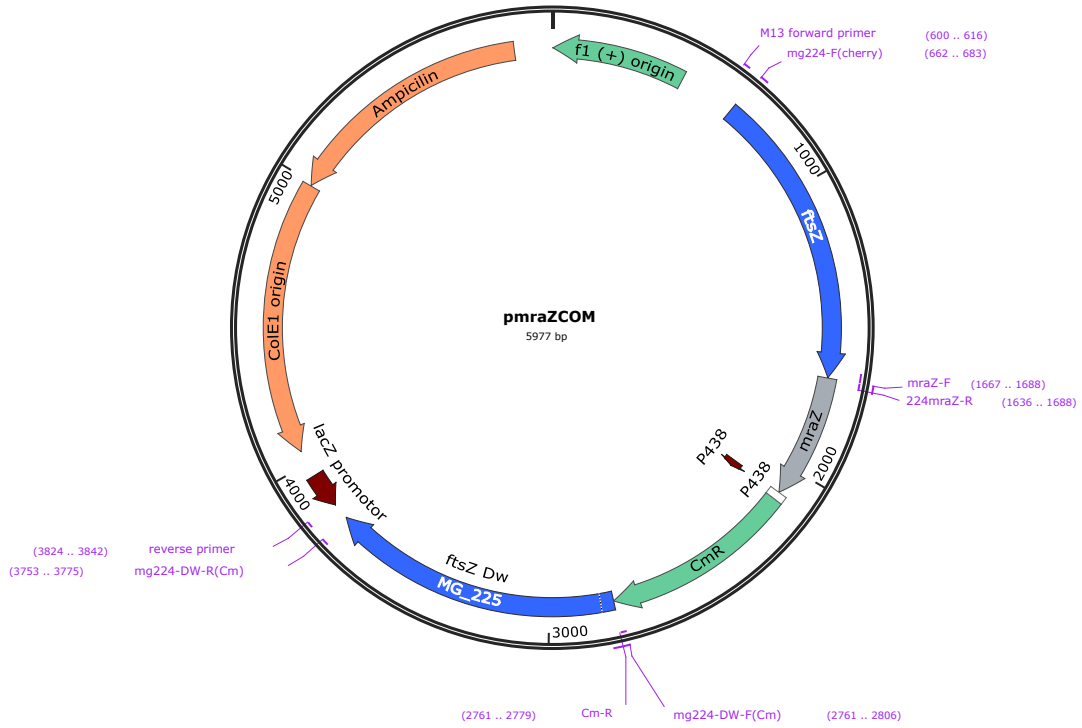

Supplementary Figure I. 5. Map of the plasmid used to complement in *cis* the *mraZ* mutant. Oligonucleotides used in its construction are highlighted.

A.1.1.4 Construction of *dcw* and *ftsZ* mutants

To delete the whole division and cell wall operon Supplementary Figure I. 6, the *mraZ* upstream region was amplified using the *mraZ upstream F* and *mraZ upstream R* primers. The downstream region was amplified using the mg224-Dw-F and mg224-Dw-R(Cm) oligonucleotides. The 3' of the first fragment and the 5' of the second fragment overlapped with the 5' and 3' of the *cat* marker, respectively. The chloramphenicol resistance was amplified using the Cm-F and Cm-R primers. Then, the three fragments were fused together with SOE-PCR.

As the first fragment (*mraZ* upstream region) ends at 80 bp of the *mraZ* ORF, the *mraZ* boxes were not present in this construction. The whole fragment was cloned into an *Eco*RV-digested pBE and later transformed into the G37 strain.

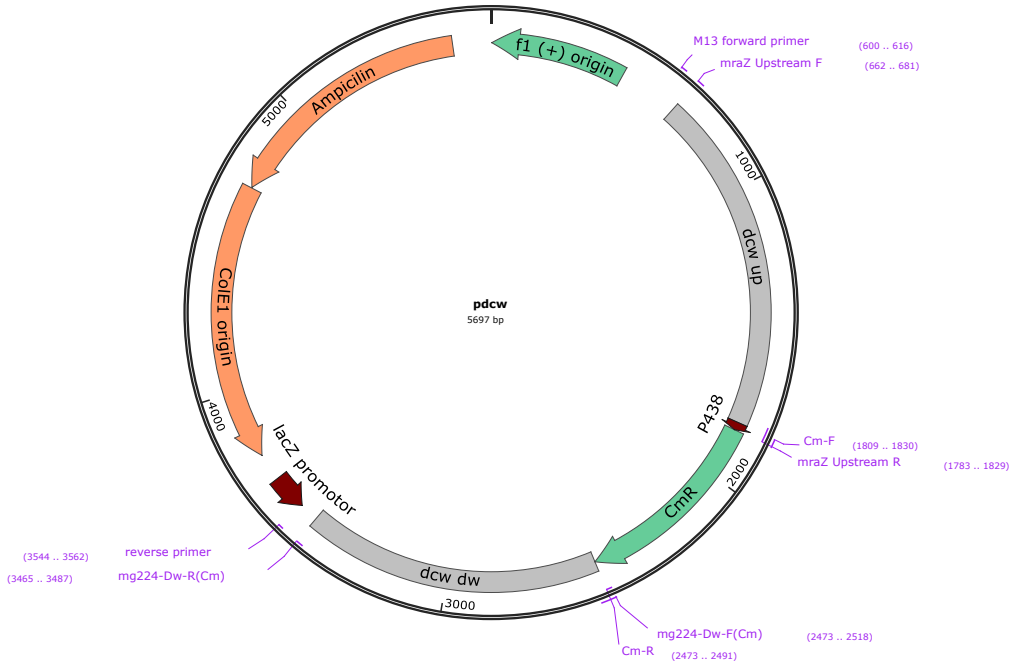

Supplementary Figure I. 6. Map of the plasmid used to delete the whole division and cell wall operon. Oligonucleotides used in its construction are highlighted.

To obtain a single knockout of the *ftsZ* gene, we replaced this gene for a chloramphenicol acetyltransferase (*cat*) resistance marker by homologous recombination Supplementary Figure I. 7. In order to do so, the upstream and downstream regions of *ftsZ* were amplified using two pairs of oligonucleotides: mraW(Dw-F) and 223p438(XhoI)-R for the upstream region and mg224-Dw-F and mg224-Dw-R(Cm) for the downstream fragment. The CmR was amplified with the Cm-F and Cm-R primers, as already described. The 3' of the first fragment and the 5' of the second fragment overlapped with the 5' and 3' of the *cat* resistance, respectively. Thus, all three fragments were joined together with SOE-PCR and cloned in an *Eco*RV-digested pBE. This construction was transformed into the G37 strain.

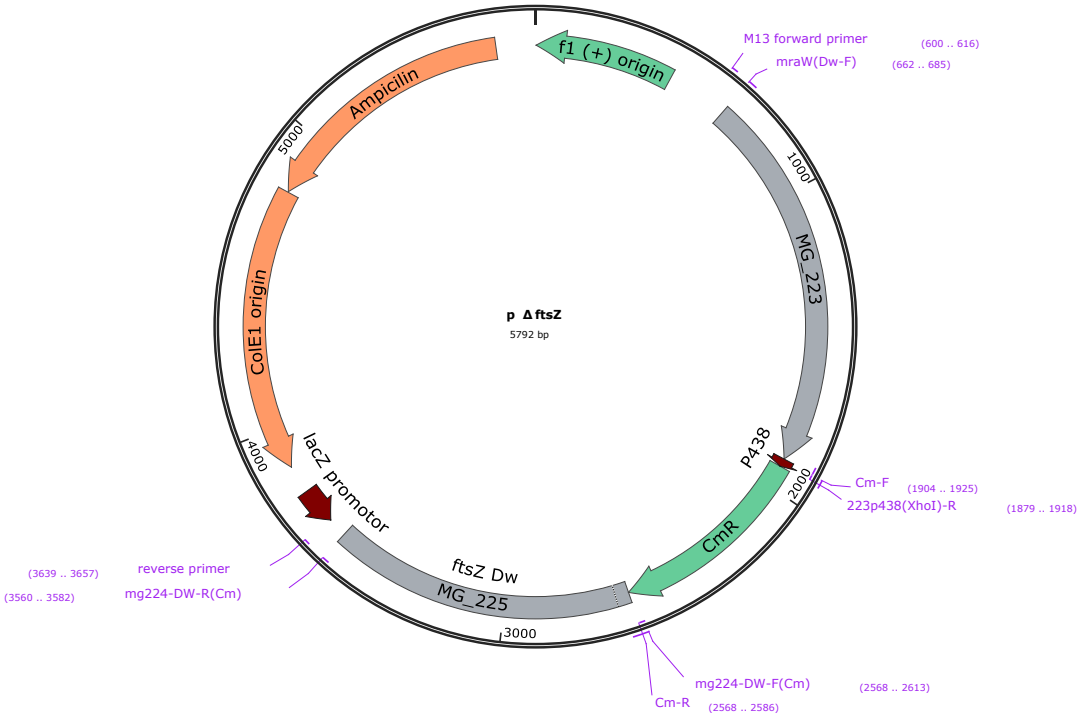

Supplementary Figure I. 7. Map of pΔftsZ plasmid. Oligonucleotides used in its construction are highlighted.

A.1.1.5 Construction of *ftsZCh* and *217YFP* strains

Two new constructions were created to fuse a fluorescent reporter to FtsZ and MG217 by homologous recombination. As for the former, the *ftsZ* gene was fused to the *mCherry* reporter (Supplementary Figure I. 8). In order to do this, a large portion of the *ftsZ* gene was amplified with the *mg224-F(cherry)* and mg224-R(cherry) oligonucleotides. Then, the downstream region (which contained an intergenic region between *ftsZ* and MG_225 and a part of MG_225) was also amplified using the *mg224-Dw-F* and *mg224-Dw-R(Cm)* primers. The *mg224-R(cherry)* and *mg224-Dw-F* contained an overhang end that overlapped with the 5' of the *mCherry* reporter and the 3' of the *cat* resistance marker, respectively. The *mCherry* and *cat* cassette was amplified from the pMG_428:Ch plasmid (Torres-Puig et al., 2015) with the *Cherry-F* and *Cm-R* oligonucleotides. Then, the three fragments were joined by SOE-PCR and cloned into an *Eco*RV-digested pBE and later transformed into the G37, *mraZ* and *mraW* strains.

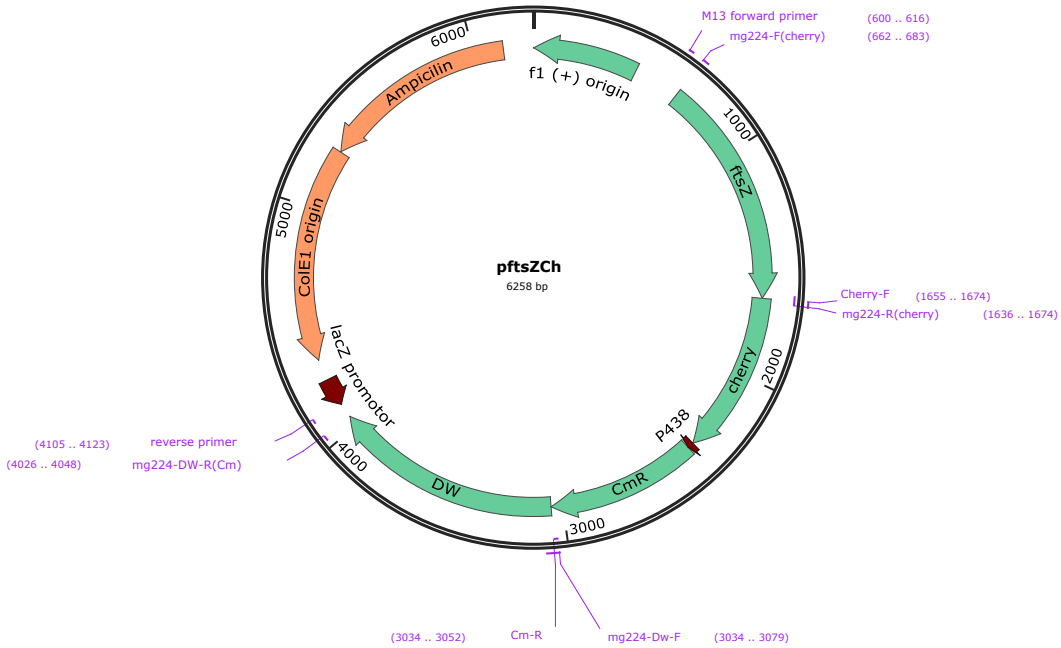

Supplementary Figure I. 8. Map of the pftsZCh plasmid. Oligonucleotides used in its construction are highlighted.

Regarding the plasmid that introduced the *eYFP* marker after the MG_217 gene (Supplementary Figure I. 9), it was constructed in a similar way. The upstream region was amplified using the *mg217-YFP-F* and *mg217-YFP-R* oligonucleotides, and the downstream region was also amplified by PCR with the *mg217Dw-PAC-F* and *mg217Dw-R* primers. In this case, the cassette containing the eYFP and *pac* markers was amplified from the pTnMG_428:YFP plasmid (Torres-Puig et al., 2018) using the *YFP-F* and *Pac-R (BamHI)* oligonucleotides. The three fragments were then fused by SOE-PCR, as the *mg217-YFP-R* and *mg217Dw-PAC-F* oligonucleotides contained an overhang that overlapped with the 5' of the *eYFP* marker and the 3' of the puromycin resistance, respectively. Then, this construction was cloned into an *Eco*RV-digested pBE and later transformed into the G37 and *mraZ* strains.

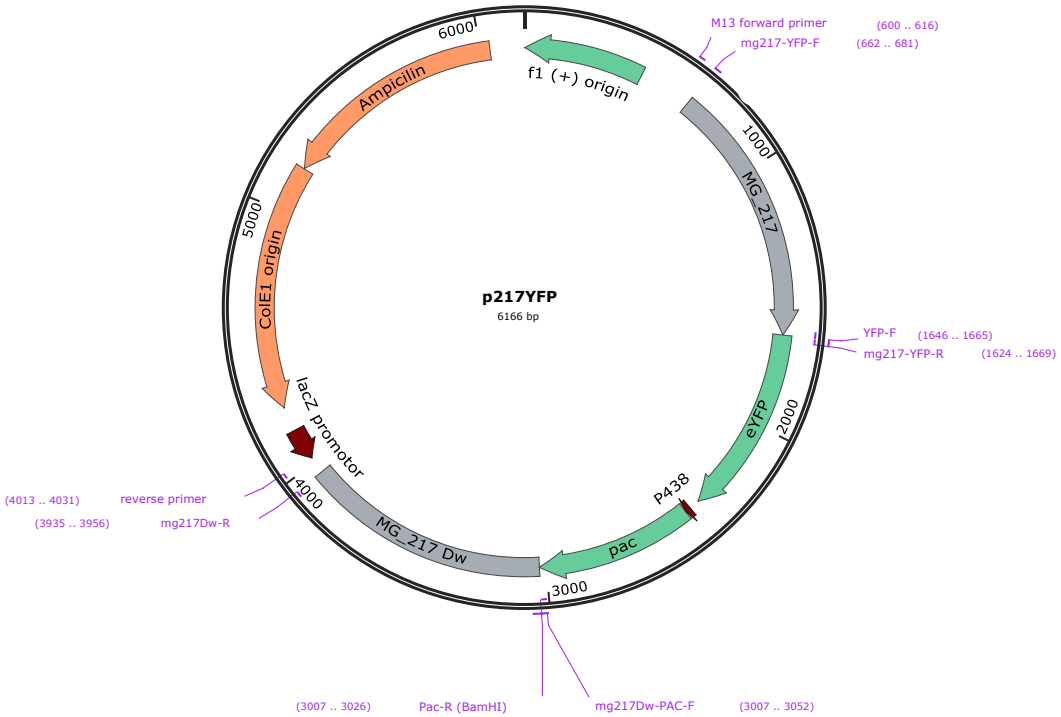

Supplementary Figure I. 9. Map of the p217YFP plasmid. Oligonucleotides used in its construction are highlighted.

A.1.2 Oligonucleotides

Supplementary Table I. 2. Oligonucleotides used in Chapter I.

Aim	Primer name	Sequence (5'-3')
Mutants	mraZ Upstream F	GTTACACCTACTAACAACAC
	mraZ Upstream R	TTTATTAATTCTAAATACTACAATTCTACAACTTAAATTAACCCTTG
	mraW Downstream F	CGATGAGTGGCAGGGCGGGGCGTAAATGTACAAACCAAAAAATATTAAC
	mraW Downstream R	TTGATAAGTGCAACATTAGC
	TetTer-3'	CAAGGGTTAATTTAAGTTGTAGCTCGAGCTAAAAATCTGTTTTTTGGT
	TetTer-5'	CTTTTTGTCCAAAATGAAATGAATTCTAGTATTTAGAATTAATAAAG
	mraZ-F	ATGCTGCTAGGTACCTTTAATC
	mraZ Up-R	CTACAACTTAAATTAACCCTTG
	mraZProm(Dw-F)	TCATTTCATTTTGGACAAAAAG
	mraW-F	TCATTTCATTTTGGACAAAAAGAAATTTTTATGCTAAGATAAAAGTGTTTAAAAGTGTCGCAAAGTGTGACAAAGTGGAAAAAATGCTAAATAACCAACAGATC
	mraZ-R	ATATTTTTTGGTTTGTACATTTATTTAGCATCTTTCATCC
	mraW(Dw-F)	ATGTACAAACCAAAAAATATTAAC
	mraW+Prom(Dw-F)	TCATTTCATTTTGGACAAAAAGAAATTTTTATGCTAAGATAAAAGTGTTTAAAAGTGTCGCAAAGTGTGACAAAGTGGAAAAAATGTACAAACCAAAAAATATTAAC
	Tc-F (or Cm-F or Pac-F)	CTCGAGTAGTATTTAGAATTAATAAAG (sequence of the MG_438 promoter)
	Cm-R	TTACGCCCCGCCCTGCCAC
	223p438(XhoI)-R	AATTCTAAATACTACTCGAGAGTTATTTAACCAAGCGTTGG
	mg224-F(cherry)	CACTATCCTAATTTAGCAAGTG
	mg224-DW-F(Cm)	GTGGCAGGGCGGGGCGTAATTAATTTAATTTATCGTTTAGAATTGC
	mg224-DW-R(Cm)	CTTTCTGGAGTTGGCAATAATAG
	224mraZ-R	GATTAAAGGTACCTAGCAGCATATTAGTAGATTTGGTTTTGGTGC
	mg217-YFP-F	CAGCAATTTAATCAACCAGG
	mg217-YFP-R	CAGCTCCTCGCCCTTGCTCACGTTATTGTTATTGTTATTGTTATTTTCATAGAAGTCATCACGGTAA
	mg217Dw-PAC-F	CTAGAAAACCTGGTGCTTAAAAAGCGTGTTTTAACTAATGAAA
	mg217Dw-R	TAAGTTGTTTAGCTACATCATC
	Pac-R (BamHI)	GCGGGATCCTTAAGCACCAGGTTTTCTAG
	YFP-F	ATGGTGAGCAAGGGCGAGGA

	MG221P221-F(ApaI)	ATTGGGCCCCAAGGGTTAATTTAAGTTGTAGTC
	COMmg221-F(ApaI)	ATTGGGCCCTAGTATTTAGAATTAATAAAGTATGCTGCTAGGTACCTTTAATC
	COM221mut-F (ApaI)	ATTGGGCCCTAGTATTTAGAATTAATAAAGTATGCTGCTAGAGTACCTTTAATC
	COMmg221-R(XhoI)	ATTCTCGAGTTATTTAGCATCTTTCATCCTTTC
Screening	mg220(Up-F)	GTGATCCTGATCCAATCCAA
	mg226(Up-R)	ATTAATTCTAAATACTATCTAGAGCCCAACATCAAACATGGTC
qRT-PCR	RTPCRmg177-F	TGAGTGTCCAGCTGGTTTTG
	RTPCRmg177-R	AACCGGGGAAAAGTTAGCAT
	RTPCRmg418-F	TGTTGACGCTAGTGGTTTGG
	RTPCRmg418-R	TTCCACCCATGTATTGAGAGTG
	RTPCRmg430-F	GGAAGCAGTTGGATTGCCTA
	RTPCRmg430-R	ATGCACTCCTCCATTGGAAA
	RTPCRmg221-F	CCTTGATAACAAGAACAGAA
	RTPCRmg221-R	GGAAGTTATTAAAGGTTTGAAA
	RTPCRmg222-F	AGGGTTTGCAGGACACAGTC
	RTPCRmg222-R	TCCCATCAAACTTGGTTATTGA
	RTPCRmg223-F	TGATGATCAAAACCAGTTCAACA
	RTPCRmg223-R	TCAGTTCAGCGAGAACAACAA
	RTPCRmg224-F	GGATGAAAATGAAACTCAATTC
	RTPCRmg224-R	CTTGCTAAATTAGGATAGTGATAA
	RTPCRmg220-F	AAACCGTGCGGTGTTAAAGT
	RTPCRmg220-R	GCTAAGCAAGTTGTTGGTGGA
	RTPCRmg225-F	TCGGAAGTTTAGCGAAAAGC
	RTPCRmg225-R	AAAGCCGTGCGAATGATAAG
Sequencing	Fup-24	CGCCAGGGTTTTCCCAGTCACGAC
	Rup-24	TCACACAGGAAACAGCTATGACCA
	TetUp	TTCCTGCATCAACATGAG
	TetDown	GTCGTCCAAATAGTCGGA
	CmUp	CAACGGTGGTATATCCAG
	CmDown	CAGTACTGCGATGAGTGGCA
	PacUp	GTAGCTAATCTAACAGTAGG
	PacDown	GTCCTAGAACTTGGTGTATG

A.1.3 qRT-PCR primer efficiency

Supplementary Table I. 3. Amplification efficiency for each pair of primers used in qRT-PCR analysis of the *dcw* operon. The efficiency was calculated as described in M.3.2.1 Primer Design and Amplification Efficiency. Efficiencies ranging from 85 to 110% are considered suitable for qRT-PCR analysis.

Gene	Efficiency (%)
mraZ	87.32%
mraW	91.51%
MG_223	92.25%
ftsZ	90.67%

A.1.4 RNAseq data

Supplementary Table I. 4. Transcription changes in the division and cell wall operon and its immediate upstream and downstream genes in the *mraREF*, *mraZ* and *mraW* mutants compared to the G37 strain. There were not any other genes above or under the arbitrary cutoff fold change of log2 ± 1. In bold, those values above or under the cutoff.

Gene	*mraREF*		*mraZ*		*mraW*	
	Log2 Fold change	p-value	Log2 Fold change	p-value	Log2 Fold change	p-value
mraZ	0.666	0	**-3.076**	0	0.801	0
mraW	0.549	0	**3.572**	0	**-2.181**	0
MG_223	0.315	0.0001569	**2.97**	0	0.242	0.0242
ftsZ	0.281	0.0008091	**2.811**	0	0.158	0.0974
MG_220	0.564	0	0.78	0	0.646	0
MG_225	0.077	0.3049	0.775	0	0.076	0.3875

A.1.5 Proteomics data

Supplementary Table I. 5. Differentially expressed proteins in a *mraZ* background. The Copy Number (CN) of the proteins in the three strains is specified as well as the Fold Change (FC) with respect to the G37 strain. The gene name is stated when characterized. Biologically significant fold changes (>2, <0.5) are highlighted in bold. ND stands for Not Detected.

Overexpressed							
Locus tag	Gene	Gene product	G37	mraZ		mraW	
			CN	CN	FC	CN	FC
MG_224	*ftsZ*	Cell division protein *ftsZ*	$4.40 \cdot 10^6$	$1.10 \cdot 10^8$	**24.96**	$8.50 \cdot 10^6$	1.93
MG_222	*mraW*	Ribosomal RNA small subunit methyltransferase H	$4.17 \cdot 10^7$	$5.95 \cdot 10^8$	**14.28**	ND	–
MG_091	*ssb*	Single-stranded DNA-binding protein	$1.10 \cdot 10^7$	$1.53 \cdot 10^8$	**13.94**	$1.38 \cdot 10^8$	**12.58**
MG_516		UPF0154 protein	$7.70 \cdot 10^6$	$5.65 \cdot 10^7$	**7.34**	$4.90 \cdot 10^6$	0.64
MG_306		Uncharacterized membrane protein	$3.10 \cdot 10^6$	$1.65 \cdot 10^7$	**5.32**	$6.80 \cdot 10^6$	**2.19**
MG_318	*p32*	P32 adhesin	$1.54 \cdot 10^8$	$6.57 \cdot 10^8$	**4.28**	$1.51 \cdot 10^8$	0.99
MG_042	*potA*	Spermidine/putrescine import ATP-binding protein	$3.65 \cdot 10^7$	$1.23 \cdot 10^8$	**3.38**	$9.18 \cdot 10^7$	**2.52**
MG_233		Uncharacterized protein	$8.40 \cdot 10^6$	$2.60 \cdot 10^7$	**3.10**	$3.85 \cdot 10^7$	**4.58**
MG_326		DegV domain-containing protein	$5.22 \cdot 10^7$	$1.04 \cdot 10^8$	**2.00**	$4.82 \cdot 10^7$	0.92

Underexpressed							
Locus tag	Gene	Gene product	G37	mraZ		mraW	
			CN	CN	FC	CN	FC
MG_261	*dnaE*	DNA polymerase III subunit alpha	$3.48 \cdot 10^7$	$1.69 \cdot 10^7$	**0.48**	$2.27 \cdot 10^7$	0.65
MG_445	*trmD*	tRNA (guanine-N(1)-)-methyltransferase	$4.66 \cdot 10^7$	$2.20 \cdot 10^7$	**0.47**	$3.28 \cdot 10^7$	0.70
MG_075		Uncharacterized protein	$1.92 \cdot 10^8$	$8.83 \cdot 10^7$	**0.46**	$1.10 \cdot 10^8$	0.57
MG_460	*ldh*	L-lactate dehydrogenase	$5.57 \cdot 10^9$	$2.47 \cdot 10^9$	**0.44**	$2.55 \cdot 10^9$	**0.46**
MG_077	*oppB*	Oligopeptide transport system permease protein	$9.22 \cdot 10^7$	$3.88 \cdot 10^7$	**0.42**	$4.50 \cdot 10^7$	**0.49**
MG_320		Uncharacterized membrane protein	$3.85 \cdot 10^7$	$1.36 \cdot 10^7$	**0.35**	$3.55 \cdot 10^7$	0.92
MG_068		Uncharacterized lipoprotein	$1.41 \cdot 10^7$	$2.70 \cdot 10^6$	**0.19**	ND	-
MG_289	*p37*	High affinity transport system protein p37	$1.14 \cdot 10^8$	$1.83 \cdot 10^7$	**0.16**	$8.17 \cdot 10^7$	0.72

Supplementary Table I. 6. Proteins detected in the *mraZ* mutant and not in the wild-type strain and viceversa.

Detected in *mraZ* and not in G37					
Locus tag	Gene	Gene product	G37	mraZ	mraW
			CN	CN	CN
MG_027	*nusB*	Transcription termination/antitermination protein	ND	$9.20 \cdot 10^7$	$6.70 \cdot 10^7$
MG_452		Uncharacterized membrane protein	ND	$4.03 \cdot 10^7$	ND
MG_044	*potC*	Spermidine/putrescine transport system permease protein	ND	$1.70 \cdot 10^7$	ND
MG_057	*rnmV*	Ribonuclease M5	ND	$1.40 \cdot 10^7$	ND
MG_011		Uncharacterized protein	ND	$1.28 \cdot 10^7$	ND
MG_447		Uncharacterized membrane protein	ND	$1.20 \cdot 10^7$	$9.30 \cdot 10^6$
MG_223		Uncharacterized protein	ND	$7.88 \cdot 10^6$	ND
MG_463	*rsmA*	Ribosomal RNA small subunit methyltransferase A	ND	$6.90 \cdot 10^6$	ND
MG_360		DNA polymerase involved in DNA repair	ND	$6.85 \cdot 10^6$	$7.00 \cdot 10^6$
MG_477		Uncharacterized protein	ND	$6.60 \cdot 10^6$	ND
MG_411		Phosphate transport system permease protein PstA homolog	ND	$6.30 \cdot 10^6$	ND
MG_043	*potB*	Spermidine/putrescine transport system permease protein	ND	$3.15 \cdot 10^6$	$1.30 \cdot 10^6$

Detected in G37 and not in *mraZ*					
Locus tag	Gene	Gene product	G37	mraZ	mraW
			CN	CN	CN
MG_221	*mraZ*	Transcriptional regulator MraZ	$4.12 \cdot 10^8$	ND	$4.65 \cdot 10^8$
MG_226		Amino acid-polyamine-organocation (APC) permease family protein	$1.80 \cdot 10^7$	ND	ND
MG_147		Uncharacterized membrane protein	$7.80 \cdot 10^6$	ND	$8.40 \cdot 10^6$
MG_440		Uncharacterized lipoprotein	$4.40 \cdot 10^6$	ND	ND

Supplementary Table I. 7. Differentially expressed proteins in the *mraW* mutant. Only proteins with a fold change (FC) over 2 compared to the G37 strain were considered. CN stands for Copy Number.

Overexpressed							
Locus tag	Gene	Gene product	G37	mraZ		mraW	
			CN	CN	FC	CN	FC
MG_091	*ssb*	Single stranded DNA binding protein	$1.10 \cdot 10^7$	$1.53 \cdot 10^8$	**13.94**	$1.38 \cdot 10^8$	**12.58**
MG_233		Uncharacterized protein	$8.40 \cdot 10^6$	$2.60 \cdot 10^7$	**3.10**	$3.85 \cdot 10^7$	**4.58**
MG_042	*potA*	Spermidine/putrescine import ATP-binding protein	$3.65 \cdot 10^7$	$1.23 \cdot 10^8$	**3.38**	$9.18 \cdot 10^7$	**2.52**
MG_306		Uncharacterized membrane protein	$3.10 \cdot 10^6$	$1.65 \cdot 10^7$	**5.32**	$6.80 \cdot 10^6$	**2.19**
MG_473	*rpmG2*	50S ribosomal protein L33 type 2	$2.70 \cdot 10^7$	$4.85 \cdot 10^7$	1.80	$5.80 \cdot 10^7$	**2.15**

Underexpressed							
Locus tag	Gene	Gene product	G37	mraZ		mraW	
			CN	CN	FC	CN	FC
MG_179	*ecfA1*	Energy-coupling factor transporter ATP-binding protein EcfA1	$1.24 \cdot 10^8$	$9.70 \cdot 10^7$	0.78	$6.13 \cdot 10^7$	**0.50**
MG_077	*oppB*	Oligopeptide transport system permease protein	$9.22 \cdot 10^7$	$3.88 \cdot 10^7$	**0.42**	$4.50 \cdot 10^7$	**0.49**
MG_332		~~Probable transcriptional regulatory protein~~ Uncharacterized protein	$1.92 \cdot 10^8$	$1.60 \cdot 10^8$	0.83	$9.37 \cdot 10^7$	**0.49**
MG_250	*dnaG*	DNA primase	$3.08 \cdot 10^7$	$2.47 \cdot 10^7$	0.80	$1.49 \cdot 10^7$	**0.48**
MG_373		Uncharacterized protein	$6.00 \cdot 10^7$	$6.10 \cdot 10^7$	1.02	$2.87 \cdot 10^7$	**0.48**
MG_206	*uvrC*	UvrABC system protein C	$4.53 \cdot 10^7$	$3.67 \cdot 10^7$	0.81	$2.14 \cdot 10^7$	**0.47**
MG_366		Uncharacterized protein	$1.90 \cdot 10^7$	$1.63 \cdot 10^7$	0.86	$8.93 \cdot 10^6$	**0.47**
MG_197	*rpmI*	50S ribosomal protein L35	$2.80 \cdot 10^8$	$2.30 \cdot 10^8$	0.82	$1.31 \cdot 10^8$	**0.47**
MG_304		Putative ABC transporter ATP-binding protein	$2.27 \cdot 10^7$	$1.38 \cdot 10^7$	0.61	$1.04 \cdot 10^7$	**0.46**
MG_460	*ldh*	L-lactate dehydrogenase	$5.57 \cdot 10^9$	$2.47 \cdot 10^9$	**0.44**	$2.55 \cdot 10^9$	**0.46**
MG_388	*ybeY*	Endoribonuclease YbeY	$1.30 \cdot 10^7$	$1.10 \cdot 10^7$	0.85	$5.80 \cdot 10^6$	**0.45**
MG_047	*metK*	S-adenosylmethionine synthase, AdoMet synthase	$6.75 \cdot 10^7$	$4.02 \cdot 10^7$	0.60	$3.00 \cdot 10^7$	**0.44**
MG_252		Uncharacterized tRNA/rRNA methyltransferase	$5.18 \cdot 10^7$	$2.98 \cdot 10^7$	0.58	$2.27 \cdot 10^7$	**0.44**
MG_040		Uncharacterized lipoprotein	$5.07 \cdot 10^8$	$3.27 \cdot 10^8$	0.64	$2.13 \cdot 10^8$	**0.42**
MG_103		Probable transcriptional regulator WhiA	$1.66 \cdot 10^7$	$1.16 \cdot 10^7$	0.70	$6.90 \cdot 10^6$	**0.42**
MG_024	*ychF*	Ribosome-binding ATPase	$8.12 \cdot 10^7$	$4.13 \cdot 10^7$	0.51	$3.33 \cdot 10^7$	**0.41**

Supplementary Table I. 8. Subset of proteins above the detection threshold in *mraW* and not detected in G37 and vice versa.

Detected in *mraW* and not in G37					
Locus tag	Gene	Gene product	G37	mraZ	mraW
			CN	CN	CN
MG_027	*nusB*	Transcription termination/antitermination protein	ND	$9.20 \cdot 10^7$	$6.70 \cdot 10^7$
MG_447		Uncharacterized membrane protein	ND	$1.20 \cdot 10^7$	$9.30 \cdot 10^6$
MG_521		Uncharacterized membrane protein	ND	ND	$9.30 \cdot 10^6$
MG_360		DNA polymerase involved in DNA repair	ND	$6.85 \cdot 10^6$	$7.00 \cdot 10^6$
MG_358	*ruvA*	Holliday junction ATP-dependent DNA helicase RuvA	ND	ND	$6.90 \cdot 10^6$
MG_291	*p69*	ABC transport system permease protein p69	ND	ND	$4.80 \cdot 10^6$
MG_339	*recA*	Protein RecA	ND	ND	$3.70 \cdot 10^6$
MG_043	*potB*	Spermidine/putrescine transport system permease protein	ND	$3.15 \cdot 10^6$	$1.30 \cdot 10^6$

Detected in G37 and not in *mraW*					
Locus tag	Gene	Gene product	G37	mraZ	mraW
			CN	CN	CN
MG_222	*mraW*	Ribosomal RNA small subunit methyltransferase H	$4.17 \cdot 10^7$	$5.95 \cdot 10^8$	ND
MG_184		Uncharacterized adenine-specific methylase	$2.40 \cdot 10^7$	$1.50 \cdot 10^7$	ND
MG_226		Amino acid-polyamine-organocation (APC) permease family protein	$1.80 \cdot 10^7$	ND	ND
MG_068		Uncharacterized lipoprotein	$1.41 \cdot 10^7$	$2.70 \cdot 10^6$	ND
MG_294		Uncharacterized protein	$1.27 \cdot 10^7$	$1.50 \cdot 10^7$	ND
MG_293		Glycerophosphoryl diester phosphodiesterase family protein	$1.18 \cdot 10^7$	$6.85 \cdot 10^6$	ND
MG_505		Putative pre-16S rRNA nuclease	$1.02 \cdot 10^7$	$1.30 \cdot 10^7$	ND
MG_440		Uncharacterized lipoprotein	$4.40 \cdot 10^6$	ND	ND

A.1.6 Growth data

Supplementary Table I. 9. Growth data for all the characterized strains in chapter I. The doubling time, the number of biological repeats and the standard deviation are stated for all the strains. In addition, the percentual increase in growth time with respect to the wild-type and the p-value are also calculated. The statistical significance was assessed with Student's T test. Statistically significant values (p-value < 0.05) are highlighted in bold.

Strain	Doubling time (h)	Sample (n)	SD*	% vs WT	p-value
G37	8.380	19	0.284	-	-
mraREF	8.810	6	0.288	5.135%	0.120
mraZ	11.536	7	0.385	37.660%	**$7.20 \cdot 10^{-8}$**
mraZ COM	8.530	6	0.379	1.786%	0.522
mraW	9.963	5	0.529	18.890%	**0.006**
ftsZ	8.289	2	0.088	-1.082%	0.431
dcw	10.126	4	0.331	20.841%	**0.013**

*SD: Standard deviation

A.1.7 Cell length and single cell percentage

Supplementary Table I. 10. Single and doubling cell length of all the characterized strains in chapter I. The standard deviation and the sample size for each strain are also stated.

Strain	Single cell length ± SD* (µm) (N)	Doubling cell length ± SD (µm) (N)
G37	0.598 ± 0.074 (133)	1.118 ± 0.177 (24)
mraREF	0.633 ± 0.088 (280)	1.230 ± 0.310 (102)
mraZ	0.723 ± 0.130 (295)	1.651 ± 0.372 (96)
mraZ COM	0.607 ± 0.083 (178)	1.210 ± 0.219 (25)
mraW	0.592 ± 0.084 (213)	1.210 ± 0.180 (42)
ftsZ	0.650 ± 0.094 (256)	1.295 ± 0.196 (89)
dcw	0.671 ± 0.092 (279)	1.259 ± 0.174 (136)

*SD: Standard deviation

Supplementary Table I. 11. Percentage of single and dividing cells in each of the characterized strains.

Strain	Single cells percentage	Dividing cells percentage	Sample size
G37	86.65%	13.35%	427
mraREF	87.01%	12.99%	1001
mraZ	61.56%	38.44%	809
mraZ COM	84.73%	15.27%	845
mraW	81%	19%	606
ftsZ	77.56%	22.44%	1680
dcw	69.47%	30.53%	1592

A.1.8 Fluorescence analysis

Supplementary Table I. 12. Number and percentage of Cherry fluorescent cells in the ftsZCh, *mraZ ftsZCh* and *mraW ftsZCh* strains. The cells were counted and organized using the ImageJ suite.

Strain	Cherry Fluorescent cells (% of total cells)	Sample size
ftsZCh	0 (0%)	2772
mraZ ftsZCh	6458 (56.63%)	11403
mraW ftsZCh	110 (1.58%)	6942

Supplementary Table I. 13. YFP fluorescent foci in the 217YFP strain used to pinpoint the terminal organelle. The total number of cells was calculated through Hoechst staining and the ImageJ suite. As there was often more than one YFP focus per cell because of the replication of the terminal organelle, the number of total YFP foci is higher than the number of Hoechst-stained cells.

Strain	YFP Fluorescent foci (% of total cells) [YFP foci/cell]	Sample size
217YFP	4147 (100%) [1.49]	2780
mraZ ftsZCh 217YFP	5641 (100%) [1.51]	3746

A.2 Appendix of Chapter II

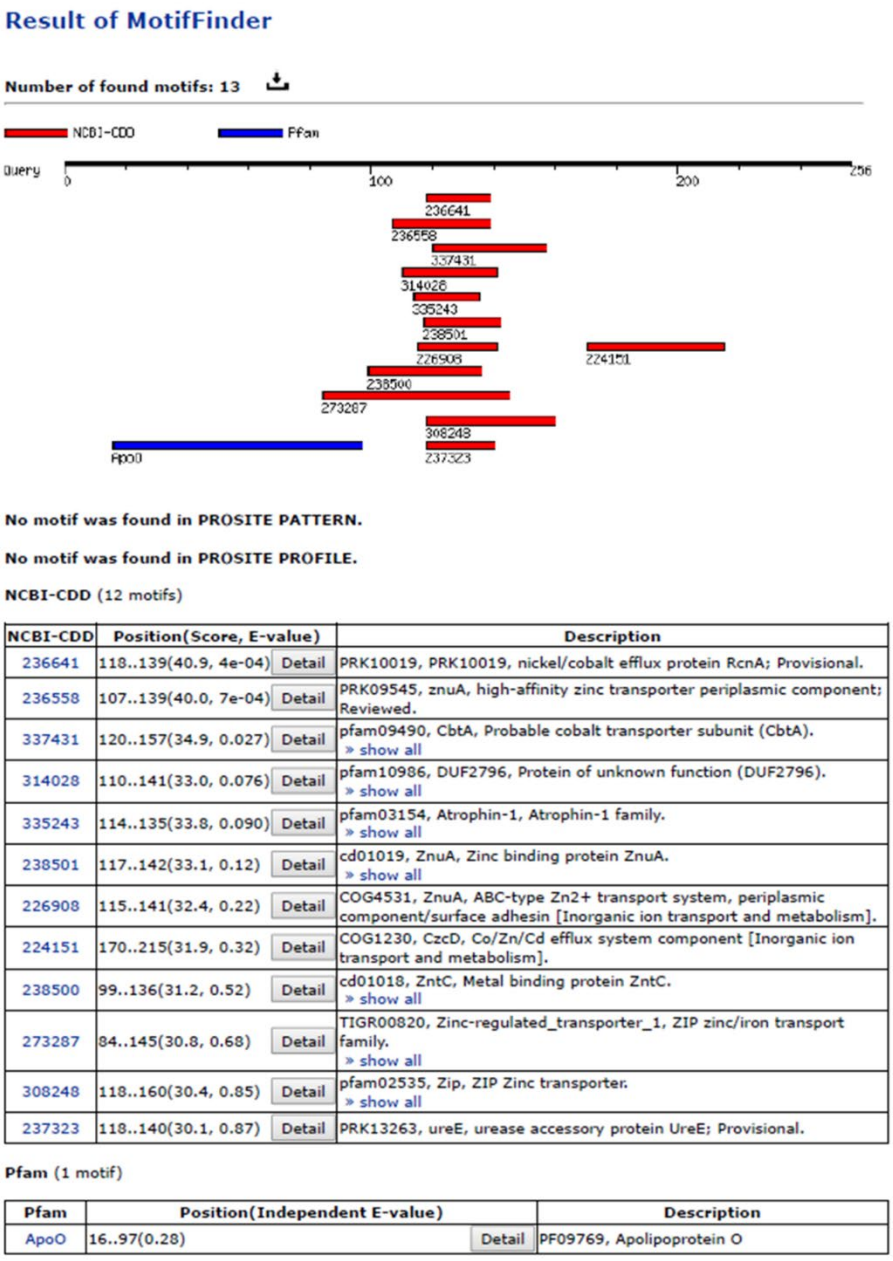

Supplementary Figure II. 1. Search for conserved domains within the Hrl (MG149) polypeptide without the putative signal peptide using MotifFinder.

A.2.1 Plasmid constructions

Supplementary Table II. 1. Plasmids used in this chapter.

Plasmid name	Description	Source
pΔMG_236	Suicide vector pBE (Pich, Burgos, Planell, et al., 2006) derivative used to create an MG_236 defective mutant. Selectable marker: tetracycline.	This work
pMTnCatMG_236	Minitransposon miniTn4001 (Calisto et al., 2012) derivative bearing an ectopic copy of MG_236 to complement the defective mutant. Selectable marker: chloramphenicol.	This work
pMTnWT149CatCh	Minitransposon miniTn4001 derivative carrying a chloramphenicol acetyl transferase resistance marker fused to an mCherry tag. Used to create the G37 *hrl*$_{WT}$:CatCh strain. Selectable marker: puromycin.	This work
pMTnMUT149CatCh	Minitransposon miniTn4001 derivative carrying a chloramphenicol acetyl transferase resistance marker fused to an mCherry tag. Selectable marker: puromycin.	This work
pC1wtCatCh	Suicide vector pBE derivative used to create the *fur hrl*$_{WT}$:CatCh strain. Selectable marker: puromycin.	This work
pC1mutCatCh	Suicide vector pBE derivative used to create the G37 *hrl*$_{mut}$:CatCh and *fur hrl*$_{mut}$:CatCh strains. Selectable marker: puromycin.	This work

pΔMG_236. This suicide plasmid was used to generate a *M. genitalium fur* null mutant by homologous recombination (HR). The MG_236 upstream region (UR) was amplified with the primers mg236 Up-F and mg236 Up-R and the downstream region (DR) was amplified with the mg236 Down-F and mg236 Down-R primers. The tetracycline resistance marker under the control of a constitutive promoter of *M. genitalium* (tetM438) was amplified with the primers Tc-F and Tc-R. Then, the UR and the tetM438 PCR products were joined by Splicing by Overlap Extension (SOE) PCR with the mg236 Up-F and Tc-R primers. Next, the product of the SOE-PCR and the DR were also joined using SOE-PCR with the mg236 Up-F and mg236 Down-R primers. The resulting PCR product was cloned into an *Eco*RV-digested pBE plasmid (Pich, Burgos, Planell, et al., 2006). In order to reduce the polar effects derived from the insertion of the resistance marker, we cloned a transcription terminator after tetM438. This terminator sequence is present between the metal acquisition operon (MG_304-MG_302) and the *dnaK* gene (MG_305) and was identified using the TransTermHP software (Kingsford et al., 2007). This transcriptional terminator was amplified using the TER305-F and TER305-R primers and digested with *Bam*HI. The plasmid was also digested with *Bam*HI and dephosphorylated to prevent self-ligation. Then, the terminator was cloned into the plasmid (Supplementary Figure II. 2).

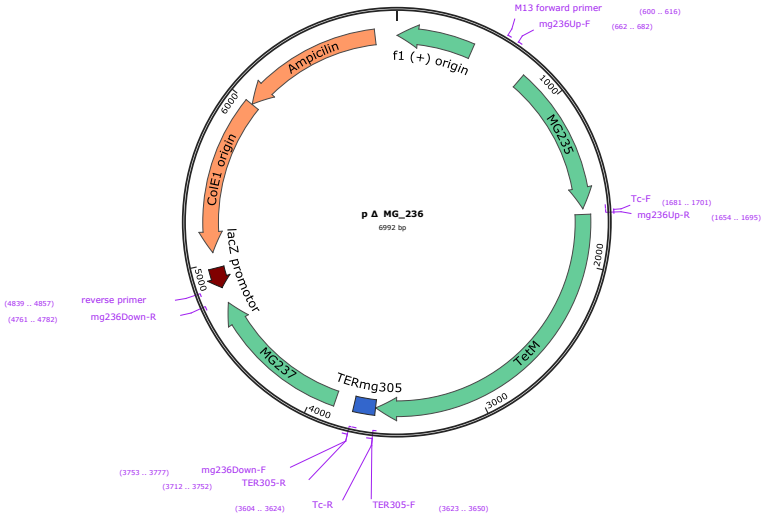

Supplementary Figure II. 2. Map of the pΔMG_236 plasmid. Oligonucleotides used in its construction are highlighted.

pMTnCatMG_236. This plasmid contains a minitransposon carrying a wild-type copy of the *fur* allele under its own promoter and was used to restore the wild-type phenotype of the *fur* mutant. The plasmid contains a chloramphenicol resistance marker. The MG_236 allele was amplified by PCR with the COMmg236-F (*Xba*I) and COMmg236-R (*Not*I), digested with *Xba*I and *Not*I and ligated into a digested pMTnCat plasmid (Calisto et al., 2012) (Supplementary Figure II. 3).

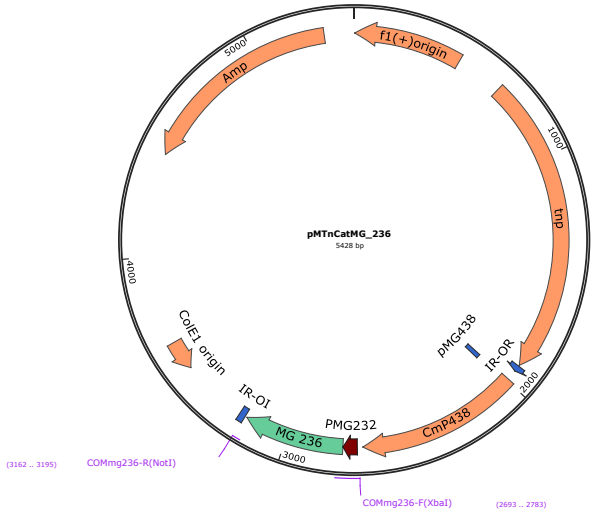

Supplementary Figure II. 3. Map of the pMTnCatMG_236 plasmid. Oligonucleotides used in its construction are highlighted.

pMTnWT149CatCh. This plasmid carries a chloramphenicol acetyl transferase resistance marker fused to an mCherry tag (Cat:Ch) under the control of the promoter region of *hrI* (gcttatttagaaaaattcaaaataagcaaatTATAAT), which contains a putative *fur* box. The selectable marker fused to the fluorescent tag was amplified from a pCat:Ch plasmid (Torres-Puig et al., 2015) with the wtMG149furbox-F and Ch-R primers. This PCR product was later digested with *Apa*I and *Xho*I and inserted in a similarly digested pMTnPac plasmid (Torres-Puig et al., 2018), which carries a minitransposon with a puromycin resistance cassette (Supplementary Figure II. 4).

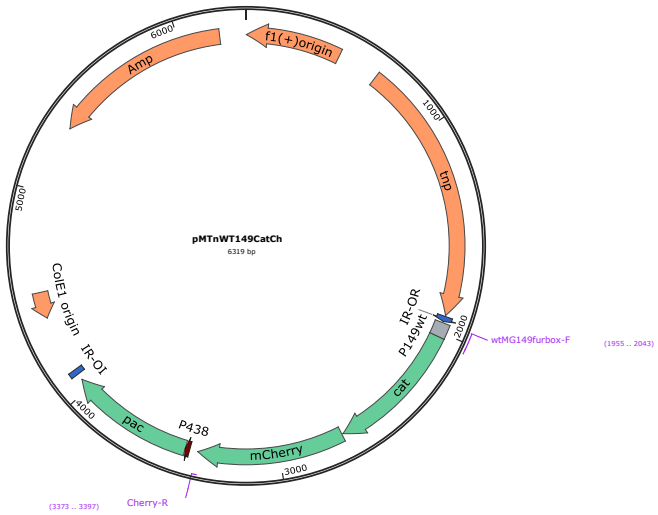

Supplementary Figure II. 4. Map of the pMTnWT149CatCh plasmid. Oligonucleotides used in its construction are highlighted.

pMTnMUT149CatCh. This plasmid carries a chloramphenicol acetyl transferase resistance marker fused to a mCherry tag under the control of a the *hrl* promoter with a scrambled sequence (gct**ac**t**a**tag**t**aaaat**a**caaa**tct**agcaaatTATAAT) at the putative *fur* box. This plasmid was constructed following the same steps as for the construction of the pMTnWT149CatCh, except that we used a different forward primer (mutMG149furbox-F) in order to alter the sequence of the putative *fur* box.

pC1wtCatCh. This plasmid was created to introduce a Cat:Ch fusion under the control of the *hrl* promoter region (gcttatttagaaaaattcaaaataagcaaatTATAAT) in the same exact chromosomic location as in the G37 hrl_{WT}:CatCh C1 strain, in order to compare the reporter fluorescence in a wild-type (G37 strain) and fur mutant background. We obtained the genomic DNA of the G37 hrl_{WT}:CatCh C1 strain and we determined the insertion point of the transposon by Sanger sequencing. Next, we amplified 1 kb upstream and downstream of the insertion point with the C1wt149CatCh-F and C1wt149CatCh-R primers. The PCR product including the upstream region, the Cat:Ch fusion under the control of the *hrl* promoter region, and the downstream region was cloned into a *Eco*RV-digested pBE to create pC1wtCatCh (Supplementary Figure II. 5).

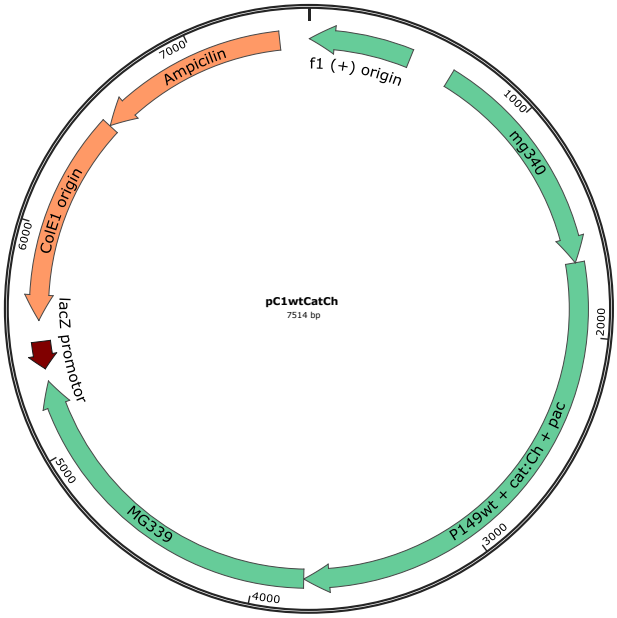

Supplementary Figure II. 5. Map of the pC1wtCatCh plasmid. Oligonucleotides used in its construction are highlighted.

pC1mutCatCh. This plasmid bears a copy of the Cat:Ch fusion under the control of the *hrl* promoter bearing the same scrambled *fur* box sequence used in the construction of the pMTnMUT149CatCh plasmid (gctactatagttaaaatacaaatctagcaaatTATAAT), in order to test the reporter fluorescence with an altered operator. The pC1wtCatCh plasmid was digested with ApaI and XhoI to excise the cassette containing the Cat:Ch fusion under the control of the *hrl* promoter. The pMTnMUT149CatCh was digested similarly with *Apa*I and *Xho*I. Then, the construction bearing the Cat:Ch fusion regulated by the *hrl* promoter with the scrambled putative *fur* box was ligated into the backbone of the pC1wtCatCh plasmid.

A.2.2 Oligonucleotides

Supplementary Table II. 2. Primers used in this study.

Aim	Primer name	Sequence (5'-3')
Mutants	mg236 Up-F	CTTTGCAGGACAAAATGTTGC
	mg236 Up-R	TAATTCTAAATACTAGAATTCACATAACTAGTTAGCATCTGG
	mg236 Down-F	CAATAAAATAACTTAGGGATCCCCTTACCTTTAACAGATGGC
	mg236 Down-R	CATCTTTTGTATCTACTAGTGC
	TER305-F	GCGGGATCCCACAAGCAAAATAACCTGTTC
	TER305-R	GCGGGATCCCTCGAGCTAAAAATCTGTTTTTTGGT
	COMmg236-F (*Xba*I)	AGTTCTAGAGTTTGTTCTATCTAACTATTAAAGCAGTTAGAATTTGTT AGAATTACTTGTTTTAAAACTATGCTAACTAGTTATGTGAAGG
	COMmg236-R (*Not*I)	AAAGCGGCCGCTTAATCATTGTTTATCTCACCCC
	wtMG149furbox-F	ATTGGGCCCGCTTATTTAGAAAAATTCAAAATAAGCAAATTATAATTA GGTGTCTTTCTTTACTAAAAATATGGAGAAAAAAATCACTGG
	mutMG149furbox-F	ATTGGGCCCGCTACTATAGTAAAATACAAATCTAGCAAATTATAATTA GGTGTCTTTCTTTACTAAAAATATGGAGAAAAAAATCACTGG
	C1wt149CatCh-F	GATTGCTGCTCAATCAATTG
	C1wt149CatCh-R	GACAACGCTTCAAAATTCACC
	Cherry-R	AGTCTCGAGTTACTTGTACAGCTCGTCC
	Tc-F	GAATTCTAGTATTTAGAATTAATAAAG
	Tc-R	GGATCCCTAAGTTATTTTATTGAAC
Screening	mg236SCR-F	GTTGGTCAGATTATCTATAG
	mg236SCR-R	CTCAACTTCCAAACAAAGAC
	mg293SCR-F	GAAAACTAGCTAGTCAACAAG
	mg293SCR-R	CGTCTTAAAAGTCTTCTTAC
qRT-PCR	RTPCRmg177-F	TGAGTGTCCAGCTGGTTTTG
	RTPCRmg177-R	AACCGGGGAAAAGTTAGCAT
	RTPCRmg418-F	TGTTGACGCTAGTGGTTTGG
	RTPCRmg418-R	TTCCACCCATGTATTGAGAGTG
	RTPCRmg430-F	GGAAGCAGTTGGATTGCCTA
	RTPCRmg430-R	ATGCACTCCTCCATTGGAAA
	RTPCRmg236-F	AATTGAACACCAAGATTGGC
	RTPCRmg236-R	AGATAGATATGGTTATGCTC
	RTPCRmg149-F	ACCAGGGATATGCACTAGCA
	RTPCRmg149-R	TGCAACACTTTGGGTAGCTG
	RTPCRmg304-F	GCTGATACACTCCACCAGGAA

	RTPCRmg304-R	CAAGCAAAAACAGCACGTTG
	RTPCRmCherry-F	GCCCCTAATGCAGAAGAAG
	RTPCRmCherry-R	GTGTAGTCCTCGTTGTGGGA
	RTPCRmg239-F	ATGCGAGAAAGCGCTAATGT
	RTPCRmg239-R	TGCAGTTACCAAAGCAGCAC
	RTPCRmg305-F	ATTTTGCTTGTGGACCTTGT
	RTPCRmg305-R	GATATTAGCAAGTCCTGATG
	RTPCRmg355-F	CACACCTGCTGGTGAAAATC
	RTPCRmg355-R	CCAACTCCAGGTTCACCAAT
Sequencing	Fup-24	CGCCAGGGTTTTCCCAGTCACGAC
	Rup-24	TCACACAGGAAACAGCTATGACCA
	TetUp	TTCCTGCATCAACATGAG
	TetDown	GTCGTCCAAATAGTCGGA
	CmUp	CAACGGTGGTATATCCAG
	CmDown	CAGTACTGCGATGAGTGGCA
	PacUp	GTAGCTAATCTAACAGTAGG
	PacDown	GTCCTAGAACTTGGTGTATG
Primer extension reactions	PEmg236 (I)	[6-FAM]CACTTTAATAAAGCAATCCG
	PEmg236 (II)	[6-FAM]GGATCTACAAAGATGTTAATC
	PEmg235 (int)	[6-FAM]GTTAAGTCTCTGCCTATCTC
	PEmg233	[6-FAM]CAGCAAACAAAGCATGACCT
	PEmg232	[6-FAM]ATCACACAAACAACCTTAGC

A.2.3 RNAseq data

Supplementary Table II. 3. Differentially expressed genes in *M. genitalium* upon metal starvation with 2,2'-bipyridyl identified by RNA-Seq analysis. Cutoff log2 ± 1.

Up-regulated				
Locus tag	Gene	Gene product	log2 Fold Change	p-value
MG_355	*clpB*	Chaperone protein ClpB	3.84	2.09E-144
MG_241		Uncharacterized protein MG241	3.19	2.39E-98
MG_239	*lon*	Lon protease	2.84	9.87E-211
MG_242		Uncharacterized protein MG242	2.66	8.28E-60
MG_304		ABC transporter ATP-binding protein MG304	2.59	6.49E-94
MG_080	*oppF*	Oligopeptide transport ATP-binding protein OppF	2.47	2.23E-147
MG_303		ABC transporter ATP-binding protein MG303	2.42	7.56E-56
MG_244	*uvrD*	DNA helicase II homolog	2.33	5.32E-38
MG_302		Uncharacterized protein	2.22	5.71E-21
MG_079	*oppD*	Oligopeptide transport ATP-binding protein OppD	2.16	1.12E-79
MG_524		Uncharacterized protein MG384.1	2.14	1.71E-13
MG_078	*oppC*	Oligopeptide transport system permease protein OppC	2.12	2.60E-50
MG_149	*hrl*	Uncharacterized lipoprotein MG149	2.12	3.73E-113
MG_305	*dnaK*	Chaperone protein DnaK	2.01	8.67E-57
MG_439		Uncharacterized lipoprotein MG439	1.94	5.13E-31
MG_077	*oppB*	Oligopeptide transport system permease protein OppB	1.93	8.60E-51
MG_316		Uncharacterized protein MG316	1.85	7.12E-08
MG_192.1		Uncharacterized small protein MG192.1	1.74	6.27E-20
MG_321		Uncharacterized lipoprotein MG321	1.65	2.68E-55
MG_339	*recA*	Protein RecA	1.64	2.94E-43
MG_033	*glpF*	Glycerol uptake facilitator protein	1.60	1.21E-47
MG_083	*pth*	Peptidyl-tRNA hydrolase	1.53	2.49E-51
MG_084	*tilS*	tRNA(Ile)-lysidine synthase	1.50	9.12E-44
MG_085	*hprK*	HPr kinase/phosphorylase	1.49	5.32E-44
MG_384	*obg*	GTPase Obg	1.49	2.56E-37
MG_389		Uncharacterized protein MG389	1.47	5.86E-05
MG_390		ABC transporter ATP-binding protein MG390	1.37	5.37E-34
MG_282	*greA*	Transcription elongation factor GreA	1.36	4.84E-63
MG_478		Uncharacterized protein MG149.1	1.32	5.04E-17
MG_521		Uncharacterized protein MG350.1	1.31	0.0178199

MG_081	*rplK*	50S ribosomal protein L11	1.31	9.44E-35
MG_098		Uncharacterized protein MG098	1.30	1.23E-22
MG_441		Uncharacterized protein MG441	1.29	0.00079279
MG_245		5-formyltetrahydrofolate cyclo-ligase	1.28	9.94E-06
MG_012		Uncharacterized protein MG012	1.25	6.17E-10
MG_206	*uvrC*	UvrABC system protein C	1.21	6.69E-24
MG_074		Uncharacterized protein MG074	1.19	0.00038207
MG_082	*rplA*	50S ribosomal protein L1	1.16	4.78E-26
MG_385		Uncharacterized protein MG385	1.14	4.81E-18
MG_237		Uncharacterized protein MG237	1.13	7.28E-23
MG_064		Uncharacterized ABC transporter permease MG064	1.10	4.54E-24
MG_075		Uncharacterized protein MG075	1.08	5.38E-35
MG_365	*fmt*	Methionyl-tRNA formyltransferase	1.07	5.47E-08
MG_246		Putative phosphatase/phosphodiesterase MG246	1.06	1.08E-13
MG_236	*fur*	Ferric uptake regulation protein	1.03	5.40E-15
MG_358	*ruvA*	Holliday junction ATP-dependent DNA helicase RuvA	1.03	3.31E-13

Down-regulated

Locus tag	Gene	Gene product	log2 Fold Change	p-value
MG_189		ABC transporter permease protein MG189	-1.98	6.16E-46
MG_188		ABC transporter permease protein MG188	-1.73	1.85E-33
MG_511		tRNA-Val	-1.42	2.68E-04
MG_489		tRNA-Asp	-1.39	9.82E-05
MG_512		tRNA-Thr	-1.35	1.59E-05
MG_485		tRNA-Met	-1.34	3.23E-06
MG_112	*rpe*	Ribulose-phosphate 3-epimerase	-1.33	8.21E-15
MG_501		tRNA-Lys	-1.31	3.06E-04
MG_434	*pyrH*	Uridylate kinase	-1.31	1.68E-30
MG_350		Uncharacterized protein MG350	-1.29	1.77E-14
MG_187		ABC transporter ATP-binding protein MG187	-1.28	1.20E-29
MG_483		tRNA-Cys	-1.28	1.33E-04
MG_111	*pgi*	Glucose-6-phosphate isomerase	-1.27	8.22E-36
MG_453	*galU*	Glucose-1-phosphate uridylyltransferase	-1.23	5.48E-20
MG_500		tRNA-Leu	-1.22	1.50E-04
MG_132		Uncharacterized HIT-like protein MG132	-1.2	7.65E-14

MG_484		tRNA-Pro	-1.19	3.72E-03
MG_324	*pepP*	Putative Xaa-Pro aminopeptidase	-1.17	4.16E-21
MG_526		ABC transporter ATP-binding protein MG468.1	-1.13	6.15E-18
MG_510		tRNA-Thr	-1.13	5.44E-04
MG_513		tRNA-Glu	-1.11	1.26E-03
MG_186		Uncharacterized lipoprotein MG186	-1.11	4.12E-11
MG_507		tRNA-Ser	-1.09	1.21E-03
MG_515		Uncharacterized protein MG323.1	-1.08	4.21E-17
MG_024	*ychF*	Ribosome-binding ATPase YchF	-1.08	1.34E-19
MG_072	*secA*	Protein translocase subunit SecA	-1.08	5.23E-22
MG_514		tRNA-Asn	-1.07	1.32E-04
MG_488		tRNA-Met	-1.07	1.66E-03
MG_023	*fba*	Fructose-bisphosphate aldolase	-1.07	3.76E-20
MG_506		tRNA-Ser	-1.02	2.83E-02
MG_494		Uncharacterized protein MG255.1	-1.02	3.37E-03
MG_278	*relA*	Guanosine-3',5'-bis(diphosphate) 3'-pyrophosphohydrolase	-1.02	3.18E-15
MG_190	*nrnA*	Bifunctional oligoribonuclease and PAP phosphatase NrnA	-1.02	9.17E-23
MG_435	*frr*	Ribosome-recycling factor	-1.01	1.05E-11
MG_262	*polA*	5'-3' exonuclease	-1	2.08E-07

Supplementary Table II. 4. Differentially expressed genes in a *M. genitalium fur* mutant and the corresponding complemented strain derivative compared to the wild-type strain identified by RNA-Seq analysis. Cutoff log 2 ± 1.

Locus tag	Gene	Gene product	*fur*		*furCOM*	
			Log2 fold change	p-value	Log2 fold change	p-value
MG_149		Uncharacterized lipoprotein MG149	**2.45**	$2.1 \cdot 10^{-144}$	-0.95	$1.9 \cdot 10^{-11}$
MG_304		ABC transporter ATP-binding protein MG304	**2.2**	$9.9 \cdot 10^{-211}$	-0.35	0.10
MG_303		ABC transporter ATP-binding protein MG303	**2.06**	$6.5 \cdot 10^{-94}$	-0.97	$6.9 \cdot 10^{-05}$
MG_302		Uncharacterized protein MG302	**1.45**	$7.6 \cdot 10^{-56}$	-0.37	0.47
MG_236	*fur*	Ferric uptake regulation protein	**-5.77**	$3.1 \cdot 10^{-41}$	**3.53**	$3.0 \cdot 10^{-293}$
MG_237		Uncharacterized protein MG237	**-1.25**	$1.5 \cdot 10^{-5}$	**-1.22**	$4.3 \cdot 10^{-14}$

Supplementary Table II. 5. Differentially expressed genes in a *M. genitalium fur* mutant upon metal deprivation with 2,2'-bipyridyl identified by RNA-Seq analysis. Cutoff log2 ± 1.

Up-regulated				
Locus tag	Gene	Gene product	log2 Fold Change	p-value
MG_355	*clpB*	Chaperone protein ClpB	4.33	2.35E-202
MG_241		Uncharacterized protein MG241	3.69	3.97E-99
MG_239	*lon*	Lon protease	3.02	3.42E-66
MG_079	*oppD*	Oligopeptide transport ATP-binding protein OppD	2.77	2.38E-90
MG_078	*oppC*	Oligopeptide transport system permease protein OppC	2.66	6.15E-63
MG_080	*oppF*	Oligopeptide transport ATP-binding protein OppF	2.58	7.58E-57
MG_083	*pth*	Peptidyl-tRNA hydrolase	2.57	1.53E-29
MG_242		Uncharacterized protein MG242	2.49	3.24E-33
MG_081	*rplK*	50S ribosomal protein L11	2.40	8.93E-31
MG_082	*rplA*	50S ribosomal protein L1	2.37	1.87E-36
MG_244	*uvrD*	DNA helicase II homolog	2.36	8.01E-51
MG_077	*oppB*	Oligopeptide transport system permease protein OppB	2.17	8.69E-64
MG_305	*dnaK*	Chaperone protein DnaK	2.09	6.78E-35
MG_321		Uncharacterized lipoprotein MG321	2.07	4.19E-48
MG_339	*recA*	Protein RecA	2.05	1.79E-22
MG_478		Uncharacterized protein MG149.1	1.91	1.78E-17
MG_084	*tilS*	tRNA(Ile)-lysidine synthase	1.88	1.64E-38
MG_012		Uncharacterized protein MG012	1.78	3.20E-15
MG_282	*greA*	Transcription elongation factor GreA	1.77	8.59E-20
MG_174	*rpmJ*	50S ribosomal protein L36	1.73	2.11E-09
MG_246		Putative phosphatase/phosphodiesterase MG246	1.72	4.62E-16
MG_384	*obg*	GTPase Obg	1.70	1.35E-17
MG_439		Uncharacterized lipoprotein MG439	1.70	3.08E-12
MG_085	*hprK*	HPr kinase/phosphorylase	1.61	3.06E-25
MG_098		Uncharacterized protein MG098	1.58	1.45E-29
MG_358	*ruvA*	Holliday junction ATP-dependent DNA helicase RuvA	1.57	3.59E-10
MG_393	*groES*	10 kDa chaperonin	1.56	1.54E-12
MG_206	*uvrC*	UvrABC system protein C	1.54	6.62E-14
MG_353		Uncharacterized protein MG353	1.52	1.18E-19
MG_142	*infB*	Translation initiation factor IF-2	1.46	4,36E-09
MG_521		Uncharacterized protein MG350.1	1.44	1.90E-02
MG_392	*groL*	60 kDa chaperonin	1.31	3.49E-19

MG_245		5-formyltetrahydrofolate cyclo-ligase	1.31	0.0004
MG_149	*hrl*	Uncharacterized lipoprotein MG149	1.30	4.13E-14
MG_340	*rpoC*	DNA-directed RNA polymerase subunit beta'	1.28	6.92E-14
MG_440		Uncharacterized protein MG440	1.28	4,49E-12
MG_359	*ruvB*	Holliday junction ATP-dependent DNA helicase RuvB	1.24	2.22E-09
MG_192.1		Uncharacterized small protein MG192.1	1.21	6.35E-07
MG_179	*ecfA1*	Energy-coupling factor transporter ATP-binding protein EcfA1	1.19	2.03E-09
MG_173	*infA*	Translation initiation factor IF-1	1.17	3.20E-06
MG_238	*tig*	Trigger factor	1.15	5.74E-08
MG_058	*prs*	Ribose-phosphate pyrophosphokinase	1.13	2.72E-09
MG_473	*rpmG2*	50S ribosomal protein L33 2	1.12	7.99E-07
MG_161	*rplN*	50S ribosomal protein L14	1.12	3.06E-05
MG_011		Uncharacterized protein MG011	1.06	1.93E-04
MG_164	*rpsN*	30S ribosomal protein S14 type Z	1.06	1.16E-04
MG_100	*gatB*	Aspartyl/glutamyl-tRNA(Asn/Gln) amidotransferase subunit B	1.05	2.17E-12
MG_237		Uncharacterized protein MG237	1.05	4.53E-06
MG_158	*rplP*	50S ribosomal protein L16	1.05	1.53E-05
MG_180	*ecfA2*	Energy-coupling factor transporter ATP-binding protein EcfA2	1.03	1.41E-10
MG_316		Uncharacterized protein MG316	1.02	9.22E-02
MG_160	*rpsQ*	30S ribosomal protein S17	1.00	3.38E-04

Down-regulated				
Locus tag	Gene	Gene product	log2 Fold Change	p-value
MG_452		Uncharacterized protein MG452	-2.31	3.56E-09
MG_505		Putative pre-16S rRNA nuclease	-1.93	3.97E-03
MG_007		Uncharacterized protein MG007	-1.91	1.05E-03
MG_494		Uncharacterized protein MG255.1	-1.87	4.82E-04
MG_522	*rpsT*	30S ribosomal protein S20	-1.86	6.78E-06
MG_039		Uncharacterized protein MG039	-1.73	9.02E-18
MG_189		ABC transporter permease protein MG189	-1.71	4.90E-21
MG_453	*galU*	Glucose-1-phosphate uridylyltransferase	-1.7	4.92E-16
MG_350		Uncharacterized protein MG350	-1.68	9.45E-10
MG_409		Uncharacterized protein MG409	-1.53	1.42E-04
MG_435	*frr*	Ribosome-recycling factor	-1.51	1.39E-07
MG_188		ABC transporter permease protein MG188	-1.5	5.10E-16
MG_437	*cdsA*	Phosphatidate cytidylyltransferase	-1.48	4.61E-11

MG_010		Uncharacterized protein MG010	-1.48	1.24E-02
MG_001	*dnaN*	Beta sliding clamp	-1.44	9.69E-03
MG_380	*rsmG*	Ribosomal RNA small subunit methyltransferase G	-1.42	9.40E-03
MG_515		Uncharacterized protein MG323.1	-1.41	3.17E-07
MG_526		ABC transporter ATP-binding protein MG468.1	-1.41	3.02E-12
MG_071	*pacL*	Cation-transporting P-type ATPase	-1.38	1.23E-14
MG_429	*ptsI*	Phosphoenolpyruvate-protein phosphotransferase	-1.34	1.89E-19
MG_255		Uncharacterized protein MG255	-1.31	5.66E-14
MG_495		tRNA-Arg	-1.3	1.74E-04
MG_431	*tpiA*	Triosephosphate isomerase	-1.26	1.96E-09
MG_428		Alternative sigma factor σ20	-1.26	4.96E-05
MG_248		tRNA methyltransferase MG248	-1.25	3.30E-06
MG_262	*polA*	5'-3' exonuclease	-1.25	8.83E-08
MG_325	*rpmG1*	50S ribosomal protein L33 1	-1.24	1.07E-07
MG_112	*rpe*	Ribulose-phosphate 3-epimerase	-1.24	1.25E-05
MG_438		Type-1 restriction enzyme specificity protein	-1.24	6.66E-14
MG_110	*rsgA*	Small ribosomal subunit biogenesis GTPase RsgA	-1.22	1.95E-04
MG_111	*pgi*	Glucose-6-phosphate isomerase	-1.2	1.11E-11
MG_422		Uncharacterized protein MG422	-1.2	5.02E-03
MG_447		Uncharacterized protein MG447	-1.19	1.45E-03
MG_507		tRNA-Ser	-1.19	2.37E-05
MG_470		ParA family protein MG470	-1.18	9.71E-11
MG_370		Uncharacterized RNA pseudouridine synthase MG370	-1.16	5.53E-03
MG_296		Uncharacterized protein MG296	-1.14	2.84E-03
MG_520		tRNA-Leu	-1.12	1.12E-04
MG_485		tRNA-Met	-1.12	1.50E-04
MG_463	*rsmA*	Ribosomal RNA small subunit methyltransferase A	-1.12	2.09E-04
MG_074		Uncharacterized protein MG074	-1.12	1.88E-03
MG_123		Uncharacterized protein MG123	-1.11	1.79E-07
MG_047	*metK*	S-adenosylmethionine synthase	-1.09	2.61E-10
MG_135		Uncharacterized protein MG135	-1.07	1.21E-05
MG_240		Uncharacterized protein MG240	-1.04	7.16E-06
MG_140		Uncharacterized ATP-dependent helicase MG140	-1.04	2.37E-15
MG_132		Uncharacterized HIT-like protein MG132	-1.04	5.33E-07
MG_372	*thiI*	Probable tRNA sulfurtransferase	-1.04	7.28E-05
MG_324	*pepP*	Putative Xaa-Pro aminopeptidase	-1.02	2.60E-13
MG_382	*udk*	Uridine kinase	-1.01	2.31E-03
MG_343		Uncharacterized protein MG343	-1.01	1.21E-02

A.2.4 Proteomics data

Supplementary Table II. 6. Differentially expressed proteins observed in the DIGE proteomic analysis of the *fur* mutant.

Spot #	Id Score[1]	Peptides[1]	% SC[1]	Accession[2]	Entry Name[2]	Protein	Locus tag	Gene	log2 FC	p-value
1766	460	10	54.1	P47648	MSRA_MYCGE	Peptide methionine sulfoxide reductase MsrA	MG_408	*msrA*	2.49	$1.6 \cdot 10^{-2}$
2076	314	6	28.0	P47648	MSRA_MYCGE	Peptide methionine sulfoxide reductase MsrA	MG_408	*msrA*	2.42	$6.0 \cdot 10^{-3}$
2065	116	2	12.1	P47648	MSRA_MYCGE	Peptide methionine sulfoxide reductase MsrA	MG_408	*msrA*	2.23	$3.0 \cdot 10^{-3}$
2118	167	5	14.4	P47515	ODPB_MYCGE	Pyruvate dehydrogenase E1 component E1, subunit beta	MG_273	*pdhB*	2.64	$2.3 \cdot 10^{-3}$
1771	84	3	23.2	P47334	RS7_MYCGE	30S ribosomal protein S7	MG_088	*rpsG*	2.54	$2.0 \cdot 10^{-3}$
2143	163	4	26.5	P47656	RS9_MYCGE	30S ribosomal protein S9	MG_417	*rpsI*	2.19	$2.6 \cdot 10^{-2}$
1838	114	3	21.2	P47656	RS9_MYCGE	30S ribosomal protein S9	MG_417	*rpsI*	2.08	$2.0 \cdot 10^{-3}$
2064	235	5	14.6	P47395	Y149_MYCGE	Histidine-rich lipoprotein MG149	MG_149	*hrl*	2.60	$3.2 \cdot 10^{-4}$
1808	112	2	6.4	P47395	Y149_MYCGE	Histidine-rich lipoprotein MG149	MG_149	*hrl*	2.22	$1.3 \cdot 10^{-2}$
1810	122	2	1.8	P47580	Y338_MYCGE	Uncharacterized lipoprotein MG338	MG_338		2.60	$3.0 \cdot 10^{-3}$
2075	192	4	3.1	P47580	Y338_MYCGE	Uncharacterized lipoprotein MG338	MG_338		2.45	$6.0 \cdot 10^{-3}$

[1]Protein Identification Score in Mascot MSMS search, number of unique peptides identified and % sequence coverage.

[2]UniProt/SwissProt identifiers.

A.2.5 Insertion sites

Supplementary Table II. 7. Insertion site of the TnPac*hrI*$_{WT}$:*cat*:*mcherry* transposon in the genome of two different G37 *hrI*$_{WT}$ CatCh clones.

G37 *hrI*$_{WT}$ CatCh clone	Fluorescence	Insertion site (bp)	Gene truncated
C1	Marginal	430390	None
C5	Marginal	72884	*fruK* (MG_063)

A.2.6 ICP-MS data

Supplementary Table II. 8. Concentration of some transition metals in the SP-4 medium determined by ICP-MS analysis (n=10).

Element	Mean (µg/L)	Standard Deviation
Mn	27.1	2.47
Fe	691.3	33.55
Co	9.72	0.64
Ni	5.52	1.11
Cu	33.7	3.83
Zn	948.5	39.31

BIBLIOGRAPHY

Adams, D. W., & Errington, J. (2009). Bacterial cell division: Assembly, maintenance and disassembly of the Z ring. In *Nature Reviews Microbiology* (Vol. 7, Issue 9, pp. 642–653). Nature Publishing Group. https://doi.org/10.1038/nrmicro2198

Adams, M. A., Udell, C. M., Pal, G. P., & Jia, Z. (2005). MraZ from Escherichia coli: Cloning, purification, crystallization and preliminary X-ray analysis. *Acta Crystallographica Section F: Structural Biology and Crystallization Communications*, *61*(4), 378–380. https://doi.org/10.1107/S1744309105007657

Algire, M. A., Lartigue, C., Thomas, D. W., Assad-Garcia, N., Glass, J. I., & Merryman, C. (2009). New selectable marker for manipulating the simple genomes of Mycoplasma species. *Antimicrobial Agents and Chemotherapy*, *53*(10), 4429–4432. https://doi.org/10.1128/AAC.00388-09

Althaus, E. W., Outten, C. E., Olson, K. E., Cao, H., & O'Halloran, T. V. (1999). The ferric uptake regulation (Fur) repressor is a zinc metalloprotein. *Biochemistry*, *38*(20), 6559–6569. https://doi.org/10.1021/bi982788s

Anagrius, C., Loré, B., & Jensen, J. S. (2005). Mycoplasma genitalium: Prevalence, clinical significance, and transmission. *Sexually Transmitted Infections*, *81*(6), 458–462. https://doi.org/10.1136/sti.2004.012062

Anderson, L. M., & Yang, H. (2008). DNA looping can enhance lysogenic CI transcription in phage lambda. *Proceedings of the National Academy of Sciences of the United States of America*, *105*(15), 5827–5832. https://doi.org/10.1073/pnas.0705570105

Andreini, C., Bertini, I., Cavallaro, G., Holliday, G. L., & Thornton, J. M. (2008). Metal ions in biological catalysis: From enzyme databases to general principles. *Journal of Biological Inorganic Chemistry*, *13*(8), 1205–1218. https://doi.org/10.1007/s00775-008-0404-5

Aparicio, D., Scheffer, M. P., Marcos-Silva, M., Vizarraga, D., Sprankel, L., Ratera, M., Weber, M. S., Seybert, A., Torres-Puig, S., Gonzalez-Gonzalez, L., Reitz, J., Querol, E., Piñol, J., Pich, O. Q., Fita, I., & Frangakis, A. S. (2020). Structure and mechanism of the Nap adhesion complex from the human pathogen Mycoplasma genitalium. *Nature Communications*, *11*(1). https://doi.org/10.1038/s41467-020-16511-2

Aparicio, D., Torres-Puig, S., Ratera, M., Querol, E., Piñol, J., Pich, O. Q., & Fita, I. (2018). Mycoplasma genitalium adhesin P110 binds sialic-acid human receptors. *Nature*

Communications, *9*(1), 1–11. https://doi.org/10.1038/s41467-018-06963-y

Ayala, J. A., Garrido, T., De Pedro, M. A., & Vicente, M. (1994). Molecular biology of bacterial septation. *New Comprehensive Biochemistry*, *27*(C), 73–101. https://doi.org/10.1016/S0167-7306(08)60408-1

Barden, J. A., & Decker, J. L. (1971). Mycoplasma Hyorhinis Swine Arthritis. I. Clinical and Microbiologic Features. *Arthritis & Rheumatism*, *14*(2), 193–201. https://doi.org/10.1002/art.1780140202

Baseman, J. B., Cole, R. M., Krause, D. C., & Leith, D. K. (1982). Molecular basis for cytadsorption of Mycoplasma pneumoniae. *Journal of Bacteriology*, *151*(3), 1514–1522. https://doi.org/10.1128/jb.151.3.1514-1522.1982

Baseman, Joel B., & Tully, J. G. (1997). Mycoplasmas: Sophisticated, Reemerging, and Burdened by Their Notoriety. *Emerging Infectious Diseases*, *3*(1), 21–32. https://doi.org/10.3201/eid0301.970103

Baumann, L., Cina, M., Egli-Gany, D., Goutaki, M., Halbeisen, F. S., Lohrer, G. R., Ali, H., Scott, P., & Low, N. (2018). Prevalence of Mycoplasma genitalium in different population groups: systematic review and meta-analysis. *Sexually Transmitted Infections*, *94*(4), 255–262. https://doi.org/10.1136/sextrans-2017-053384

Beall, B., & Lutkenhaus, J. (1991). FtsZ in Bacillus subtilis is required for vegetative septation and for asymmetric septation during sporulation. *Genes and Development*, *5*(3), 447–455. https://doi.org/10.1101/gad.5.3.447

Becskel, A., & Serrano, L. (2000). Engineering stability in gene networks by autoregulation. *Nature*, *405*(6786), 590–593. https://doi.org/10.1038/35014651

Benders, G. A., Powell, B. C., & Hutchison, C. A. (2005). Transcriptional analysis of the conserved ftsZ gene cluster in Mycoplasma genitalium and Mycoplasma pneumoniae. *Journal of Bacteriology*, *187*(13), 4542–4551. https://doi.org/10.1128/JB.187.13.4542-4551.2005

Bergemann, A. D., Whitley, J. C., & Finch, L. R. (1989). Homology of mycoplasma plasmid pADB201 and staphylococcal plasmid pE194. *Journal of Bacteriology*, *171*(1), 593–595. https://doi.org/10.1128/jb.171.1.593-595.1989

Bernhardt, T. G., & De Boer, P. A. J. (2005). SlmA, a nucleoid-associated, FtsZ binding protein required for blocking septal ring assembly over chromosomes in E. coli. *Molecular Cell*, *18*(5), 555–564. https://doi.org/10.1016/j.molcel.2005.04.012

Bisson-Filho, A. W., Hsu, Y. P., Squyres, G. R., Kuru, E., Wu, F., Jukes, C., Sun, Y., Dekker,

C., Holden, S., VanNieuwenhze, M. S., Brun, Y. V., & Garner, E. C. (2017). Treadmilling by FtsZ filaments drives peptidoglycan synthesis and bacterial cell division. *Science*, *355*(6326), 739–743. https://doi.org/10.1126/science.aak9973

Blötz, C., Lartigue, C., Timana, Y. V., Ruiz, E., Paetzold, B., Busse, J., & Stülke, J. (2018). Development of a replicating plasmid based on the native oriC in mycoplasma pneumoniae. *Microbiology (United Kingdom)*, *164*(11), 1372–1382. https://doi.org/10.1099/mic.0.000711

Blötz, C., & Stülke, J. (2017). Glycerol metabolism and its implication in virulence in Mycoplasma. *FEMS Microbiology Reviews*, *41*(5), 640–652. https://doi.org/10.1093/femsre/fux033

Bohorquez, L. C., Surdova, K., Jonker, M. J., & Hamoen, L. W. (2018). The conserved DNA binding protein WhiA influences chromosome segregation in Bacillus subtilis. *Journal of Bacteriology*, *200*(8). https://doi.org/10.1128/JB.00633-17

Bousis, S., Setyawati, I., Diamanti, E., Slotboom, D. J., & Hirsch, A. K. H. (2019). Energy-Coupling Factor Transporters as Novel Antimicrobial Targets. *Advanced Therapeutics*, *2*(2), 1800066. https://doi.org/10.1002/adtp.201800066

Braam, J. F., van Dommelen, L., Henquet, C. J. M., van de Bovenkamp, J. H. B., & Kusters, J. G. (2017). Multidrug-resistant Mycoplasma genitalium infections in Europe. *European Journal of Clinical Microbiology and Infectious Diseases*, *36*(9), 1565–1567. https://doi.org/10.1007/s10096-017-2969-9

Bradshaw, C. S., Chen, M. Y., & Fairley, C. K. (2008). Persistence of Mycoplasma genitalium following azithromycin therapy. *PLoS ONE*, *3*(11), e3618. https://doi.org/10.1371/journal.pone.0003618

Bradshaw, C. S., Horner, P. J., Jensen, J. S., & White, P. J. (2018). Syndromic management of STIs and the threat of untreatable Mycoplasma genitalium. In *The Lancet Infectious Diseases* (Vol. 18, Issue 3, pp. 251–252). Lancet Publishing Group. https://doi.org/10.1016/S1473-3099(18)30080-X

Breton, M., Sagné, E., Duret, S., Béven, L., Citti, C., & Renaudin, J. (2010). First report of a tetracycline-inducible gene expression system for mollicutes. *Microbiology*, *156*(1), 198–205. https://doi.org/10.1099/mic.0.034074-0

Bullen, J. J., Rogers, H. J., Spalding, P. B., & Ward, C. G. (2005). Iron and infection: the heart of the matter. *FEMS Immunology & Medical Microbiology*, *43*(3), 325–330. https://doi.org/10.1016/j.femsim.2004.11.010

Burgos, R., Pich, O. Q., Ferrer-Navarro, M., Baseman, J. B., Querol, E., & Piñol, J. (2006).

Mycoplasma genitalium P140 and P110 cytadhesins are reciprocally stabilized and required for cell adhesion and terminal-organelle development. *Journal of Bacteriology*, *188*(24), 8627–8637. https://doi.org/10.1128/JB.00978-06

Burgos, R., Pich, O. Q., Querol, E., & Piñol, J. (2007). Functional analysis of the Mycoplasma genitalium MG312 protein reveals a specific requirement of the MG312 N-terminal domain for gliding motility. *Journal of Bacteriology*, *189*(19), 7014–7023. https://doi.org/10.1128/JB.00975-07

Burgos, R., Pich, O. Q., Querol, E., & Piñol, J. (2008). Deletion of the Mycoplasma genitalium MG_217 gene modifies cell gliding behaviour by altering terminal organelle curvature. *Molecular Microbiology*, *69*(4), 1029–1040. https://doi.org/10.1111/j.1365-2958.2008.06343.x

Burgos, R., Wood, G. E., Iverson-Cabral, S. L., & Tottena, P. A. (2018). Mycoplasma genitalium nonadherent phase variants arise by multiple mechanisms and escape antibody-dependent growth inhibition. *Infection and Immunity*, *86*(4). https://doi.org/10.1128/IAI.00866-17

Butcher, J., Sarvan, S., Brunzelle, J. S., Couture, J. F., & Stintzi, A. (2012). Structure and regulon of Campylobacter jejuni ferric uptake regulator fur define apo-Fur regulation. *Proceedings of the National Academy of Sciences of the United States of America*, *109*(25), 10047–10052. https://doi.org/10.1073/pnas.1118321109

Calisto, B. M., Broto, A., Martinelli, L., Querol, E., Piñol, J., & Fita, I. (2012). The EAGR box structure: A motif involved in mycoplasma motility. *Molecular Microbiology*, *86*(2), 382–393. https://doi.org/10.1111/j.1365-2958.2012.08200.x

Carpenter, B. M., Gilbreath, J. J., Pich, O. Q., McKelvey, A. M., Maynard, E. L., Li, Z. Z., & Scott Merrell, D. (2013). Identification and characterization of novel helicobacter pylori apo-Fur-Regulated target genes. *Journal of Bacteriology*, *195*(24), 5526–5539. https://doi.org/10.1128/JB.01026-13

Chandrangsu, P., Rensing, C., & Helmann, J. D. (2017). Metal homeostasis and resistance in bacteria. In *Nature Reviews Microbiology* (Vol. 15, Issue 6, pp. 338–350). Nature Publishing Group. https://doi.org/10.1038/nrmicro.2017.15

Chang, T. H., Huang, H. Da, Wu, L. C., Yeh, C. T., Liu, B. J., & Horng, J. T. (2009). Computational identification of riboswitches based on RNA conserved functional sequences and conformations. *RNA*, *15*(7), 1426–1430. https://doi.org/10.1261/rna.1623809

Chen, S., Jancrick, J., Yokota, H., Kim, R., & Kim, S. H. (2004). Crystal structure of a protein associated with cell division from Mycoplasma pneumoniae (GI: 13508053): A novel

fold with a conserved sequence motif. *Proteins: Structure, Function and Genetics*, *55*(4), 785–791. https://doi.org/10.1002/prot.10593

Cheng, J., Poduska, B., Morton, R. A., & Finan, T. M. (2011). An ABC-type cobalt transport system is essential for growth of Sinorhizobium meliloti at trace metal concentrations. *Journal of Bacteriology*, *193*(17), 4405–4416. https://doi.org/10.1128/JB.05045-11

Christen, B., Abeliuk, E., Collier, J. M., Kalogeraki, V. S., Passarelli, B., Coller, J. A., Fero, M. J., McAdams, H. H., & Shapiro, L. (2011). The essential genome of a bacterium. *Molecular Systems Biology*, *7*(1). https://doi.org/10.1038/msb.2011.58

Commichau, F. M., & Stülke, J. (2008). Trigger enzymes: Bifunctional proteins active in metabolism and in controlling gene expression. In *Molecular Microbiology* (Vol. 67, Issue 4, pp. 692–702). https://doi.org/10.1111/j.1365-2958.2007.06071.x

Couldwell, D. L., & Lewis, D. A. (2015). Mycoplasma genitalium infection: Current treatment options, therapeutic failure, and resistance-associated mutations. *Infection and Drug Resistance*, *8*, 147–161. https://doi.org/10.2147/IDR.S48813

Crooks, G. E., Hon, G., Chandonia, J. M., & Brenner, S. E. (2004). WebLogo: A sequence logo generator. *Genome Research*, *14*(6), 1188–1190. https://doi.org/10.1101/gr.849004

Cross, C. E., Halliwell, B., Borish, E. T., Pryor, W. A., Ames, B. N., Saul, R. L., McCord, J. M., & Harman, D. (1987). Oxygen radicals and human disease. In *Annals of Internal Medicine* (Vol. 107, Issue 4, pp. 526–545). American College of Physicians. https://doi.org/10.7326/0003-4819-107-4-526

D'Autréaux, B., Pecqueur, L., De Peredo, A. G., Diederix, R. E. M., Caux-Thang, C., Tabet, L., Bersch, B., Forest, E., & Michaud-Soret, I. (2007). Reversible redox- and zinc-dependent dimerization of the Escherichia coli fur protein. *Biochemistry*, *46*(5), 1329–1342. https://doi.org/10.1021/bi061636r

Dai, K., & Lutkenhaus, J. (1991). ftsZ Is an essential cell division gene in Escherichia coli. *Journal of Bacteriology*, *173*(11), 3500–3506. https://doi.org/10.1128/jb.173.11.3500-3506.1991

De Lorenzo, V., Wee, S., Herrero, M., & Neilands, J. B. (1987). Operator sequences of the aerobactin operon of plasmid colV--K30 binding the ferric uptake regulation (fur) repressor. *Journal of Bacteriology*, *169*(6), 2624–2630. https://doi.org/10.1128/jb.169.6.2624-2630.1987

Deguchi, T. (2017). Proposed treatment strategies for non-gonococcal urethritis. In *The*

Lancet Infectious Diseases (Vol. 17, Issue 11, pp. 1121–1122). Lancet Publishing Group. https://doi.org/10.1016/S1473-3099(17)30571-6

Deigan, K. E., & Ferré-D'Amaré, A. R. (2011). Riboswitches: Discovery of drugs that target bacterial gene-regulatory RNAs. *Accounts of Chemical Research*, *44*(12), 1329–1338. https://doi.org/10.1021/ar200039b

Delany, I., Rappuoli, R., & Scarlato, V. (2004). Fur functions as an activator and as a repressor of putative virulence genes in Neisseria meningitidis. *Molecular Microbiology*, *52*(4), 1081–1090. https://doi.org/10.1111/j.1365-2958.2004.04030.x

Deng, X., Sun, F., Ji, Q., Liang, H., Missiakas, D., Lan, L., & He, C. (2012). Expression of multidrug resistance efflux pump gene norA Is iron responsive in Staphylococcus aureus. *Journal of Bacteriology*, *194*(7), 1753–1762. https://doi.org/10.1128/JB.06582-11

Dhandayuthapani, S., Rasmussen, W. G., & Baseman, J. B. (1999). Disruption of gene mg218 of Mycoplasma genitalium through homologous recombination leads to an adherence-deficient phenotype. *Proceedings of the National Academy of Sciences of the United States of America*, *96*(9), 5227–5232. https://doi.org/10.1073/pnas.96.9.5227

Dodd, I. B., Perkins, A. J., Tsemitsidis, D., & Egan, J. B. (2001). Octamerization of λ CI repressor is needed for effective repression of PRM and efficient switching from lysogeny. *Genes and Development*, *15*(22), 3013–3022. https://doi.org/10.1101/gad.937301

Dorman, C. J., & Dorman, M. J. (2016). DNA supercoiling is a fundamental regulatory principle in the control of bacterial gene expression. In *Biophysical Reviews* (Vol. 8, Issue 3, pp. 209–220). Springer Verlag. https://doi.org/10.1007/s12551-016-0205-y

Ebersbach, G., Galli, E., Møller-Jensen, J., Löwe, J., & Gerdes, K. (2008). Novel coiled-coil cell division factor ZapB stimulates Z ring assembly and cell division. *Molecular Microbiology*, *68*(3), 720–735. https://doi.org/10.1111/j.1365-2958.2008.06190.x

Edwards, D. H., & Errington, J. (1997). The Bacillus subtilis DivIVA protein targets to the division septum and controls the site specificity of cell division. *Molecular Microbiology*, *24*(5), 905–915. https://doi.org/10.1046/j.1365-2958.1997.3811764.x

Eraso, J. M., Markillie, L. M., Mitchell, H. D., Taylor, R. C., Orr, G., & Margolin, W. (2014). The highly conserved MraZ protein is a transcriptional regulator in Escherichia coli.

Journal of Bacteriology, *196*(11), 2053–2066. https://doi.org/10.1128/JB.01370-13

Errington, J., Daniel, R. A., & Scheffers, D.-J. (2003). Cytokinesis in Bacteria. *Microbiology and Molecular Biology Reviews*, *67*(1), 52–65. https://doi.org/10.1128/mmbr.67.1.52-65.2003

Escolar, L., Pérez-Martín, J., & De Lorenzo, V. (1998). Binding of the Fur (ferric uptake regulator) repressor of Escherichia coli to arrays of the GATAAT sequence. *Journal of Molecular Biology*, *283*(3), 537–547. https://doi.org/10.1006/jmbi.1998.2119

Escolar, L., Pérez-Martín, J., & De Lorenzo, V. (1999). Opening the iron box: Transcriptional metalloregulation by the fur protein. In *Journal of Bacteriology* (Vol. 181, Issue 20, pp. 6223–6229). American Society for Microbiology Journals. https://doi.org/10.1128/jb.181.20.6223-6229.1999

Espéli, O., Borne, R., Dupaigne, P., Thiel, A., Gigant, E., Mercier, R., & Boccard, F. (2012). A MatP-divisome interaction coordinates chromosome segregation with cell division in *E. coli*. *The EMBO Journal*, *31*(14), 3198–3211. https://doi.org/10.1038/emboj.2012.128

Fernández-Huerta, M., Barberá, M. J., Serra-Pladevall, J., Esperalba, J., Martínez-Gómez, X., Centeno, C., Pich, O. Q., Pumarola, T., & Espasa, M. (2020). Mycoplasma genitalium and antimicrobial resistance in Europe: a comprehensive review. In *International Journal of STD and AIDS* (Vol. 31, Issue 3, pp. 190–197). SAGE Publications Ltd. https://doi.org/10.1177/0956462419890737

Fillat, M. F. (2014). The FUR (ferric uptake regulator) superfamily: Diversity and versatility of key transcriptional regulators. *Archives of Biochemistry and Biophysics*, *546*, 41–52. https://doi.org/10.1016/J.ABB.2014.01.029

Fisunov, G. Y., Evsyutina, D. V., Semashko, T. A., Arzamasov, A. A., Manuvera, V. A., Letarov, A. V., & Govorun, V. M. (2016). Binding site of MraZ transcription factor in Mollicutes. *Biochimie*, *125*, 59–65. https://doi.org/10.1016/j.biochi.2016.02.016

Fisunov, G.Y., Evsyutina, D. V., Semashko, T. A., Arzamasov, A. A., Manuvera, V. A., Letarov, A. V., & Govorun, V. M. (2016). Binding site of MraZ transcription factor in Mollicutes. *Biochimie*, *125*, 59–65. https://doi.org/10.1016/J.BIOCHI.2016.02.016

Fisunov, Gleb Y., Garanina, I. A., Evsyutina, D. V., Semashko, T. A., Nikitina, A. S., & Govorun, V. M. (2016). Reconstruction of transcription control networks in mollicutes by high-throughput identification of promoters. *Frontiers in Microbiology*, *7*(DEC), 1977. https://doi.org/10.3389/fmicb.2016.01977

Fraser, C. M., Gocayne, J. D., White, O., Adams, M. D., Clayton, R. A., Fleischmann, R. D.,

Bult, C. J., Kerlavage, A. R., Sutton, G., Kelley, J. M., Fritchman, J. L., Weidman, J. F., Small, K. V., Sandusky, M., Fuhrmann, J., Nguyen, D., Utterback, T. R., Saudek, D. M., Phillips, C. A., … Lucier, T. S. (1995). The Minimal Gene Complement of Mycoplasma genitalium. *Science*, *270*(5235), 397–404. https://doi.org/10.1126/science.270.5235.397

Fu, X. (2001). The MinE ring required for proper placement of the division site is a mobile structure that changes its cellular location during the Escherichia coli division cycle. *Proceedings of the National Academy of Sciences*, *98*(3), 980–985. https://doi.org/10.1073/pnas.031549298

Fuangthong, M., & Helmann, J. D. (2003). Recognition of DNA by Three Ferric Uptake Regulator (Fur) Homologs in Bacillus subtilis. *Journal of Bacteriology*, *185*(21), 6348–6357. https://doi.org/10.1128/JB.185.21.6348-6357.2003

Furukawa, K., Ramesh, A., Zhou, Z., Weinberg, Z., Vallery, T., Winkler, W. C., & Breaker, R. R. (2015). Bacterial Riboswitches Cooperatively Bind Ni2+ or Co2+ Ions and Control Expression of Heavy Metal Transporters. *Molecular Cell*, *57*(6), 1088–1098. https://doi.org/10.1016/j.molcel.2015.02.009

Gancz, H., Jones, K. R., & Merrell, D. S. (2008). Sodium chloride affects Helicobacter pylori growth and gene expression. *Journal of Bacteriology*, *190*(11), 4100–4105. https://doi.org/10.1128/JB.01728-07

Gancz, H., & Merrell, D. S. (2011). The Helicobacter pylori Ferric Uptake Regulator (Fur) is essential for growth under sodium chloride stress. *Journal of Microbiology*, *49*(2), 294–298. https://doi.org/10.1007/s12275-011-0396-7

García-Morales, L., González-González, L., Querol, E., & Piñol, J. (2016). A minimized motile machinery for *Mycoplasma genitalium*. *Molecular Microbiology*, *100*(1), 125–138. https://doi.org/10.1111/mmi.13305

Gibson, D. G., Benders, G. A., Andrews-Pfannkoch, C., Denisova, E. A., Baden-Tillson, H., Zaveri, J., Stockwell, T. B., Brownley, A., Thomas, D. W., Algire, M. A., Merryman, C., Young, L., Noskov, V. N., Glass, J. I., Venter, J. C., Hutchison, C. A., & Smith, H. O. (2008). Complete chemical synthesis, assembly, and cloning of a Mycoplasma genitalium genome. *Science*, *319*(5867), 1215–1220. https://doi.org/10.1126/science.1151721

Gibson, D. G., Glass, J. I., Lartigue, C., Noskov, V. N., Chuang, R. Y., Algire, M. A., Benders, G. A., Montague, M. G., Ma, L., Moodie, M. M., Merryman, C., Vashee, S., Krishnakumar, R., Assad-Garcia, N., Andrews-Pfannkoch, C., Denisova, E. A., Young, L., Qi, Z. N., Segall-Shapiro, T. H., … Venter, J. C. (2010). Creation of a bacterial cell controlled by a chemically synthesized genome. *Science*, *329*(5987), 52–56.

https://doi.org/10.1126/science.1190719

Giedroc, D. P., & Arunkumar, A. I. (2007). Metal sensor proteins: Nature's metalloregulated allosteric switches. *Dalton Transactions*, *29*, 3107–3120. https://doi.org/10.1039/b706769k

Glasgow, L. R., & Hill, R. L. (1980). Interaction of Mycoplasma gallisepticum with sialyl glycoproteins. *Infection and Immunity*, *30*(2), 353–361.

Glass, J. I., Assad-Garcia, N., Alperovich, N., Yooseph, S., Lewis, M. R., Maruf, M., Hutchison, C. A., Smith, H. O., & Venter, J. C. (2006). Essential genes of a minimal bacterium. *Proceedings of the National Academy of Sciences of the United States of America*, *103*(2), 425–430. https://doi.org/10.1073/pnas.0510013103

Gnanadurai, R., & Fifer, H. (2020). Mycoplasma genitalium: A review. In *Microbiology (United Kingdom)* (Vol. 166, Issue 1, pp. 21–29). Microbiology Society. https://doi.org/10.1099/mic.0.000830

Goret, J., Le Roy, C., Touati, A., Mesureur, J., Renaudin, H., Claverol, S., Bébéar, C., Béven, L., & Pereyre, S. (2016). Surface lipoproteome of Mycoplasma hominis PG21 and differential expression after contact with human dendritic cells. *Future Microbiology*, *11*(2), 179–194. https://doi.org/10.2217/fmb.15.130

Großhennig, S., Schmidl, S. R., Schmeisky, G., Busse, J., & Stülke, J. (2013). Implication of glycerol and phospholipid transporters in Mycoplasma pneumoniae growth and virulence. *Infection and Immunity*, *81*(3), 896–904. https://doi.org/10.1128/IAI.01212-12

Güell, M., Van Noort, V., Yus, E., Chen, W. H., Leigh-Bell, J., Michalodimitrakis, K., Yamada, T., Arumugam, M., Doerks, T., Kühner, S., Rode, M., Suyama, M., Schmidt, S., Gavin, A. C., Bork, P., & Serrano, L. (2009). Transcriptome complexity in a genome-reduced bacterium. *Science*, *326*(5957), 1268–1271. https://doi.org/10.1126/science.1176951

Halbedel, S., Eilers, H., Jonas, B., Busse, J., Hecker, M., Engelmann, S., & Stülke, J. (2007). Transcription in Mycoplasma pneumoniae: Analysis of the Promoters of the ackA and ldh Genes. *Journal of Molecular Biology*, *371*(3), 596–607. https://doi.org/10.1016/j.jmb.2007.05.098

Halbedel, S., Hames, C., & Stülke, J. (2007). Regulation of Carbon Metabolism in the Mollicutes and Its Relation to Virulence. *Journal of Molecular Microbiology and Biotechnology*, *12*(1–2), 147–154. https://doi.org/10.1159/000096470

Hallamaa, K. M., Tang, S. L., Ficorilli, N., & Browning, G. F. (2008). Differential expression

of lipoprotein genes in Mycoplasma pneumoniae after contact with human lung epithelial cells, and under oxidative and acidic stress. *BMC Microbiology*, *8*, 124. https://doi.org/10.1186/1471-2180-8-124

Hames, C., Halbedel, S., Hoppert, M., Frey, J., & Stülke, J. (2009). Glycerol metabolism is important for cytotoxicity of Mycoplasma pneumoniae. *Journal of Bacteriology*, *191*(3), 747–753. https://doi.org/10.1128/JB.01103-08

Haney, S. A., Glasfeld, E., Hale, C., Keeney, D., He, Z., & De Boer, P. (2001). Genetic analysis of the Escherichia coli FtsZ·ZipA interaction in the yeast two-hybrid system. Characterization of FtsZ residues essential for the interactions with ZipA and with FtsA. *Journal of Biological Chemistry*, *276*(15), 11980–11987. https://doi.org/10.1074/jbc.M009810200

Hardy, R. D., Coalson, J. J., Peters, J., Chaparro, A., Techasaensiri, C., Cantwell, A. M., Kannan, T. R., Baseman, J. B., & Dube, P. H. (2009). Analysis of Pulmonary Inflammation and Function in the Mouse and Baboon after Exposure to Mycoplasma pneumoniae CARDS Toxin. *PLoS ONE*, *4*(10), e7562. https://doi.org/10.1371/journal.pone.0007562

Harris, K. A., & Breaker, R. R. (2018). Large Noncoding RNAs in Bacteria. *Microbiology Spectrum*, *6*(4). https://doi.org/10.1128/microbiolspec.rwr-0005-2017

Hartig, S. M. (2013). Basic image analysis and manipulation in imageJ. *Current Protocols in Molecular Biology*, *Chapter 14*(SUPPL.102). https://doi.org/10.1002/0471142727.mb1415s102

Hasselbring, B. M., Jordan, J. L., Krause, R. W., & Krause, D. C. (2006). Terminal organelle development in the cell wall-less bacterium Mycoplasma pneumoniae. *Proceedings of the National Academy of Sciences of the United States of America*, *103*(44), 16478–16483. https://doi.org/10.1073/pnas.0608051103

Hasselbring, B. M., & Krause, D. C. (2007). Proteins P24 and P41 function in the regulation of terminal-organelle development and gliding motility in Mycoplasma pneumoniae. *Journal of Bacteriology*, *189*(20), 7442–7449. https://doi.org/10.1128/JB.00867-07

Hatchel, J. M., & Balish, M. F. (2008). Attachment organelle ultrastructure correlates with phylogeny, not gliding motility properties, in Mycoplasma pneumoniae relatives. *Microbiology (Reading, England)*, *154*(Pt 1), 286–295. https://doi.org/10.1099/mic.0.2007/012765-0

Hauryliuk, V., Atkinson, G. C., Murakami, K. S., Tenson, T., & Gerdes, K. (2015). Recent functional insights into the role of (p)ppGpp in bacterial physiology. In *Nature*

Reviews Microbiology (Vol. 13, Issue 5, pp. 298–309). Nature Publishing Group. https://doi.org/10.1038/nrmicro3448

Havill, J. T., Bhatiya, C., Johnson, S. M., Sheets, J. D., & Thompson, J. S. (2014). A new approach for detecting riboswitches in DNA sequences. *Bioinformatics (Oxford, England)*, *30*(21), 3012–3019. https://doi.org/10.1093/bioinformatics/btu479

Hedreyda, C. T., Lee, K. K., & Krause, D. C. (1993). Transformation of Mycoplasma pneumoniae with Tn4001 by Electroporation. *Plasmid*, *30*(2), 170–175. https://doi.org/10.1006/plas.1993.1047

Hempel, K., Herbst, F. A., Moche, M., Hecker, M., & Becher, D. (2011). Quantitative proteomic view on secreted, cell surface-associated, and cytoplasmic proteins of the methicillin-resistant human pathogen staphylococcus aureus under iron-limited conditions. *Journal of Proteome Research*, *10*(4), 1657–1666. https://doi.org/10.1021/pr1009838

Hermsen, R., Ursem, B., & ten Wolde, P. R. (2010). Combinatorial gene regulation using auto-regulation. *PLoS Computational Biology*, *6*(6), 1–13. https://doi.org/10.1371/journal.pcbi.1000813

Hernández-Solans, M., Torres-Puig, S., Querol, E., Piñol, J., & Pich, O. Q. (2016). *Development Of A Replicable OriC Plasmid For Mycoplasma genitalium*. Poster.

Hiron, A., Posteraro, B., Carrière, M., Remy, L., Delporte, C., La Sorda, M., Sanguinetti, M., Juillard, V., & Borezée-Durant, E. (2010). A nickel ABC-transporter of Staphylococcus aureus is involved in urinary tract infection. *Molecular Microbiology*, *77*(5), 1246–1260. https://doi.org/10.1111/j.1365-2958.2010.07287.x

Hochschild, A., & Lewis, M. (2009). The bacteriophage λ CI protein finds an asymmetric solution. In *Current Opinion in Structural Biology* (Vol. 19, Issue 1, pp. 79–86). Elsevier Current Trends. https://doi.org/10.1016/j.sbi.2008.12.008

Holm, R. H., Kennepohl, P., & Solomon, E. I. (1996). Structural and functional aspects of metal sites in biology. *Chemical Reviews*, *96*(7), 2239–2314. https://doi.org/10.1021/cr9500390

Hood, M. I., & Skaar, E. P. (2012). Nutritional immunity: Transition metals at the pathogen-host interface. In *Nature Reviews Microbiology* (Vol. 10, Issue 8, pp. 525–537). Nature Publishing Group. https://doi.org/10.1038/nrmicro2836

Horner, P. J., Blee, K., Falk, L., van der Meijden, W., & Moi, H. (2016). 2016 European guideline on the management of non-gonococcal urethritis. *International Journal*

of STD and AIDS, *27*(11), 928–937. https://doi.org/10.1177/0956462416648585

Hu, P. C., Schaper, U., Collier, A. M., Clyde, W. A., Horikawa, M., Huang, Y. S., & Barile, M. F. (1987). A Mycoplasma genitalium protein resembling the Mycoplasma pneumoniae attachment protein. *Infection and Immunity*, *55*(5), 1126–1131. https://doi.org/10.1128/iai.55.5.1126-1131.1987

Hu, Z., & Lutkenhaus, J. (2003). A conserved sequence at the C-terminus of MinD is required for binding to the membrane and targeting MinC to the septum. *Molecular Microbiology*, *47*(2), 345–355. https://doi.org/10.1046/j.1365-2958.2003.03321.x

Huang, K. H., Durand-Heredia, J., & Janakiraman, A. (2013). FtsZ ring stability: Of bundles, tubules, crosslinks, and curves. In *Journal of Bacteriology* (Vol. 195, Issue 9, pp. 1859–1868). American Society for Microbiology Journals. https://doi.org/10.1128/JB.02157-12

Hutchison, C. A., Chuang, R.-Y., Noskov, V. N., Assad-Garcia, N., Deerinck, T. J., Ellisman, M. H., Gill, J., Kannan, K., Karas, B. J., Ma, L., Pelletier, J. F., Qi, Z.-Q., Richter, R. A., Strychalski, E. A., Sun, L., Suzuki, Y., Tsvetanova, B., Wise, K. S., Smith, H. O., … Venter, J. C. (2016). Design and synthesis of a minimal bacterial genome. *Science*, *351*(6280), aad6253–aad6253. https://doi.org/10.1126/science.aad6253

Hutchison, Clyde A., Peterson, S. N., Gill, S. R., Cline, R. T., White, O., Fraser, C. M., Smith, H. O., & Venter, J. C. (1999). Global transposon mutagenesis and a minimal mycoplasma genome. *Science*, *286*(5447), 2165–2169. https://doi.org/10.1126/science.286.5447.2165

Ishag, H. Z.A., Liu, M. J., Yang, R. S., Xiong, Q. Y., Feng, Z. X., & Shao, G. Q. (2016). A replicating plasmid-based vector for GFP expression in Mycoplasma hyopneumoniae. *Genetics and Molecular Research*, *15*(2). https://doi.org/10.4238/gmr.15027832

Ishag, Hassan Z.A., Xiong, Q., Liu, M., Feng, Z., & Shao, G. (2017). Development of oriC-plasmids for use in Mycoplasma hyorhinis. *Scientific Reports*, *7*(1). https://doi.org/10.1038/s41598-017-10519-3

Ito, S., Abe, Y., Kinomoto, K., Saitoh, T., Kato, T., Kohli, Y., Kuriyama, M., Sakai, T., & Ishizaki, T. (1995). Fulminant Mycoplasma Pneumoniae Pneumonia with Marked Elevation of Serum Soluble Interleukin-2 Receptor. *Internal Medicine*, *34*(5), 430–435. https://doi.org/10.2169/internalmedicine.34.430

Iverson-Cabral, S. L., Astete, S. G., Cohen, C. R., Rocha, E. P. C., & Totten, P. A. (2006). Intrastrain heterogeneity of the mgpB gene in Mycoplasma genitalium is extensive

in vitro and in vivo and suggests that variation is generated via recombination with repetitive chromosomal sequences. *Infection and Immunity*, *74*(7), 3715–3726. https://doi.org/10.1128/IAI.00239-06

Iverson-Cabral, S. L., Astete, S. G., Cohen, C. R., & Totten, P. A. (2007). mgpB and mgpC sequence diversity in Mycoplasma genitalium is generated by segmental reciprocal recombination with repetitive chromosomal sequences. *Molecular Microbiology*, *66*(1), 55–73. https://doi.org/10.1111/j.1365-2958.2007.05898.x

Iverson-Cabral, S. L., Wood, G. E., & Totten, P. A. (2015). Analysis of the Mycoplasma genitalium MgpB Adhesin to Predict Membrane Topology, Investigate Antibody Accessibility, Characterize Amino Acid Diversity, and Identify Functional and Immunogenic Epitopes. *PLOS ONE*, *10*(9), e0138244. https://doi.org/10.1371/journal.pone.0138244

Jemiolo, D. K., Zwieb, C., & Dahlberg, A. E. (1985). Point mutations in the 3' minor domain of 16S rRNA of E.coli. *Nucleic Acids Research*, *13*(23), 8631–8643. https://doi.org/10.1093/nar/13.23.8631

Jensen, J.S., Cusini, M., Gomberg, M., & Moi, H. (2016). 2016 European guideline on *Mycoplasma genitalium* infections. *Journal of the European Academy of Dermatology and Venereology*, *30*(10), 1650–1656. https://doi.org/10.1111/jdv.13849

Jensen, Jørgen S., Bradshaw, C. S., Tabrizi, S. N., Fairley, C. K., & Hamasuna, R. (2008). Azithromycin Treatment Failure in Mycoplasma genitalium –Positive Patients with Nongonococcal Urethritis Is Associated with Induced Macrolide Resistance . *Clinical Infectious Diseases*, *47*(12), 1546–1553. https://doi.org/10.1086/593188

Jensen, Jørgen Skov. (2017). Mycoplasma genitalium: yet another challenging STI. In *The Lancet Infectious Diseases* (Vol. 17, Issue 8, pp. 795–796). Lancet Publishing Group. https://doi.org/10.1016/S1473-3099(17)30364-X

Johnson, A. D., Meyer, B. J., & Ptashne, M. (1979). Interactions between DNA-bound repressors govern regulation by the λ phage repressor. *Proceedings of the National Academy of Sciences of the United States of America*, *76*(10), 5061–5065. https://doi.org/10.1073/pnas.76.10.5061

Kaiser, B. K., & Stoddard, B. L. (2011). DNA recognition and transcriptional regulation by the WhiA sporulation factor. *Scientific Reports*, *1*(1), 1–9. https://doi.org/10.1038/srep00156

Kani, K. (2017). Quantitative proteomics using SILAC. In *Methods in Molecular Biology* (Vol. 1550, pp. 171–184). Humana Press Inc. https://doi.org/10.1007/978-1-4939-

6747-6_13

Kannan, T. R., & Baseman, J. B. (2006). ADP-ribosylating and vacuolating cytotoxin of Mycoplasma pneumoniae represents unique virulence determinant among bacterial pathogens. *Proceedings of the National Academy of Sciences of the United States of America*, *103*(17), 6724–6729. https://doi.org/10.1073/pnas.0510644103

Karr, J. R., Sanghvi, J. C., MacKlin, D. N., Gutschow, M. V., Jacobs, J. M., Bolival, B., Assad-Garcia, N., Glass, J. I., & Covert, M. W. (2012). A whole-cell computational model predicts phenotype from genotype. *Cell*, *150*(2), 389–401. https://doi.org/10.1016/j.cell.2012.05.044

Kasai, T., Nakane, D., Ishida, H., Ando, H., Kiso, M., & Miyata, M. (2013). Role of binding in Mycoplasma mobile and Mycoplasma pneumoniae gliding analyzed through inhibition by synthesized sialylated compounds. *Journal of Bacteriology*, *195*(3), 429–435. https://doi.org/10.1128/JB.01141-12

Kawai, Y., Mickiewicz, K., & Errington, J. (2018). Lysozyme Counteracts β-Lactam Antibiotics by Promoting the Emergence of L-Form Bacteria. *Cell*, *172*(5), 1038-1049.e10. https://doi.org/10.1016/j.cell.2018.01.021

Keçeli, S. A., & Miles, R. J. (2002). Differential inhibition of mollicute growth: An approach to development of selective media for specific mollicutes. *Applied and Environmental Microbiology*, *68*(10), 5012–5016. https://doi.org/10.1128/AEM.68.10.5012-5016.2002

Kehl-Fie, T. E., & Skaar, E. P. (2010). Nutritional immunity beyond iron: a role for manganese and zinc. In *Current Opinion in Chemical Biology* (Vol. 14, Issue 2, pp. 218–224). NIH Public Access. https://doi.org/10.1016/j.cbpa.2009.11.008

Kimura, S., & Suzuki, T. (2010). Fine-tuning of the ribosomal decoding center by conserved methyl-modifications in the Escherichia coli 16S rRNA. *Nucleic Acids Research*, *38*(4), 1341–1352. https://doi.org/10.1093/nar/gkp1073

Kingsford, C. L., Ayanbule, K., & Salzberg, S. L. (2007). Rapid, accurate, computational discovery of Rho-independent transcription terminators illuminates their relationship to DNA uptake. *Genome Biology*, *8*(2), R22. https://doi.org/10.1186/gb-2007-8-2-r22

Klieneberger, E. (1935). The natural occurrence of pleuropneumonia-like organism in apparent symbiosis with Streptobacillus moniliformis and other bacteria. *The Journal of Pathology and Bacteriology*, *40*(1), 93–105. https://doi.org/10.1002/path.1700400108

Krause, D C, Leith, D. K., Wilson, R. M., & Baseman, J. B. (1982). Identification of Mycoplasma pneumoniae proteins associated with hemadsorption and virulence. *Infection and Immunity*, *35*(3), 809–817. http://www.ncbi.nlm.nih.gov/pubmed/6802761

Krause, Duncan C. (1996). Mycoplasma pneumoniae cytadherence: Unravelling the tie that binds. In *Molecular Microbiology* (Vol. 20, Issue 2, pp. 247–253). https://doi.org/10.1111/j.1365-2958.1996.tb02613.x

Krause, Duncan C., & Balish, M. F. (2001). Structure, function, and assembly of the terminal organelle of Mycoplasma pneumoniae . *FEMS Microbiology Letters*, *198*(1), 1–7. https://doi.org/10.1111/j.1574-6968.2001.tb10610.x

Krause, Duncan C., & Balish, M. F. (2004). Cellular engineering in a minimal microbe: structure and assembly of the terminal organelle of Mycoplasma pneumoniae. *Molecular Microbiology*, *51*(4), 917–924. https://doi.org/10.1046/j.1365-2958.2003.03899.x

Krishnakumar, R., Assad-Garcia, N., Benders, G. A., Phan, Q., Montague, M. G., & Glass, J. I. (2010). Targeted chromosomal knockouts in mycoplasma pneumoniae. *Applied and Environmental Microbiology*, *76*(15), 5297–5299. https://doi.org/10.1128/AEM.00024-10

Krupka, M., Cabré, E. J., Jiménez, M., Rivas, G., Rico, A. I., & Vicente, M. (2014). Role of the FtsA C terminus as a switch for polymerization and membrane association. *MBio*, *5*(6). https://doi.org/10.1128/mBio.02221-14

Kumar, A., Rahal, A., Chakraborty, S., Verma, A. K., & Dhama, K. (2014). Mycoplasma agalactiae, an etiological agent of contagious agalactia in Small ruminants: A review. In *Veterinary Medicine International* (Vol. 2014). Hindawi Publishing Corporation. https://doi.org/10.1155/2014/286752

Kyuma, T., Kimura, S., Hanada, Y., Suzuki, T., Sekimizu, K., & Kaito, C. (2015). Ribosomal RNA methyltransferases contribute to *Staphylococcus aureus* virulence. *FEBS Journal*, *282*(13), 2570–2584. https://doi.org/10.1111/febs.13302

Lartigue, C., Blanchard, A., Renaudin, J., Thiaucourt, F., & Sirand-Pugnet, P. (2003). Host specificity of mollicutes oriC plasmids: functional analysis of replication origin . *Nucleic Acids Research*, *31*(22), 6610–6618. https://doi.org/10.1093/nar/gkg848

Lavrrar, J. L., & McIntosh, M. A. (2003). Architecture of a Fur binding site: A comparative analysis. *Journal of Bacteriology*, *185*(7), 2194–2202. https://doi.org/10.1128/JB.185.7.2194-2202.2003

Le, T. B. K., Imakaev, M. V., Mirny, L. A., & Laub, M. T. (2013). High-resolution mapping of the spatial organization of a bacterial chromosome. *Science*, *342*(6159), 731–734. https://doi.org/10.1126/science.1242059

Leaver, M., Domínguez-Cuevas, P., Coxhead, J. M., Daniel, R. A., & Errington, J. (2009). Life without a wall or division machine in Bacillus subtilis. *Nature*, *457*(7231), 849–853. https://doi.org/10.1038/nature07742

Lee, J. H., Jeong, H., Kim, Y., & Lee, H. S. (2020). Corynebacterium glutamicum whiA plays roles in cell division, cell envelope formation, and general cell physiology. *Antonie van Leeuwenhoek, International Journal of General and Molecular Microbiology*, *113*(5), 629–641. https://doi.org/10.1007/s10482-019-01370-9

Lee, J. W., & Helmann, J. D. (2007). Functional specialization within the fur family of metalloregulators. *BioMetals*, *20*(3–4), 485–499. https://doi.org/10.1007/s10534-006-9070-7

Lee, S.-W., Browning, G. F., & Markham, P. F. (2008). Development of a replicable oriC plasmid for Mycoplasma gallisepticum and Mycoplasma imitans, and gene disruption through homologous recombination in M. gallisepticum. *Microbiology*, *154*(9), 2571–2580. https://doi.org/10.1099/mic.0.2008/019208-0

Létoffé, S., Delepelaire, P., & Wandersman, C. (2006). The housekeeping dipeptide permease is the Escherichia coli heme transporter and functions with two optional peptide binding proteins. *Proceedings of the National Academy of Sciences of the United States of America*, *103*(34), 12891–12896. https://doi.org/10.1073/pnas.0605440103

Li, G., Fan, L., Wang, Y., Huang, L., Wang, M., Zhu, C., Hao, C., Ji, W., Liang, H., Yan, Y., & Chen, Z. (2019). High co-expression of TNF-α and CARDS toxin is a good predictor for refractory Mycoplasma pneumoniae pneumonia. *Molecular Medicine*, *25*(1). https://doi.org/10.1186/s10020-019-0105-2

Li, J., Zhang, J., Zhang, N., Zhang, Y., Wu, W., & Li, J. (2015). Development of a replicative plasmid for gene expression in Mycoplasma bovis. *Journal of Microbiological Methods*, *108*, 12–18. https://doi.org/10.1016/j.mimet.2014.11.005

Liang, W., Ouyang, S., Shaw, N., Joachimiak, A., Zhang, R., & Liu, Z. (2011). Conversion of d -ribulose 5-phosphate to D -xylulose 5-phosphate: new insights from structural and biochemical studies on human RPE . *The FASEB Journal*, *25*(2), 497–504. https://doi.org/10.1096/fj.10-171207

Lillis, R. A., Martin, D. H., & Nsuami, M. J. (2019). Mycoplasma genitalium Infections in Women Attending a Sexually Transmitted Disease Clinic in New Orleans. *Clinical*

Infectious Diseases : An Official Publication of the Infectious Diseases Society of America, *69*(3), 459–465. https://doi.org/10.1093/cid/ciy922

Lis, R., Rowhani-Rahbar, A., & Manhart, L. E. (2015). Mycoplasma genitalium infection and female reproductive tract disease: a meta-analysis. *Clinical Infectious Diseases : An Official Publication of the Infectious Diseases Society of America*, *61*(3), 418–426. https://doi.org/10.1093/cid/civ312

Litwin, C. M., & Calderwood, S. B. (1993). Role of iron in regulation of virulence genes. *Clinical Microbiology Reviews*, *6*(2), 137–149. https://doi.org/10.1128/CMR.6.2.137

Lloréns-Rico, V., Lluch-Senar, M., & Serrano, L. (2015). Distinguishing between productive and abortive promoters using a random forest classifier in Mycoplasma pneumoniae. *Nucleic Acids Research*, *43*(7), 3442–3453. https://doi.org/10.1093/nar/gkv170

Lluch-Senar, M., Querol, E., & Piñol, J. (2010). Cell division in a minimal bacterium in the absence of ftsZ. *Molecular Microbiology*, *78*(2), 278–289. https://doi.org/10.1111/j.1365-2958.2010.07306.x

Lluch-Senar, M., Delgado, J., Chen, W., Lloréns-Rico, V., O'Reilly, F. J., Wodke, J. A., Unal, E. B., Yus, E., Martínez, S., Nichols, R. J., Ferrar, T., Vivancos, A., Schmeisky, A., Stülke, J., Noort, V., Gavin, A., Bork, P., & Serrano, L. (2015). Defining a minimal cell: essentiality of small ORF s and nc RNA s in a genome-reduced bacterium . *Molecular Systems Biology*, *11*(1), 780. https://doi.org/10.15252/msb.20145558

Loomes, L. M., Uemura, K. ichi, Childs, R. A., Paulson, J. C., Rogers, G. N., Scudder, P. R., Michalski, J. C., Hounsell, E. F., Taylor-Robinson, D., & Feizi, T. (1984). Erythrocyte receptors for mycoplasma pneumoniae are sialylated oligosaccharides of I antigen type. *Nature*, *307*(5951), 560–563. https://doi.org/10.1038/307560a0

Loose, M., & Mitchison, T. J. (2014). The bacterial cell division proteins ftsA and ftsZ self-organize into dynamic cytoskeletal patterns. *Nature Cell Biology*, *16*(1), 38–46. https://doi.org/10.1038/ncb2885

Lyon, B. R., May, J. W., & Skurray, R. A. (1984). Tn 4001: A gentamicin and kanamycin resistance transposon in Staphylococcus aureus. *MGG Molecular & General Genetics*, *193*(3), 554–556. https://doi.org/10.1007/BF00382099

Ma, L., Jensen, J. S., Mancuso, M., Hamasuna, R., Jia, Q., McGowin, C. L., & Martin, D. H. (2010). Genetic Variation in the Complete MgPa Operon and Its Repetitive Chromosomal Elements in Clinical Strains of Mycoplasma genitalium. *PLoS ONE*, *5*(12), e15660. https://doi.org/10.1371/journal.pone.0015660

Ma, L., Jensen, J. S., Myers, L., Burnett, J., Welch, M., Jia, Q., & Martin, D. H. (2007). Mycoplasma genitalium: An efficient strategy to generate genetic variation from a minimal genome. *Molecular Microbiology*, *66*(1), 220–236. https://doi.org/10.1111/j.1365-2958.2007.05911.x

Machtel, P., Bąkowska-Żywicka, K., & Żywicki, M. (2016). Emerging applications of riboswitches – from antibacterial targets to molecular tools. In *Journal of Applied Genetics* (Vol. 57, Issue 4, pp. 531–541). Springer Verlag. https://doi.org/10.1007/s13353-016-0341-x

Madsen, M. L., Nettleton, D., Thacker, E. L., & Minion, F. C. (2006). Transcriptional profiling of Mycoplasma hyopneumoniae during iron depletion using microarrays. *Microbiology*, *152*(4), 937–944. https://doi.org/10.1099/mic.0.28674-0

Maeda, T., Tanaka, Y., Takemoto, N., Hamamoto, N., & Inui, M. (2016). RNase III mediated cleavage of the coding region of mraZ mRNA is required for efficient cell division in Corynebacterium glutamicum. *Molecular Microbiology*, *99*(6), 1149–1166. https://doi.org/10.1111/mmi.13295

Maeda, Y. T., & Sano, M. (2006). Regulatory Dynamics of Synthetic Gene Networks with Positive Feedback. *Journal of Molecular Biology*, *359*(4), 1107–1124. https://doi.org/10.1016/j.jmb.2006.03.064

Maes, D., Sibila, M., Kuhnert, P., Segalés, J., Haesebrouck, F., & Pieters, M. (2018). Update on Mycoplasma hyopneumoniae infections in pigs: Knowledge gaps for improved disease control. *Transboundary and Emerging Diseases*, *65*, 110–124. https://doi.org/10.1111/tbed.12677

Manhart, L. E., Gillespie, C. W., Lowens, M. S., Khosropour, C. M., Colombara, D. V, Golden, M. R., Hakhu, N. R., Thomas, K. K., Hughes, J. P., Jensen, N. L., & Totten, P. A. (2013). Standard treatment regimens for nongonococcal urethritis have similar but declining cure rates: a randomized controlled trial. *Clinical Infectious Diseases : An Official Publication of the Infectious Diseases Society of America*, *56*(7), 934–942. https://doi.org/10.1093/cid/cis1022

Manhart, L. E., Gillespie, C. W., Lowens, M. S., Khosropour, C. M., Colombara, D. V, Golden, M. R., Hakhu, N. R., Thomas, K. K., Hughes, J. P., Jensen, N. L., Totten, P. A., Cohen, C. R., Nosek, M., Meier, A., Astete, S. G., Iverson-Cabral, S., Mugo, N. R., & Totten, P. A. (2013). *Mycoplasma genitalium* infection and persistence in a cohort of female sex workers in Nairobi, Kenya. *Sexually Transmitted Diseases*, *34*(5), 274–279.

Manhart, L. E., Jensen, J. S., Bradshaw, C. S., Golden, M. R., & Martin, D. H. (2015). Efficacy of Antimicrobial Therapy for Mycoplasma genitalium Infections. *Clinical*

Infectious Diseases : An Official Publication of the Infectious Diseases Society of America, *61 Suppl 8*, S802-17. https://doi.org/10.1093/cid/civ785

Manhart, L. E., Mostad, S. B., Baeten, J. M., Astete, S. G., Mandaliya, K., & Totten, P. A. (2008). High *Mycoplasma genitalium* Organism Burden Is Associated with Shedding of HIV-1 DNA from the Cervix. *The Journal of Infectious Diseases*, *197*(5), 733–736. https://doi.org/10.1086/526501

Margolin, W. (2000). Themes and variations in prokaryotic cell division. In *FEMS Microbiology Reviews* (Vol. 24, Issue 4, pp. 531–548). No longer published by Elsevier. https://doi.org/10.1016/S0168-6445(00)00038-3

Margolin, W., Wang, R., & Kumar, M. (1996). Isolation of an ftsZ homolog from the archaebacterium Halobacterium salinarium: Implications for the evolution of FtsZ and tubulin. *Journal of Bacteriology*, *178*(5), 1320–1327. https://doi.org/10.1128/jb.178.5.1320-1327.1996

Mariscal, A. M., González-González, L., Querol, E., & Piñol, J. (2016). All-in-one construct for genome engineering using Cre-lox technology. *DNA Research*, *23*(3), 263–270. https://doi.org/10.1093/dnares/dsw015

Mariscal, A. M., Kakizawa, S., Hsu, J. Y., Tanaka, K., González-González, L., Broto, A., Querol, E., Lluch-Senar, M., Piñero-Lambea, C., Sun, L., Weyman, P. D., Wise, K. S., Merryman, C., Tse, G., Moore, A. J., Hutchison, C. A., Smith, H. O., Tomita, M., Venter, J. C., … Suzuki, Y. (2018). Tuning Gene Activity by Inducible and Targeted Regulation of Gene Expression in Minimal Bacterial Cells. *ACS Synthetic Biology*, *7*(6), 1538–1552. https://doi.org/10.1021/acssynbio.8b00028

Martin, D. H., Manhart, L. E., & Workowski, K. A. (2017). Mycoplasma genitalium From Basic Science to Public Health: Summary of the Results From a National Institute of Allergy and Infectious Disesases Technical Consultation and Consensus Recommendations for Future Research Priorities. *The Journal of Infectious Diseases*, *216*(suppl_2), S427–S430. https://doi.org/10.1093/infdis/jix147

Martínez-Torró, C., Torres-Puig, S., Monge, M., Sánchez-Alba, L., González-Martín, M., Marcos-Silva, M., Perálvarez-Marín, A., Canals, F., Querol, E., Piñol, J., & Pich, O. Q. (2020). Transcriptional response to metal starvation in the emerging pathogen Mycoplasma genitalium is mediated by Fur-dependent and –independent regulatory pathways. *Emerging Microbes and Infections*, *9*(1), 5–19. https://doi.org/10.1080/22221751.2019.1700762

Martis B., S., Forquet, R., Reverchon, S., Nasser, W., & Meyer, S. (2019). DNA Supercoiling: an Ancestral Regulator of Gene Expression in Pathogenic Bacteria? In *Computational and Structural Biotechnology Journal* (Vol. 17, pp. 1047–1055).

Elsevier B.V. https://doi.org/10.1016/j.csbj.2019.07.013

Mathieu, S., Cissé, C., Vitale, S., Ahmadova, A., Degardin, M., Pérard, J., Colas, P., Miras, R., Boturyn, D., Covès, J., Crouzy, S., & Michaud-Soret, I. (2016). From Peptide Aptamers to Inhibitors of FUR, Bacterial Transcriptional Regulator of Iron Homeostasis and Virulence. *ACS Chemical Biology*, *11*(9), 2519–2528. https://doi.org/10.1021/acschembio.6b00360

Maurer, R., Meyer, B. J., & Ptashne, M. (1980). Gene regulation at the right operator (OR) of bacteriophage λ. I. OR3 and autogenous negative control by repressor. *Journal of Molecular Biology*, *139*(2), 147–161. https://doi.org/10.1016/0022-2836(80)90302-2

Mazin, P. V, Fisunov, G. Y., Gorbachev, A. Y., Kapitskaya, K. Y., Altukhov, I. A., Semashko, T. A., Alexeev, D. G., & Govorun, V. M. (2014). Transcriptome analysis reveals novel regulatory mechanisms in a genome-reduced bacterium. *Nucleic Acids Research*, *42*(21), 13254–13268. https://doi.org/10.1093/nar/gku976

McGowin, C. L., & Anderson-Smits, C. (2011). Mycoplasma genitalium: An Emerging Cause of Sexually Transmitted Disease in Women. *PLoS Pathogens*, *7*(5), e1001324. https://doi.org/10.1371/journal.ppat.1001324

McGowin, C. L., Annan, R. S., Quayle, A. J., Greene, S. J., Ma, L., Mancuso, M. M., Adegboye, D., & Martin, D. H. (2012). Persistent Mycoplasma genitalium infection of human endocervical epithelial cells elicits chronic inflammatory cytokine secretion. *Infection and Immunity*, *80*(11), 3842–3849. https://doi.org/10.1128/IAI.00819-12

McGowin, C. L., Liang, M., Martin, D. H., & Pyles, R. B. (2009). Mycoplasma genitalium-encoded MG309 activates NF-κB via toll-like receptors 2 and 6 to elicit proinflammatory cytokine secretion from human genital epithelial cells. *Infection and Immunity*, *77*(3), 1175–1181. https://doi.org/10.1128/IAI.00845-08

McGowin, C. L., Popov, V. L., & Pyles, R. B. (2009). Intracellular mycoplasma genitalium infection of human vaginal and cervical epithelial cells elicits distinct patterns of inflammatory cytokine secretion and provides a possible survival niche against macrophage-mediated killing. *BMC Microbiology*, *9*(1), 139. https://doi.org/10.1186/1471-2180-9-139

McGowin, C. L., & Totten, P. A. (2017). The Unique Microbiology and Molecular Pathogenesis of Mycoplasma genitalium. *The Journal of Infectious Diseases*, *216*(suppl_2), S382–S388. https://doi.org/10.1093/infdis/jix172

Merchant, S. S., & Helmann, J. D. (2012). Elemental Economy. Microbial Strategies for

Optimizing Growth in the Face of Nutrient Limitation. In *Advances in Microbial Physiology* (Vol. 60, pp. 91–210). Academic Press. https://doi.org/10.1016/B978-0-12-398264-3.00002-4

Mercier, R., Domínguez-Cuevas, P., & Errington, J. (2012). Crucial Role for Membrane Fluidity in Proliferation of Primitive Cells. *Cell Reports*, *1*(5), 417–423. https://doi.org/10.1016/j.celrep.2012.03.008

Mercier, R., Kawai, Y., & Errington, J. (2014). General principles for the formation and proliferation of a wall-free (L-form) state in bacteria. *ELife*, *3*. https://doi.org/10.7554/eLife.04629

Mernaugh, G. R., Dallo, S. F., Holt, S. C., & Baseman, J. B. (1993). Properties of Adhering and Nonadhering Populations of Mycoplasma genitalium. *Clinical Infectious Diseases*, *17*(Supplement_1), S69–S78. https://doi.org/10.1093/clinids/17.supplement_1.s69

Merrell, D. S., Thompson, L. J., Kim, C. C., Mitchell, H., Tompkins, L. S., Lee, A., & Falkow, S. (2003). Growth Phase-Dependent Response of Helicobacter pylori to Iron Starvation. *Infection and Immunity*, *71*(11), 6510–6525. https://doi.org/10.1128/IAI.71.11.6510-6525.2003

Messer, W., & Weigel, C. (1997). DnaA initiator - Also a transcription factor. In *Molecular Microbiology* (Vol. 24, Issue 1, pp. 1–6). Blackwell Publishing Ltd. https://doi.org/10.1046/j.1365-2958.1997.3171678.x

Meyer, B. J., Maurer, R., & Ptashne, M. (1980). Gene regulation at the right operator (OR) of bacteriophage λ. II. OR1, OR2, and OR3: Their roles in mediating the effects of repressor and cro. *Journal of Molecular Biology*, *139*(2), 163–194. https://doi.org/10.1016/0022-2836(80)90303-4

Meyer, B. J., & Ptashne, M. (1980). Gene regulation at the right operator (OR) of bacteriophage λ. III. λ Repressor directly activates gene transcription. *Journal of Molecular Biology*, *139*(2), 195–205. https://doi.org/10.1016/0022-2836(80)90304-6

Milano, A., Forti, F., Sala, C., Riccardi, G., & Ghisotti, D. (2001). Transcriptional regulation of furA and katG upon oxidative stress in Mycobacterium smegmatis. *Journal of Bacteriology*, *183*(23), 6801–6806. https://doi.org/10.1128/JB.183.23.6801-6806.2001

Minion, F. C. (2002). Molecular pathogenesis of mycoplasma animal respiratory pathogens. *Frontiers in Bioscience : A Journal and Virtual Library*, *7*, d1410-22. http://www.ncbi.nlm.nih.gov/pubmed/12045010

Moi, H., Blee, K., & Horner, P. J. (2015). Management of non-gonococcal urethritis. In *BMC Infectious Diseases* (Vol. 15, Issue 1, p. 294). BioMed Central Ltd. https://doi.org/10.1186/s12879-015-1043-4

Monahan, L. G., Robinson, A., & Harry, E. J. (2009). Lateral FtsZ association and the assembly of the cytokinetic Z ring in bacteria. *Molecular Microbiology*, *74*(4), 1004–1017. https://doi.org/10.1111/j.1365-2958.2009.06914.x

Monahan, L. G., Turnbull, L., Osvath, S. R., Birch, D., Charles, I. G., & Whitchurch, C. B. (2014). Rapid conversion of Pseudomonas aeruginosa to a spherical cell morphotype facilitates tolerance to carbapenems and penicillins but increases susceptibility to antimicrobial peptides. *Antimicrobial Agents and Chemotherapy*, *58*(4), 1956–1962. https://doi.org/10.1128/AAC.01901-13

Montero-Blay, A., Miravet-Verde, S., Lluch-Senar, M., Piñero-Lambea, C., & Serrano, L. (2019). SynMyco transposon: Engineering transposon vectors for efficient transformation of minimal genomes. *DNA Research*, *26*(4), 327–339. https://doi.org/10.1093/dnares/dsz012

Morrison-Plummer, J., Lazzell, A., & Baseman, J. B. (1987). Shared epitopes between Mycoplasma pneumoniae major adhesin protein P1 and a 140-kilodalton protein of Mycoplasma genitalium. *Infection and Immunity*, *55*(1), 49–56.

Mukherjee, A., & Lutkenhaus, J. (1998). Dynamic assembly of FtsZ regulated by GTP hydrolysis. *The EMBO Journal*, *17*(2), 462–469. https://doi.org/10.1093/emboj/17.2.462

Mukherjee, S., Barash, D., & Sengupta, S. (2017). Comparative genomics and phylogenomic analyses of lysine riboswitch distributions in bacteria. *PLoS ONE*, *12*(9). https://doi.org/10.1371/journal.pone.0184314

Mukherjee, S., & Sengupta, S. (2016). Riboswitch Scanner: an efficient pHMM-based web-server to detect riboswitches in genomic sequences. *Bioinformatics (Oxford, England)*, *32*(5), 776–778. https://doi.org/10.1093/bioinformatics/btv640

Mulhbacher, J., Brouillette, E., Allard, M., Fortier, L.-C., Malouin, F., & Lafontaine, D. A. (2010). Novel Riboswitch Ligand Analogs as Selective Inhibitors of Guanine-Related Metabolic Pathways. *PLoS Pathogens*, *6*(4), e1000865. https://doi.org/10.1371/journal.ppat.1000865

Musatovova, O., Dhandayuthapani, S., & Baseman, J. B. (2006). Transcriptional heat shock response in the smallest known self-replicating cell, Mycoplasma genitalium. *Journal of Bacteriology*, *188*(8), 2845–2855. https://doi.org/10.1128/JB.188.8.2845-2855.2006

Nagai, R., & Miyata, M. (2006). Gliding motility of Mycoplasma mobile can occur by repeated binding to N-acetylneuraminyllactose (sialyllactose) fixed on solid surfaces. *Journal of Bacteriology*, *188*(18), 6469–6475. https://doi.org/10.1128/JB.00754-06

Nahvi, A., Sudarsan, N., Ebert, M. S., Zou, X., Brown, K. L., & Breaker, R. R. (2002). Genetic control by a metabolite binding mRNA. *Chemistry and Biology*, *9*(9), 1043–1049. https://doi.org/10.1016/S1074-5521(02)00224-7

Nakane, D., Adan-Kubo, J., Kenri, T., & Miyata, M. (2011). Isolation and characterization of P1 adhesin, a leg protein of the gliding bacterium mycoplasma pneumoniae. *Journal of Bacteriology*, *193*(3), 715–722. https://doi.org/10.1128/JB.00796-10

Neumann, W., Gulati, A., & Nolan, E. M. (2017). Metal homeostasis in infectious disease: recent advances in bacterial metallophores and the human metal-withholding response. In *Current Opinion in Chemical Biology* (Vol. 37, pp. 10–18). Elsevier Ltd. https://doi.org/10.1016/j.cbpa.2016.09.012

Nicholas, R. A. J., & Ayling, R. D. (2003). Mycoplasma bovis: Disease, diagnosis, and control. In *Research in Veterinary Science* (Vol. 74, Issue 2, pp. 105–112). Res Vet Sci. https://doi.org/10.1016/S0034-5288(02)00155-8

Nikfarjam, L., & Farzaneh, P. (2012). Prevention and detection of mycoplasma contamination in cell culture. In *Cell Journal* (Vol. 13, Issue 4, pp. 203–212). Royan Institute.

Párraga-Niño, N., Colomé-Calls, N., Canals, F., Querol, E., & Ferrer-Navarro, M. (2012). A comprehensive proteome of mycoplasma genitalium. In *Journal of Proteome Research* (Vol. 11, Issue 6, pp. 3305–3316). J Proteome Res. https://doi.org/10.1021/pr300084c

Peterson, S. N., Bailey, C. C., Jensen, J. S., Borre, M. B., King, E. S., Bott, K. F., & Hutchison, C. A. (1995). Characterization of repetitive DNA in the Mycoplasma genitalium genome: Possible role in the generation of antigenic variation. *Proceedings of the National Academy of Sciences of the United States of America*, *92*(25), 11829–11833. https://doi.org/10.1073/pnas.92.25.11829

Pich, O. Q., Burgos, R., Ferrer-Navarro, M., Querol, E., & Piñol, J. (2006). Mycoplasma genitalium mg200 and mg386 genes are involved in gliding motility but not in cytadherence. *Molecular Microbiology*, *60*(6), 1509–1519. https://doi.org/10.1111/j.1365-2958.2006.05187.x

Pich, O. Q., Burgos, R., Planell, R., Querol, E., & Piñol, J. (2006). Comparative analysis of antibiotic resistance gene markers in Mycoplasma genitalium: Application to

studies of the minimal gene complement. *Microbiology*, *152*(2), 519–527. https://doi.org/10.1099/mic.0.28287-0

Pich, O. Q., Burgos, R., Querol, E., & Piñol, J. (2009). P110 and P140 Cytadherence-Related Proteins Are Negative Effectors of Terminal Organelle Duplication in Mycoplasma genitalium. *PLoS ONE*, *4*(10), e7452. https://doi.org/10.1371/journal.pone.0007452

Pich, O. Q., Carpenter, B. M., Gilbreath, J. J., & Merrell, D. S. (2012). Detailed analysis of Helicobacter pylori Fur-regulated promoters reveals a Fur box core sequence and novel Fur-regulated genes. *Molecular Microbiology*, *84*(5), 921–941. https://doi.org/10.1111/j.1365-2958.2012.08066.x

Pich, O. Q., & Merrell, D. S. (2013). The ferric uptake regulator of Helicobacter pylori: A critical player in the battle for iron and colonization of the stomach. In *Future Microbiology* (Vol. 8, Issue 6, pp. 725–738). Future Medicine Ltd London, UK . https://doi.org/10.2217/fmb.13.43

Pichoff, S., & Lutkenhaus, J. (2002). Unique and overlapping roles for ZipA and FtsA in septal ring assembly in Escherichia coli. *The EMBO Journal*, *21*(4), 685–693. https://doi.org/10.1093/emboj/21.4.685

Pilo, P., Vilei, E. M., Peterhans, E., Bonvin-Klotz, L., Stoffel, M. H., Dobbelaere, D., & Frey, J. (2005). A metabolic enzyme as a primary virulence factor of Mycoplasma mycoides subsp. mycoides small colony. *Journal of Bacteriology*, *187*(19), 6824–6831. https://doi.org/10.1128/JB.187.19.6824-6831.2005

Pollack, J. D. (1997). Mycoplasma genes: a case for reflective annotation. *Trends in Microbiology*, *5*(10), 413–419. https://doi.org/10.1016/s0966-842x(97)01113-x

Pour-El, I., Adams, C., & Minion, F. C. (2002). Construction of mini-Tn4001tet and its use in Mycoplasma gallisepticum. *Plasmid*, *47*(2), 129–137. https://doi.org/10.1006/plas.2001.1558

Proft, T., & Herrmann, R. (1994). Identification and characterization of hitherto unknown *Mycoplasma pneumoniae* proteins. *Molecular Microbiology*, *13*(2), 337–348. https://doi.org/10.1111/j.1365-2958.1994.tb00427.x

Provost, A., Perreau, P., Breard, A., Goff, C. Le, Martel, J. L., Cottew, G. S., & Le Goff, C. (1987). *Contagious bovine pleuropneumonia.*

Ptashne, M., Backman, K., Humayun, M. Z., Jeffrey, A., Maurer, R., Meyer, B., & Sauer, R. T. (1976). Autoregulation and function of a repressor in bacteriophage lambda. In *Science* (Vol. 194, Issue 4261, pp. 156–161). American Association for the

Advancement of Science. https://doi.org/10.1126/science.959843

Qi, L. S., Larson, M. H., Gilbert, L. A., Doudna, J. A., Weissman, J. S., Arkin, A. P., & Lim, W. A. (2013). Repurposing CRISPR as an RNA-guided platform for sequence-specific control of gene expression. *Cell*, *152*(5), 1173–1183. https://doi.org/10.1016/j.cell.2013.02.022

Radisic, M., Torn, A., Gutierrez, P., Defranchi, H. A., & Pardo, P. (2000). Severe Acute Lung Injury Caused by *Mycoplasma pneumoniae* : Potential Role for Steroid Pulses in Treatment. *Clinical Infectious Diseases*, *31*(6), 1507–1511. https://doi.org/10.1086/317498

Ramijan, K., Ultee, E., Willemse, J., Zhang, Z., Wondergem, J. A. J., van der Meij, A., Heinrich, D., Briegel, A., van Wezel, G. P., & Claessen, D. (2018). Stress-induced formation of cell wall-deficient cells in filamentous actinomycetes. *Nature Communications*, *9*(1), 1–13. https://doi.org/10.1038/s41467-018-07560-9

Raskin, D. M., & De Boer, P. A. J. (1999). Rapid pole-to-pole oscillation of a protein required for directing division to the middle of Escherichia coli. *Proceedings of the National Academy of Sciences of the United States of America*, *96*(9), 4971–4976. https://doi.org/10.1073/pnas.96.9.4971

Rawadi, G., & Roman-Roman, S. (1996). Mycoplasma membrane lipoproteins induce proinflammatory cytokines by a mechanism distinct from that of lipopolysaccharide. *Infection and Immunity*, *64*(2), 637–643. https://doi.org/10.1128/iai.64.2.637-643.1996

Razin, S. (1985). Molecular biology and genetics of mycoplasmas (Mollicutes). In *Microbiological Reviews* (Vol. 49, Issue 4, pp. 419–455). American Society for Microbiology (ASM). https://doi.org/10.1128/mmbr.49.4.419-455.1985

Razin, Shmuel. (2006). The Genus Mycoplasma and Related Genera (Class Mollicutes). In *The Prokaryotes* (pp. 836–904). Springer US. https://doi.org/10.1007/0-387-30744-3_29

Razin, Shmuel, Yogev, D., & Naot, Y. (1998). Molecular Biology and Pathogenicity of Mycoplasmas. *Microbiology and Molecular Biology Reviews*, *62*(4), 1094–1156. https://doi.org/10.1128/mmbr.62.4.1094-1156.1998

Reddy, S. P., Rasmussen, W. G., & Baseman, J. B. (1996). Isolation and characterization of transposon Tn 4001 -generated, cytadherence-deficient transformants of Mycoplasma pneumoniae and Mycoplasma genitalium . *FEMS Immunology & Medical Microbiology*, *15*(4), 199–211. https://doi.org/10.1111/j.1574-695x.1996.tb00086.x

Roberts, D. D., Olson, L. D., Barile, M. F., Ginsburg, V., & Krivan, H. C. (1989). Sialic acid-dependent adhesion of Mycoplasma pneumoniae to purified glycoproteins. *Journal of Biological Chemistry*, *264*(16), 9289–9293.

Rodionov, D. A., Hebbeln, P., Eudes, A., Ter Beek, J., Rodionova, I. A., Erkens, G. B., Slotboom, D. J., Gelfand, M. S., Osterman, A. L., Hanson, A. D., & Eitinger, T. (2009). A novel class of modular transporters for vitamins in prokaryotes. *Journal of Bacteriology*, *91*(1), 42–51. https://doi.org/10.1128/JB.01208-08

Rodionov, D. A., Hebbeln, P., Gelfand, M. S., & Eitinger, T. (2006). Comparative and functional genomic analysis of prokaryotic nickel and cobalt uptake transporters: Evidence for a novel group of ATP-binding cassette transporters. *Journal of Bacteriology*, *188*(1), 317–327. https://doi.org/10.1128/JB.188.1.317-327.2006

Rodrigue, A., Effantin, G., & Mandrand-Berthelot, M. A. (2005). Identification of rcnA (yohM), a nickel and cobalt resistance gene in Escherichia coli. *Journal of Bacteriology*, *187*(8), 2912–2916. https://doi.org/10.1128/JB.187.8.2912-2916.2005

Rosenfeld, N., Elowitz, M. B., & Alon, U. (2002). Negative autoregulation speeds the response times of transcription networks. *Journal of Molecular Biology*, *323*(5), 785–793. https://doi.org/10.1016/S0022-2836(02)00994-4

Roth, J. R., Lawrence, J. G., Rubenfield, M., Kieffer-Higgins, S., & Church, G. M. (1993). Characterization of the cobalamin (vitamin B12) biosynthetic genes of Salmonella typhimurium. *Journal of Bacteriology*, *175*(11), 3303–3316. https://doi.org/10.1128/jb.175.11.3303-3316.1993

Rottem, S., & Barile, M. F. (1993). Beware of mycoplasmas. In *Trends in Biotechnology* (Vol. 11, Issue 4, pp. 143–151). Elsevier Current Trends. https://doi.org/10.1016/0167-7799(93)90089-R

Rozen, S., & Skaletsky, H. (2000). Primer3 on the WWW for general users and for biologist programmers. *Methods in Molecular Biology (Clifton, N.J.)*, *132*, 365–386. https://doi.org/10.1385/1-59259-192-2:365

Runde, S., Molière, N., Heinz, A., Maisonneuve, E., Janczikowski, A., Elsholz, A. K. W., Gerth, U., Hecker, M., & Turgay, K. (2014). The role of thiol oxidative stress response in heat-induced protein aggregate formation during thermotolerance in Bacillus subtilis. *Molecular Microbiology*, *91*(5), 1036–1052. https://doi.org/10.1111/mmi.12521

Sarvan, S., Charih, F., Askoura, M., Butcher, J., Brunzelle, J. S., Stintzi, A., & Couture, J. F. (2018). Functional insights into the interplay between DNA interaction and metal

coordination in ferric uptake regulators. *Scientific Reports*, *8*(1), 1–14. https://doi.org/10.1038/s41598-018-25157-6

Schäfer, H., Heinz, A., Sudzinová, P., Voß, M., Hantke, I., Krásný, L., & Turgay, K. (2018). Spx, the central regulator of the heat and oxidative stress response in *B. subtilis* , can repress transcription of translation-related genes. *Molecular Microbiology*, *111*(2), mmi.14171. https://doi.org/10.1111/mmi.14171

Schalk, I. J. (2008). Metal trafficking via siderophores in Gram-negative bacteria: Specificities and characteristics of the pyoverdine pathway. *Journal of Inorganic Biochemistry*, *102*(5–6), 1159–1169. https://doi.org/10.1016/j.jinorgbio.2007.11.017

Schalk, I. J., & Cunrath, O. (2016). An overview of the biological metal uptake pathways in Pseudomonas aeruginosa. *Environmental Microbiology*, *18*(10), 3227–3246. https://doi.org/10.1111/1462-2920.13525

Schmidl, S. R., Otto, A., Lluch-Senar, M., Piñol, J., Busse, J., Becher, D., & Stülke, J. (2011). A Trigger Enzyme in Mycoplasma pneumoniae: Impact of the Glycerophosphodiesterase GlpQ on Virulence and Gene Expression. *PLoS Pathogens*, *7*(9), e1002263. https://doi.org/10.1371/journal.ppat.1002263

Seña, A. C., Lee, J. Y., Schwebke, J., Philip, S. S., Wiesenfeld, H. C., Rompalo, A. M., Cook, R. L., & Hobbs, M. M. (2018). A Silent Epidemic: The Prevalence, Incidence and Persistence of Mycoplasma genitalium Among Young, Asymptomatic High-Risk Women in the United States. *Clinical Infectious Diseases : An Official Publication of the Infectious Diseases Society of America*, *67*(1), 73–79. https://doi.org/10.1093/cid/ciy025

Serganov, A., & Nudler, E. (2013). A decade of riboswitches. In *Cell* (Vol. 152, Issues 1–2, pp. 17–24). Cell Press. https://doi.org/10.1016/j.cell.2012.12.024

Seto, S., Layh-Schmitt, G., Kenri, T., & Miyata, M. (2001). Visualization of the attachment organelle and cytadherence proteins of Mycoplasma pneumoniae by immunofluorescence microscopy. *Journal of Bacteriology*, *183*(5), 1621–1630. https://doi.org/10.1128/JB.183.5.1621-1630.2001

Shahid, M. A., Marenda, M. S., Markham, P. F., & Noormohammadi, A. H. (2014). Development of an oriC vector for use in Mycoplasma synoviae. *Journal of Microbiological Methods*, *103*, 70–76. https://doi.org/10.1016/j.mimet.2014.05.014

Shimada, Y., Deguchi, T., Nakane, K., Masue, T., Yasuda, M., Yokoi, S., Ito, S. ichi, Nakano, M., Ito, S., & Ishiko, H. (2010). Emergence of clinical strains of Mycoplasma

genitalium harbouring alterations in ParC associated with fluoroquinolone resistance. *International Journal of Antimicrobial Agents*, *36*(3), 255–258. https://doi.org/10.1016/j.ijantimicag.2010.05.011

Shimizu, T. (2016). Inflammation-inducing factors of Mycoplasma pneumoniae. In *Frontiers in Microbiology* (Vol. 7, Issue MAR). https://doi.org/10.3389/fmicb.2016.00414

Shimizu, T., Kida, Y., & Kuwano, K. (2007). Triacylated lipoproteins derived from Mycoplasma pneumoniae activate nuclear factor-?B through toll-like receptors 1 and 2. *Immunology*, *121*(4), 473–483. https://doi.org/10.1111/j.1365-2567.2007.02594.x

Shimizu, T., Kida, Y., & Kuwano, K. (2008). A triacylated lipoprotein from Mycoplasma genitalium activates NF-κB through Toll-like receptor 1 (TLR1) and TLR2. *Infection and Immunity*, *76*(8), 3672–3678. https://doi.org/10.1128/IAI.00257-08

Soni, S., Alexander, S., Verlander, N., Saunders, P., Richardson, D., Fisher, M., & Ison, C. (2010). The prevalence of urethral and rectal Mycoplasma genitalium and its associations in men who have sex with men attending a genitourinary medicine clinic. *Sexually Transmitted Infections*, *86*(1), 21–24. https://doi.org/10.1136/sti.2009.038190

Sonnenberg, P., Ison, C. A., Clifton, S., Field, N., Tanton, C., Soldan, K., Beddows, S., Alexander, S., Khanom, R., Saunders, P., Copas, A. J., Wellings, K., Mercer, C. H., & Johnson, A. M. (2015). Epidemiology of Mycoplasma genitalium in British men and women aged 16–44 years: evidence from the third National Survey of Sexual Attitudes and Lifestyles (Natsal-3). *International Journal of Epidemiology*, *44*(6), 1982–1994. https://doi.org/10.1093/ije/dyv194

Stintzi, A., Barnes, C., Xu, J., & Raymond, K. N. (2000). Microbial iron transport via a siderophore shuttle: A membrane ion transport paradigm. *Proceedings of the National Academy of Sciences of the United States of America*, *97*(20), 10691–10696. https://doi.org/10.1073/pnas.200318797

Stipkovits, L., & Kempf, I. (1996). Mycoplasmoses in poultry. *OIE Revue Scientifique et Technique*, *15*(4), 1495–1525. https://doi.org/10.20506/rst.15.4.986

Stroud, R. M., Miercke, L. J. W., O'Connell, J., Khademi, S., Lee, J. K., Remis, J., Harries, W., Robles, Y., & Akhavan, D. (2003). Glycerol facilitator GlpF and the associated aquaporin family of channels. In *Current Opinion in Structural Biology* (Vol. 13, Issue 4, pp. 424–431). Elsevier Ltd. https://doi.org/10.1016/S0959-440X(03)00114-3

Sun, Q., & Margolin, W. (1998). FtsZ dynamics during the division cycle of live Escherichia

coli cells. *Journal of Bacteriology*, *180*(8), 2050–2056. https://doi.org/10.1128/jb.180.8.2050-2056.1998

Surdova, K., Gamba, P., Claessen, D., Siersma, T., Jonker, M. J., Errington, J., & Hamoena, L. W. (2013). The Conserved DNA-Binding protein WhiA is involved in cell division in bacillus subtilis. *Journal of Bacteriology*, *195*(24), 5450–5460. https://doi.org/10.1128/JB.00507-13

Suvorova, I. A., Korostelev, Y. D., & Gelfand, M. S. (2015). GntR Family of Bacterial Transcription Factors and Their DNA Binding Motifs: Structure, Positioning and Co-Evolution. *PLOS ONE*, *10*(7), e0132618. https://doi.org/10.1371/journal.pone.0132618

Tan, S., Noto, J. M., Romero-Gallo, J., Peek, R. M., & Amieva, M. R. (2011). Helicobacter pylori Perturbs Iron Trafficking in the Epithelium to Grow on the Cell Surface. *PLoS Pathogens*, *7*(5), e1002050. https://doi.org/10.1371/journal.ppat.1002050

Tan, S., Tompkins, L. S., & Amieva, M. R. (2009). Helicobacter pylori Usurps Cell Polarity to Turn the Cell Surface into a Replicative Niche. *PLoS Pathogens*, *5*(5), e1000407. https://doi.org/10.1371/journal.ppat.1000407

Tanaka, K. J., & Pinkett, H. W. (2019). Oligopeptide-binding protein from nontypeable Haemophilus influenzae has ligand-specific sites to accommodate peptides and heme in the binding pocket. *Journal of Biological Chemistry*, *294*(3), 1070–1082. https://doi.org/10.1074/jbc.RA118.004479

Taylor-Robinson, D., & Jensen, J. S. (2011). Mycoplasma genitalium: From chrysalis to multicolored butterfly. *Clinical Microbiology Reviews*, *24*(3), 498–514. https://doi.org/10.1128/CMR.00006-11

Teixidó, L., Carrasco, B., Alonso, J. C., Barbé, J., & Campoy, S. (2011). Fur activates the expression of salmonella enterica pathogenicity island 1 by directly interacting with the hilD operator in Vivo and in Vitro. *PLoS ONE*, *6*(5). https://doi.org/10.1371/journal.pone.0019711

Ter Beek, J., Duurkens, R. H., Erkens, G. B., & Slotboom, D. J. (2011). Quaternary structure and functional unit of Energy Coupling Factor (ECF)-type transporters. *Journal of Biological Chemistry*, *286*(7), 5471–5475. https://doi.org/10.1074/jbc.M110.199224

Thomas, D. C. (2017). The phagocyte respiratory burst: Historical perspectives and recent advances. In *Immunology Letters* (Vol. 192, pp. 88–96). Elsevier B.V. https://doi.org/10.1016/j.imlet.2017.08.016

Torres-Puig, S. (2017). Study of a master regulator of recombination in Mycoplasma genitalium. In *TDX (Tesis Doctorals en Xarxa)*. Universitat Autònoma de Barcelona.

Torres-Puig, S., Broto, A., Querol, E., Piñol, J., & Pich, O. Q. (2015). A novel sigma factor reveals a unique regulon controlling cell-specific recombination in Mycoplasma genitalium. *Nucleic Acids Research*, *43*(10), 4923–4936. https://doi.org/10.1093/nar/gkv422

Torres-Puig, S., Martínez-Torró, C., Granero-Moya, I., Querol, E., Piñol, J., & Pich, O. Q. (2018). Activation of σ20-dependent recombination and horizontal gene transfer in Mycoplasma genitalium. *DNA Research*, *25*(4), 383–393. https://doi.org/10.1093/dnares/dsy011

Troxell, B., & Hassan, H. M. (2013). Transcriptional regulation by Ferric Uptake Regulator (Fur) in pathogenic bacteria. *Frontiers in Cellular and Infection Microbiology*, *4*(OCT), 59. https://doi.org/10.3389/fcimb.2013.00059

Trussart, M., Yus, E., Martinez, S., Baù, D., Tahara, Y. O., Pengo, T., Widjaja, M., Kretschmer, S., Swoger, J., Djordjevic, S., Turnbull, L., Whitchurch, C., Miyata, M., Marti-Renom, M. A., Lluch-Senar, M., & Serrano, L. (2017). Defined chromosome structure in the genome-reduced bacterium Mycoplasma pneumoniae. *Nature Communications*, *8*(1), 1–13. https://doi.org/10.1038/ncomms14665

Tryon, V. V., & Baseman, J. B. (1987). The acquisition of human lactoferrin by Mycoplasma pneumoniae. *Microbial Pathogenesis*, *3*(6), 437–443. https://doi.org/10.1016/0882-4010(87)90013-1

Tseng, C. W., Chiu, C. J., Kanci, A., Citti, C., Rosengarten, R., Browning, G. F., & Markham, P. F. (2017). The oppD gene and putative peptidase genes may be required for virulence in Mycoplasma gallisepticum. *Infection and Immunity*, *85*(6). https://doi.org/10.1128/IAI.00023-17

Tully, J. G., Taylor-Robinson, D., Cole, R. M., & Rose, D. L. (1981). A newly discovered mycoplasma in the human urogenital tract. *Lancet (London, England)*, *1*(8233), 1288–1291. https://doi.org/10.1016/s0140-6736(81)92461-2

Vandepitte, J., Weiss, H. A., Bukenya, J., Kyakuwa, N., Muller, E., Buvé, A., Van Der Stuyft, P., Hayes, R. J., & Grosskurth, H. (2014). Association between Mycoplasma genitalium infection and HIV acquisition among female sex workers in Uganda: Evidence from a nested case-control study. *Sexually Transmitted Infections*, *90*(7), 545–549. https://doi.org/10.1136/sextrans-2013-051467

Vannini, A., Roncarati, D., Spinsanti, M., Scarlato, V., & Danielli, A. (2014). In depth analysis of the Helicobacter pylori cag pathogenicity island transcriptional

responses. *PLoS ONE*, *9*(6). https://doi.org/10.1371/journal.pone.0098416

Vicente, M., Gomez, M. J., & Ayala, J. A. (1998). Regulation of transcription of cell division genes in the Eschericia coli dcw cluster. *Cellular and Molecular Life Sciences*, *54*(4), 317–324. https://doi.org/10.1007/s000180050158

Vickers, C. E. (2016). The minimal genome comes of age. In *Nature Biotechnology* (Vol. 34, Issue 6, pp. 623–624). Nature Publishing Group. https://doi.org/10.1038/nbt.3593

Vilei, E. M., & Frey, J. (2001). Genetic and biochemical characterization of glycerol uptake in Mycoplasma mycoides subsp. mycoides SC: Its impact on H2O2 production and virulence. *Clinical and Diagnostic Laboratory Immunology*, *8*(1), 85–92. https://doi.org/10.1128/CDLI.8.1.85-92.2001

Vizarraga, D., Kawamoto, A., Matsumoto, U., Illanes, R., Perez-Luque, R., Martin, J., Mazzolini, R., Bierge, P., Pich, O., Mateu, E., Sanfeliu, I., Esperalba, J., Fernandez-Huerta, M., Scheffer, M., Piñol, J., Frangakis, A., Lluch-Senar, M., Mori, S., Shibayama, K., … Aparicio, D. (n.d.). Immunodominant proteins P1 and P40/P90 from human pathogen Mycoplasma pneumoniae. *Nature Communications*.

Waites, K. B., & Talkington, D. F. (2004). Mycoplasma pneumoniae and Its Role as a Human Pathogen. *Clinical Microbiology Reviews*, *17*(4), 697–728. https://doi.org/10.1128/CMR.17.4.697-728.2004

Washington, T. A., Smith, J. L., & Grossman, A. D. (2017). Genetic networks controlled by the bacterial replication initiator and transcription factor DnaA in *Bacillus subtilis*. *Molecular Microbiology*, *106*(1), 109–128. https://doi.org/10.1111/mmi.13755

Waterhouse, A., Bertoni, M., Bienert, S., Studer, G., Tauriello, G., Gumienny, R., Heer, F. T., de Beer, T. A. P., Rempfer, C., Bordoli, L., Lepore, R., & Schwede, T. (2018). SWISS-MODEL: homology modelling of protein structures and complexes. *Nucleic Acids Research*, *46*(W1), W296–W303. https://doi.org/10.1093/nar/gky427

Weinberg, E. D. (1975). Nutritional immunity. Host's attempt to withold iron from microbial invaders. *JAMA: The Journal of the American Medical Association*, *231*(1), 39–41. https://doi.org/10.1001/jama.231.1.39

Weiner III, J., Herrmann, R., & Browning, G. F. (2000). Transcription in Mycoplasma pneumoniae. *Nucleic Acids Research*, *28*(22), 4488–4496. https://doi.org/10.1093/nar/28.22.4488

White, C., Lee, J., Kambe, T., Fritsche, K., & Petris, M. J. (2009). A role for the ATP7A

copper-transporting ATPase in macrophage bactericidal activity. *Journal of Biological Chemistry*, *284*(49), 33949–33956. https://doi.org/10.1074/jbc.M109.070201

Woese, C. R., Maniloff, J., & Zablen, L. B. (1980). Phylogenetic analysis of the mycoplasmas. *Proceedings of the National Academy of Sciences of the United States of America*, *77*(1), 494–498. https://doi.org/10.1073/pnas.77.1.494

Wood, G. E., Iverson-Cabral, S. L., Patton, D. L., Cummings, P. K., Cosgrove Sweeney, Y. T., & Tottena, P. A. (2013). Persistence, immune response, and antigenic variation of mycoplasma genitalium in an experimentally infected pig-tailed macaque (macaca nemestrina). *Infection and Immunity*, *81*(8), 2938–2951. https://doi.org/10.1128/IAI.01322-12

Wu, L. J., & Errington, J. (2004). Coordination of cell division and chromosome segregation by a nucleoid occlusion protein in Bacillus subtilis. *Cell*, *117*(7), 915–925. https://doi.org/10.1016/j.cell.2004.06.002

Wu, Y., Qiu, H., Zeng, Y., You, X., Deng, Z., Yu, M., & Zhu, C. (2008). Mycoplasma genitalium lipoproteins induce human monocytic cell expression of proinflammatory cytokines and apoptosis by activating nuclear factor kappaB. *Mediators of Inflammation*, *2008*, 195427. https://doi.org/10.1155/2008/195427

Xu, X., Zhang, H., Huang, Y., Zhang, Y., Wu, C., Gao, P., Teng, Z., Luo, X., Peng, X., Wang, X., Wang, D., Pu, J., Zhao, H., Lu, X., Lu, S., Ye, C., Dong, Y., Lan, R., & Xu, J. (2019). Beyond a Ribosomal RNA Methyltransferase, the Wider Role of MraW in DNA Methylation, Motility and Colonization in Escherichia coli O157:H7. *Frontiers in Microbiology*, *10*, 2520. https://doi.org/10.3389/fmicb.2019.02520

Yamamoto, K. (2014). The hierarchic network of metal-response transcription factors in Escherichia coli. In *Bioscience, Biotechnology and Biochemistry* (Vol. 78, Issue 5, pp. 737–747). Japan Society for Bioscience Biotechnology and Agrochemistry. https://doi.org/10.1080/09168451.2014.915731

Yang, X., Lyu, Z., Miguel, A., McQuillen, R., Huang, K. C., & Xiao, J. (2017). GTPase activity-coupled treadmilling of the bacterial tubulin FtsZ organizes septal cell wall synthesis. *Science*, *355*(6326), 744–747. https://doi.org/10.1126/science.aak9995

Yus, E., Güell, M., Vivancos, A. P., Chen, W. H., Lluch-Senar, M., Delgado, J., Gavin, A. C., Bork, P., & Serrano, L. (2012). Transcription start site associated RNAs in bacteria. *Molecular Systems Biology*, *8*, 585. https://doi.org/10.1038/msb.2012.16

Yus, E., Lloréns-Rico, V., Martínez, S., Gallo, C., Eilers, H., Blötz, C., Stülke, J., Lluch-Senar, M., & Serrano, L. (2019). Determination of the Gene Regulatory Network of a

Genome-Reduced Bacterium Highlights Alternative Regulation Independent of Transcription Factors. *Cell Systems*, *9*(2), 143-158.e13. https://doi.org/10.1016/j.cels.2019.07.001

Yus, E., Maier, T., Michalodimitrakis, K., Van Noort, V., Yamada, T., Chen, W. H., Wodke, J. A. H., Güell, M., Martínez, S., Bourgeois, R., Kühner, S., Raineri, E., Letunic, I., Kalinina, O. V., Rode, M., Herrmann, R., Gutiérrez-Gallego, R., Russell, R. B., Gavin, A. C., … Serrano, L. (2009). Impact of genome reduction on bacterial metabolism and its regulation. *Science*, *326*(5957), 1263–1268. https://doi.org/10.1126/science.1177263

Zhang, P. (2013). Structure and mechanism of energy-coupling factor transporters. In *Trends in Microbiology* (Vol. 21, Issue 12, pp. 652–659). Elsevier Current Trends. https://doi.org/10.1016/j.tim.2013.09.009

Zhang, P., Wang, J., & Shi, Y. (2010). Structure and mechanism of the S component of a bacterial ECF transporter. *Nature*, *468*(7324), 717–720. https://doi.org/10.1038/nature09488

Zhang, W., & Baseman, J. B. (2011a). Transcriptional response of Mycoplasma genitalium to osmotic stress. *Microbiology*, *157*(2), 548–556. https://doi.org/10.1099/mic.0.043984-0

Zhang, W., & Baseman, J. B. (2011b). Transcriptional regulation of MG-149, an osmoinducible lipoprotein gene from Mycoplasma genitalium. *Molecular Microbiology*, *81*(2), 327–339. https://doi.org/10.1111/j.1365-2958.2011.07717.x

Zhao, S., Cao, S., Luo, L., Zhang, Z., Yuan, G., Zhang, Y., Yang, Y., Guo, W., Wang, L., Chen, F., Wu, Q., & Li, L. (2018). A preliminary investigation of metal element profiles in the serum of patients with bloodstream infections using inductively-coupled plasma mass spectrometry (ICP-MS). *Clinica Chimica Acta*, *485*, 323–332. https://doi.org/10.1016/j.cca.2018.07.013

Zhao, Y., Hammond, R. W., Lee, I. M., Roe, B. A., Lin, S., & Davis, R. E. (2004). Cell Division Gene Cluster in Spiroplasma kunkelii: Functional Characterization of ftsZ and the First Report of ftsA in Mollicutes. *DNA and Cell Biology*, *23*(2), 127–134. https://doi.org/10.1089/104454904322759948

Zheleznova, E. E., Crosa, J. H., & Brennan, R. G. (2000). Characterization of the DNA- and metal-binding properties of Vibrio anguillarum Fur reveals conservation of a structural Zn2+ ion. *Journal of Bacteriology*, *182*(21), 6264–6267. https://doi.org/10.1128/JB.182.21.6264-6267.2000

Zou, J., Zhang, W., Zhang, H., Zhang, X. D., Peng, B., & Zheng, J. (2018). Studies on

aminoglycoside susceptibility identify a novel function of KsgA to secure translational fidelity during antibiotic stress. *Antimicrobial Agents and Chemotherapy*, *62*(10). https://doi.org/10.1128/AAC.00853-18